Toughening of A Polyester and Epoxy Molecular Network System

by

Mavyn McAuliffe

B.S. Materials Science and Engineering (1995)

Massachusetts Institute of Technology

Submitted to the Department of Materials Science and Engineering
in Partial Fulfillment of the Requirements for the Degree of
Master of Science in Materials Science and Engineering

at the

Massachusetts Institute of Technology

February 1997

Signature of Author . . . . . .
Department of Materials Science and Engineering
January 17, 1997

Certified by . . . . . .
Professor Frederick J. McGarry
Professor of Polymer Engineering
Thesis Supervisor

Accepted by . . . . . .
Professor Linn W. Hobbes
John F. Elliott Professor of Materials
Chairman, Department Committee on Graduate Students

Toughening of A Polyester and Epoxy Molecular Network System

by

Mavyn McAuliffe

Submitted to the Department of Materials Science and Engineering
on January 17, 1997 in Partial Fulfillment of the
Requirements for the Degree of Master of Science
in Materials Science and Engineering

ABSTRACT

Lightweight polymer based composites are finding increased applications in the areas of surface transportation and infrastructure. Polyester resins are the most common matrix material for a major class of these composites known as sheet molding compounds (SMC's). However, polyesters are inherently brittle. Thus, these resins must be toughened if their use is to be expanded.

This study investigated a system of unsaturated polyester and epoxy modified with an amine terminated poly (butadiene-co-acrylonitrile) (ATBN) liquid rubber. At less than 9% ATBN, the morphology of this molecular network system (MNS) consisted of a continuous polyester-rich matrix with discrete rubber-rich domains, and produced only small increases in toughness properties. On the other hand, at higher rubber contents, the morphology changed to a continuous rubber-rich phase with discrete brittle polyester-rich domains. This morphology led the plane strain fracture toughness (K_{Ic}) to increase by a factor of 1.7 and the strain energy release rate (G_{Ic}) to increase by a factor of 3.2. The toughness properties continued to increase with increasing rubber content. However, the mechanical and thermal properties were significantly diminished as a result of the high rubber contents.

Several types of second phase particles were added to MNS compositions containing low rubber contents. While the resulting increases in toughness properties were measurable, they were not as substantial as expected. This was generally due to poor adhesion or location of these particles, which prevented them from initiating adequate energy absorbing mechanisms. However, a sample containing well-adhered hollow glass microspheres located within the discrete ATBN-rich domains showed a large amount of deformation and exhibited a 1.8 fold increase in K_{Ic}, a 4.2 fold increase in G_{Ic}, and minimal decreases in mechanical and thermal properties.

Thesis Supervisor: Professor Frederick J. McGarry
Title: Professor of Polymer Engineering

To Mom and Dad

Acknowledgments

First of all, I would like to thank my advisor and mentor, Professor McGarry. Under his tutelage, I have gained an immeasurable amount of both technical knowledge and real-world experience. He taught me to trust my instincts and think creatively.

I would also like to thank my officemates. Firstly, thank you to Ramnath Subramaniam for getting me started on this research project, and for teaching me that the proper method for cleaning the lab floor requires doing the twist. Also thank you Bizhong Zhu for being patient with me in my few synthesis attempts, and for being a resource any time I encountered anything related to chemistry. Rizwan Gul was also instrumental in introducing me to the lab, as well as for coming to the rescue whenever the Instron decided not to behave. Deborah Spence deserves special recognition for being a valuable resource to bounce ideas off of, as well as for being a true friend who spent a lot of time listening. She also taught me that there are not many problems in life that chocolate can't solve. I would also like to thank Diane for help with the ins and outs of MIT bureaucracy. She saved me many headaches during the last two years. Finally, thank you to my UROP, Mon Fen Hong, who kept my sanity intact by performing hours of dektak runs for me last term.

I would also like to extend a special thank you to Dr. Carol Schutte at NIST for her support and guidance. She sparked my interest in polymers, taught me how to be successful in the lab, and showed me how to handle real world issues. I consider her to be an exceptional role model for me in my future career.

I could not have made it through MIT without the best group of friends a person could have. Kristen, Holly, Shraddha, Ranjini, Ranee, Ross, Joel, Nitin, Scott L., Scott M., Minh, and Jean; you guys are truly the best. Michael, I will value your friendship always, and I thank you for always being there for me and for helping me to believe in myself as much as you believed in me.

Finally, I would like to acknowledge the most important people in my life--my parents. Mom and Dad, you are truly exceptional people. You gave me all the tools to make it though life, and then stood back to let me give it my best shot while always being nearby in case I needed support. Thank you for all your patience, support and lengthy phone calls these past few years. I couldn't have done it without you.

INDEX

1.0 Introduction 21
- 1.1 General Deformation Mechanisms 22
  - 1.1.1 Global Methods 22
  - 1.1.2 Local Methods 23
    - 1.1.2.1 Crazing 23
    - 1.1.2.2 Shear Banding 27
- 1.2 Toughening Mechanisms 27
  - 1.2.1 In-Situ Particle Formation 28
  - 1.2.2 Role of Rubber Particles 30
    - 1.2.2.1 In Materials that Craze 32
    - 1.2.2.2 In Materials that Shear Band 32
    - 1.2.2.3 Modifier Properties 35

2.0 Previous Work 36
- 2.1 Toughening Mechanisms- Thermoplastics 36
  - 2.1.1 Effect of Particle Size 37
    - 2.1.2 Effect of Matrix Properties 38
- 2.2 Toughening Mechanisms- Thermosets 38
  - 2.2.1 Epoxies 38
    - 2.2.1.1 Effect of Modifier Type 39
      - 2.2.1.1.1 In-Situ Particles 39
      - 2.2.1.1.2 Pre-Formed Particles 40
    - 2.2.1.2 Effect of Phase Separation 41
      - 2.2.1.2.1 Fracture Toughness 41
      - 2.2.1.2.2 Mechanical Properties 42
    - 2.2.1.3 Effect of Particle Size 43
    - 2.2.1.4 Effect of Particle Adhesion 44
    - 2.2.1.5 Effect of Matrix Properties 45
  - 2.2.2 Polyesters 45
    - 2.2.2.1 Effect of Modifier Type 46
    - 2.2.2.2 Effect of Phase Separation 47
    - 2.2.2.3 Effect of Particle Size 48
    - 2.2.2.4 Effect of Particle Adhesion 49
- 2.3 IPN's 50
  - 2.3.1 General Toughening Mechanisms 50
- 2.4 MNS 51
  - 2.4.1 Structure 51
  - 2.4.2 Morphology 52
  - 2.4.3 Mechanical Properties 53
- 2.5 Objective 53

3.0 Experimental 54
3.1 Materials 54
3.1.1 Primary Components 54
3.1.2 Pre-Formed Particles 54
3.2 Castings 56
3.3 Mechanical Properties 57
3.3.1 Tensile Properties 57
3.3.2 Plane Strain Fracture Toughness 57
3.3.3 Flexural Modulus 58
3.4 Scanning Electron Microscopy 58
3.5 Dynamic Mechanical Analysis 59

4.0 Results and Discussion 59
4.1 Neat MNS Compositions 59
4.1.1 Mechanical Properties 59
4.1.1.1 Tensile Properties 59
4.1.1.2 Plane Strain Fracture Toughness 64
4.1.2 Scanning Electron Microscopy 66
4.1.2 Dynamic Mechanical Analysis 79
4.2 Compositions Containing Pre-Formed Particles 91
4.2.1 Nipol and Paraloid Particles 92
4.2.1.1 Plane Strain Fracture Toughness 92
4.2.1.2 Scanning Electron Microscopy 100
4.2.1.2.1 Nipol Particles 100
4.2.1.2.2 Paraloid Particles 106
4.2.1.2.3 Fumed Silica Particles 109
4.2.1.3 Dynamic Mechanical Analysis 112
4.2.2 CTBN Liquid Rubber 115
4.2.2.1 Plane Strain Fracture Toughness 115
4.2.2.2 Scanning Electron Microscopy 118
4.2.2.2.1 Middle Region 118
4.2.2.2.2 Top Region 125
4.2.2.2.3 Transition Regions 127
4.2.2.3 Dynamic Mechanical Analysis 130
4.2.3 Core-Shell Particles 133
4.2.3.1 Plane Strain Fracture Toughness 133
4.2.3.2 Scanning Electron Microscopy 140
4.2.3.2.1 EXL 5136 Particles 140
4.2.3.2.2 EXL 2691 Particles 144
4.2.3.2.3 EXL 2330 Particles 147
4.2.3.3 Dynamic Mechanical Analysis 150
4.2.4 Glass Particles 153
4.2.4.1 Plane Strain Fracture Toughness 153
4.2.4.2 Scanning Electron Microscopy 159
4.2.4.2.1 Solid Glass Spheres (Z6020) 159
4.2.4.2.2 Solid Glass Spheres (Z6040) 162

4.2.4.2.3 Hollow Glass Spheres (Z6020) 162
4.2.4.3 Dynamic Mechanical Analysis 167
4.2.5 PDMS Particles 170
4.2.5.1 Plane Strain Fracture Toughness 170
4.2.5.2 Scanning Electron Microscopy 176
4.2.5.2.1 Amino PDMS Particles 176
4.2.5.2.2 Epoxy PDMS Particles 180
4.2.5.2.3 Silanol PDMS Particles 183
4.2.5.3 Dynamic Mechanical Analysis 186
4.2.6 12% ATBN and Glass Spheres 188
4.2.6.1 Plane Strain Fracture Toughness 189
4.2.6.2 Scanning Electron Microscopy 192

5.0 Conclusions 198

Appendix 202

References 204

LIST OF FIGURES

Figure 1.1	Schematic of shear yielding, crazing and shear banding mechanisms.	22
Figure 1.2	Schematic of craze structure.	24
Figure 1.3	Schematic of the sequence of craze initiation, propagation and failure.	26
Figure 1.4	Schematic of the process of rubber particle cavitation.	31
Figure 1.5	Schematic of tearing of a rubber particle.	31
Figure 1.6	Schematic of deformation in a craze induced by a rubber particle.	33
Figure 1.7	Schematic of craze arrest mechanisms.	34
Figure 2.1	Schematic of reactions possible in crosslinked MNS.	52
Figure 4.1	Variation of ultimate tensile strength with rubber content of MNS samples.	61
Figure 4.2	Variation of strain to failure with rubber content of MNS samples.	62
Figure 4.3	Variation of tensile modulus with rubber content of MNS samples.	63
Figure 4.4	Variation of plane strain fracture toughness with rubber content of MNS samples.	65
Figure 4.5	Backscattered image of discrete rubber-rich domains on the fracture surface of an MNS specimen containing 7.0% ATBN.	67
Figure 4.6	Backscattered image of glassy polyester-rich occlusions in a rubber-rich domain on the fracture surface of an MNS specimen containing 7.0% ATBN.	67
Figure 4.7	Backscattered image of numerous rubber-rich domains on the fracture surface of an MNS specimen containing 7.5% ATBN.	68

Figure 4.8	Backscattered image of the discrete rubber-rich domains on the fracture surface of a second MNS specimen containing 7.5% ATBN.	68
Figure 4.9	Backscattered image of the discrete rubber-rich domains on the fracture surface of an MNS specimen containing 8.0% ATBN.	70
Figure 4.10	Backscattered image of the discrete rubber-rich domains on the fracture surface of an MNS specimen containing 8.5% ATBN.	70
Figure 4.11	Backscattered image of large glassy occlusions in the rubber-rich domains on the fracture surface of an MNS specimen containing 8.0% ATBN.	71
Figure 4.12	Backscattered image of large glassy occlusions in the rubber-rich domains on the fracture surface of an MNS specimen containing 8.5% ATBN.	71
Figure 4.13	Backscattered image of the forming polyester-rich domains in a continuous polyester-rich matrix on the fracture surface of an MNS specimen with 9.0% ATBN.	72
Figure 4.14	Backscattered image of discrete polyester-rich domains on the fracture surface of an MNS specimen containing 9.0% ATBN.	72
Figure 4.15	Backscattered image of a rubber-rich occlusion in a polyester-rich domain on the fracture surface of an MNS specimen containing 9.0% ATBN.	73
Figure 4.16	Backscattered image of distinct polyester-rich domains on the fracture surface of an MNS sample containing 9.5% ATBN.	73
Figure 4.17	Backscattered image of a polyester-rich domain on the fracture surface of an MNS sample containing 9.5% ATBN.	74
Figure 4.18	Backscattered image of rubber-rich occlusions in a polyester-rich domain on the fracture surface of an MNS specimen containing 9.5% ATBN.	74
Figure 4.19	Backscattered image of large, distinct polyester-rich domains on the fracture surface of an MNS sample	75

containing 10.0% ATBN.

Figure 4.20 Backscattered image of rubber-rich occlusions in two polyester-rich domains on the fracture surface of an MNS sample containing 10.0% ATBN. 75

Figure 4.21 Backscattered image of distinct polyester-rich domains on the fracture surface of an MNS sample containing 10.5% ATBN. 77

Figure 4.22 Backscattered image of a small, pulled-out polyester-rich domain on the fracture surface of an MNS sample containing 10.5% ATBN. 77

Figure 4.23 Backscattered image of the hole left by a pulled-out polyester-rich domain on the fracture surface of an MNS sample containing 10.5% ATBN. 78

Figure 4.24 Backscattered image of a rubber-rich occlusion in a polyester-rich domain on the fracture surface of an MNS sample containing 10.5% ATBN. 78

Figure 4.25 Tanδ curves as a function of temperature for pure polyester specimens tested in tensile mode at a heating rate of 2°C/min and a frequency of 5 hz. 81

Figure 4.26 Tanδ curves as a function of temperature for the first and second heating of a pure polyester specimen. 83

Figure 4.27 Tanδ curves as a function of temperature for samples of pure polyester, and MNS with 0%, 7.5% or 9.5% ATBN. 84

Figure 4.28 Tanδ curves as a function of temperature for MNS specimens containing various rubber contents. 87

Figure 4.29 Variation of Tg for both primary and secondary transitions in MNS with increasing rubber content. 88

Figure 4.30 Variation of tanδ for both primary and secondary transitions in MNS with increasing rubber content. 89

Figure 4.31 Fracture toughness values for MNS compact tension specimens containing 7.5% ATBN, and samples with 7.5% ATBN and either 5% Nipol, 5% Paraloid or 2.5% fumed silica particles. 94

Figure 4.32	Load versus displacement curve for an MNS compact tension specimen containing 7.5% ATBN.	96
Figure 4.33	Load versus displacement curve for an MNS compact tension specimen containing 7.5% ATBN and 5% Nipol particles.	97
Figure 4.34	Load versus deflection curves for rubber-modified epoxy associated with different types of crack growth.	98
Figure 4.35	G_{Ic} values for MNS compact tension specimens containing 7.5% ATBN and samples containing 7.5% ATBN and either 5% Nipol or 5% Paraloid particles.	99
Figure 4.36	Load versus displacement curve for an MNS compact tension specimen containing 7.5% ATBN and 5% Paraloid particles.	101
Figure 4.37	Load versus displacement curve for an MNS compact tension specimen containing 7.5% ATBN and 2.5% fumed silica particles tested at a rate of 0.2 in/min.	102
Figure 4.38	Fracture surface of an MNS compact tension specimen containing 7.5% ATBN and 5% Nipol particles.	104
Figure 4.39	Backscattered image of the polished surface of an MNS specimen containing 7.5% ATBN and 5% Nipol particles.	104
Figure 4.40	Backscattered image of the phase separation in a rubber-rich domain on the polished surface of an MNS specimen containing 7.5% ATBN and 5% Nipol particles.	105
Figure 4.41	Fracture surface of an MNS compact tension specimen containing 7.5% ATBN and 5% Paraloid particles.	107
Figure 4.42	Paraloid particles within the circular domains on the fracture surface of an MNS compact tension specimen containing 7.5% ATBN and 5% Paraloid particles.	107
Figure 4.43	Backscattered image of the polished surface of an MNS specimen containing 7.5% ATBN and 5% Paraloid particles.	108
Figure 4.44	Backscattered image of a magnified rubber-rich domain containing Paraloid particles on the polished surface of	108

an MNS sample containing 7.5% ATBN and 5% Paraloid particles.

Figure 4.45 Fracture surface of an MNS compact tension specimen containing 7.5% ATBN and 2.5% fumed silica. 110

Figure 4.46 Backscattered image of the polished surface of an MNS sample containing 7.5% ATBN and 2.5% fumed silica. 110

Figure 4.47 Backscattered image of fumed silica particles in ATBN-rich domains on the polished surface of an MNS specimen containing 7.5% ATBN and 2.5% fumed silica. 111

Figure 4.48 Tanδ curves as a function of temperature for MNS specimens containing 7.5% ATBN and samples with 7.5% ATBN and either 5% Nipol, 5% Paraloid or 2.5% Cabosil fumed silica particles. 114

Figure 4.49 Fracture toughness values for MNS compact tension specimens taken from the top and middle of a casting containing 7.5% ATBN and 2.5% CTBN. 116

Figure 4.50 Load versus displacement curve for a compact tension specimen from the middle region of an MNS casting containing 7.5% ATBN and 2.5% CTBN. 117

Figure 4.51 G_{Ic} values for MNS compact tension specimens containing 7.5% ATBN and samples from the top portion of a sample containing 7.5% ATBN and 2.5% CTBN. 119

Figure 4.52 Load versus displacement curve for a compact tension specimen taken from the top region of an MNS casting containing 7.5% ATBN and 2.5% CTBN. 120

Figure 4.53 Fracture surface of a compact tension specimen taken from the middle region of an MNS casting containing 7.5% ATBN and 2.5% CTBN. 121

Figure 4.54 Two types of cavitation behavior on the fracture surface of a sample taken from the middle region of an MNS casting containing 7.5% ATBN and 2.5% CTBN. 121

Figure 4.55 Backscattered image of a cavitated domain on the polished surface of a sample taken from the middle 122

region of an MNS casting containing 7.5% ATBN and 2.5% CTBN.

Figure 4.56 Crater left by a pulled-out rubber domain on the fracture surface of a sample taken from the middle region of an MNS casting containing 7.5% ATBN and 2.5% CTBN. 122

Figure 4.57 Three different types of rubber-rich domains on the fracture surface of a sample taken from the middle region of an MNS sample containing 7.5% ATBN and 2.5% CTBN. 123

Figure 4.58 Two-phase rubber-rich domain on the fracture surface of a sample taken from the middle region of an MNS sample containing 7.5% ATBN and 2.5% CTBN. 123

Figure 4.59 Plastic flow on the fracture surface of a sample taken from the top region of an MNS casting containing 7.5% ATBN and 2.5% CTBN. 126

Figure 4.60 Backscattered image of discrete polyester-rich domains on the polished surface of a sample taken from the top region of an MNS casting containing 7.5% ATBN and 2.5% CTBN. 126

Figure 4.61 Transition zone between the top and middle regions of an MNS casting containing 7.5% ATBN and 2.5% CTBN. 128

Figure 4.62 Rubber-rich domains near the transition zone between the top and middle regions of an MNS casting containing 7.5% ATBN and 2.5% CTBN. 128

Figure 4.63 Morphology of the top portion of the middle region of a sample taken from an MNS casting containing 7.5% ATBN and 2.5% CTBN. 129

Figure 4.64 Transition zone between the middle and bottom regions of an MNS casting containing 7.5% ATBN and 2.5% CTBN. 129

Figure 4.65 Tanδ curves as a function of temperature for samples taken from the top and middle portions of an MNS casting containing 7.5% ATBN and 2.5% CTBN as determined by DMA. 131

Figure 4.66	Fracture toughness values for MNS compact tension samples containing 7.5% ATBN and 5% core-shell particles.	134
Figure 4.67	Load versus displacement curve for an MNS compact tension specimen containing 7.5% ATBN and 5% EXL 5136 particles.	136
Figure 4.68	Load versus displacement curve for an MNS compact tension specimen containing 7.5% ATBN and 5% EXL 2691 particles.	137
Figure 4.69	Load versus displacement curve for an MNS compact tension specimen containing 7.5% ATBN and 5% EXL 2330 particles.	138
Figure 4.70	G_{Ic} values for MNS compact tension samples containing 7.5% ATBN and 5% core-shell particles.	139
Figure 4.71	Fracture surface of an MNS compact tension specimen containing 7.5% ATBN and 5% EXL 5136 core-shell particles.	141
Figure 4.72	Clusters of EXL 5136 particles surrounding an ATBN-rich domain on the fracture surface of a compact tension specimen containing 7.5% ATBN and 5% EXL 5136 particles.	141
Figure 4.73	Backscattered image of the polished surface of an MNS specimen containing 7.5% ATBN and 5% EXL 5136 particles.	142
Figure 4.74	Backscattered image of well-adhered particles on the polished surface of an MNS specimen containing 7.5% ATBN and 5% EXL 5136 particles.	142
Figure 4.75	Backscattered image of trapped ATBN in a particle cluster on the polished surface of an MNS sample containing 7.5% ATBN and 5% EXL 5136 particles.	143
Figure 4.76	Fracture surface of an MNS compact tension specimen containing 7.5% ATBN and 5% EXL 2691 core-shell particles.	145
Figure 4.77	EXL 2691 particles within the smooth region of a rubber rich domain on the fracture surface of an MNS	145

compact tension specimen containing 7.5% ATBN and 5% EXL 2691 particles.

Figure 4.78 EXL 2691 particles in the rough region of a rubber-rich region of an MNS compact tension specimen containing 7.5% ATBN and 5% EXL 2691 particles. 146

Figure 4.79 Backscattered image of the polished surface of an MNS specimen containing 7.5% ATBN and 5% EXL 2691 core-shell particles. 146

Figure 4.80 Fracture surface of an MNS compact tension specimen containing 7.5% ATBN and 5% EXL 2330 particles. 148

Figure 4.81 EXL 2330 particles within an amorphous rubber-rich domain on the fracture surface of an MNS compact tension specimen containing 7.5% ATBN and 5% EXL 2330 particles. 148

Figure 4.82 Backscattered image of the polished surface of an MNS specimen containing 7.5% ATBN and 5% EXL 2330 particles. 149

Figure 4.83 Backscattered image of particle containing domains on the polished surface of an MNS specimen containing 7.5% ATBN and 5% EXL 2330 particles. 149

Figure 4.84 Tanδ curves as a function of temperature for MNS specimens containing 7.5% ATBN and 5% core-shell particles. 152

Figure 4.85 Fracture toughness values for MNS compact tension samples containing 7.5% ATBN and 5% solid glass spheres reacted with either epoxy or amino coupling agent or 5% hollow glass spheres reacted with Z6020 coupling agent. 154

Figure 4.86 Load versus displacement curve for an MNS compact tension specimen containing 7.5% ATBN and 5% solid glass spheres reacted with Z6020 coupling agent. 155

Figure 4.87 Load versus displacement curve for an MNS compact tension specimen containing 7.5% ATBN and 5% solid glass spheres reacted with Z6040 coupling agent. 156

Figure 4.88	Load versus displacement curve for an MNS compact tension specimen containing 7.5% ATBN and 5% hollow glass spheres reacted with Z6020 coupling agent.	157
Figure 4.89	Average G_{Ic} values for MNS compact tension samples containing 7.5% ATBN and 5% solid glass spheres reacted with Z6040 coupling agent.	158
Figure 4.90	Fracture surface of an MNS compact tension specimen containing 7.5% ATBN and 5% solid glass spheres reacted with Z6020 coupling agent.	160
Figure 4.91	Glass spheres in an ATBN-rich domain on the fracture surface of an MNS sample containing 7.5% ATBN and 5% solid glass spheres reacted with epoxy coupling agent.	160
Figure 4.92	Backscattered image of the polished surface of an MNS specimen containing 7.5% ATBN and 5% solid glass spheres reacted with an Z6020 coupling agent.	161
Figure 4.93	Fracture surface of an MNS compact tension specimen containing 7.5% ATBN and 5% solid glass spheres reacted with an Z6040 coupling agent.	163
Figure 4.94	Well-adhered glass spheres on the fracture surface of an MNS compact tension specimen containing 7.5% ATBN and 5% solid glass spheres reacted with an Z6040 coupling agent.	163
Figure 4.95	Backscattered image of the polished surface of an MNS specimen containing 7.5% ATBN and 5% solid glass spheres reacted with an Z6040 coupling agent.	164
Figure 4.96	Fracture surface of an MNS compact tension specimen containing 7.5% ATBN and 5% hollow glass spheres reacted with the Z6040 coupling agent.	164
Figure 4.97	Glass spheres in rubber-rich domains on the fracture surface of an MNS compact tension specimen containing 7.5% ATBN and 5% hollow glass sphere reacted with the Z6020 coupling agent.	165
Figure 4.98	Well-adhered glass spheres on the fracture surface of an MNS compact tension specimen containing 7.5% ATBN and 5% hollow glass spheres reacted with the Z6020 coupling agent.	165

Figure 4.99	Backscattered image of the polished surface of an MNS specimen containing 7.5% ATBN and 5% hollow glass spheres reacted with Z6020 coupling agent.	166
Figure 4.100	Tanδ curves as a function of temperature for MNS specimens containing 7.5% ATBN and either 5% solid glass beads reacted Z6020 coupling agent, solid glass beads reacted with Z6040 coupling agent, or hollow glass beads reacted with Z6020 coupling agent.	169
Figure 4.101	Fracture toughness values for MNS compact tension samples containing 9.5% ATBN and 5% PDMS particles.	171
Figure 4.102	Load versus displacement curve for an MNS compact tension specimen containing 9.5% ATBN and 5% amino PDMS particles.	172
Figure 4.103	Load versus displacement curve for an MNS compact tension specimen containing 9.5% ATBN and 5% epoxy PDMS particles.	173
Figure 4.104	Load versus displacement curve for an MNS compact tension specimen containing 9.5% ATBN and 5% silanol PDMS particles.	174
Figure 4.105	Average G_{Ic} values for MNS compact tension samples containing 9.5% ATBN and 5% PDMS particles.	175
Figure 4.106	Fracture surface of an MNS compact tension specimen containing 9.5% ATBN and 5% amino PDMS particles.	177
Figure 4.107	Evidence of pulled out particles in a rubber-rich domain on the fracture surface of an MNS compact tension specimen containing 9.5% ATBN and 5% amino PDMS particles.	177
Figure 4.108	Backscattered image of the polished surface of an MNS sample containing 9.5% ATBN and 5% amino PDMS particles.	178
Figure 4.109	Backscattered image of PDMS particles in a rubber-rich domain on the polished surface of an MNS sample containing 9.5% ATBN and 5% amino PDMS particles.	178

Figure 4.110	Backscattered image of poorly-adhered PDMS particles on the polished surface of an MNS sample containing 9.5% ATBN and 5% amino PDMS particles.	179
Figure 4.111	Fracture surface of an MNS compact tension specimen containing 9.5% ATBN and 5% Epoxy PDMS particles.	181
Figure 4.112	Poorly-adhered PDMS particles in a rubber-rich domain on the fracture surface of an MNS sample containing 9.5% ATBN and 5% Epoxy PDMS particles.	181
Figure 4.113	Backscattered image of the polished surface of an MNS specimen containing 9.5% ATBN and 5% Epoxy PDMS particles.	182
Figure 4.114	Fracture surface of an MNS compact tension specimen containing 9.5% ATBN and 5% Silanol PDMS particles.	184
Figure 4.115	Poorly-adhered PDMS particles in a rubber-rich domain on the fracture surface of an MNS sample containing 9.5% ATBN and 5% Silanol PDMS particles.	184
Figure 4.116	Backscattered image of the polished surface of an MNS sample containing 9.5% ATBN and 5% Silanol PDMS particles.	185
Figure 4.117	Backscattered image of an ATBN-rich domain on the polished surface of an MNS sample containing 9.5% ATBN and 5% Silanol PDMS particles.	185
Figure 4.118`	Tanδ curves as a function of temperature for MNS specimens containing 9.5% ATBN and 5% PDMS particles.	187
Figure 4.119	Fracture toughness values for MNS compact tension samples containing 7.5% ATBN and 5% solid glass spheres reacted with either Z6020 or Z6040 coupling agent or 5% hollow glass spheres reacted with epoxy coupling, or 12% ATBN with 5% hollow glass spheres reacted with Z6020 coupling agent.	190
Figure 4.120	Average G_{Ic} values for MNS compact tension samples containing 7.5% ATBN and 5% solid glass spheres reacted with either Z6020 or Z6040 coupling agent or 5% hollow glass spheres reacted with Z6020 coupling, or 12% ATBN with 5% hollow glass spheres	191

reacted with Z6020 coupling agent.

Figure 4.121 Fracture surface of an MNS compact tension specimen containing 12% ATBN and 5% hollow glass spheres reacted with Z6020 coupling agent. 194

Figure 4.122 Glass spheres within a highly deformed rubber-rich domain on the fracture surface of an MNS specimen containing 12% ATBN and 5% hollow glass spheres reacted with Z6020 coupling agent. 194

Figure 4.123 Extensive plastic flow emanating from glass spheres in a rubber-rich domain on the fracture surface of an MNS sample containing 12% ATBN and 5% hollow glass spheres reacted with an Z6020 coupling agent. 195

Figure 4.124 Small rubber-rich domains and well-adhered glass spheres on the fracture surface of an MNS compact tension specimen containing 12% ATBN and 5% hollow glass spheres reacted with an Z6020 coupling agent. 195

Figure 4.125 Well-adhered glass spheres on the fracture surface of an MNS compact tension specimen containing 12% ATBN and 5% hollow glass spheres reacted with an Z6020 coupling agent. 196

Figure 4.126 Well-adhered glass spheres on the fracture surface of an MNS compact tension specimen containing 12% ATBN and 5% hollow glass spheres reacted with an Z6020 coupling agent. 196

Figure 4.127 Cleaved glass spheres on the fracture surface of an MNS compact tension specimen containing 12% ATBN and 5% hollow glass spheres reacted with Z6020 coupling agent. 197

Figure A3.1 Geometry of compact tension specimen, per ASTM D 5045-93. 202

LIST OF TABLES

Table 3.1	Types of second phase particles used in this study.	55
Table 4.1	Mechanical properties of MNS with various rubber contents.	60
Table 4.2	Values of Tg and tan(d) for both primary and secondary transitions in MNS samples with various rubber contents.	86
Table 4.3	Fracture toughness values for MNS compact tension specimens with various rubber contents.	93
Table 4.4	Values of Tg and tan(d) for both primary and secondary transitions in MNS samples containing 7.5% ATBN and samples with 7.5% ATBN and either 5% Nipol, 5% Paraloid, or 2.5% Cabosil fumed silica particles.	113
Table 4.5	Values of Tg and tan(d) for both primary and secondary transitions in for MNS samples containing 7.5% ATBN and samples taken from the top and middle regions of the casting containing 7.5% ATBN and 2.5% CTBN.	130
Table 4.6	Values of Tg and tan(d) for both primary and secondary transitions in for MNS samples containing 7.5% ATBN and 5% core-shell particles.	151
Table 4.7	Values of Tg and tan(d) for both primary and secondary transitions in for MNS samples containing 7.5% ATBN and either 5% solid glass spheres reacted Z6020 coupling agent, solid glass spheres reacted with Z6040 coupling agent, or hollow glass spheres reacted with Z6020 coupling agent.	168
Table 4.8	Values of Tg and tan(d) for both primary and secondary transitions in for MNS samples containing 9.5% ATBN and 5% PDMS particles.	186
Table 4.9	Fracture toughness values for MNS compact tension specimens containing 7.5% ATBN or 12% ATBN with 5% glass spheres reacted with Z6020 coupling agent.	189

1.0 Introduction

Polymer based composites combine the properties of strong, stiff fibers with a tough, lightweight, inexpensive polymer matrix to yield a material with specific strengths and moduli that are generally superior to those of common metals.[1-2] Therefore, it is not surprising that the use of composites to replace such materials in structural applications is increasing. One of the new markets for mid-range performance polymer matrix composites is surface transportation. According to a study conducted by the Advanced Technologies Program (ATP) at the National Institute of Standards and Technology (NIST),[3] an additional several hundred kilograms of composite materials could be added to each automobile. The increased use of lightweight composites over metal alloys would significantly reduce the weight of the average automobile and greatly improve its fuel efficiency.

Many of the composite parts found in automobiles are derived from sheet molding compounds (SMC's). A typical SMC consists of a continuous sheet of fibers and fillers encapsulated in a thermosetting resin. The uncured sheet is cut to the desired shape and molded using heat to form a cured part. This approach has the advantage that parts with very complex shapes can be formed in one process. This allows for parts consolidation and, therefore, the elimination of costly secondary operations.[4]

Polyester resins are the most common thermosets used for SMC's. Polyesters generally possess low viscosity, high stiffness, high chemical resistance, are easy to process and are inexpensive.[5-6] However, they have a very highly crosslinked network structure, which makes them extremely brittle. Therefore, polyesters also have low toughness, poor impact properties and are prone to catastrophic failure.[6-8] In addition, they have a high coefficient of thermal expansion that leads to a large difference in the shrinkage rates between the resin and the fibers and fillers in the SMC during cooling of the part. As a result, microcracking in the resin and warpage of the part may occur.[8] Thus, a mechanism for toughening the polyester resin is necessary before the use of polyester based SMC's can be expanded to applications in which fracture and impact resistance is important.

1.1 General Deformation Mechanisms

1.1.1 Global Methods

In order for a material to exhibit high fracture toughness or impact properties, it must be able to absorb large amounts of energy without failing. The means by which a polymer absorbs this energy either can be through local or global deformations. Global deformation of a sample is known as shear yielding, and consists of large scale orientation of the polymer chains in response to an applied load (Figure 1.1a).[9-10] This orientation of the chains can absorb large amounts of energy. However, the shear yielding process requires a large amount of chain motion, both for the orientation of the chains and to compensate for the contraction in the directions perpendicular to the loading direction that results from the need to preserve constant volume. Thus, shear yielding only occurs in polymers that are ductile below their glass transition temperature.[9,11]

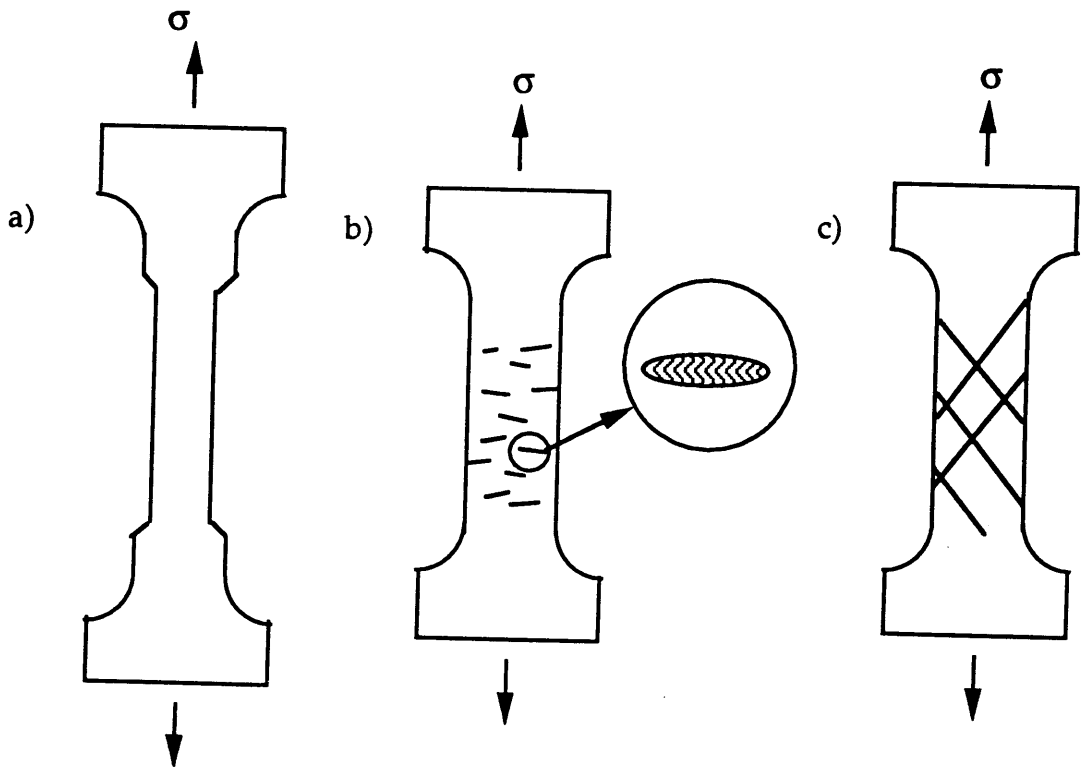

Figure 1.1- Schematic of a) shear yielding, b) crazing, and c) shear banding.

1.1.2 Local Methods

Most of the common structural polymers are required to have high strengths and moduli. Therefore, these materials are generally relatively brittle at temperatures below their glass transition temperature. Thus, they are not capable of undergoing global shear yielding at typical operating temperatures. In these cases, local deformation mechanisms become the main sources of energy dissipation. These local mechanisms only require the orientation of small regions of polymer chains at a time and, therefore, can occur in materials with lower ductility. The local methods of deformation can be divided into crazing and shear banding (Figure 1.1b and 1.1c). As will be discussed in the following sections, materials that are highly entangled tend to form shear bands, while longer entanglement lengths are needed for the large amount of orientation involved in craze formation.

1.1.2.1 Crazing

Crazes consist of cavitated regions of material that resemble small cracks. However, unlike true cracks, crazes are bridged by highly drawn and oriented polymer fibrils. These fibrils have diameters of around 20 nanometers, and separate voids of similar size (Figure 1.2). The void content in a craze is extremely high, and comprises about 40-50% of the craze volume.[13] Since the formation of each of these voids increases the amount of free surface area, crazes dissipate a large amount of energy by turning strain energy into surface free energy.[12]

Crazes tend to form under tensile stresses in materials with relatively long entanglement lengths and bulky side groups. While shear yielding can occur under compressive stresses, at least some tensile component is necessary for the formation of crazes. The bulky side groups and long entanglement lengths result in loose packing and higher mobility of the chains, which is necessary for the large amounts of reorganization necessary for craze formation. Polymers with bulky units in the backbone and short entanglement lengths tend to undergo shear yielding, which does not require quite as much mobility.[11]

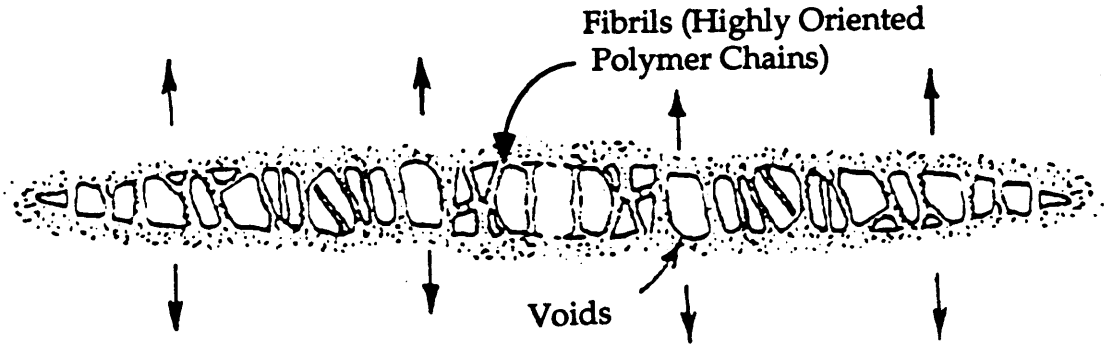

Figure 1.2- Schematic of the craze structure.

Crazing is a time-dependent viscoelastic process that is similar to creep in its stress and time dependence.[12] Crazes tend to form at surfaces, or in regions of high stress concentration (scratches, dust particles, frozen-in tensions, etc.), where localized plastic flow results in the creation of small voids by shear at the molecular scale.[9] When a polymer with chains of suitably large entanglement lengths is subjected to a tensile load, there will be an instantaneous elastic and then a more time-dependent anelastic deformation of the segments that results in accumulation of stored elastic energy. This energy either can be used by local shear displacement of the segments, or by orientational and conformational reorganization. It has been proposed that in the formation of a craze, the later process is the dominant mechanism. This results in an unstable reorientation of the chain segments in the direction of the applied stress while preserving the entanglements which already existed in this direction. The coiled chain segments cannot move individually due to the large number of entanglements, but a small reorganization of the segments can be achieved by breaking of secondary bonds between segments while keeping the entanglements intact.
The molecular segment coils will unwind a bit to partially assume their extended length, but at a certain point lateral constraints will prevent further

uncoiling. If the entanglement density of the matrix is sufficiently high, the stretching in one direction will result in contractive stresses in the other two directions due to volume conservation principles. These stresses can be alleviated either at a surface, at soft inclusions, or by contraction of the sample if the specimen is either very thin or sufficiently ductile. With continued straining, the local deformation caused by segment rotation and relief of lateral contraction becomes more difficult and the consequences will be one of the following: (1) if break up of the continuous matrix occurs to form voids in the deformed region, a craze results; (2) if, instead, localized plastic deformation occurs, a shear band is formed; (3) if a slow-down of the reorganization within the local region occurs, this could result in a general increase in the stress level, which could lead to stress relief through initiation of crazes or shear bands in other sites or to other forms of deformation, such as shear yielding.[9]

The chains in a forming craze always rotate to align themselves with the direction of maximum applied tensile load. Thus, the polymer fibrils in a craze are always aligned parallel to the direction of applied stress, and the craze itself is always oriented perpendicular to the direction of maximum applied tensile stress. Figure 1.3 shows a schematic of the craze initiation and growth process. A craze grows by nucleating another cavity beyond the existing craze tip where stresses are highest.[13] The new cavity then grows until it joins with the existing filimentary region in which the voids are interconnected. Thickening of the craze occurs by fibrillation of further matrix material,[9] as well as by drawing out and thinning down of the filaments. Growth of the craze in the lateral direction occurs more rapidly than in the thickness direction.[13] The thinning down of the stretched filaments increases the true strain in the filaments. As the stress in the filaments can be 40% to 140% higher than in the surrounding matrix material,[10] the highly stretched fibrils are prone to failure, which then results in the formation of a small crack.[14]

The failure mechanism of the fibrils depends on the properties of the network as well as the testing conditions. Under rapid loading, or with highly entangled networks, the fibrils will break by chain scission. At higher temperature, or with shorter chain lengths, the fibrils will fail by chain slip.[14]

Finally, under long-term testing or fatigue loading, the fibrils will fail by chain disentanglement.[9] As the stress in the specimen is fairly high at this point, small cracks can propagate quickly to lead to catastrophic failure. Thus, despite the extensive energy absorption that accompanies (1) craze formation, (2) craze deformation under stress, (3) creation of new surface area through void formation, and (4) breaking of chemical bonds, materials that craze are generally brittle unless the growth of the crazes can be restricted.[11, 13]

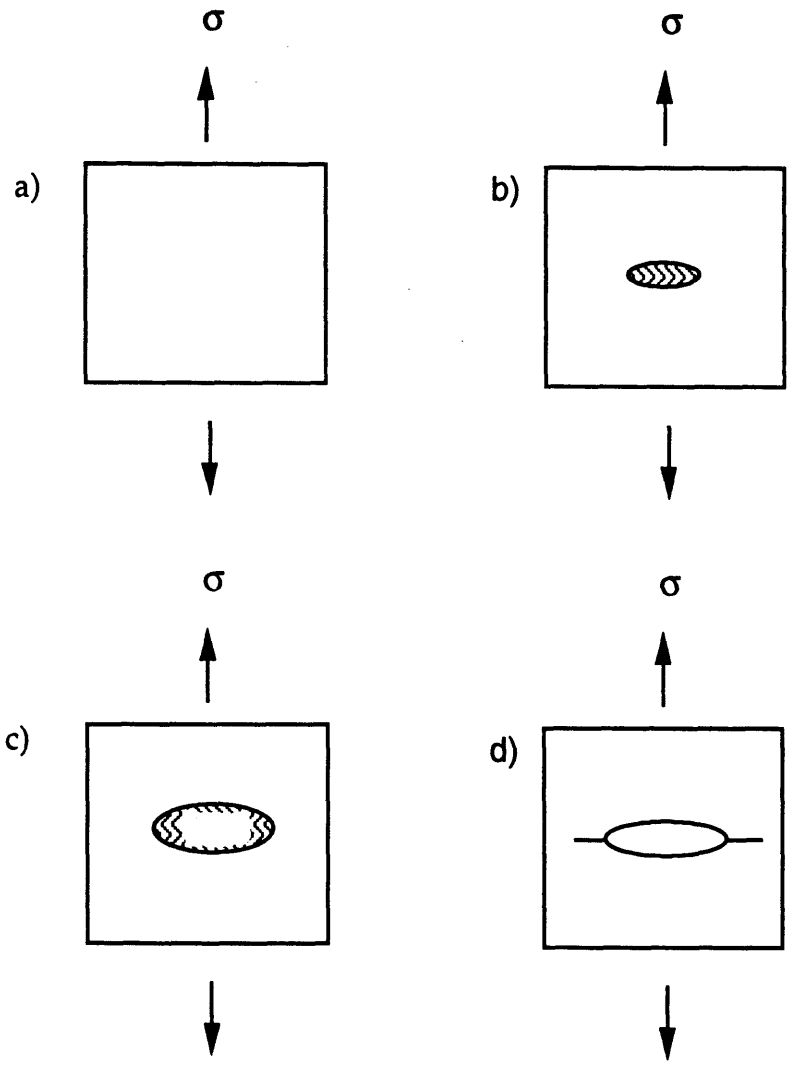

Figure 1.3- Response of craze-forming material to increased tensile loading a) under low loads, no crazes form, b) increase the tensile load and a craze forms, c) increase the load further and the craze grows longer and wider until some fibrils break or pull apart, d) increase the load even further and all fibrils pull apart to produce a crack which can propagate to lead to catastrophic failure.

1.1.2.2 Shear Banding

Shear bands are regions of drawn but unfibrillated material that grow in glassy polymers with short chain lengths between entanglements (Figure 1.1c). Because strain hardening occurs at relatively low strain levels in polymers with short entanglement lengths, the tendency for any locally deformed region to form a craze is suppressed.[14] It was found that the deformation mode of cross-linked polystyrene changed from crazing to shear banding when the number of cross-links or entanglement points was increased.[15] The extension ratio in shear bands is considerably lower than in crazes. The high extension ratios for crazes have been explained by the occurrence of chain scission or slippage during the creation of the void-filled networks. On the other hand, the formation of shear bands only involves local orientation of polymer chains, but with limited amounts of chain breakage and slippage. Since only orientation is involved in the formation of shear bands, these form much more quickly than do crazes.[14]
Another difference between crazes and shear bands is that shear bands tend to form at a 45° angle to the tensile stress, where shear stresses are the highest. In addition, as mentioned earlier, shear bands can form under either tensile or compressive stresses, while crazes can only form if there is a tensile component.

Shear bands also do not tend to fail in the same catastrophic manner as crazes, so materials which form shear bands are not as brittle as those that craze. However, since the formation of shear bands only requires orientation of chains, not as much energy is absorbed as for crazing, which requires void formation. Also, shear bands are a very localized phenomena. Thus, it is necessary to maximize the number of shear bands formed to achieve the greatest amount of energy dissipation.

1.2 Toughening Mechanisms

The most common approach for toughening both thermoplastics and thermosets is the addition of a small amount of elastomeric phase.[16] The technique of using rubber to toughen otherwise brittle polymers was first applied to thermoplastics back in 1948, when it was used to increase the

fracture toughness of polystyrene. Since then, it has been applied to most of the other common thermoplastics (including polypropylene (PP), polycarbonate (PC), and rigid poly (vinyl chloride)(PVC)), and even to some of the less highly crosslinked thermosetting resins (such as epoxies). Between 5% and 20% of the appropriate elastomer is added in the form of particles with diameters that generally range from 0.1 to 5 microns.[2] These particles can be either pre-formed or, as discussed below, can form in-situ via phase separation. In addition, thermoplastic particles, glass spheres, and voids have been used toughen these resins.[2]

1.2.1 In-Situ Particle Formation

In order to describe the formation of in-situ particles, the case of a reactive liquid rubber and epoxy resin system will be discussed. Liquid rubber additives completely dissolve in the uncured epoxy resin,[17] but the compatibility of the rubber with the epoxy decreases with cure until eventually phase separation occurs and rubber-rich domains precipitate in the epoxy matrix.[16-17] The phase separation process involves the two competing mechanisms of the kinetics of phase separation and the viscosity increases accompanying epoxy network formation.[18] As the epoxy network forms, the diffusivity of the rubber in the epoxy decreases, but the driving function for phase separation increases as the molecular weight increases with cure.[17] Eventually, gelation occurs, and the particle size of the phase separated domains becomes fixed.[12, 16-17] The result is a two-phase system of cross-linked rubber domains that are well bonded to the epoxy matrix.

As will be shown later, the size of the particles formed often plays a major role in their ability to toughen. The size of the second phase domains formed in-situ can be controlled by four main factors: (1) the rate of reaction of the epoxy network, (2) the molecular weight of the rubber, (3) the reactivity of the rubber with the epoxy matrix, and (4) the solubility of the liquid rubber in the epoxy resin.[16-17] The rate of reaction of the epoxy resin can be controlled by the cross-linking agent used,[16] or the temperature of cure. If a good cross-linking agent is used or the curing temperature is high, gelation will be fast. As diffusion is generally a slow process, the particles will not have time to adequately phase separate. Relatively small particles will result.

On the other hand, a poor cross-linking agent or low temperatures lead to long gelation times. The rubber will have adequate time to phase separate, and larger particles will result.[17]

Higher molecular weights tend to result in larger particles. In amine terminated polysulphone (PSF) modified epoxies, a critical molecular weight of PSF oligomers was required to produce a two-phase microstructure. If the molecular weight was too low, the compatibility of the epoxy with the PSF was too high, and the PSF remained dissolved in the matrix. The two-phase morphology became more pronounced, and the particle size increased with increasing molecular weight of the PSF.[19]

The reactivity of the elastomer with the epoxy also determines the particle size. Sankaran et al.[20] showed that a chemically reacted system of epoxy and hydroxyl-terminated poly(butadiene-co-acrylonitrile) (HTBN) rubber formed a greater number of particles than a system in which HTBN was physically reacted into the epoxy. The particles in the chemically reacted system were also smaller and had a narrower size distribution than their counterparts in the physically reacted system.

Finally, the initial compatibility of the modifier with the epoxy plays an important role in determining the ultimate particle size of the resulting domains. For example, increasing the acrylonitrile content of carboxyl terminated poly (butadiene-co-acrylonitrile) (CTBN) has universally been found to increase its compatibility with the epoxy resin and to result in smaller particles[12,21] as they will precipitate at a later stage of cure.[16-17] In fact, the compatibility of poly (butylene phthalate) (PBP) polyester with epoxy was so high that no second phase particles were observed.[22] Excessive compatibility and chemical interaction between modifier and epoxy may lead to a one phase morphology with the modifier remaining dissolved in the matrix. This is generally an unstable morphology.[23]

It is generally acknowledged that phase-separated rubber domains are not completely composed of pure rubber. Manzione et al.[24] found that in a CTBN modified epoxy system, the volume fraction of rubber domains on the surface of a transmission electron microscopy (TEM) specimen was greater

than the volume fraction of rubber added. In addition, the rubber domains were found to be larger than the length of the CTBN chains based on their molecular weights. Kunz et al.[25] found the same phenomenon. However, their nuclear magnetic resonance (NMR) work showed that the amount of mobile material present in the material did approximately match that added to the material in the form of the rubber. Both studies concluded that the dispersed rubber phase probably contains immobile epoxy segments. In fact, TEM performed by Manzione et al. showed the presence of epoxy inclusions.[24] Kinloch et al.[26] came to a slightly different conclusion as stained rubbery domains in CTBN modified epoxy did not show detectable regions of epoxy. They concluded that the epoxy served to chain extend the CTBN and this resulted in the large CTBN domains.

1.2.2 Role of Rubber Particles

The presence of a rubber particle in itself can provide toughening either through debonding, cavitation, or tearing mechanisms. If adhesion between the particles and matrix is poor, the particles will debond and a small amount of energy will be absorbed. On the other hand, if the particles are well-adhered, they can either cavitate or tear. Since a rubber particle has less cohesive strength than the matrix, it can fail by internal voiding (cavitation) (Figure 1.4). This cavitation process absorbs a fair amount of energy as it involves both deformation and creation of new free surface area. Finally, some rubber particles are capable of elongating to large critical extensions before failing by tearing (Figure 1.5).[27] Both the elongation and tearing processes absorb energy.[25, 27, 28-29] In addition, tearing is thought to relax the strain at a fixed crack opening. Continuous tearing of a particle was found to require a continuously increasing crack opening as the chains are found to rupture successively by the propagation of a tear which originates at a flaw.[27] However, even larger amounts of energy can be absorbed when second phase particles are combined with local deformation mechanisms such as crazes or shear bands.

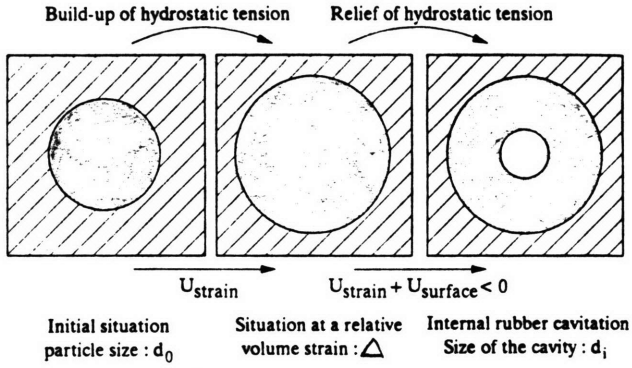

Figure 1.4- A schematic representation of the different steps in rubber cavitation.[58]

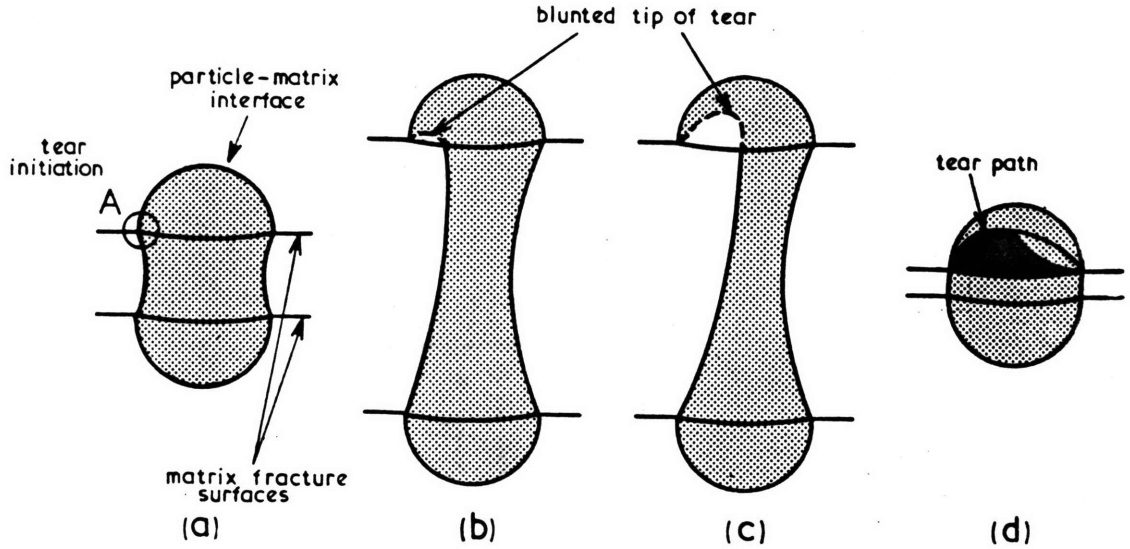

Figure 1.5- Schematic representation of tearing of a rubber particle. Closure of the matrix crack (d) shows the tearing path within the hemispherical region of the particle.[59]

1.2.2.1 In Materials that Craze

As mentioned earlier, although the formation and deformation of crazes absorb a considerable amount of energy, the breakdown of crazes into cracks can result in catastrophic failure. As a result, the material actually behaves in a brittle manner. If the crazes can be stopped before they grow too large, the energy absorption can be taken advantage of without the problems associated with crack formation. The growth of crazes can be stopped if: (1) the craze hits an obstacle which prevents further fibrillation of matrix material, (2) the craze has grown so large that the initiating crack is blunted and no longer critical, or (3) the craze interacts with other crazes.[9]

When rubber particles are added to a material which supports crazes, the benefits are three-fold. First, the particles act as stress concentrators which can initiate multiple craze formation at their interfaces under lower applied stresses than in the unmodified matrix. Then the particle can deform with the crazed matrix to stabilize it against fracture (Figure 1.6).[2,12] At this point the energy absorbing processes consists of craze formation, craze deformation, cavitation of the rubber particles and deformation of the particles. The third benefit of rubber particles is their ability to limit craze growth. A craze initiated at one rubber particle will grow until it hits another rubber particle (Figure 1.7a). Therefore, if the interparticle distance is small enough, craze growth will be stopped before any large cracks are formed. Thus, a large amount of energy is absorbed, but catastrophic failure does not occur.[11,13] Shear bands can also serve to stop growth of crazes.[13] Since shear bands form at an angle of 45° to the applied load, while crazes form perpendicular to tensile stress, shear bands can be oriented in different directions from crazes, so that the craze stops when it encounters the oriented material of a shear band (Figure 1.7b).

1.2.2.2 In Materials that Shear Band

The addition of rubber particles also increases the toughness of materials prone to shear band formation. Due to their low cohesive strength, rubber particles are not capable of sustaining as large of a load as the matrix material. Thus, when a system containing rubber particles is subjected to

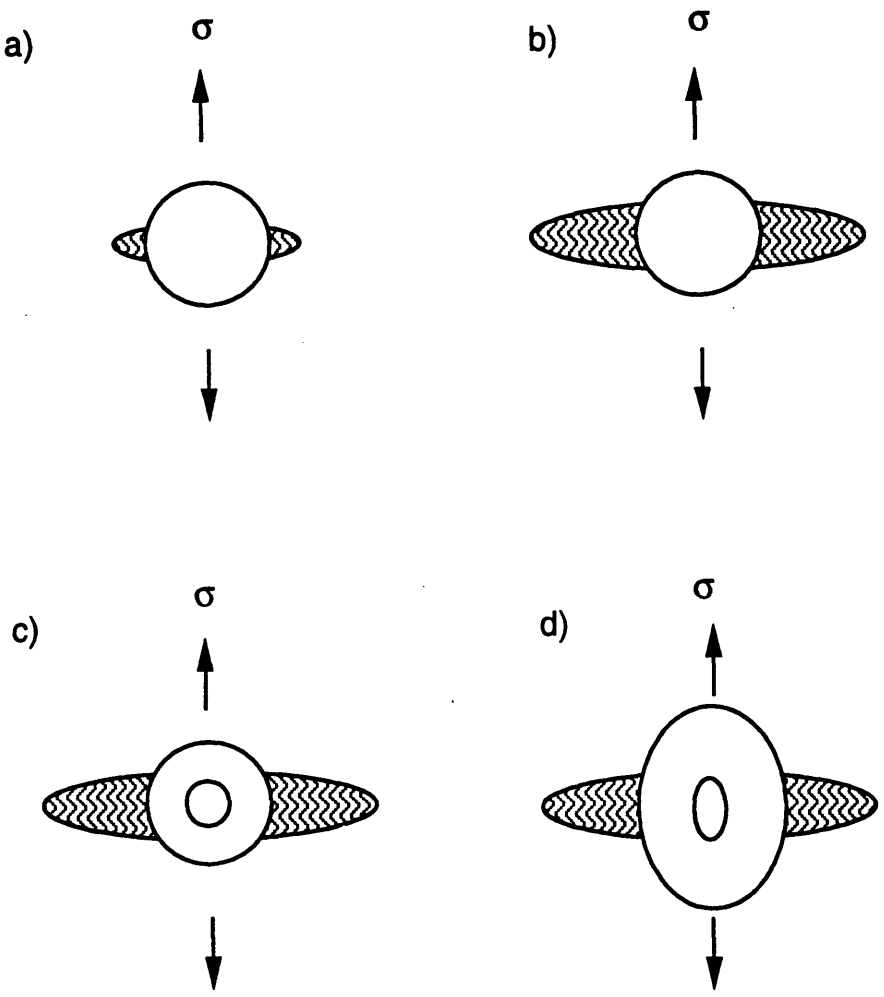

Figure 1.6- Schematic representation of the deformation mechanisms in a craze induced by a rubber particle. a) craze induced by stress concentration at the surface of the rubber particles, b) growth of craze due to increasing tensile load, c) cavitation of the rubber particle due to triaxial stresses ahead of the crack tip, and d) deformation of cavitated rubber particle with increasing load.

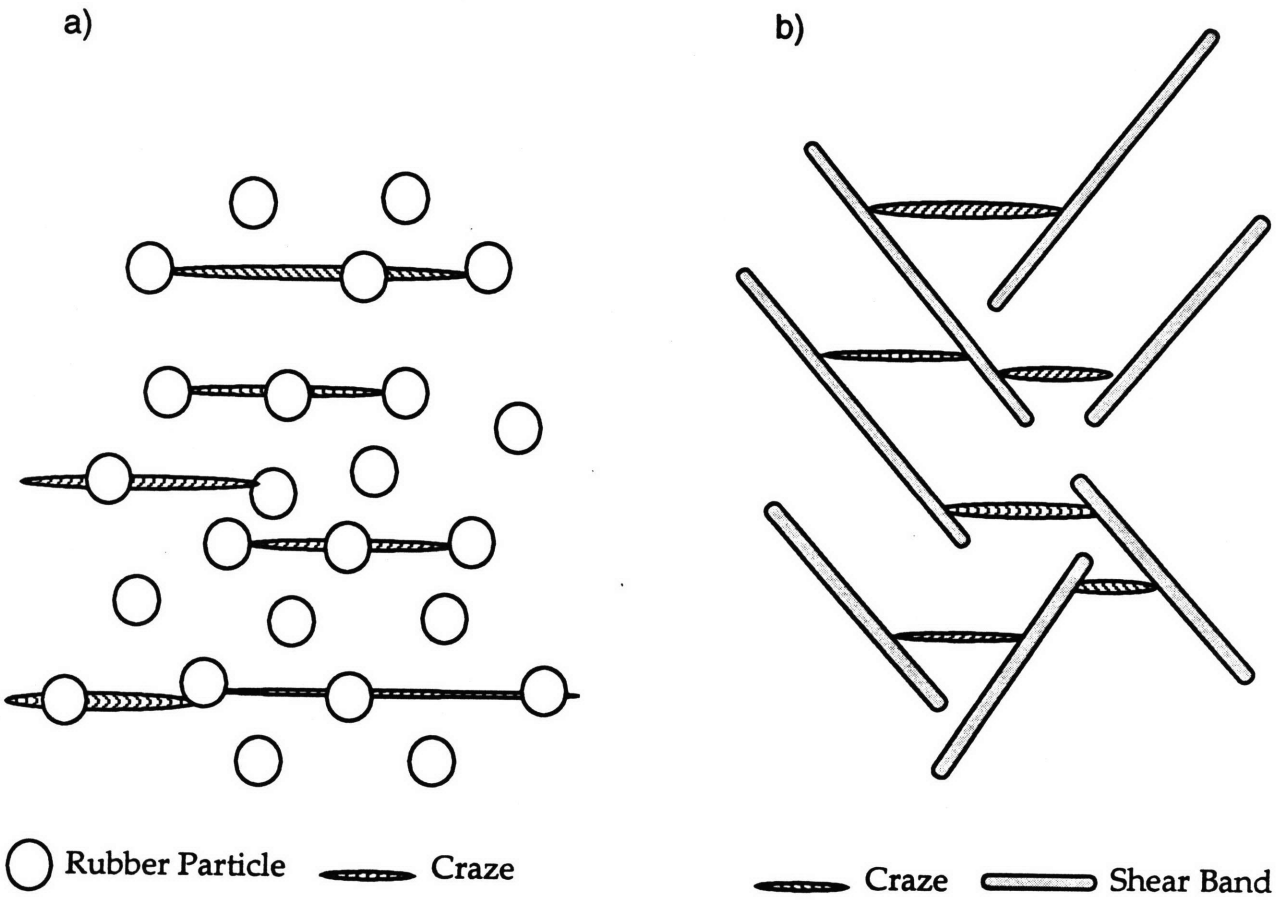

Figure 1.7- Schematic representation of the arrest of craze growth due to interactions with a) rubber particles or b) previously oriented material in shear bands.

stresses, the particles generally respond by either debonding from the matrix (if the adhesion is low), or cavitating in the center (if adhesion is high). The cavitation process absorbs energy in its own right, but cavitation is sometimes cited as a pre-requisite for the production of higher energy absorbing mechanisms, such as shear yielding.[30-32]

When a material containing rubber particles is subjected to stresses, cavitation or debonding (depending on the degree of adhesion) of the particle occurs as a result of triaxial stresses ahead of the crack tip.[26] Some studies suggest that the voids formed by cavitation or debonding of the particles may increase the stress concentration at the equator of these particles, and at the same time relieve the constraint in the matrix in the vicinity of the failed particle. Without the cavitation of the rubber particles, stress concentration occurs but additional shear deformation is not induced. The greater the number of cavitated particles, the higher the constraint relief effect will be. This results in localized regions of low yield stress, which promotes further shear yielding.[26, 33] The shear yielding is said to be localized as shear bands are thought to originate at one particle and terminate at another.[26] Some studies have suggested that the number of shear bands that form is dependent on the matrix properties of the resin, with highly cross-linked matrices suppressing the formation of the bands.[28]

As stated earlier, the distance between rubber particles is an important factor in stopping craze growth. One study claims that it also plays an important role in ductile materials that deform by cavitation of rubber particles and shear yielding. If the voids formed in the cavitated particles are close enough, the thin ligaments of remaining material between the particles will undergo local yielding. With enough void and ligament formation, the yielding process can span the entire deformation zone allowing the material to behave in a ductile manner.[38]

1.2.2.3 Modifier Properties

While the failure mechanisms generated by the presence of these modifiers are different for each resin, and there is considerable controversy

over the exact mechanism in many cases, the following factors are universally acknowledged to be related to the degree of toughening achieved:[12,16,21,35,34-37]

- Particle size / Particle size distribution
- Compatibility of the rubber modifiers with the resin (homogeneous versus heterogeneous morphology)
- Reactivity/ Adhesion between modifier and the matrix resin
- Molecular weight of the rubber
- Modifier content/ Volume fraction/ Interparticle distance
- The basic properties of the matrix (i.e., inherent ductility)

The above considerations will now be discussed for both thermoplastics and thermosets.

2.0 Previous Work

2.1 Toughening Mechanisms -Thermoplastics

The main source of energy absorption in brittle thermoplastics, such as polystyrene (PS) and styrene acrylonitrile copolymer (SAN), comes from the initiation, grown and breakdown of crazes that initiate ahead of the crack tip.[28,40] In more ductile thermoplastics, such as PC, PVC, and polyamides (PA), shear yielding is thought to be the main source of energy dissipation.[38]

However, the type of deformation phenomenon may also depend on the test rate. In fast fracture of rubber modified PC, cavitation of the rubber particles was observed, but little evidence of plastic flow was present.[30] It is possible that while the rubber particles cavitated, there was insufficient time for the formation of the shear bands.[39] Studies on PVC and methyl methacrylate-butadiene-styrene copolymer blends found that rubber cavitation was essential for initiating matrix shear yielding at high test rates, where constraint relief was needed to induce shear yielding under the short times of the test.[40] Therefore, the only energy absorption mechanism at high test speeds may be cavitation, while shear yielding is more likely at slower test speeds .[39]

2.1.1 Effect of Particle Size

Particle size and particle size distribution are the most commonly cited factors for determining the failure mechanism and degree of toughening in a thermoplastic material. Several studies showed that as the size of the rubber particle decreases, its resistance to cavitation increases.[35, 38, 40] Therefore, it has been proposed that a minimum particle diameter is required to produce cavitation.[38] The ability of the rubber particle to cavitate is an important parameter as cavitation is usually necessary to relieve the hydrostatic tension and induce shear yielding.[35] If a particle is too small to cavitate, matrix voiding occurs in the form of crazes.[38] This matrix voiding was found for PVC, poly (methyl methacrylate) (PMMA), and nylon-6. If the strain necessary to promote cavitation of the particles is higher than that required for the initiation of crazing in the matrix, crazing will occur and the material will fail in a brittle manner through craze breakdown.[35] One study believes that rubber particles toughen PMMA by changing the failure mechanism from crazing to shear yielding.[38]

In acrylic particle modified PMMA, particles with diameters of 200nm were found to produce optimal toughness and mechanical properties.[39] Particles smaller than 200nm were thought to be capable of creating large amounts of crazes and shear bands, but their small size prevented them from providing adequate reinforcement for control of crack propagation. Particles larger than 200nm were not be able to initiate as many crazes and shear bands. This size effect occurs because a greater number of small particles than large particles can be formed from a given volume fraction of rubber. Thus, fewer sites of initiation existed in the system containing the larger particles.[39]

Some studies report that the size distribution of particles also affects the level of toughness achieved. For instance, in a rubber toughened PMMA system with a twin population of rubber particles, it was found that the small particles (below 1 micron) initiated the damage (crazing in this case) while those above 1 micron arrested and controlled the propagation of the damage. The study found that a 50/50 population of these two particle types promoted the highest synergy effect and, therefore, produced the highest toughness.[41] This toughness increase was especially reflected in greatly increased resistance

to crack propagation in terms of the strain energy release rate (G_{Ic}). A bidistribution of particle sizes was also found to produce the highest degree of toughening in acrylonitrile-butadiene-styrene (ABS), methyl methacrylate-butadiene-styrene (MBS), and high impact polystyrene (HIPS), which deformed by crazes or a mixed mode of crazes and shear.[41]

2.1.2 Effect of Matrix Properties

The ability of a material to be toughened also appears to be related to the inherent ductility of the matrix material. A study found that SAN copolymers have more inherent ductility than basic PS and were, therefore, were more easily toughened. Similarly, styrene-maleic anhydride (SMA) copolymers, which have less inherent ductility than PS, were more difficult to toughen with impact modifiers. The study concluded that increasing the acrylonitrile content in the formulations increased the inherent ductility of the material and this was thought to contribute strongly to the overall toughness of the blend.[36]

2.2 Toughening Mechanisms - Thermosets

2.2.1 Epoxies

The discussion of the toughening of thermosets will begin with epoxies, as the majority of literature on toughening of thermosets is dedicated to these materials. While graced with high tensile strength and modulus, good chemical and corrosion resistance, good dimensional stability, good thermal resistance, and low creep, epoxies are also plagued with being inherently brittle.[19,26,48] There are several theories regarding the toughening mechanisms for epoxies. The two most often cited mechanisms of energy dissipation in rubber-modified epoxies are: (1) localized shear bands initiated by stress concentrations produced by the presence of rubber particles, and (2) particle void growth produced by either by cavitation of the particle or debonding at the particle/matrix interface.[26,28,33,42] However, the formation of shear bands is generally acknowledged to be the major source of energy dissipation.[26,28]

Some studies also report that crack bridging and tearing of rubber particles provide a major source of energy dissipation in epoxy resins. One study claims that the increase in toughness of a rubber modified epoxy material can be estimated from the volume fraction and bulk tear energy of the rubber.[27] However, another study of both rubber and microvoid toughened epoxies observed that both systems exhibited the same failure mechanisms. This would seem to contradict the assertion that crack bridging plays a large role in toughening of epoxy resins.[43]

There is some debate over the plausibility of crazing as a failure mechanism for toughened epoxies. Many studies have found no evidence of crazes in rubber modified epoxies.[12,26-27] They suggest that crazing cannot occur in pure or rubber modified epoxies because of the high crosslink density of the material and the short chain lengths in between crosslinks.[12, 19,26] One study that did observe crazes found that the craze length was significantly shorter than the interparticle distance, and concluded that rubber particles do not play a significant role as crack stoppers as suggested for rubber toughened crazible thermoplastics.[27] However, other studies have found crazing to be a major toughening mechanism for epoxy resins.[29] A study of CTBN-toughened epoxy found that the particles were elongated in the direction of the tensile stress field, and that there appeared to be a microvoid associated with each particle. However, they did not observe the type of fibrous crazes generally found for thermoplastics.[12] Another study found that cavities formed around the particles during crazing, and that cavity formation and deformation are highly energy absorbent processes.[16] This study, as well as most of the others that observed crazing, found that large particles promoted crazing while smaller particles promoted shear yielding.[12, 16] A more detailed discussion of the effects of particle size on failure mechanisms follows.

2.2.1.1 Effect of Modifier Type

2.2.1.1.1 In-Situ Particles

One of the most common methods of toughening epoxy resins is to incorporate small amounts of reactive liquid rubber. The most common type of liquid rubber used for epoxy resins is CTBN liquid rubber.[16] Liquid rubbers

are responsible for greatly increasing the fracture toughness of the resin,[26] but unfortunately, they generally do so at the expense of the stiffness and tensile strength.[25] The same problem was found for chemically reacted HTBN,[20, 44] and epoxy terminated acrylonitrile butadiene (ETBN).[18] Thus, other compositions of modifiers have been investigated.

Poly (ether sulphone) (PES), which is a ductile engineering thermoplastic with a high Tg and modulus, produced measurable increases in fracture toughness of epoxy with only a slight (10-15%) decrease in the modulus. This is less than the deterioration generally caused by rubber modification.[19] Poly (ethylene phthalate) polyester (PEP) was also investigated as a modifier for epoxies. The fracture toughness of epoxy was found to increase with increasing molecular weight of PEP. However, very high levels of PEP led to a decrease in tensile strength. An optimum molecular weight of 7,200 was found to increase the fracture toughness by 150% at no expense to the tensile strength.[22] PC was also shown to be an effective modifier. The addition of 20% PC was shown to increase the fracture toughness of epoxy by a factor of 7 without sacrificing the modulus of the resin. The effectiveness of PC as a modifier is thought to be a result of the fact that the PC segments are longer and more flexible than those of the epoxy, and can, therefore, deform more easily. Thus, the addition of PC is believed to increase capability for localized plastic deformation of the epoxy network. This is supported by the decrease in yield stress with increasing PC content in the system.[45]

2.2.1.1.2 Pre-Formed Particles

Most of the modifiers mentioned above are added as liquids which phase separate to form second phase particles in-situ. Core-shell particles are another form of modifier that have successfully been used to toughen epoxies. These particles keep their integrity during the curing of the epoxy and, therefore, are not dependent on the phase separation process for their identity.[18] One final type of modifier frequently used is hollow microspheres or voids. While some studies have found that voids did not significantly increase the fracture toughness of epoxies,[27] other studies have had more

success. Hollow plastic microspheres, as well as voids created by debonding of unreactive rubber particles, have been reported to produce similar increases in fracture toughness to CTBN toughened systems. In addition, the void modified epoxies have been found to possess mechanical properties that are comparable to or even better than those of their rubber modified counterparts. In addition, the void modified systems have lower densities, and should show better low temperature properties than rubber toughened materials.[43]

2.2.1.2 Effect of Phase Separation

2.2.1.2.1 Fracture Toughness

There is some debate over whether phase separation of the modifying phase is a necessary condition for achieving increased fracture toughness of the epoxy resin. In PSF modified materials, homogeneous blends were found to fail by ductile tearing of the matrix, while heterogeneous blends showed evidence of shear bands in between the PSF particles.[37] In epoxy urethane interpenetrating polymer networks (IPN's), it was found that the homogeneous morphology had the effect of flexibilizing the matrix to result in higher impact properties, but the heterogeneous two-phase morphology increased the fracture toughness.[29, 46] Thus, the toughening effect of a given morphology may be dictated by the testing rate.

At low strain rates, a process of rubber cavitation and local plastic deformation was found to occur. However, at high strain rates, rubber domains did not have time to respond and deform and, therefore, did not act any differently from the matrix. While dispersed rubber particles did increase the impact toughness somewhat, homogeneous flexibilization of the epoxy matrix is believed to be the most effective toughening mechanism at high strain rates.[29,46] However, Min et al. found that even at low strain-rates the degree of toughening greatly improved with increasing amount of phase inverted co-continuous structure capable of ductile tearing.[37]

This leads to the theory that a combination of dissolved and phase separated rubber is necessary to achieve optimum properties. Manzione et

al.[24] suggest that to improve the toughness of epoxies under both impact and low strain rate conditions, it is necessary to combine dissolved and phase-separated rubber. In a study of polyester modified epoxy, microphase separation was found to be important for inducing delocalized plastic deformation of the material around the polyester domain. However, this study also found that a material in which the polyester did not phase separate out of the epoxy also showed an increase in the fracture toughness. The study concluded that toughening of the epoxy matrix itself is also an important condition for improving the toughness of the material.[22]

2.2.1.2.2 Mechanical Properties

Despite the debate over the necessity of a homogeneous or heterogeneous morphology for imparting optimum toughness properties, rubber has been successfully employed as a means to increase the fracture toughness of epoxies by orders of magnitude.[19, 31, 33] However, one significant drawback is that the addition of the elastomeric phase can have a detrimental effect on some of the mechanical properties of the material, such as tensile strength and modulus. The debate arises again over whether a heterogeneous or homogeneous morphology results in the greatest deterioration of mechanical properties. However, as will be seen, the homogeneous morphology is generally found to have the least adverse effect.

A study of polyester and epoxy showed that the higher molecular weight polyesters led to the greatest decrease in mechanical properties of the epoxy resin, since the higher molecular weight polyesters tended to form discrete domains while those of lower molecular weight remained more dissolved in the matrix.[22] One study of CTBN modified epoxy also found that the phase separated morphology had more of an adverse effect on the tensile modulus than did the dissolved rubber. This study found that incorporation of up to 15% dissolved CTBN produced no noticeable decrease in the modulus of the epoxy.[24] In a study of phase separated epoxy-terminated poly(n-butyl acrylate) (ETPnBA) modified epoxy containing at least 5% rubber, the tensile strength and Young's modulus decreased measurably with increasing elastomer content. This study found that it was impossible to increase the fracture toughness without reducing the other mechanical

properties by using a higher functionality and higher molecular weight rubber. This allowed significant improvement in toughness at lower rubber contents and, therefore, less deterioration of the mechanical properties.[23]

2.2.1.3 Effect of Particle Size

The size of the second phase particles plays an important role in determining the type of deformation mechanism that occurs, and hence, the amount of toughening achieved. Small particles (< 0.5 microns) tend to initiate shear yielding, while crazes and microvoids were prevalent in compositions with larger rubber particles (1-5 microns).[12, 16] Many studies have asserted that a combination of crazing and shear yielding produces the greatest toughening effect. This is due to the dual energy absorbing mechanisms provided by crazing and shear banding, as well as the ability of the shear bands to stop the growth of the crazes before they reach a critical size.[12,16] Therefore, a bidistribution of particle sizes is recommended for producing optimum fracture toughness properties.[12]

In a monodisperse system, smaller particles are generally found to toughen more effectively than their larger counterparts. [7,16,20,24,33,43-44] This is probably due to the fact that while the cavities formed by crazes in systems with large particles absorb a large amount of energy (evidenced in large increase in fracture surface work), these cavities coalesce to form cracks that lead the material to fail at relatively low average strains.[16] In addition, crazes that are thought to be produced by stress concentrations at large particles are not believed to be possible in highly cross-linked materials such as epoxies. Therefore, shear-yield inducing small particles are thought to be the most effective tougheners in these systems.[19] Hedrick et al. found that the optimum particle size for an epoxy containing thermoplastic composite particles was 1-1.5 microns. These particles were thought to induce local plastic deformation in the matrix. The study also found that increasing the number of particles caused the stress fields created by each particle to interact, and this improved the fracture toughness.[19] A study of CTBN modified epoxy found that particle sizes of 1-2 microns increased the toughness by a factor of at least one order of magnitude.[16] Particles larger or smaller than this size range were found to be less effective in toughening.

The size of a particle has also been connected to its ability to tear. One study of a chemically reacted HTBN and epoxy system found that particles with diameters greater than 3 microns showed evidence of tearing, while smaller particles showed either debonding or cavitation.[20] On the other hand, a study of crack bridging in CTBN modified epoxy found that the larger particles failed before the smaller particles.[27] In a physically blended HTBN/toluene diisocyanate (TDI) epoxy system, no evidence of particle tearing was present even in the large particles. However, this was thought to be due to the poor degree of adhesion.[44]

2.2.1.4 Effect of Particle Adhesion

It is generally agreed that a high degree of interfacial bonding at the rubber epoxy interface is necessary for effective toughening of modified epoxies. Carboxyl, hydroxyl, epoxy, mercaptan and amine have been cited as groups that react well with epoxy and are, therefore, the end groups most commonly used for liquid rubber modifiers.[23] One reason for the common use of CTBN to toughen epoxies is its ability to quickly react with epoxy resin.[47] Rubbers with terminal end groups were found to be more effective than those with pendent groups for toughening epoxy resins. In addition, it was found that liquid rubbers with approximately two reactive end groups produced the maximum fracture energy in liquid rubber modified epoxies.[12]

When physically blended polyether sulphone was used to toughen epoxies, the tough, ductile PES phase separated due the higher solubility parameter of the PES compared with the epoxy. However, the failure to significantly improve the fracture toughness of the epoxy was attributed to the poor interfacial adhesion of the PES with the epoxy.[19] Similarly, attempts to modify brittle materials with hard particles (such as glass) were believed to be unsuccessful due to poor adhesion of the glass particles.[19]

Studies performed by Sankaran et al.[20,44] present a classic case of the need for good adhesion to produce maximum enhancement of toughness properties. In their HTBN/TDI modified epoxy system, the degree of interfacial bonding was superior in chemically reacted samples than in

physically reacted ones. The result was significantly higher toughness properties for the chemically reacted system. In addition, it was found that the physically reacted system led to a significant decrease in the ultimate tensile strength (UTS) of the material. The drop in UTS for the chemically reacted system was much less severe than for the physically reacted system. As mentioned above, the poor adhesive properties of the physically blended HTBN/ TDI epoxy system prevented rubber particles from bridging the crack. Instead, these particles failed either by debonding or cavitation. The superior toughening ability of chemically reacted HTBN over the physically reacted HTBN may also be connected to the fact that the chemically reacted HTBN resulted in a large number of small particles due to its higher compatibility with the epoxy, while the physically reacted system resulted in a lower number of larger particles. It has already been acknowledged that smaller particles are generally more effective toughening agents than their larger counterparts. Finally, the superior toughening produced by the chemically reacted particles can also be attributed to the strong covalent bonds at the interphase, which have to be ruptured during failure.[44]

2.2.1.5 Effect of Matrix Properties

As has been discussed in detail, rubber particles are very effective toughening agents for epoxy resins. One of their main functions is to act as stress concentrators to induce energy absorbing mechanisms, such as localized shear yielding in the matrix. However, this mechanism relies on the matrix's ability to plastically deform. As the cross-link density of the matrix increases, it's ability to plastically deform decreases. Thus, rubber toughing becomes less effective as the cross-link density of the matrix increases.[48]

2.2.2 Polyesters

As mentioned above, the toughening ability of rubber modifiers decreases as the cross-link density of the matrix increases. The cross-link density of polyesters is generally significantly higher than that of epoxies. Thus, much fewer successful approaches to the toughening of polyester resins can be found in the literature. Some studies suggest that the failure mechanism for polyesters is very similar to that for epoxies. Rubber particles

or domains act as stress concentrators and cavitate to provide constraint relief in the surrounding matrix. This, in turn, initiates local plastic flow in the regions surrounding the particles. However, one study acknowledged that the fracture surfaces of rubber modified polyesters showed very little evidence of plastic deformation. The half rubber particles were found to have retracted due to the relief of the triaxial stress, but the surrounding polyester matrix was very flat and exhibited very little evidence of plastic deformation.[31]

Other studies suggest that the cross-link density of polyesters is too high to enable shear band formation. Instead, Kim et al.[28] found the respective energy dissipation mechanisms in hydroxyl terminated polyurethane rubber (HTPU) and isocyanate terminated polyurethane rubber (ITPU) modified unsaturated polyester resin (UPE) systems to be debonding and cavitation. In addition, they found that large rubber particles acted as crack bridges. However, this study found cavitation to be a more effective toughening mechanism for UPE than debonding or crack bridging. Thus, it was concluded that the properties of the rubber should be controlled to achieve proper cavitation resistance.

2.2.2.1 Effect of Modifier Type

Like epoxies, the main type of modifier used to toughen polyesters is reactive liquid rubbers. However, while the addition of amine terminated acrylonitrile butadiene copolymer (ATBN) liquid rubber to polyester showed a slight increase in strain to failure and fracture toughness at low rubber contents, this trend did not continue with higher rubber contents.[6] Another study found improvements in a reactive liquid rubber modified polyester at slow testing speeds, but the impact properties were found to improve only slightly.[7] The poor toughening results of liquid rubber modified polyesters are probably related to the fact that polyester is incompatible with most of the rubbers used, including those with hydroxyl, carboxyl, amine and vinyl terminal groups.[6,49] The toughness of an ATBN modified polyester system was found to be comparable to that of a CTBN system, and an HTBN modified system to that of a vinyl terminated acrylonitrile butadiene (VTBN) modified system. This was believed to be due to the fact that the pairs had similar particle sizes and distributions. The toughness of the later two

systems were found to be higher than those of the former two systems.[49] When the hydroxyl groups of hydroxyl terminated polybutadiene (HTPB) were changed to more reactive isocyanate groups, the values of the fracture toughness (K_{Ic}) and strain energy release rate (G_{Ic}) were increased from 2 to 5 times that of the unmodified polyester resin.[31] Also, when carboxyl or hydroxyl terminated liquid rubbers of sufficient molecular weight were chemically reacted with the polyester, higher toughness resulted.[49]

2.2.2.2 Effect of Phase Separation

The most effective toughening of thermosetting resins is thought to come about when the reactivity of the liquid rubber with the matrix resin is high. This results in small particles, a narrow distribution of particle sizes, and good adhesion between particle and matrix.[31] However, as stated above, the compatibility of the polyester resin with typical reactive liquid rubbers is very poor. This incompatibility leads to phase separation of the rubber into discrete domains (as described above for epoxies) with the diameters being dependent mainly on initial compatibility, reactivity, and molecular weight of the rubber.[31, 36] In CTBN modified UPE, macrophase separation was found to occur, and the resulting castings were opaque.[6] Another study found that in all cases of adding VTBN or other liquid rubbers with non-reactive groups, a broad distribution of rubber sizes and relatively large domains resulted. This study found that effective toughening could be achieved by adding a liquid rubber with highly reactive functional groups that was compatible with the UPE in the initial stages of cure. Therefore, when a triblock copolymer ETBN was used in place of CTBN, the interfacial tension was drastically reduced and the compatibility improved.[7-8]

Similar to the results found for epoxies above, studies of polyurethane (PU) elastomer modified UPE's showed that the impact strength was improved by the flexibilizing effect of a homogeneous morphology, while fracture energy was improved by the presence of second phase particles. The second phase particles were believed to toughen via the re-initiating crack mechanism. The crack is stopped by the second-phase particles, and energy is absorbed by deformation or tearing of the particles and the re-initiation of the crack in the matrix. The study also found that the mechanical properties of

the UPE were improved with incorporation of PU elastomer. This was probably due to increases in molecular weight and cross-linking brought about by either copolymerization of the UPE and PU, or by the interpenetrating structure in the graft case.[5] On the other hand, homogeneous systems of UPE toughened physically with thermoplastics, such as polyethylene glycol, showed good compatibility and good performance.[49] Another method investigated was the direct incorporation of rubber into the polymer main chains. This resulted in a microheterogeneous morphology with "superior" properties.[51] Finally, Ullett and Chartoff[50] showed that optimum properties could be achieved if enough rubber remained dissolved in the matrix of the two-phase morphology.

As was found to be the case with liquid rubber toughened epoxies, the rubber domains in the UPE are not believed to be composed of pure rubber. Since the volume fraction of rubber particles was found to exceed the amount of PU rubber incorporated into the system, it was speculated that UPE was incorporated into the rubber particles.[28]

2.2.2.3 Effect of Particle Size

In general, smaller particles were found to produce better toughening effects in UPE than large ones. One explanation for this size effect is that small particles have large interfacial areas, which enables them to dissipate a substantial amount of energy through debonding.[28] In contrast, large particles are thought to provide weak regions that the crack can pass through more easily. Stresses are believed to concentrate in these areas and lead to catastrophic failure.[7]

As mentioned earlier, CTBN has poor miscibility with UPE. As a result, large CTBN-rich domains with diameters greater than 10 microns and a large size distribution were formed in CTBN modified polyester. The improvement in fracture properties of this system was not significant, and this was thought to be the result of the large particle sizes.[7] When 10% of the CTBN was replaced by an epoxy-CTBN-epoxy triblock, smaller domains of 5-12 microns and a smaller dispersion of particle sizes were formed due to the greater compatibility between epoxy and polyester. As a result, the impact

behavior was improved. However, when large amounts of epoxy triblock were added, the particle size increased again, and the impact properties dropped.[7] It was believed that the optimum particle size for toughening is 0.5-5 microns as was found for epoxies.[7] When isocyanate-terminated polyurethane (ITPU) replaces hydroxyl-terminated polyurethane (HTPU) in a polyester system, the particle size of the rubber phase is reduced as a result of the better reactivity of the isocyanate groups with UPE.[28, 51] The addition of ITPU was found to improve the fracture toughness by 1.9 times that of the unmodified UPE.[51]

Another factor affecting the particle size is the molecular weight of the rubber. As the molecular weight of liquid polyurethane rubber decreased, the resulting particle size is also decreased.[51] However, if the molecular weight of HTPU was reduced too low, it dissolved in the UPE matrix to form a homogeneous phase.[28] A triblock of polyester and isocyanate-terminated polybutadiene (PE-ITPB-PE) was also found to decrease the particle size compared to HTPB. The small particles were found to have small voids in the center that are consistent with cavitation. In addition, the surrounding matrix showed evidence of shear yielding. The superior toughening abilities of the ITPB triblock were attributed to the smaller particles formed on phase separation as well as the chemical bonding with the UPE matrix, which increased the particle adhesion so that cavitation could take place.[31] As mentioned above, UPE's physically blended with thermoplastics, such as polyethylene glycol, polyepichlorin and polycaprolactone, showed good compatibility with the UPE and formed very small domains. The toughening ability of these systems was found to be superior to rubber modified systems, and the mechanical properties were also found to be good. The only drawback was found to be their high propensity for water absorption.[49]

2.2.2.4 Effect of Particle Adhesion

When there is poor adhesion between the rubber and the UPE, the main energy absorbing mechanism was found to be debonding. However, cavitation was found to be a more effective method of energy dissipation than debonding or particle bridging. Thus, good chemical bonding is an important factor in promoting high fracture properties. Good adhesion was necessary to

promote cavitation of PU rubber particles. The isocyanate end group of the ITPU can react with the hydroxyl or carboxylic acid group in the UPE to create good adhesion. This resulted in an increase in fracture toughness of 1.5 to 1.9 times that of the unmodified resin.[28] In general isocyanate terminated liquid rubbers are more effective modifiers than their hydroxy terminated counterparts due to this ability of the isocyanate groups to react with the polyester.[34]

Further evidence that good adhesion of the rubber particles is necessary for the improvement of toughness properties is provided by the fact that the UPE and rubber block copolymers were found to have superior mechanical properties to physically blended rubber toughened systems.[49] While the improvement of the mechanical properties could not be explained by the formation of the chemical bonds alone, good adhesion between particles and matrix also appears to be important for the mechanical properties. While the fracture toughness seems to increase with molecular weight of the ITPU rubber added, the flexural modulus was found to decrease with increasing molecular weight. However, the decrease in modulus of these ITPU modified UPE's is not significant because of the good adhesion between particles and matrix.

2.3 IPN's

2.3.1 General Toughening Mechanisms

Another approach to toughening polymers is to create interpenetrating network structures (IPN's). IPN's are traditionally defined as a blend of two or more crosslinked polymers in which the chains of one are entangled in those of the other with minimal covalent bonding between the two systems. The entanglements of the chains prevent the networks from phase separating completely as a result of the (positive or close to zero) Gibbs Free Energy of Mixing associated with most polymer systems.[6] IPN's can be formed sequentially or simultaneously. In a sequential IPN, the network formed first determines the properties of the second network. In the case of a simultaneous IPN, the network formed first will be the most complete and will have the greatest influence on the mechanical properties.[6] When IPN's

are created in which one polymer is glassy and the other is rubbery, a series of tough plastics and reinforced elastomers results.[52]

The first instance of IPN use for improving impact resistance was a system composed of natural rubber, sulfur and phenolic resin.[6] While the increased fracture toughness of liquid rubber modified epoxies was generally accompanied by a decrease in mechanical properties, PU-epoxy IPN's were found to have higher maximum tensile strengths than either component at intermediate concentrations. This phenomenon was thought to be the result of the interpenetration.[53] The same effect was found for UPE and PU IPN's in which a small amount of one or the other component was incorporated. Only small amounts of the second component were used in order to ensure complete network formation of the first network without any buildup of stresses.[54] This PU and UPE system was found to be a pure IPN with no interaction between the two networks. On the other hand, another study of a UPE and PU IPN found the properties of the IPN to be worse than those of the control UPE. They speculated that this was due to the different reaction rates of the UPE and PU (by free radical and condensation respectively), and this resulted in an imperfect network structure.[5]

Unsaturated polyesters are highly reactive as they polymerize via free radical polymerization and contain reactive carboxyl and hydroxyl end groups. Thus, it would be difficult to find another monomer system that would not react with the polyester so that a true IPN could form.[34] One study formed a one-phase IPN of UPE and PU by grafting. Grafting was found to be essential to improving the impact and fracture toughness properties of UPE's as it prevented phase separation of the components. The flexibility of the system was found to increase with PU content, thus improving the impact properties.[5]

2.4 MNS

2.4.1 Structure

Another successful method of toughening brittle polyester networks has been to combine them with a flexible network of rubber toughened epoxy.

The epoxy network is chosen as the flexibilized one due to its higher propensity to being toughened.[6] Liquid ATBN rubber and a diglycidyl ether of bisphenol-A (DGEBA) epoxy were physically blended with an unsaturated polyester resin in styrene monomer. However, it was soon found that a true IPN had not formed. While the ATBN preferentially reacts with the epoxy, the amine group is also capable of reacting with the double bond in the polyester. In addition, the epoxy and the polyester were found to react through hydrogen bonding of the carbonyl groups of the polyester and epoxy groups. The reaction sequence is believed to proceed as follows: first the ATBN, epoxy and polyester start to react, and then when the temperature of the resin becomes high enough, free radical polymerization of the polyester is initiated and this dominates.[6] Because a true IPN has not been formed, the system was termed a "Molecular Network System" (MNS) rather than an IPN. A schematic of the reaction structure is shown in Figure 2.1.

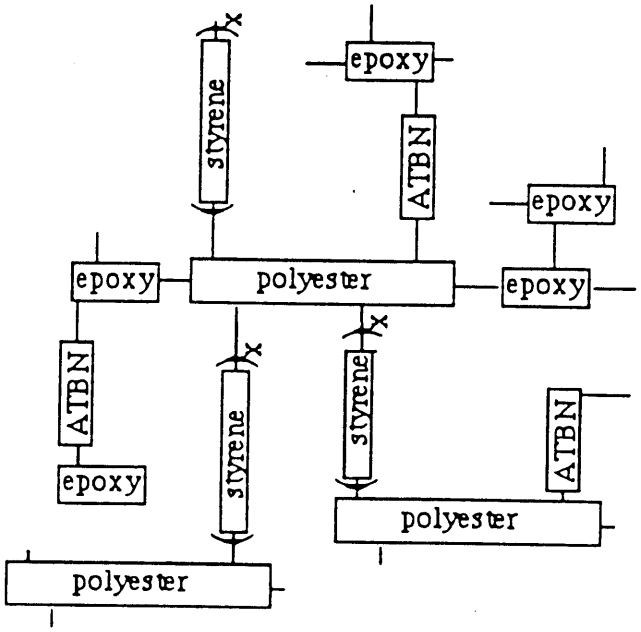

Figure 2.1- Schematic of reactions possible in crosslinked MNS. The value of x is normally between 1 and 5. Some polystyrene is also probably formed but is not shown here.[60]

2.4.2 Morphology

At low ATBN contents (below around 8%), the morphology of the MNS system consists of discrete rubber-rich domains in a polyester-rich

matrix. The volume fraction of rubber-rich domains on the surface was found to be considerably larger than the volume fraction of rubber added. Therefore, it is probable that the rubber domains contain a considerable amount of epoxy, polyester and styrene monomer. In fact, TEM showed that within the domains that are on the order of a few tens of microns, the actual rubber domains were a few hundred angstroms in size.[6] At higher rubber contents, a phase inversion occurs, and the continuous phase becomes a flexibilized rubber-rich matrix with brittle polyester-rich inclusions.

2.4.3 Mechanical Properties

At the highest rubber contents (22.5% ATBN), a 10 fold increase in G_{Ic} occurs due to the flexibilization of the matrix, which increases its ability to undergo plastic flow and blunt the crack tip. However, this increase in fracture toughness occurs at the expense of the mechanical properties. This is to be expected since the modulus of the rubber is much lower than that of the polyester. At low rubber contents, the tensile strength increased with addition of rubber, as the addition of the rubber reduced its sensitivity to defects. However, at high rubber contents the UTS began to decrease due to the increased content of low-strength rubber phase.[6]

2.5 Objective

As stated above, significant toughening of the MNS system occurred only at very high rubber contents, which resulted in the subsequent deterioration of the bulk properties. Therefore, this work focuses on increasing the toughness of MNS with ATBN contents below the phase inversion point. The first task of this study was, therefore, to locate the precise rubber content at which phase inversion occurred. Next, the focus turned to improving the toughness of a composition containing a rubber content just below the phase inversion point by the addition of pre-formed rubber particles. As mentioned previously, a twin population of particle sizes in epoxy was found to provide optimum toughening. Thus, it should be possible to add pre-formed second phase particles with diameters of around 1 micron to create a synergistic effect with the small ATBN domains in the rubber-containing regions of the MNS.

3.0 Experimental

3.1 Materials

3.1.1 Primary Components

All materials were used as received. Unsaturated polyester resin from Aristech Corporation (MR 13006) was received as a solution in 40 wt% styrene monomer. The composition of the polyester is as follows: 30% propylene glycol, 7% ethylene glycol, 4% dipropylene glycol, 53% fumarate ester and 6% maleate ester. The epoxy used was EPON 828, a diglycidyl ether of bisphenol-A (DGEBA) resin from Shell Chemical Company. BF Goodrich supplied the amine terminated acrylonitrile butadiene copolymer (ATBN 1300x16) reactive liquid rubber used in this study. The curing agent for the epoxy was Ancamine K61B, and that for the polyester was t-butyl per-benzoate. Both were purchased from Aldrich Chemical Company.

3.1.2 Pre-Formed Particles

Several types of pre-formed particles were used in this study. The compositions and sizes of all particles are listed in Table 3.1. Except where noted otherwise, all particles were used as received. Solid acrylonitrile butadiene Nipol DP5078 particles were obtained from Zeon Chemicals. These particles are the largest used in the study, with diameters close to 150 microns. Several types of core-shell particles with pMMA shells and butadiene or butyl acrylate cores were obtained from Rohm and Haas. The Paraloid KM334 particles have a butyl acrylate core and are sub-micron in size. The EXL 5136 and EXL 2330 particles have butyl acrylate cores and particle sizes of close to 1 micron and 600 nanometers respectively. The EXL 2691 particles have a butadiene core and are extremely small with a mean diameter of around 150 nanometers. The degree of crosslinking of both the pMMA shell and rubber cores are higher for the EXL particles than for the Paraloid particles. Poly (dimethyl siloxane) (PDMS) particles with either amino, epoxy or silanol functionalities were obtained from Dow Corning Company. These particles had a mean particle diameter of 5 microns.

Table 3.1- Types of second phase particles used in this study.

Particle	Supplier	Core Composition	Shell Composition	Mean Size
Nipol DP5078	Zeon Chemicals	Acrylonitrile butadiene	n/a	100 microns
Paraloid KM334	Rohm & Haas	Butyl Acrylate	pMMA	Sub-micron
Solid Glass Spheres	Potter's Industries	Borosilicate	n/a	2 microns
Hollow Glass Spheres	Potter's Industries	Borosilicate	n/a	8 microns
EXL 5136	Rohm & Haas	Very heavily cross-linked butyl acrylate	Cross-linked pMMA	~ 1 micron
EXL 2691	Rohm & Haas	Partially cross-linked butadiene	Cross-linked pMMA	150-160 nm
EXL 2330	Rohm & Haas	Partially cross-linked butyl acrylate	Cross-linked pMMA	600 nm
Amino PDMS	Dow Corning	PDMS	n/a	5 microns
Epoxy PDMS	Dow Corning	PDMS	n/a	5 microns
Silanol PDMS	Dow Corning	PDMS	n/a	5 microns

The final type of pre-formed particle used in this study was borosilicate glass spheres obtained from Potter's Industries. Both solid and hollow spheres were obtained. The solid spheres had a mean diameter of 2 microns, while the hollow spheres were slightly larger with a mean diameter of 8 microns. In order to increase the degree of adhesion of these spheres with the matrix materials, the spheres were first reacted with a coupling agent. Two types of coupling agents were used. Both these coupling agents; N-aminoethyl -2 aminopropyl trimethoxy silane (Dow Z6040), and 3-glycidoxy propyl trimethoxy silane (Dow Z6020) were obtained from Dow Corning. In both cases, a solution of 56g of isopropyl alcohol, and 0.1g of water were mixed in a 500ml 3-neck flask. To this solution was added 20g of glass spheres. The solution was mixed for 18 hours. In order to retrieve the spheres, the solution was poured through filter paper and the wet spheres were allowed to dry for 8 hours. In order to simulate a hydrating environment, the spheres were then suspended on filter paper over a beaker containing water for 16 hours. The spheres were then allowed to dry for 3 more hours before they were separated using a fine sieve.

3.2 Castings

The ratio of unsaturated polyester to epoxy for each of the castings produced in this study was kept constant at 2:1. Although the unsaturated polyester resin was already suspended in a styrene monomer carrier, additional styrene was added to maintain the ratio of reactive unsaturation in the polyester to styrene monomer at 1: 3.[6] For each casting, the liquid rubber was first dissolved in the styrene monomer. At this time, any second phase particles were added so that they could be well dispersed in the solution while the viscosity was still low. Next, the polyester resin, epoxy, and curing agents were added. Then, 1.5% by weight of t-butyl per benzoate was added. In order to ensure complete cure, the amount of ancamine added was adjusted so that the ratio of total amine functions to epoxy functions was equal to 1. In some cases, it was necessary to add fumed silica particles in order to increase the viscosity of the solution so as to prevent the pre-formed particles from either rising to the top of the mixture or falling to the bottom due to differences in density. The core-shell particles tended to rise to the top, while

the glass spheres tended to sink to the bottom. A mechanical stirrer was used to ensure that all components were evenly distributed in the resin. However, the mixing process tended to incorporate a substantial amount of air into the mixture. To remove these air bubbles, the solution was degassed under vacuum at room temperature for 15-45 minutes depending on the type of particle used. The solution was then poured between two vertical Teflon coated aluminum plates and cured at 100°C under atmospheric pressure for 2 hours. The temperature was then increased to 120°C for an additional 16 hours.

The first series of MNS castings produced in this study contained various amounts of ATBN, but no additional second phase particles. The ATBN content was varied between 7% and 12.5%, and two casting were made at each half percent rubber content spanning this range. In addition, castings were made containing 7.5% ATBN with 5% of each of the pre-formed particles discussed above. However, the castings containing 5% PDMS particles contained 9.5% ATBN. In addition, a casting containing 7.5% ATBN and 2.5% CTBN was produced.

3.3 Mechanical Properties

3.3.1 Tensile Properties

Tensile properties were obtained using dog bone shaped samples machined from the first series of MNS castings, which contained various amounts of rubber but no pre-formed particles. The tensile tests were performed on an Instron 4505 at a cross-head speed of 0.2 in./ min in accordance with ASTM D-638. For accuracy, 8 to 10 specimens of each composition were tested. The strain to failure was determined by using an extensometer. The ultimate tensile strength (UTS) and tensile modulus of each sample were also determined.

3.3.2 Plane Strain Fracture Toughness

The plane strain fracture toughness (K_{Ic}) was obtained from compact tension specimens machined from each of the MNS formulations. The

geometry of the compact tension specimen is given in Figure A 3.1. The specimens were pre-cracked using a fresh razor blade and wooden mallet. Only specimens with straight pre-cracks that met the required length specifications were tested. Between 4 and 8 good specimens of each composition were tested in accordance with ASTM D 5045-93 at a rate of 0.2 in./ min. The plane strain fracture toughness was calculated from the maximum stress value attained according to the specifications in the standard:

$$K_{IC} = (P/BW^{1/2})f(x)$$

Where P is the maximum load achieved, W is the width of the specimen, B is the thickness of the specimen, and f(x) is a function of the specimen geometry.

3.3.3 Flexural Modulus

The flexural modulus was obtained from three point bend tests performed on specimens machined from some of the MNS castings containing the pre-formed particles. The samples were tested in accordance with ATSM D790-92 at a rate of 0.11 in,/ min. The flexural modulus allowed for the calculation of the strain energy release rate (G_{IC}):[2]

$$G_{IC} = (K_{IC})^2/E$$

Where E is the modulus. For the MNS specimens without second phase particles, the modulus obtained from the tensile tests was used for the calculation of G_{IC}. The strain energy release rate reflects the material's resistance to crack propagation, while K_{IC} represents the resistance to crack initiation.

3.4 Scanning Electron Microscopy

The fracture surface of a compact tension specimen from each composition produced was examined using a Cambridge Instruments Scanning Electron Microscope (SEM). The specimens were first exposed to

osmium tetroxide vapor to preferentially stain the rubber in the sample, since osmium atoms react with the unsaturation in the butadiene. Backscattered electrons are sensitive to atomic number, and areas containing the heavy osmium atoms will appear brighter than the rest of the sample when imaged using backscattered electrons. The samples were then coated with a thin layer of gold before imaging.

3.5 Dynamic Mechanical Analysis

The mechanical properties as a function of temperature for the samples with various rubber contents, as well as for those containing the pre-formed particles, were determined using a Seiko DMS 200 dynamic mechanical analyzer (DMA) in tensile mode. Samples were machined from the compact tension specimens, and then polished to dimensions of approximately 0.7 mm by 4.0 mm with a testing gauge length of 10 mm. The samples were heated from -100°C to 250°C at a rate of 2°C per minute. The cycle frequency was fixed at 5 Hz with an amplitude of 30 microns. All measurements were carried out under a stream of nitrogen gas. Two different specimens from each composition were tested to ensure complete reproducibility. The locations and the intensities of the resulting tan δ peaks were noted.

4.0 Results and Discussion

4.1 Neat MNS Compositions

4.1.1 Mechanical Properties

4.1.1.1 Tensile Properties

The mechanical properties obtained from tensile tests performed on MNS dogbone specimens with rubber contents in the range of 7.0% to 12.5% ATBN are given in Figures 4.1 - 4.3. The average values of the mechanical properties for these samples are given in Table 4.1. Although there is a fair amount of scatter in the data, it appears that the ultimate tensile strength (UTS) generally increases with increasing rubber content between 7.0% and

Table 4.1- Mechanical Properties of MNS with various rubber contents.

Rubber Content (%)	UTS* (psi)	Modulus* (ksi)	Strain* (%)	K_{Ic}** ksi*in1/ 2	G_{Ic}** (lb/ in)
0***	8100	590	1.6	0.45	0.34
7.0	8161 (1210)	514.7 (48.0)	2.05 (0.59)	0.5372 (0.0388)	0.5607
7.5	8774 (353)	513.5 (28.6)	2.33 (0.21)	0.5591 (0.0798)	0.6087
8.0	7999 (1223)	497.8 (31.3)	2.10 (0.49)	0.5128 (0.0453)	0.5282
8.5	9028 (589)	555.6 (27.8)	2.09 (0.17)	0.4408 (0.0230)	0.3498
9.0	6942 (793)	562.5 (61.7)	1.84 (0.58)	0.7860 (0.0628)	1.0981
9.5	6322 (332)	545.8 (32.7)	1.34 (0.11)	0.7171 (0.0687)	0.9423
10.0	7444 (372)	406.6 (26.7)	2.99 (0.55)	0.7423 (0.0435)	1.3553
10.5	7551 (407)	403.6 (24.8)	2.85 (0.66)	0.7412 (0.0259)	1.3613
11.0	7556 (739)	433.2 (32.4)	2.59 (0.61)	0.7649 (0.0464)	1.3506
11.5	7755 (506)	433.4 (24.8)	2.59 (0.37)	0.7332 (0.0417)	1.2405
12.0	6967 (686)	419.7 (30.9)	2.33 (0.54)	0.7716 (0.0535)	1.4187
12.5	6666 (499)	409.4 (21.9)	2.18 (0.39)	0.7098 (0.0149)	1.2305

* Tensile Properties measured per ASTM D-638.

** Plane strain fracture toughness per ASTM D 5045-93.

*** Data per R. Subramaniam.[6]

Numbers in parentheses are standard deviations.

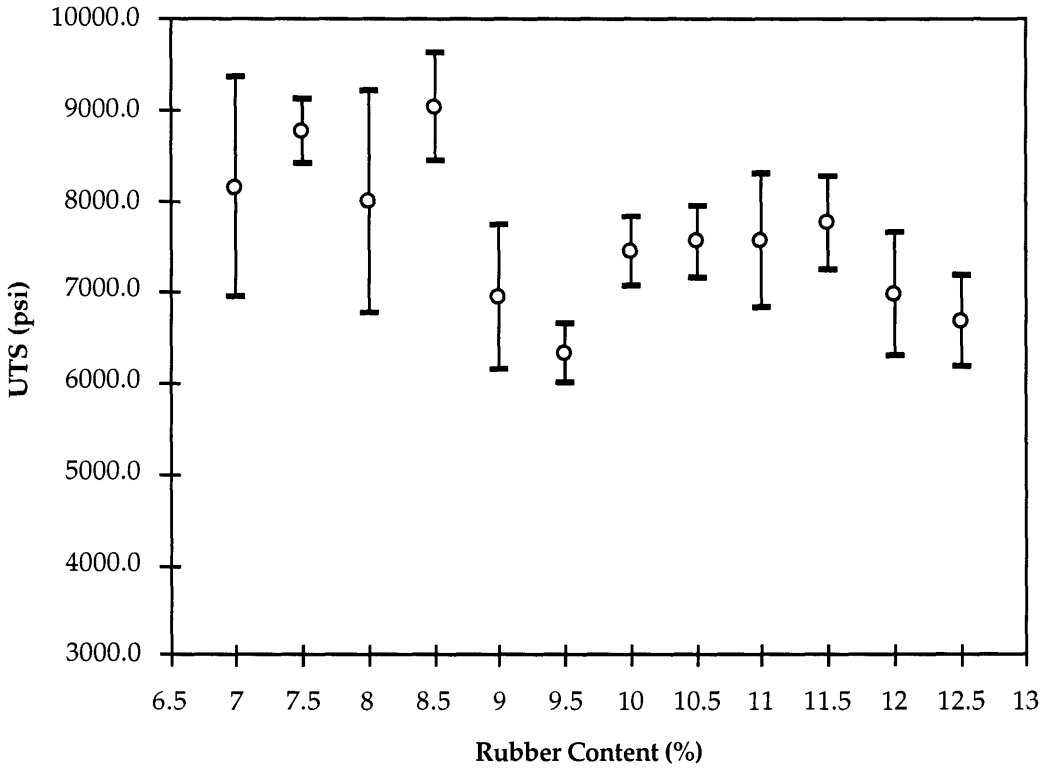

Figure 4.1- Variation of ultimate tensile strength with rubber content of MNS samples. Measured per ASTM D-638 on dog bone shaped samples at a speed of 0.2 in/min.

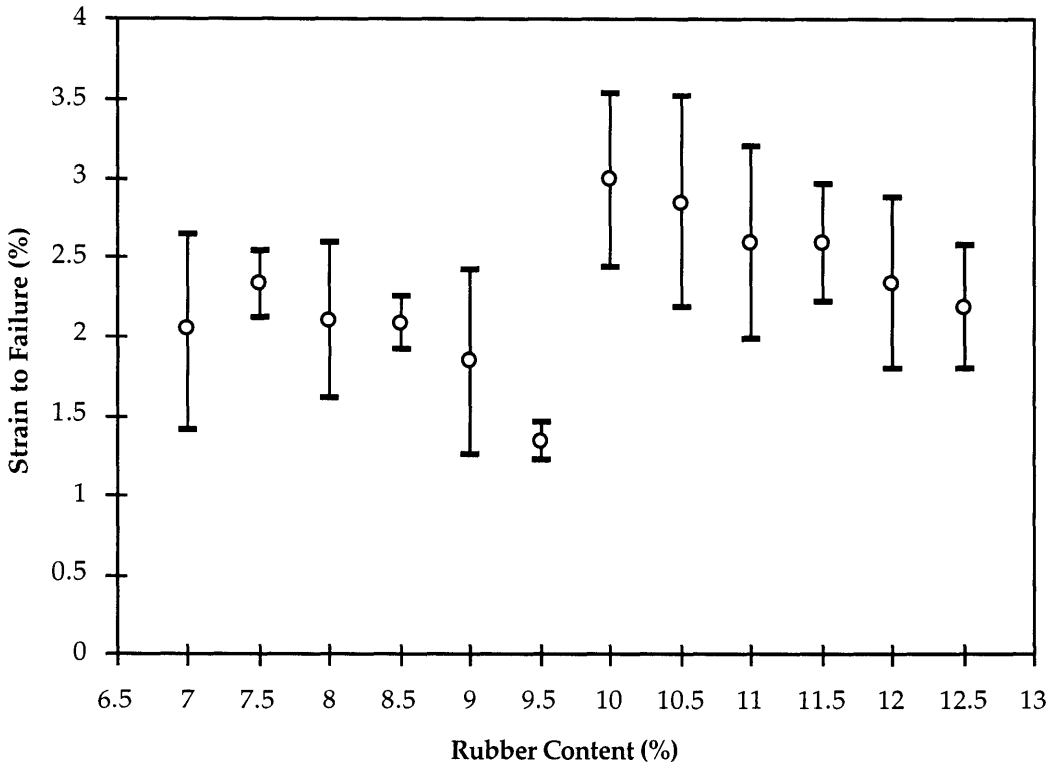

Figure 4.2- Variation of strain to failure with rubber content of MNS samples. Measured per ASTM D-638 on dog bone shaped samples at a speed of 0.2 in/min.

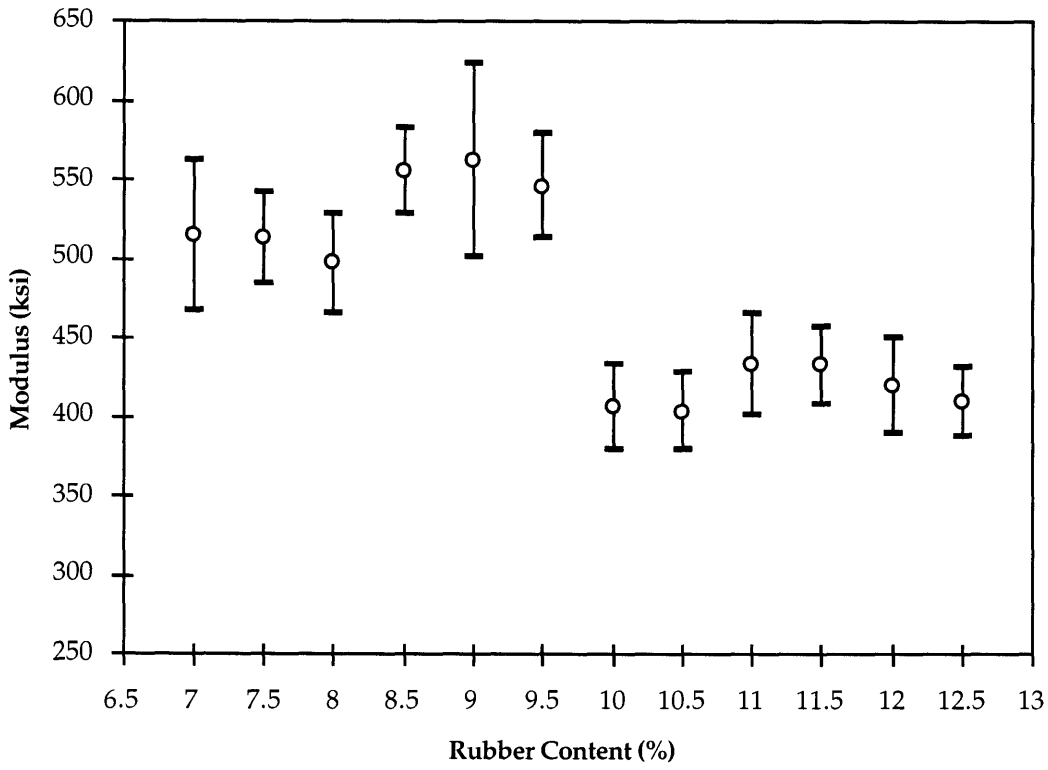

Figure 4.3- Variation of tensile modulus with rubber content of MNS samples. Measured per ASTM D-638 on dog bone shaped samples at a speed of 0.2 in/min.

8.5% ATBN. Then, between 8.5% and 9.0% ATBN, the tensile strength drops sharply from a mean values of 9028 psi at 8.5% ATBN to a mean value of 6942 psi at 9.0% ATBN. It would seem that the addition of up to 8.5% ATBN serves to toughen the matrix, and make it stronger by decreasing the sensitivity to defects. The sharp decrease in UTS between 8.5% and 9.0% is most likely due to the phase inversion which takes place near this composition. As will be confirmed by SEM micrographs later on, at about 9.0% ATBN the morphology changes from a rigid polyester-rich continuous matrix with discrete rubber domains to a flexibilized rubber-rich matrix with brittle inclusions of the polyester-rich phase. Beyond 9.0% ATBN, the tensile strength first shows a slight increase, but then begins to drop steadily as more rubber is incorporated into the network.

The strain to failure and tensile modulus also show large changes around the 9.0% ATBN composition. The strain to failure increases fairly sharply from a mean value of 1.84% at 9.0% ATBN to a mean value of 2.99% at 10% ATBN. This large increase in strain to failure is consistent with the increase in ductility that would be achieved by the change from the brittle polyester-rich matrix to the more flexibilized rubber-rich one. Similarly, the tensile modulus shows a large drop in this composition range, from a mean value of 545.8 ksi at 9.5% ATBN to a mean value of 406.6 ksi at 10.0% ATBN.

4.1.1.2 Plane Strain Fracture Toughness

Figure 4.4 shows the variation of plane strain fracture toughness with increasing rubber content, and the mean values are given in table 4.1. Although there is a fair amount of scatter in this toughness data, it is clear that there is a large increase between 8.5% ATBN and 9.0% ATBN. At 8.5% ATBN, the mean value of the fracture toughness is 0.4408 ksi*in$^{1/2}$. This increases quite sharply to 0.7860 ksi*in$^{1/2}$ at 9.0% ATBN. The data for the 8.5% ATBN samples looks fairly low, but the general increase in this area is still very substantial. The significant jump in fracture toughness between 8.5% and 9.0% ATBN supports the tensile data in suggesting that a phase inversion takes place in this composition range, since a rubber rich matrix would be more resistant to cracks than a brittle polyester-rich matrix.

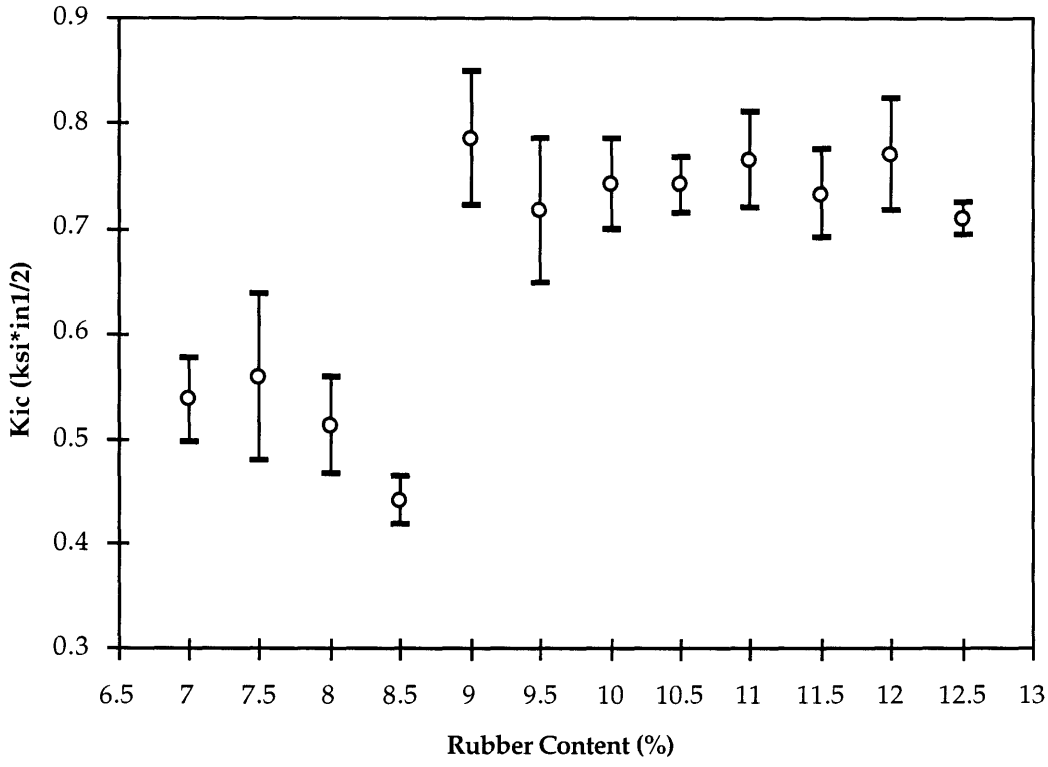

Figure 4.4- Variation of plane strain fracture toughness with rubber content. Measured per ASTM D 5045-93 on compact tension specimens with a rate of 0.2 in/min.

4.1.2 Scanning Electron Microscopy

Micrographs of the fracture surfaces of the MNS compact tension specimens containing various rubber contents are found in Figures 4.5 through 4.24. At 7.0% ATBN, the rubber-rich domains appear as light circles against the darker polyester matrix (Figure 4.5). Since the volume occupied by the rubbery domains appears to be much greater than 7.0%, it is probable that the domains contain a significant amount of the epoxy and polyester components. As mentioned earlier, this is not an uncommon occurrence. Since the reactivity of the ATBN with the epoxy is much higher than with the polyester, it is probable that most of the brittle material within the rubber-rich domains is epoxy. Note that there appears to be an interesting miscibility between the two phases as indicated by the large, glassy occlusions in the rubber-rich domains (Figure 4.6).

The micrographs taken of the 7.5% ATBN fracture surface show a considerably larger volume of rubber-rich domains than did the 7.0% ATBN sample (Figure 4.7). The rubber-rich domains are very densely packed and are no longer circular. There are also no apparent glassy occlusions in the rubber-rich domains. In attempt to account for this large change in morphology, the fracture toughness data for this specimen was examined. This sample turned out to have the highest fracture toughness of the 7.5% ATBN samples tested.

The fracture surface of a second compact tension specimen containing 7.5% ATBN, which exhibited a more average fracture toughness value, was examined. This specimen showed a fracture surface more like that of the 7.0% rubber sample (Figure 4.8). Notice also that the glassy occlusions are again present in some of the rubber-rich domains in this sample. The large difference in morphology and properties between these two specimens taken from the same casting indicates that the morphology may vary with position in the casting. This could be due to the fact that the bottom portion of the mold is closer to the heating coils in the furnace and, therefore, cures faster than the top portion. Subramaniam observed that crosslinking in MNS appeared to progress upwards from the bottom of the mold, which is closer to the heating elements of the oven. He found that the differences become more critical at compositions close to the phase inversion

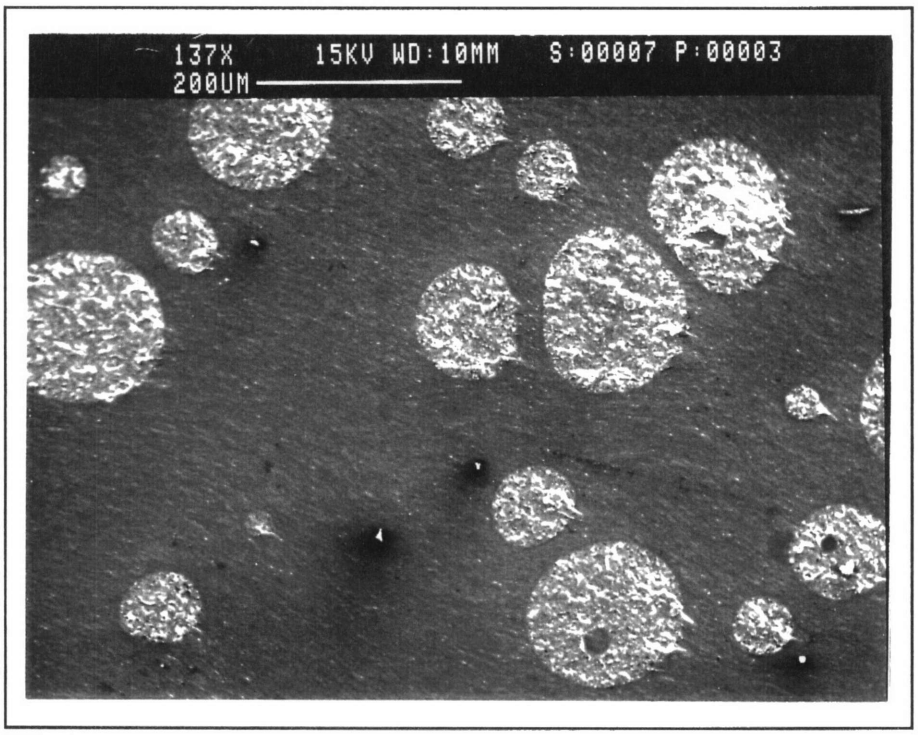

Figure 4.5- Backscattered image of discrete rubber-rich domains on the fracture surface of an MNS specimen containing 7.0% ATBN.

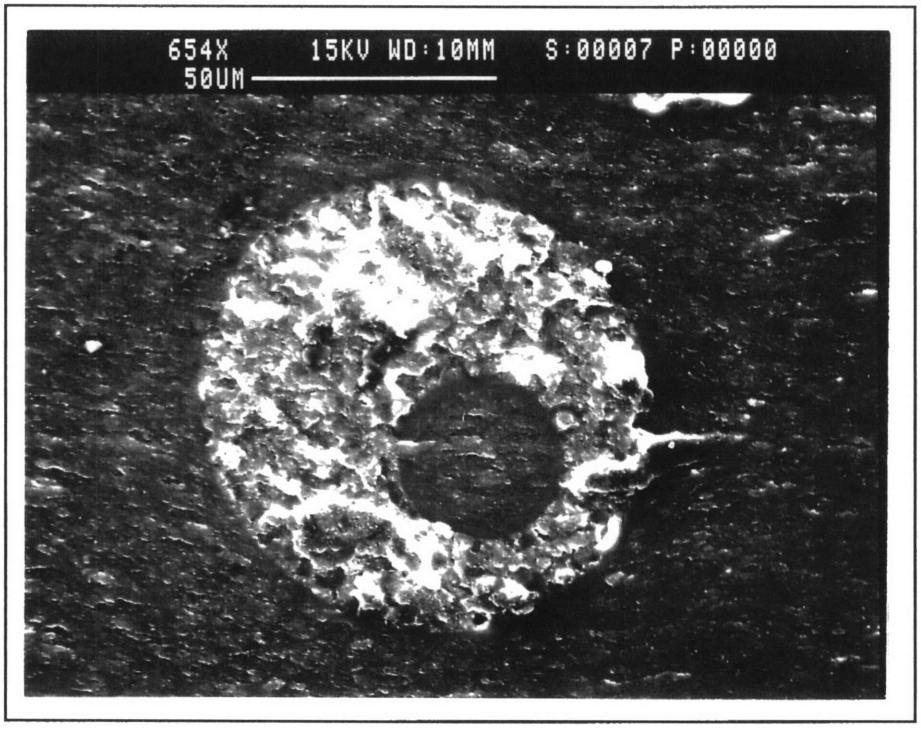

Figure 4.6- Backscattered image of glassy polyester-rich occlusions in a rubber-rich domain on the fracture surface of an MNS specimen containing 7.0% ATBN.

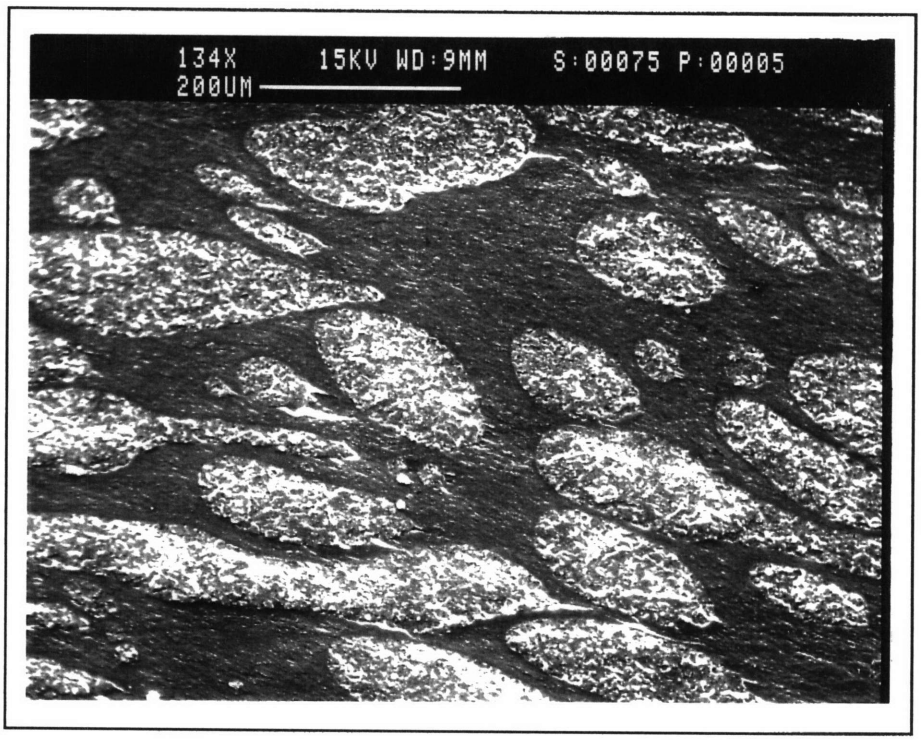

Figure 4.7- Backscattered image of numerous rubber-rich domains on the fracture surface of an MNS specimen containing 7.5% ATBN.

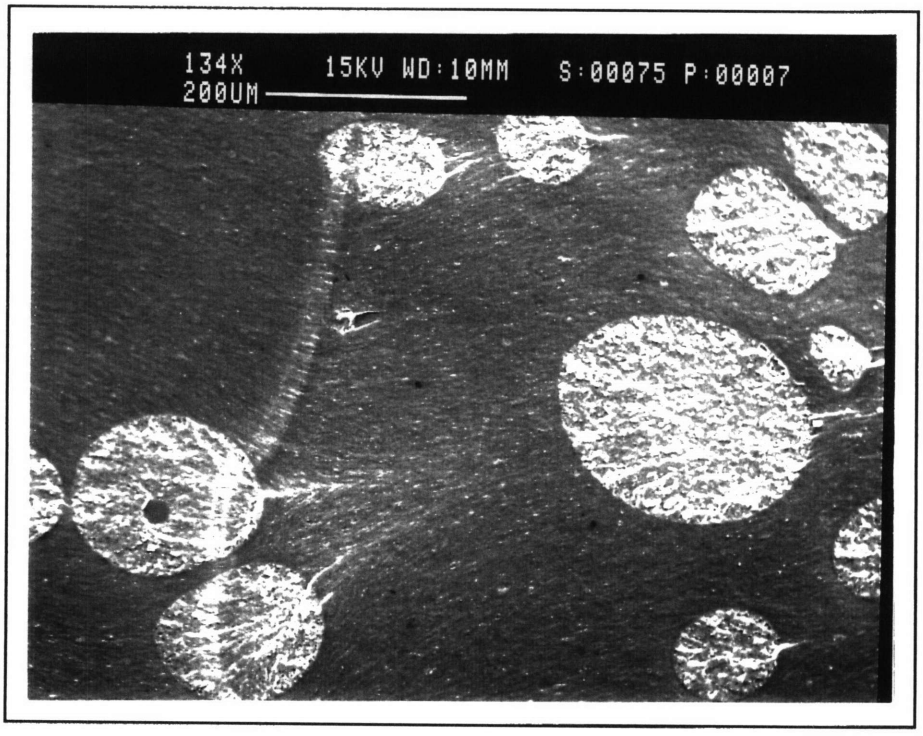

Figure 4.8- Backscattered image of the discrete rubber-rich domains on the fracture surface of a second MNS specimen containing 7.5% ATBN.

point, and that slight variations in cure can have a significant effect on the sample morphology.[6]

The fracture surfaces of the 8.0% and 8.5% ATBN specimens look very similar to those of the 7.0% and 7.5% ATBN specimens (Figures 4.9 and 4.10). The discrete rubbery domains are circular and evenly dispersed. There are large, glassy occlusions in the rubber-rich domains of these compositions, indicating the proximity to the rubber composition at which phase inversion occurs (Figures 4.11 and 4.12).

At 9.0% ATBN, the phase inversion appears to occur. The polyester-rich phase begins to form discrete circular domains, and the rubber-rich phase becomes the continuous one (Figure 4.13). The inversion does not appear to be fully complete at 9.0% ATBN as the polyester-rich domains are not very distinct (Figure 4.14). The centers of these domains are brighter than their borders and appear to have deformed a bit. Thus, the polyester-rich domains probably still contain some trapped rubber. The rubber-rich matrix now appears to occupy considerably more than 9.0% of the sample volume. Therefore, it is probable that the matrix also contains a large amount of both polyester and epoxy. It appears that the solubility diagram of this system is symmetric, because rubbery occlusions are now found in the polyester-rich domains (Figure 4.15).

The morphology of the fracture surface of the sample containing 9.5% ATBN is very similar to that of the 9.0% ATBN sample, but the polyester-rich domains have grown and have become much more distinct (Figure 4.16). The centers of these domains appear to contain a slightly deformed region which is slightly brighter than the rest of the domain (Figure 4.17). Therefore, there probably is not much rubber still trapped in the polyester-rich domains at 9.5% ATBN. There are still a large number of rubber-rich occlusions present in the polyester-rich domains (Figure 4.18). At 10% ATBN, the polyester-rich domains have continued to grow larger and are more distinct (Figure 4.19) with a large number of rubber-rich occlusions in the brittle domains (Figure 4.20).

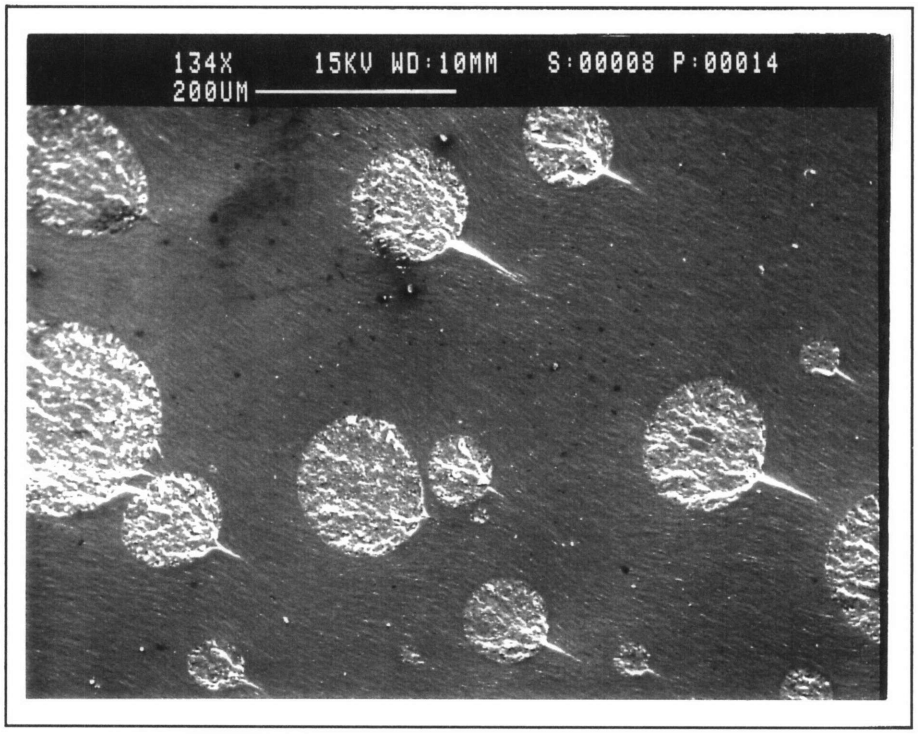

Figure 4.9- Backscattered image of the discrete rubber-rich domains on the fracture surface of an MNS specimen containing 8.0% ATBN.

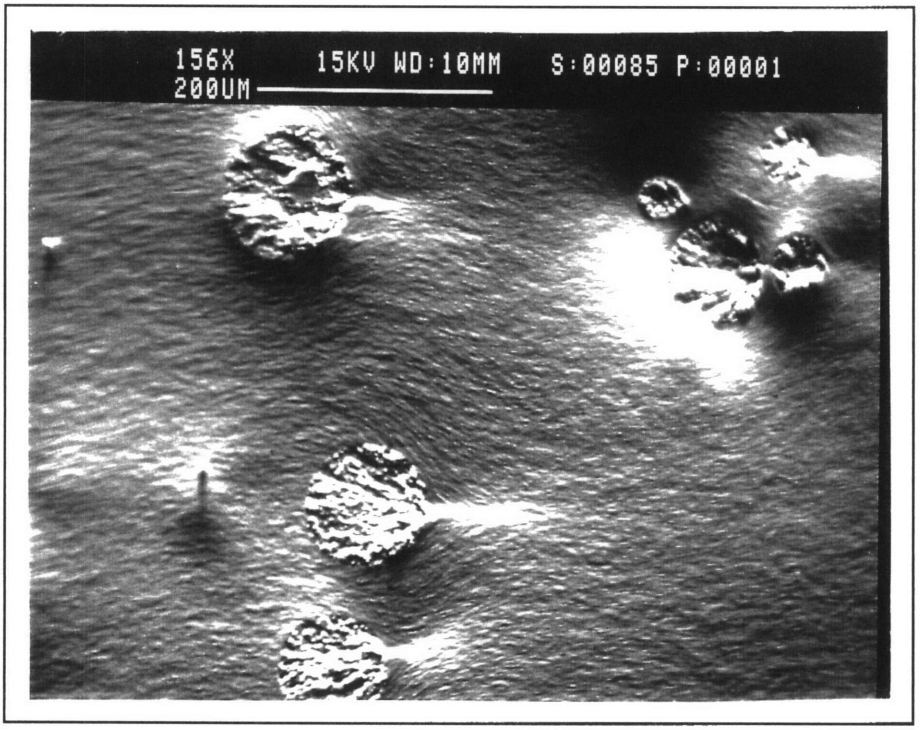

Figure 4.10- Backscattered image of the discrete rubber-rich domains on the fracture surface of an MNS specimen containing 8.5% ATBN.

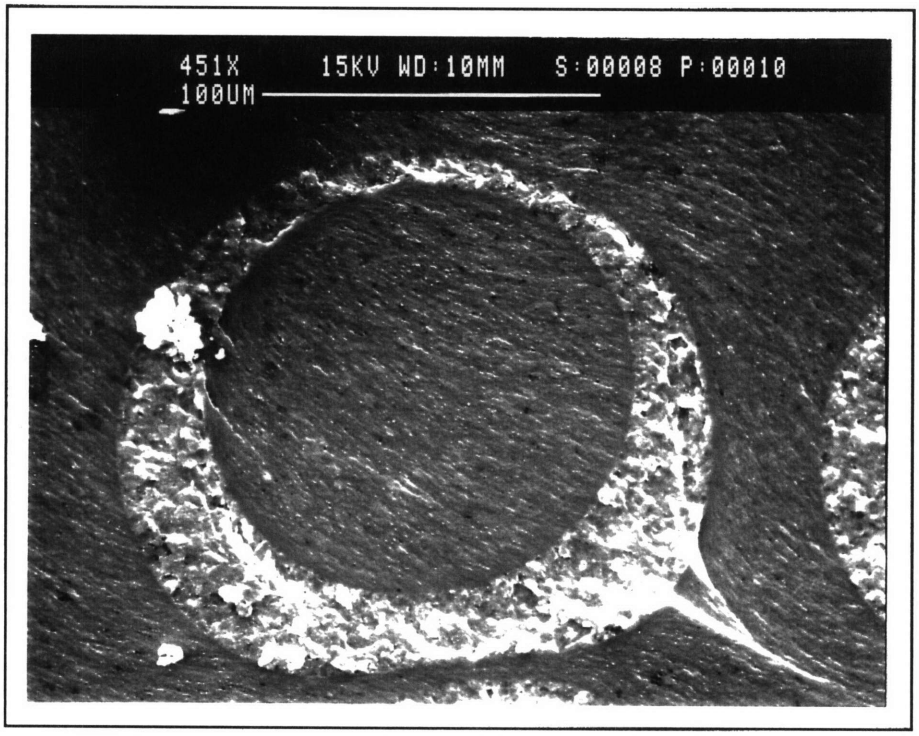

Figure 4.11- Backscattered image of large glassy occlusions in the rubber-rich domains on the fracture surface of an MNS specimen containing 8.0% ATBN.

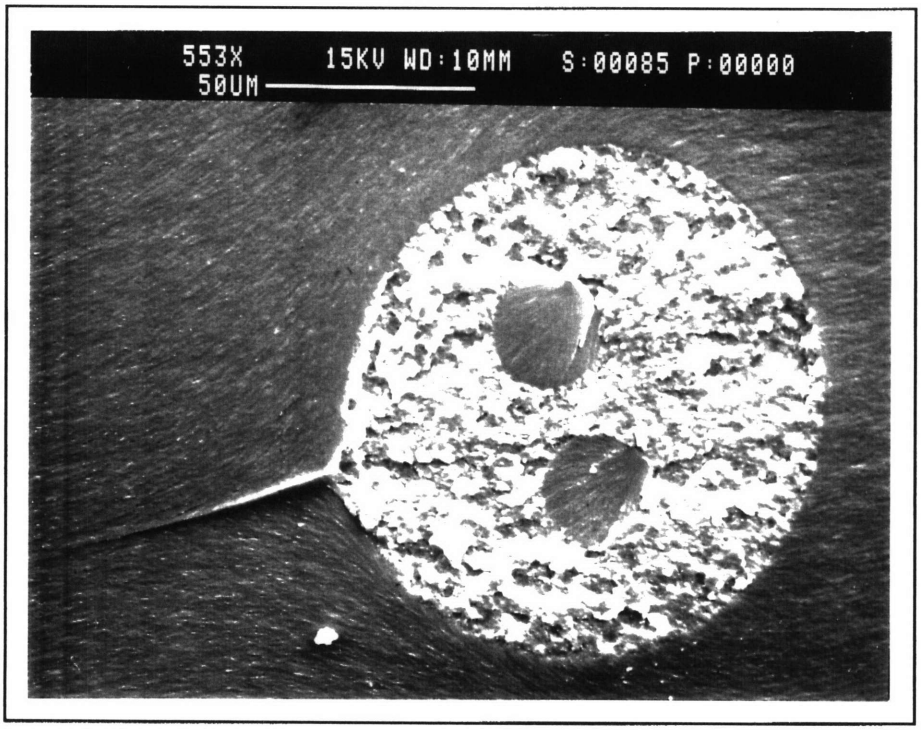

Figure 4.12- Backscattered image of large glassy occlusions in the rubber-rich domains on the fracture surface of an MNS specimen containing 8.5% ATBN.

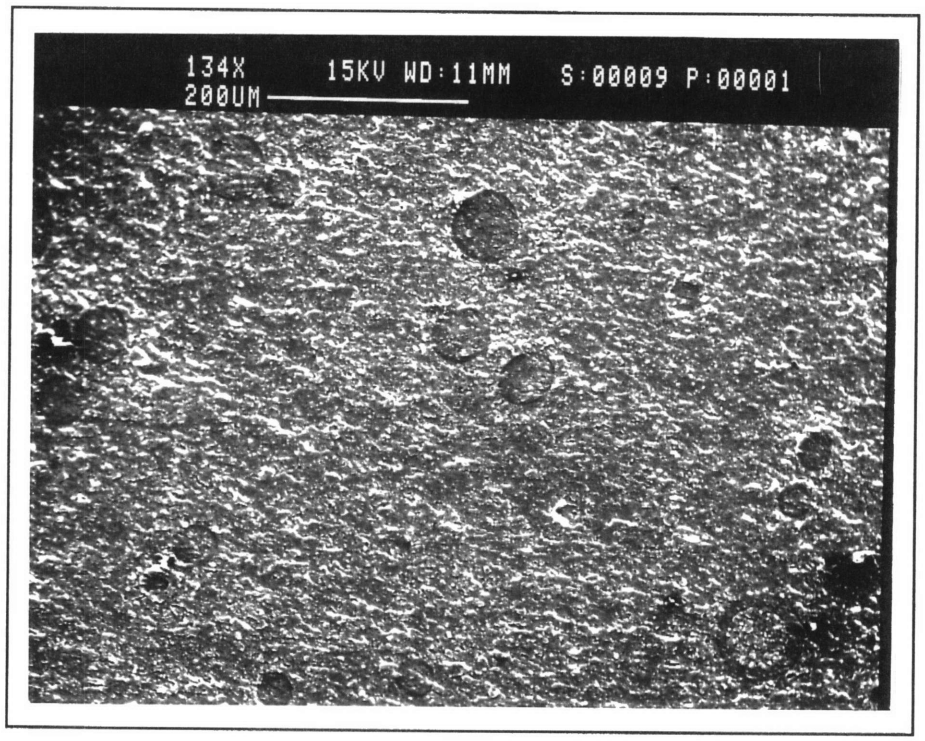

Figure 4.13- Backscattered image of the forming polyester-rich domains in a continuous polyester-rich matrix on the fracture surface of an MNS specimen with 9.0% ATBN.

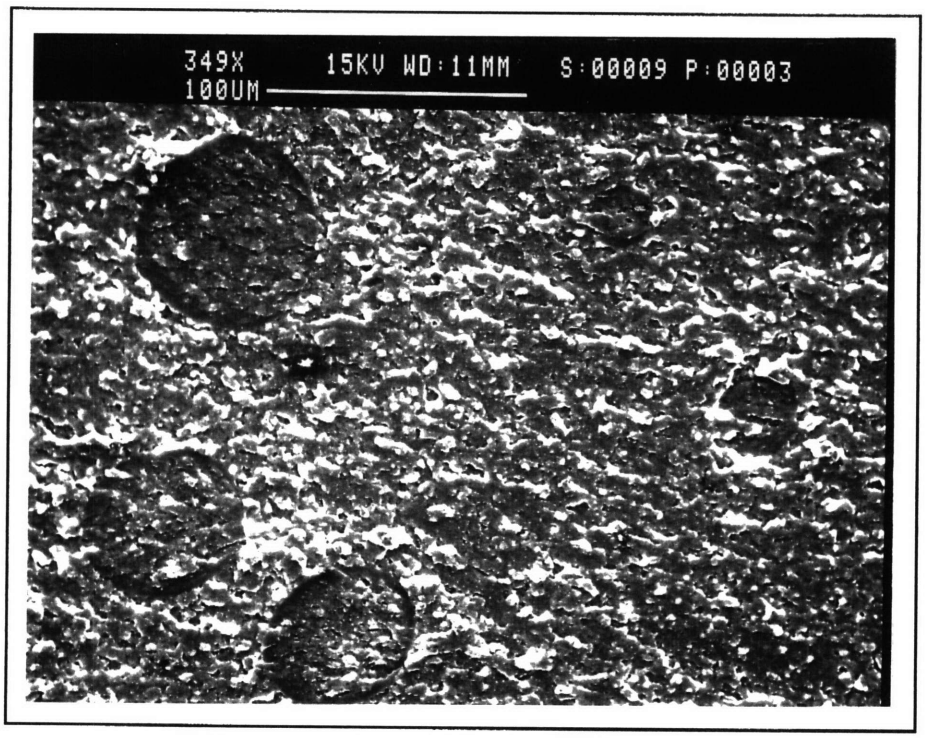

Figure 4.14- Backscattered image of discrete polyester-rich domains on the fracture surface of an MNS specimen containing 9.0% ATBN. These domains are not very distinct.

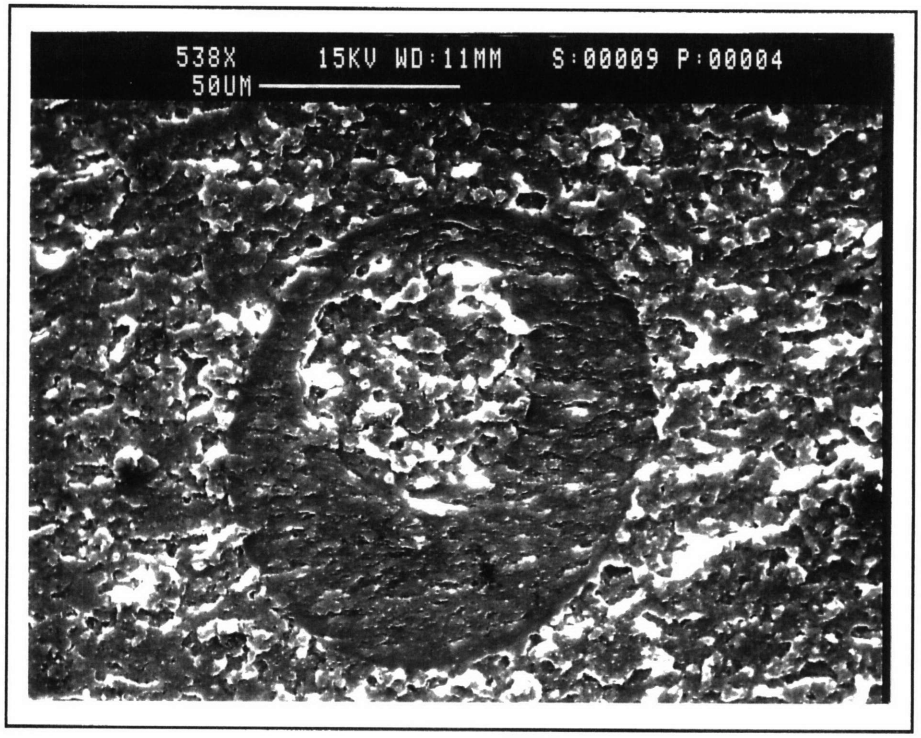

Figure 4.15- Backscattered image of a rubber-rich occlusion in a polyester-rich domain on the fracture surface of an MNS specimen containing 9.0% ATBN.

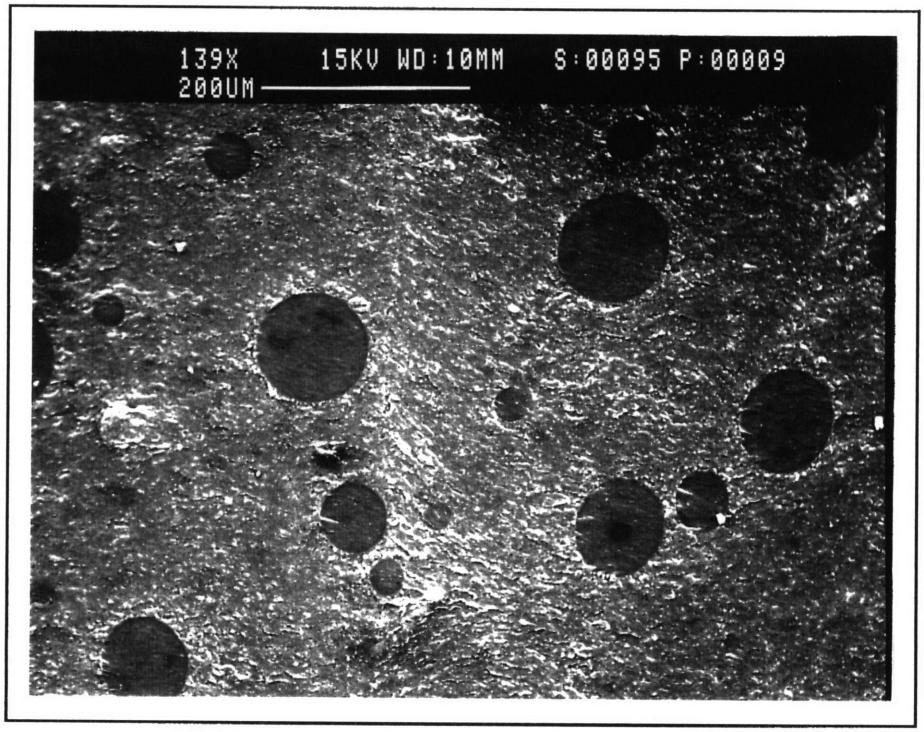

Figure 4.16- Backscattered image of distinct polyester-rich domains on the fracture surface of an MNS sample containing 9.5% ATBN.

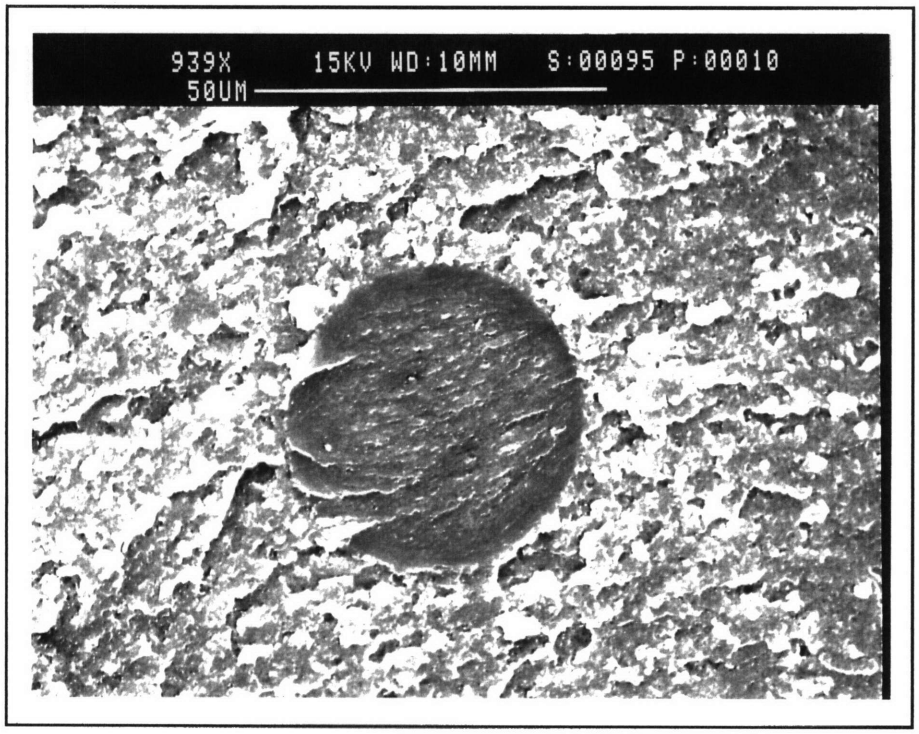

Figure 4.17- Backscattered image of a polyester-rich domain on the fracture surface of an MNS sample containing 9.5% ATBN. The center of this domain may contain ATBN.

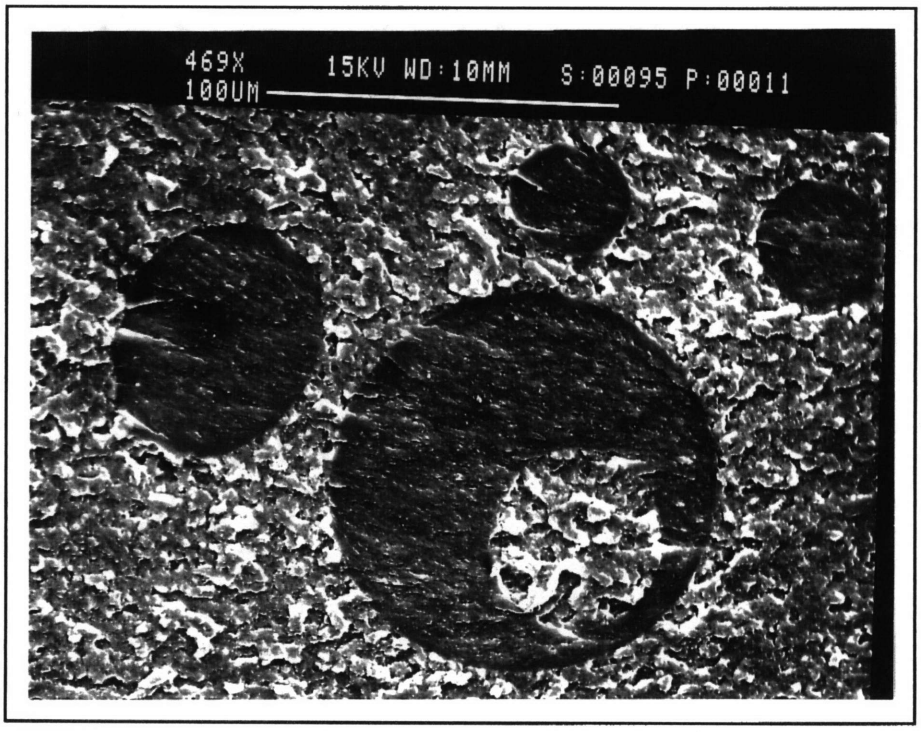

Figure 4.18- Backscattered image of rubber-rich occlusions in a polyester-rich domain on the fracture surface of an MNS specimen containing 9.5% ATBN.

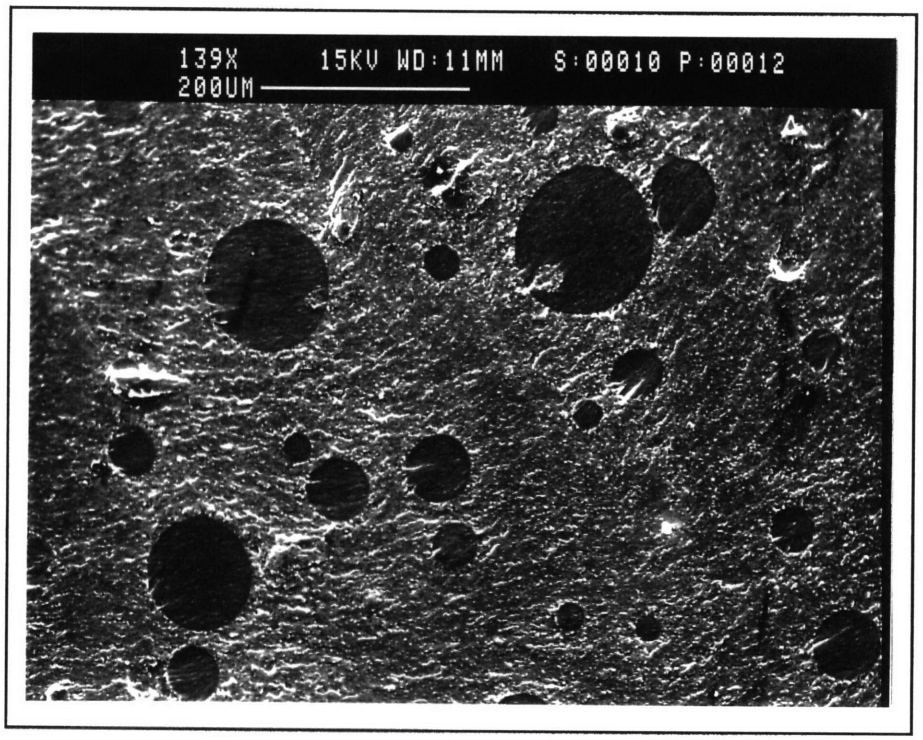

Figure 4.19- Backscattered image of large, distinct polyester-rich domains on the fracture surface of an MNS sample containing 10.0% ATBN.

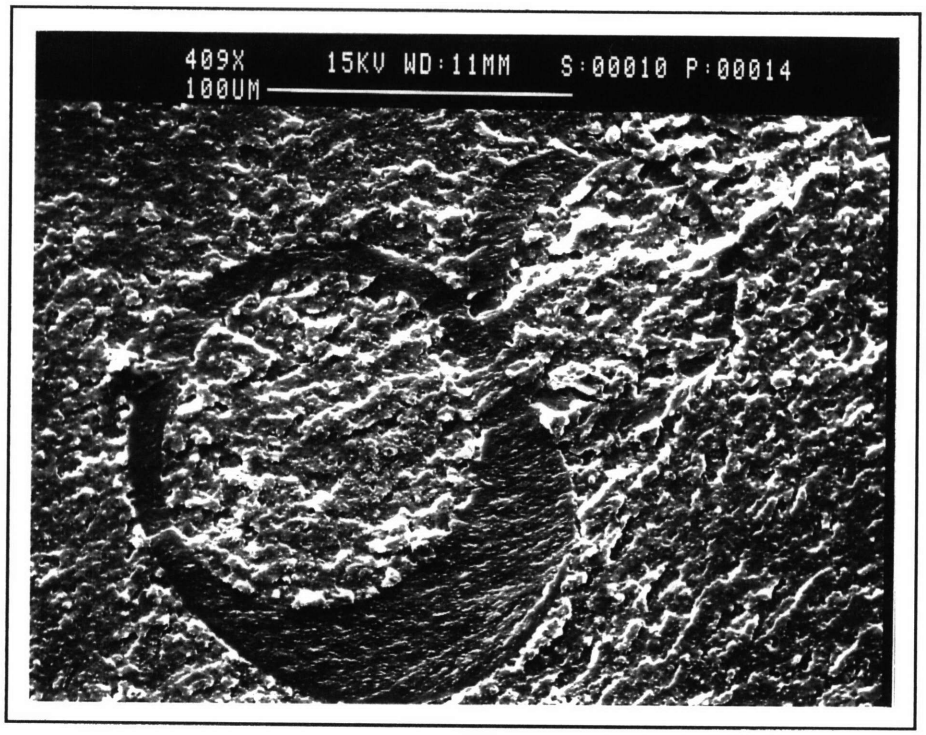

Figure 4.20- Backscattered image of rubber-rich occlusions in two polyester-rich domains on the fracture surface of an MNS sample containing 10.0% ATBN.

When 10.5% ATBN was added, the brittle polyester-rich domains became very distinct, but ceased to grow in size (Figure 4.21). Instead, the distribution in sizes of theses brittle domains is very large. Now, there is evidence that the very small polyester-rich domains have pulled free of the surface. The surface shows small spheres coated with rubber-rich material, and corresponding cavities of the same size. This would indicate particle pull-out (Figures 4.22 and 4.23). It appears that at a certain point, the rubber-rich matrix loses its strength, and it is easier for the brittle domains to be pulled free of the matrix than for the crack to propagate through the domains. This was only found to occur for the smaller domains. The presence of rubber-rich occlusions in the brittle domains is still observed (Figure 4.24).

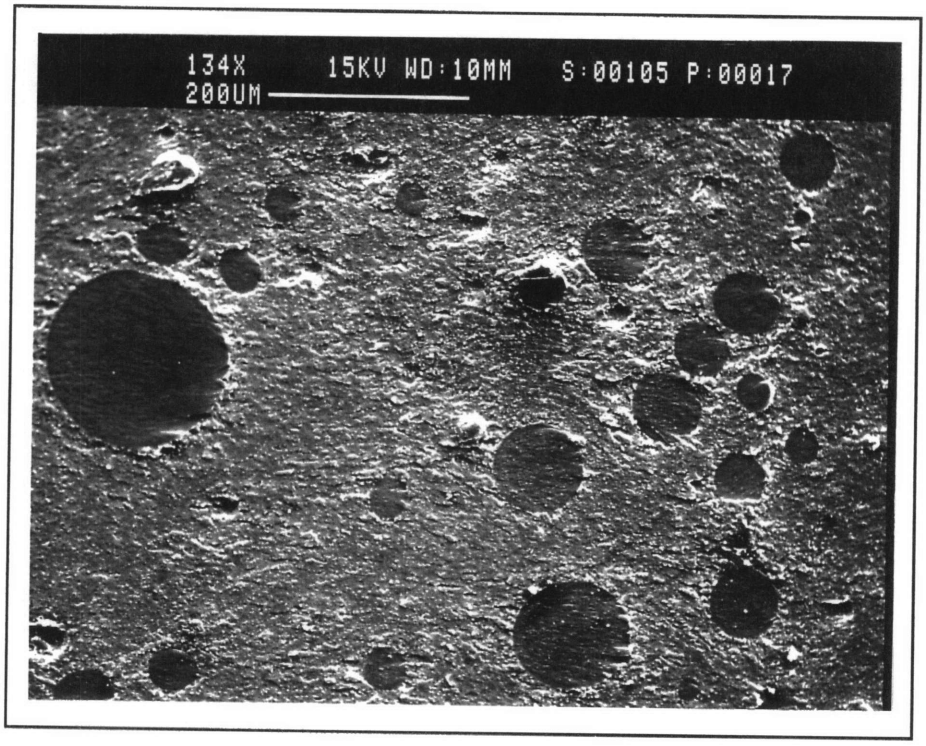

Figure 4.21- Backscattered image of distinct polyester-rich domains on the fracture surface of an MNS sample containing 10.5% ATBN.

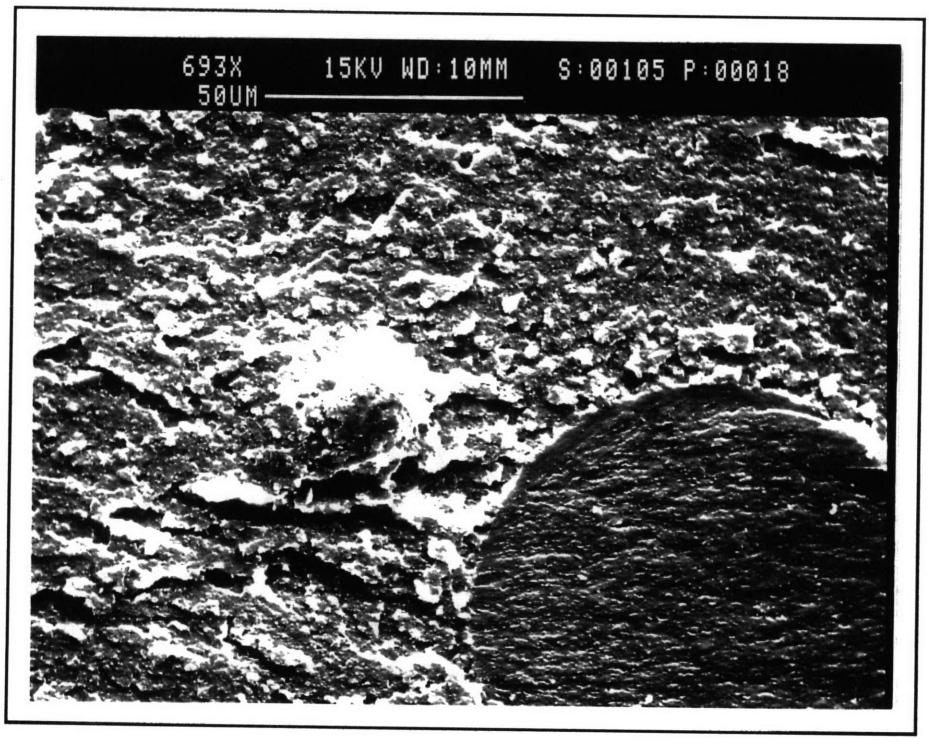

Figure 4.22- Backscattered image of a small, pulled-out polyester-rich domain on the fracture surface of an MNS sample containing 10.5% ATBN.

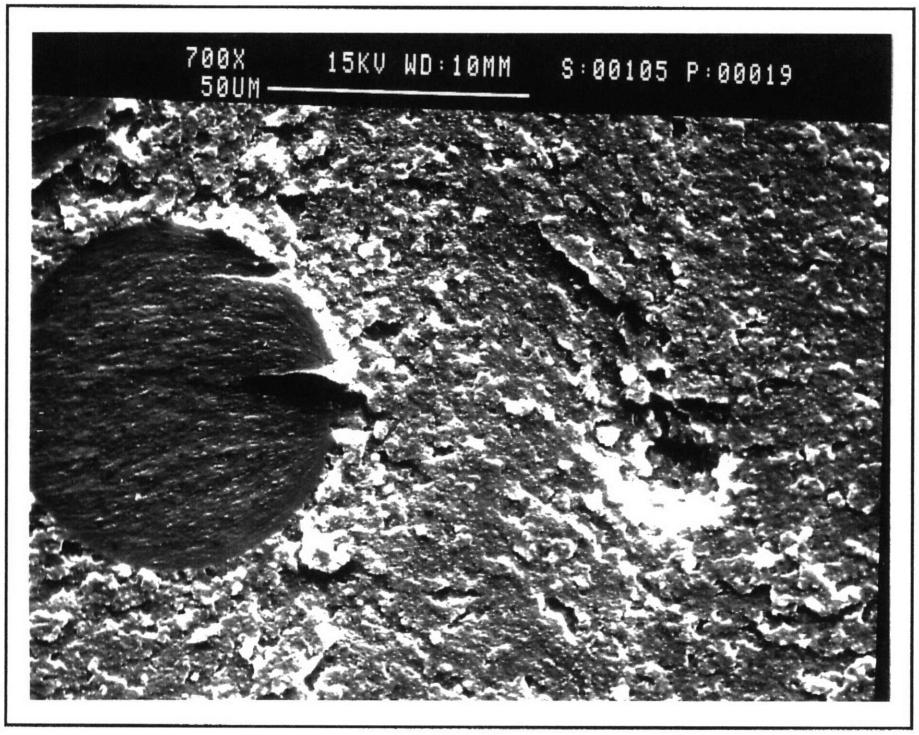

Figure 4.23- Backscattered image of the hole left by a pulled-out polyester-rich domain on the fracture surface of an MNS sample containing 10.5% ATBN.

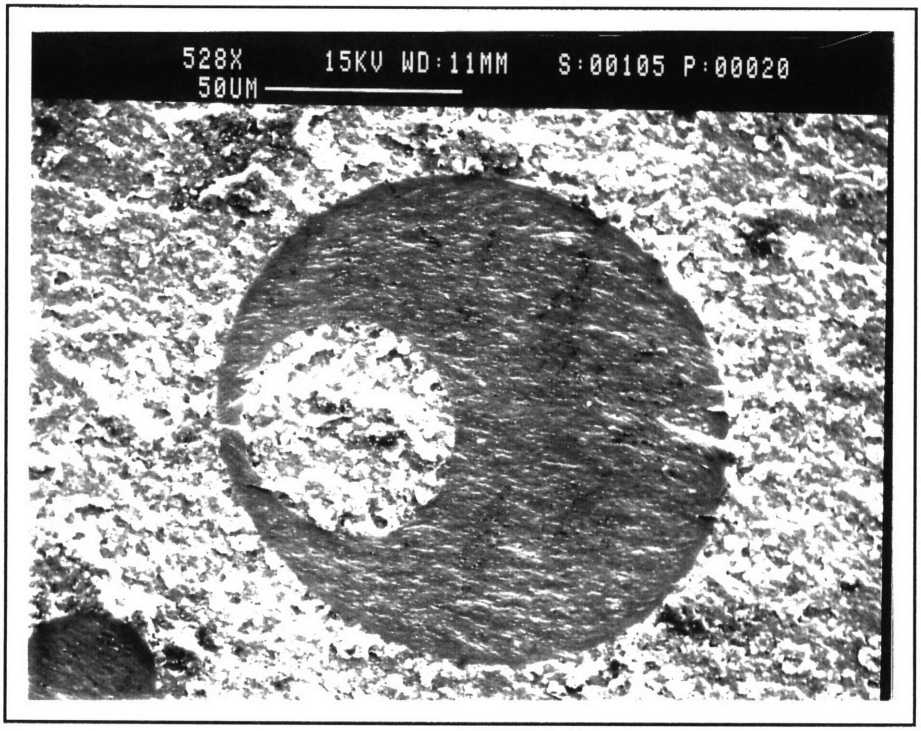

Figure 4.24- Backscattered image of a rubber-rich occlusion in a polyester-rich domain on the fracture surface of an MNS sample containing 10.5% ATBN.

4.1.3 Dynamic Mechanical Analysis

Dynamic mechanical analysis (DMA) measures a material's response to an imposed sinusoidal stress or strain with increasing temperature. Either the stress is controlled and the resulting strain in the sample is recorded, or the strain is controlled and the stress is measured. Since polymers are viscoelastic materials, only part of the material's response will be elastic. Therefore, if the strain is given by:[2]

$$\varepsilon = \varepsilon_o \cos(\omega t)$$

The resulting stress component will be out of phase by an amount δ:

$$\sigma = \sigma_o \cos(\omega t + \delta)$$

The stress can be expressed in terms of the contribution of real and imaginary components:

$$\sigma = \sigma_o' \cos(\omega t) + i\sigma_o'' \sin(\omega t)$$

The first term contains the real component. This term represents the in-phase portion of the stress response that is due to the elastic nature of the material. The second term is the out-of-phase portion of the response which reflects the ability of the material to dissipate energy through viscous mechanisms. The complex modulus of the material can be calculated by dividing the stress by the strain:

$$E^* = \sigma_o'/\varepsilon_o + \sigma''/\varepsilon_o$$

$$E^* = E' + E''$$

Where E' is the real or "storage" modulus, and E'' is the imaginary or "loss" modulus. The ratio of the loss modulus to the storage modulus is known as the tanδ:

$$\tan\delta = E''/E'$$

The plot of tanδ versus temperature can tell much about the properties of a polymeric material. If the material goes through a transition, such as the glass transition (Tg), there will be a peak in the tanδ curve representing the fact that there is a significant amount of energy absorbed through viscous motions during a transition. In addition, the intensity of this transition is directly related to the material's ability to dissipate energy through segmental motions.[6] Thus, the temperatures at which the transitions occur and the intensity of the transitions can reveal much about the mobility of a given system.

Finally, the breadth of a transition in a multi-component system is indicative of the morphology of that material. If there are multiple transitions, this indicates that there has been significant phase separation into distinct components with each component producing its own transition. However, if there is extremely good mixing, the transition will be single and narrow, and its temperature will be dependent on the Tg's of the individual components. A third possibility exists if the free energy of mixing of the system is close to zero. In this case, the components will separate into small domains (200-400nm) to form a microheterogeneous morphology representing small clusters of molecules. The transition will remain single with a temperature intermediate to the transitions involved. However, if the Tg's of the components are widely varied, the transition will be very broad due to the contributions of the various components.[53, 55] There have been reports of a microheterogeneous morphology producing a shoulder in CTBN modified polyester.[49] This shoulder is probably the result of slightly larger than microheterogeneous domains.

In order to gain better insight into the reactions between the polyester, epoxy and ATBN as the MNS system goes though the phase inversion, DMA was performed on a pure polyester sample, an MNS sample containing no rubber, and MNS samples containing 7%, 7.5%, 8%, 8.5%, 9%, 9.5%, 10%, 11% or 12.5% ATBN. Figure 4.25 shows the tanδ curves for two different samples of pure polyester. The two curves are fairly similar, which indicates good reproducibility. It is interesting to see that several different peaks appear on these curves. Kim et al. found that for pure polyester, there was a main tanδ

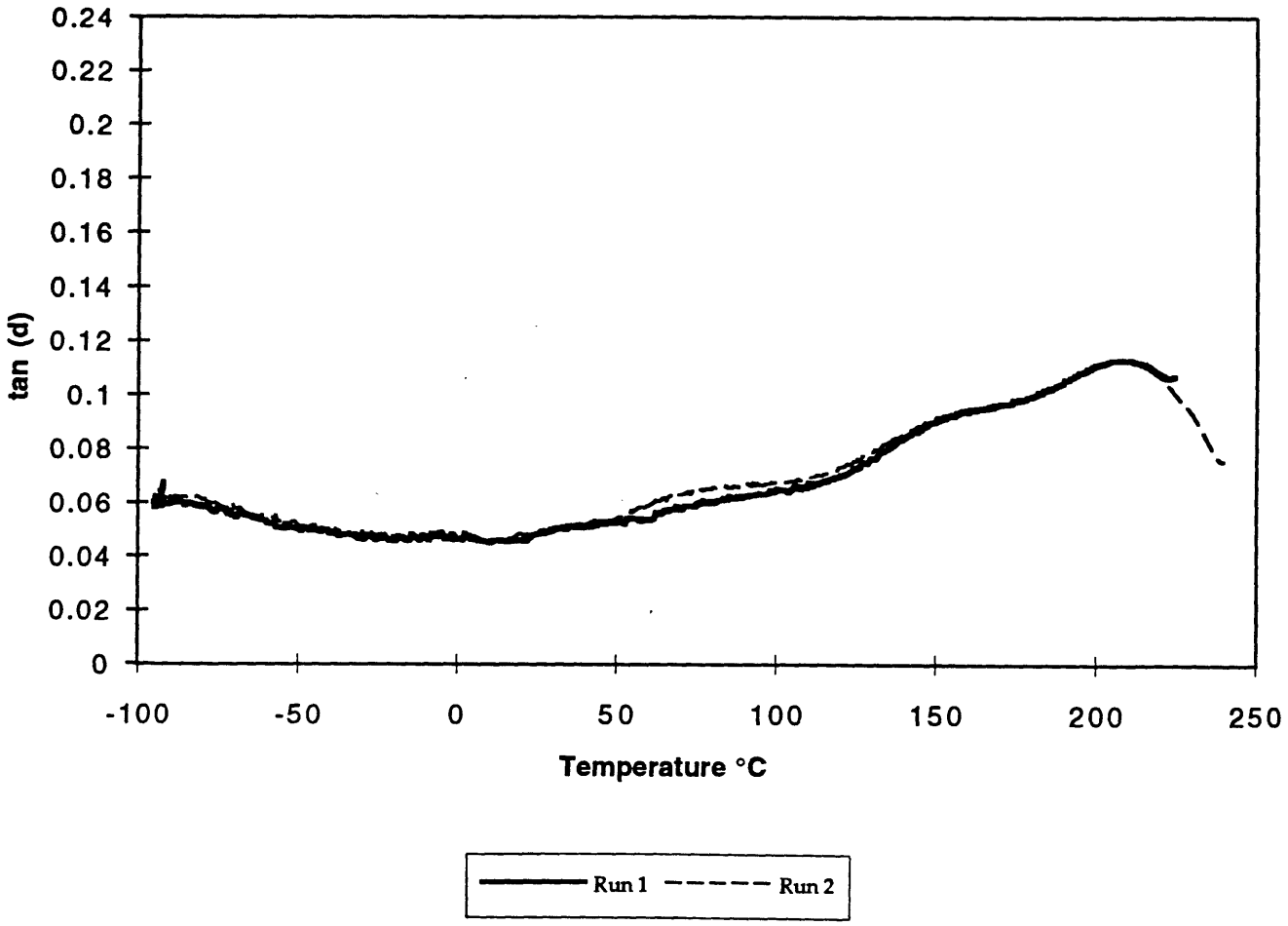

Figure 4.25- Tanδ curves as a function of temperature for pure polyester specimens tested in tensile mode at a heating rate of 2°C/min and a frequency of 5 hz.

peak at 179°C that reflected main chain movements, and a shoulder near 135°C that reflected the relaxation of either polystyrene or a polystyrene-polyester copolymer formed because styrene monomer was used as the carrier for unsaturated polyester.[28] Both the transitions in the present system occur at higher temperatures than those reported in the study. The main transition in the current study is located at 208°C, with a shoulder at 159°C. It is possible that the higher transition temperatures in the present system are due to a higher degree of cross-linking in this polyester system than for that reported in the literature.

Figure 4.25 also shows a lower temperature transition at around 78°C. This transition was more distinct in the second specimen than in the first. In order to see if this transition represented incomplete cross-linking, a sample was subjected to a second heating cycle. The tanδ curve for the second heating is compared with the curve from the first heat in Figure 4.26. The intensity of the entire tanδ curve for the second heating is considerably lower than that of the first heating. This indicates that the cross-linking increased during the heating process and restricted the mobility of the system. In addition, the shoulders are not present in the second heating. This indicates that some of the secondary relaxations have been inhibited by the increased cross-linking. Therefore, it would appear that the original shoulder was due to a polystyrene and polyester copolymer rather than pure polystyrene. During heating, the crosslink density of this copolymer probably increased, and this decreased the mobility significantly.

Figure 4.27 contains the tanδ curves for the pure polyester, MNS with 0% ATBN, MNS with 7.5% ATBN, and MNS with 9.5% ATBN. The intensity of the curve for the polyester and epoxy combination has increased considerably over that for the pure polyester. The intensity of the primary transition doubles from 0.11 to 0.22, and that of the shoulder almost doubles from 0.095 to 0.17 with the addition of epoxy. In addition, the temperatures of both the primary transition and the shoulder decrease considerably with the addition of the epoxy. The temperature of the primary transition decreases from around 208°C to 147°C, and that of the secondary shoulder decreases from around 159°C to 112°C. Both the decrease in the temperatures of the transition and the increase in intensity indicate that the mobility of the

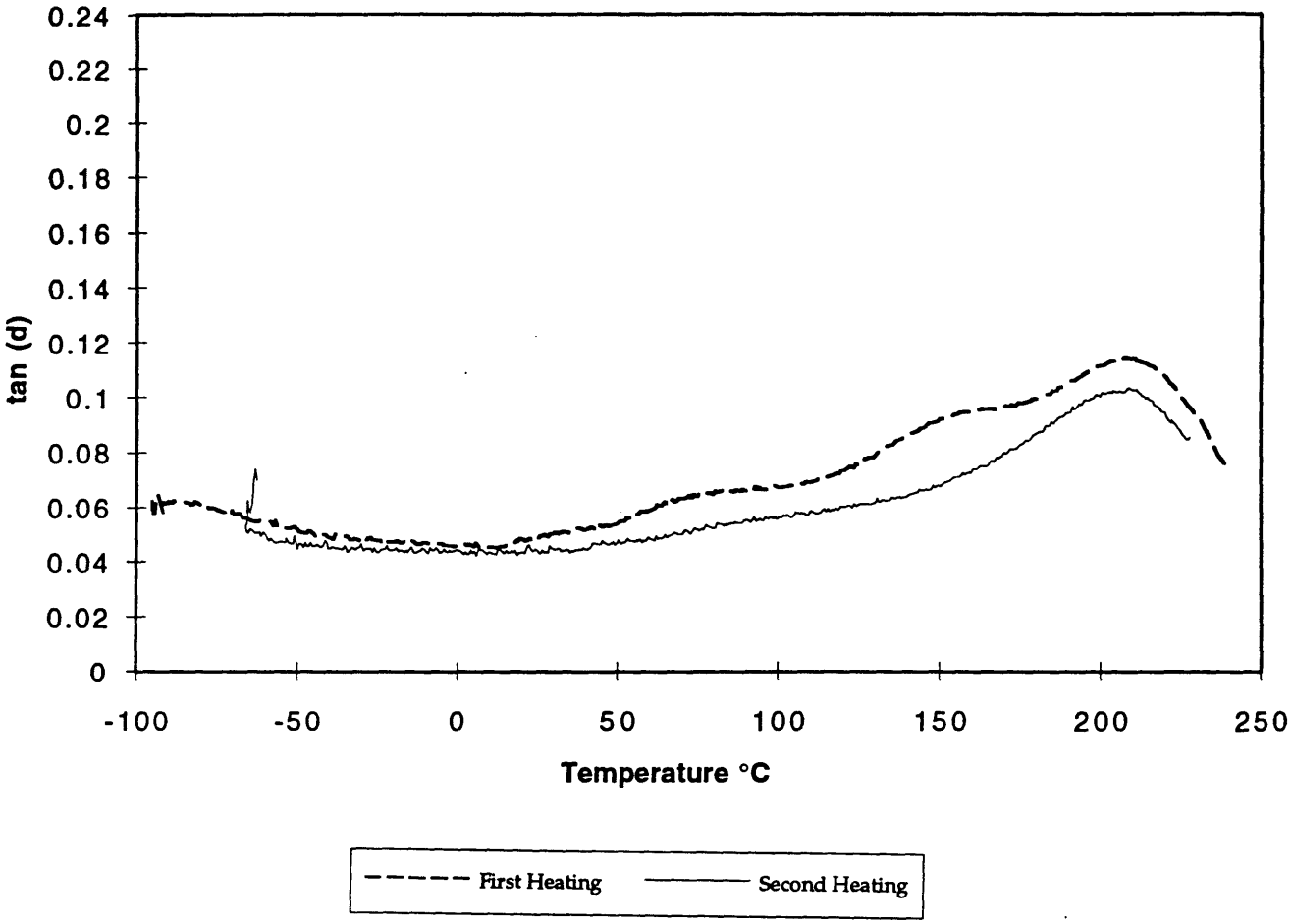

Figure 4.26- Tanδ curves as a function of temperature for the first and second heating of a pure polyester specimen tested in tensile mode at a heating rate of 2°C/min and a frequency of 5 Hz.

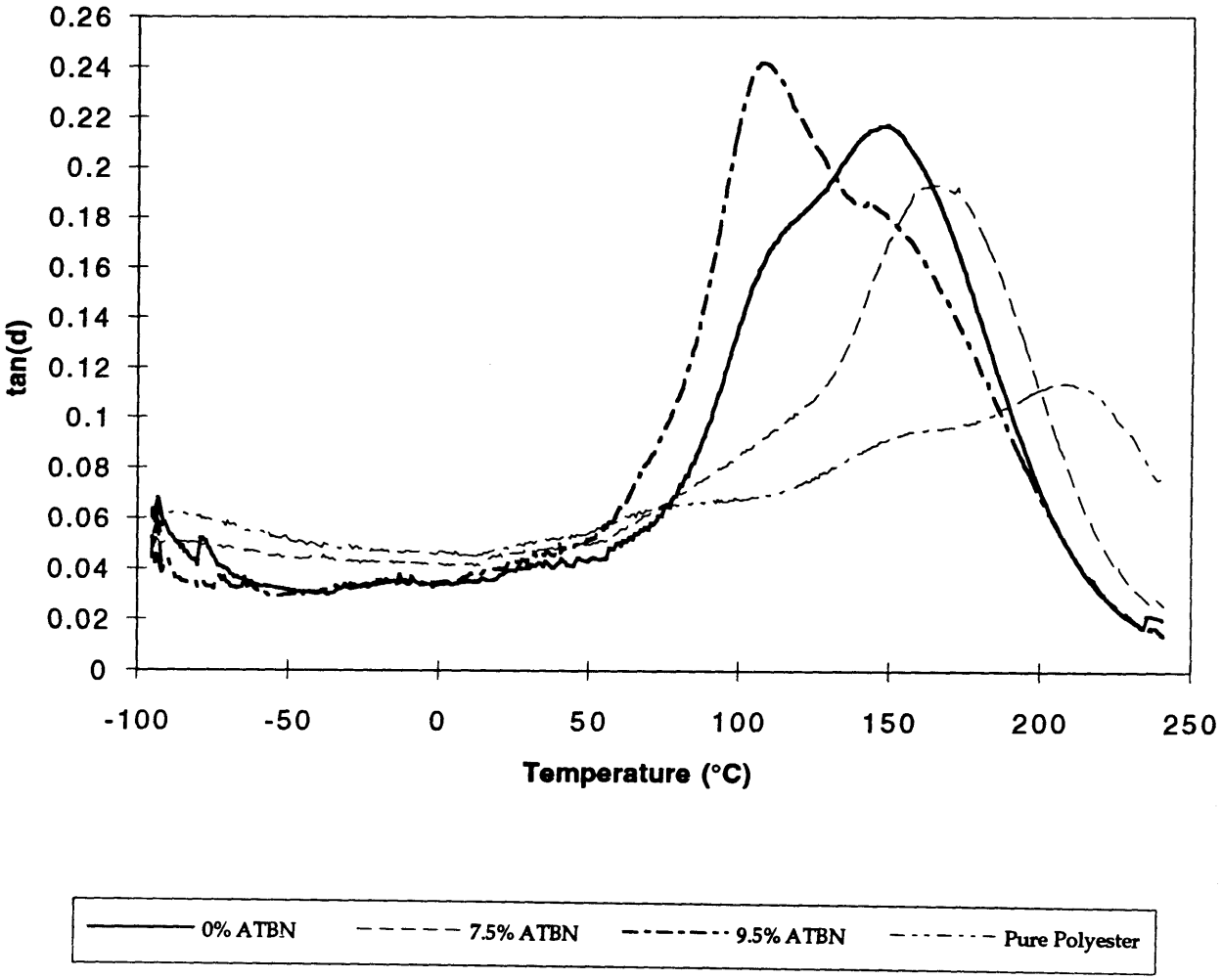

Figure 4.27- Tanδ curves as a function of temperature for samples of pure polyester, and MNS with 0%, 7.5% or 9.5% ATBN as determined by DMA in tensile mode at a heating rate of 2°C/min and a frequency of 5 Hz.

system has increased considerably. The increase in mobility could be due to the fact that the epoxy has a lower cross-link density than the polyester and, thus, has a lower temperature Tg. One study found that DMA performed on a pure epoxy specimen resulted in a single transition at a temperature of 100°C.[28] Thus, the epoxy probably serves to decrease the overall crosslink density of the system and to augment the low temperature shoulder. An interesting note is that even though the mobility of the polyester is increased significantly by the addition of the epoxy, Subramaniam showed that the fracture toughness of this composition did not increase considerably over that of pure polyester.[6]

When 7% ATBN is added to the polyester and epoxy MNS system, it is interesting to note that no low temperature peak characteristic of the rubber forms. This is probably the result of the rubber being confined to very small domains. Studies of CTBN modified epoxy found no damping peak attributed to the CTBN when the rubber was either completely blended with the epoxy or present in domains smaller than a critical size.[24] Low temperature transitions due to the presence of rubber were found when there was a large degree of phase separation, while mid-range relaxations were attributed to mixing of the elastomer and epoxies to different degrees.[26, 56] Even though there is phase separation into rubber-rich domains of around 100 microns in an MNS sample containing 7% ATBN, it was found that these domains were really composed of smaller individual domains of ATBN mixed with domains of epoxy and possibly some polyester.[6] The ATBN itself was found to occupy very small regions of around 100 nanometers.

The temperature of the high temperature transition for the 7% ATBN sample increases to around 160°C, but the intensity remains almost unchanged. This increase in the transition temperature is unexpected since the addition of dissolved rubber is generally found to modify the Tg to broaden it to lower temperatures and higher intensities for both rubber modified polyester and epoxy systems.[16-18,24,26,49] Completely phase separated rubber generally tends to create a low temperature transition, but does not generally change the transition temperature of the matrix phase.[20, 25] Equally unexpected is the significant drop in the intensity of the low temperature shoulder of the 7% ATBN sample back down to the level present in the pure

polyester sample, while the temperature remains unchanged. For the reasons just mentioned, one would expect the temperature of the transition to decrease and the intensity to increase with rubber incorporation.

In order to explore these unexpected findings, DMA was performed on further MNS samples with different rubber contents. Figure 4.28 contains the tanδ curves for MNS samples with rubber contents between 7% and 12.5%, as well as for the control MNS sample with 0% ATBN. Figures 4.29 and 4.30 show the trends of temperature and intensity of the transitions with increasing rubber content, while Table 4.2 contains the values of temperature and intensity of the transitions for each of the formulations. While both the temperature and the intensity of the high temperature transition remain pretty much unchanged for rubber contents between 7% and 9%, the intensity of the low temperature shoulder continues to decrease with increasing rubber content. The temperature of the low temperature transition, on the other hand, remains unchanged.

Table 4.2- DMA data for MNS with various rubber contents.

Rubber Content (%)	High Temperature Transition (°C)	Low Temperature Transition (°C)	High Temperature tan(d)	Low Temperature tan(d)
0	147.6	112.3	0.2173	0.1709
7.0	159.1	111.6	0.1965	0.1161
7.5	164.8	none	0.1925	none
8.0	165.4	111.7	0.1931	0.0993
8.5	165.1	none	0.1937	none
9.0	141.7	107.5	0.1902	0.2287
9.5	145.4	108.4	0.1843	0.2323
10.0	151.5	107.7	0.1789	0.2124
11.0	151.8	109.2	0.1779	0.1795
12.5	150.7	107.3	0.1731	0.1883

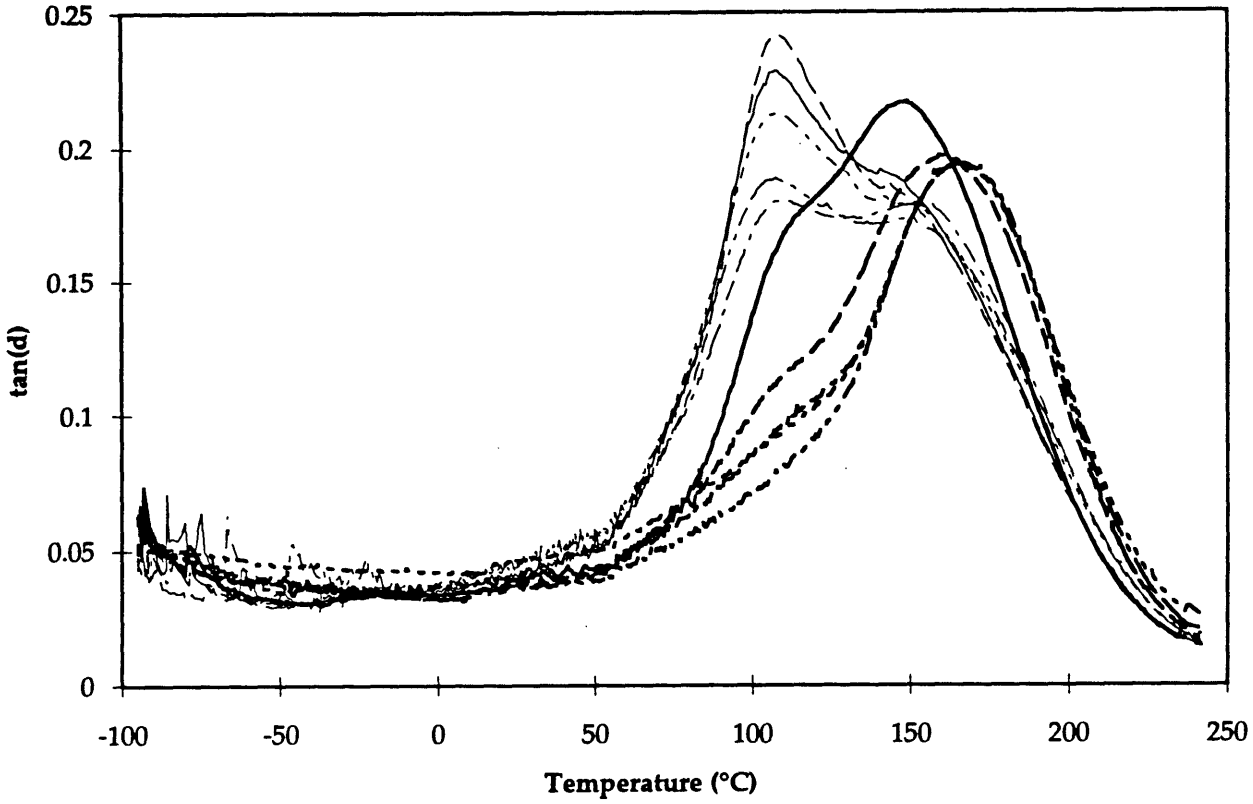

Figure 4.28- Tanδ curves as a function of temperature for MNS specimens containing various rubber contents as determined by DMA performed in tensile mode at a heating rate of 2°C/min and a frequency of 5 Hz.

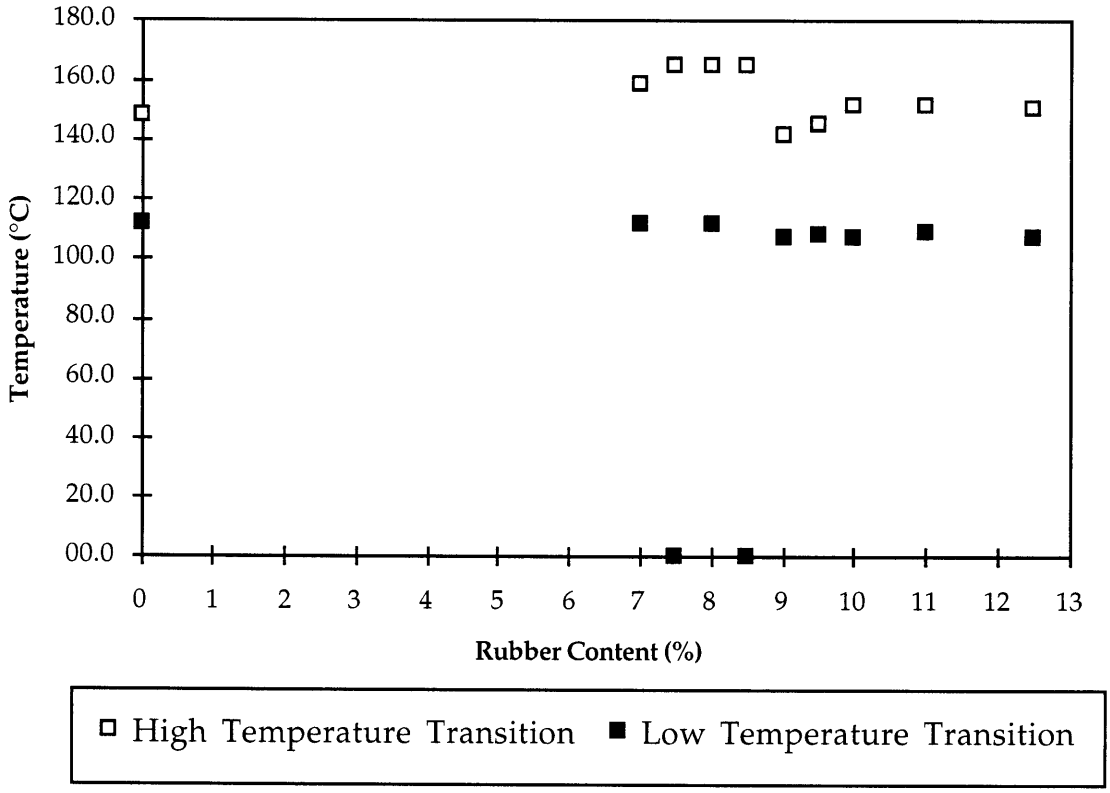

Figure 4.29- Variation of Tg for both primary and secondary transitions in MNS with increasing rubber content as determined by DMA performed at a rate of 2°C/min and a frequency of 5 Hz.

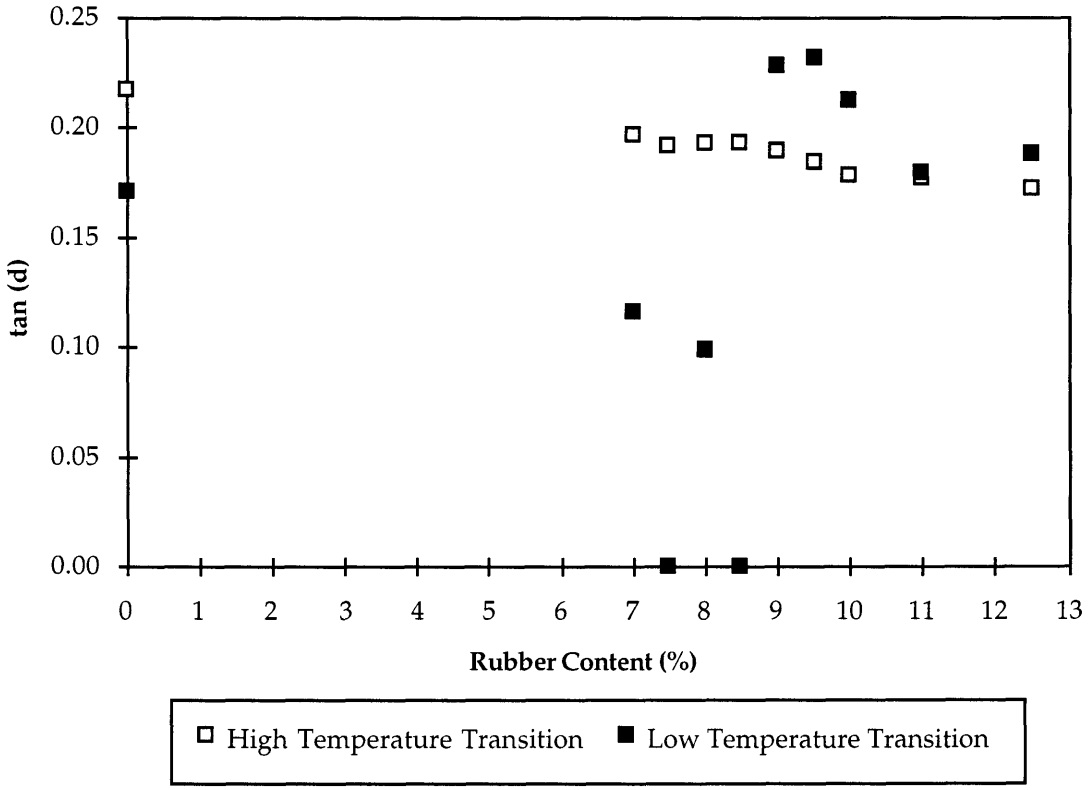

Figure 4.30- Variation of tanδ for both primary and secondary transitions in MNS with increasing rubber content as determined by DMA runs performed at a rate of 2°C/min and a frequency of 5 Hz.

After the phase inversion occurs, both the temperature and intensity of the high temperature transition decrease slightly. With further increase in rubber content, the temperature of this transition decreases sharply at first and then increases to level off to a fairly constant value that is slightly lower than before the inversion. The intensity of the high temperature transition also decreases gradually with rubber contents higher than 9%, and then levels off to a constant value that is slightly lower than that of the material prior to the inversion. On the other hand, the intensity of the low temperature transition increases dramatically after the phase inversion, while the temperature remains unaffected. As the rubber content is increased, the temperature of the low temperature transition continues to remain unchanged, but the intensity begins to decrease once again with increasing rubber content. At about 11% ATBN, the intensities of the high and low temperature transitions are equal.

The unexpected increase in the temperature of the high temperature transition of the 7% ATBN sample over that of the control MNS sample is probably due to the fact that the ATBN reacts more readily with the epoxy than with the polyester. When the epoxy reacts with the ATBN, this leaves less of the lower Tg epoxy component to react with the polyester. Thus, the Tg of the polyester increases. The decrease in the temperature of the high temperature transition at rubber contents over 9% suggests that some of the ATBN has reacted with the polyester to flexibilize it and lower the Tg. An explanation for the decrease in intensity of this transition with increasing rubber content over 9% will be presented shortly.

Now, the unexpected decrease of the intensity of the low temperature transition with increasing rubber content both before and after the phase inversion will be discussed. ATBN is known to be capable of reacting with both the epoxy and polyester, but the reaction with the epoxy is preferred. It is possible that adding the ATBN merely serves to increase the amine content in the system and, therefore, increases the crosslink density of the epoxy to reduce damping. The Tg of the epoxy doesn't increase because the ATBN probably flexibilizes the epoxy to some extent, but the increased crosslink density could counteract the mobilizing effect to render the temperature of this transition unchanged. The amount of ATBN is very low at the

compositions under consideration. Therefore, the ATBN crosslinks are probably very short and cannot absorb large amounts of energy through the typical uncoiling mechanisms. In effect, the rubber is prevented from behaving like a rubber. This would further explain the lack of a low temperature rubber transition in any of the samples examined. This also explains why the intensity of the high temperature transition decreases slightly after the inversion. After the inversion, there is enough ATBN for some to react with the polyester. This lowers the Tg of the polyester, but also increases the crosslink density and lowers the mobility.

Work done by Subramaniam showed that when the rubber content is increased to very high values of around 20% ATBN, the DMA curve exhibits a single transition at a lower temperature and much higher intensity than for the control specimens. The fracture surfaces showed no evidence of secondary domains.[6] This leads to the conclusion that at high enough rubber contents, there is enough ATBN to react both with the epoxy and with a significant portion of the polyester to result in a uniform distribution of components. In addition, the ATBN segments are probably much longer at this high rubber concentration, which could lead to more of a rubber-epoxy blend. It is at this point that the real increase in toughness properties was observed. At 12.5% ATBN, the intensities of the high and low temperature transitions are about the same. It appears that the transition is moving towards a single one, and that the morphology is becoming that of a uniform, highly flexibilized network. It is the creation of an overall flexibilized matrix that results in high toughness properties. However, as stated earlier, this comes at the expense of the other mechanical properties.

4.2 Compositions Containing Pre-Formed Particles

As shown above, the fracture toughness of the MNS systems did not increase significantly until large amounts of rubber were added so as to produce a flexibilized matrix of polyester and epoxy. However, this toughening was seen to come at the expense of the modulus, UTS, and thermal properties. As was discussed in the background section, a bidistribution of particle sizes was shown to produce the greatest toughening effects in epoxies by promoting both crazing and shear banding mechanisms.

Also, as stated earlier, the actual rubber domains within the rubber-rich phases of MNS compositions containing less than 9% ATBN were found to be extremely small (200-400nm). Therefore, it was hoped that adding additional large rubber particles (with diameters of approximately 1 micron) might improve the fracture toughness at low enough ATBN contents to preserve the mechanical properties. Thus, several types of second phase particles were added to MNS containing 7.5% ATBN (this content falls below that necessary for the phase inversion). As was discussed earlier, the additives were in the form of rubber particles, glass spheres, and reactive CTBN rubber that forms in-situ particles.

4.2.1 Nipol and Paraloid Particles

4.2.1.1 Plane Strain Fracture Toughness

The first type of second phase particles investigated was Nipol DP5078 particles from Zeon Chemicals. These acrylonitrile butadiene particles were the largest particles used in this study with diameters reported to be in the range of 100 microns. 5% Nipol particles by weight were added to the 7.5% ATBN formulation. The next type of modifier used was a Paraloid KM334 particle from Rohm and Haas. This core shell particle consisted of a pMMA shell with a butyl acrylate core and was considerably smaller than the Nipol particles with diameters reported to be in the sub-micron range. Because the Paraloid particles tended to float to the surface of the uncured resin, 1.4% cabosil fumed silica was added to the formulations containing 5% Paraloid particles in order to increase the viscosity of the resin and keep the particles in suspension. A casting of MNS with 7.5% ATBN and 2.5% fumed silica particles was also produced to see if the addition of the fumed silica particles in themselves would alter the properties of the MNS. It was possible that the small fumed silica particles would migrate to the ATBN rich domains and act as deformation promoters in their own right.

Figure 4.31 shows the plot of fracture toughness values for the control 7.5% ATBN sample, and samples with 7.5% ATBN and either 5% Nipol, 5% Paraloid or 2.5% fumed silica particles. The K_{Ic} values for these compositions

are given in Table 4.3. The sample with the Nipol particles shows a measurable increase in the fracture toughness over the control 7.5% ATBN sample. The KIc increases from an average value of 0.6465 ksi*in1/2 for the control sample to 0.7483 ksi*in1/2 for that containing the Nipol particles. This increase is not quite as significant when it is noted that the addition of the rubber particles brings the total rubber content to 12.5%. As stated earlier, the fracture toughness for an MNS sample containing 12.5% ATBN was found to be around 0.71 ksi*in$^{1/2}$. This value is only slightly lower than the average value found for the sample containing the Nipol particles.

Table 4.3- Mechanical properties of MNS samples with various second phase particles.

Sample	KIc ksi*in1/ 2	Modulus ksi	GIc lb/ in
7.5% ATBN Control	0.6465 (0.1017)	508.7	0.8380 (0.2427)
9.5% ATBN Control	0.7171 (0.0687)	545.8	0.9423 (0.1853)
5% Nipol	0.7483 (0.0393)	377.8	1.4853 (0.1546)
5% Paraloid	0.6564 (0.0616)	406.3	1.0682 (0.1947)
2.5% Cabosil	0.6654 (0.0265)		
2.5% CTBN middle	0.6782 (0.0527)	425.1	1.0873 (0.1709)
2.5% CTBN top	1.0969 (0.0596)		
5% EXL 5136	0.7072 (0.0369)	344.1	1.4567 (0.1514)
5% EXL 2691	0.7197 (0.0498)	378.0	1.3756 (0.1895)
5% EXL 2330	0.7082 (0.0718)	368.9	1.3710 (0.2827)
5% Solid Glass 6020	0.6195 (0.0609)		
5% Hollow Glass 6020	0.8093 (0.0402)		
5% Solid Glass 6040	0.5151 (0.0562)	495.5	0.5409 (0.1210)
5% Amino PDMS*	0.6872 (0.0211)	315.1	1.5001 (0.0919)
5% Epoxy PDMS*	0.7169 (0.0347)	338.8	1.5200 (0.1469)
5% Silanol PDMS*	0.6446 (0.0250)	334.9	1.2421 (0.0958)

* Samples contain 9.5% ATBN. All others contain 7.5% ATBN.

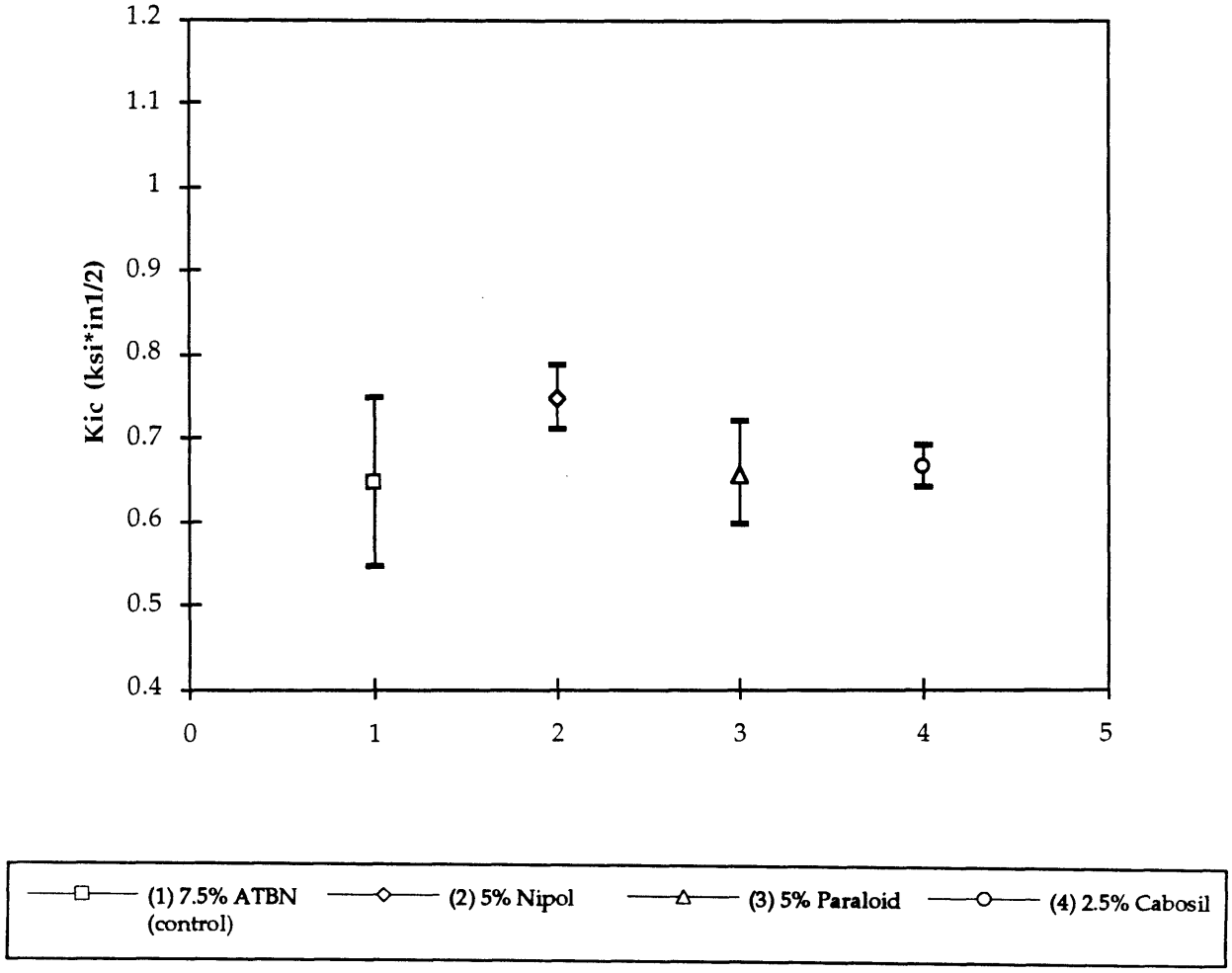

Figure 4.31- Fracture toughness values for MNS compact tension specimens containing 7.5% ATBN, and samples with 7.5% ATBN and either 5% Nipol, 5% Paraloid or 2.5% fumed silica particles tested according to ASTM D 5045-93 at a rate of 0.2 in./min.

The load versus displacement curve for the sample containing Nipol particles and that of a 7.5% ATBN MNS control sample are shown in Figures 4.32 and 4.33. The load displacement profile during fracture for the sample with Nipol particles has a larger area under the curve than the 7.5% ATBN control sample, and the sample with Nipol particles has more than one peak in the curve. Typical load versus displacement curves for rubber toughened materials are shown in figure 4.34. A curve with only a single, sharp peak represents stable, brittle crack growth, while a broad and rounded peak indicates ductile, stable crack growth. Somewhere in between these two extremes is a curve with one sharp primary peak and several sharp secondary peaks. This type of curve represent brittle, unstable crack growth. The first peak represents the initial propagation stage, while the secondary peaks represent subsequent arrest and reinitiation mechanisms as the crack proceeds through the sample. A reinitiating crack absorbs more energy than a stable brittle crack, while a ductile stable crack growth mechanism absorbs the most energy of all. It appears that the addition of the Nipol particles has increased the ability of the sample to arrest the propagating crack. The greater area under the curve for the sample containing the Nipol particles also represents greater energy absorption. It is, therefore, surprising that the fracture toughness of the sample containing the Nipol particles is not substantially higher than that of the 7.5% ATBN control specimen. It is possible that the Nipol particle are too large to effectively toughen the sample. They appear to be effective in arresting crack propagation, but the presence of such large areas of weaker material may prevent them from actually toughening the material against crack initiation.

In order to determine if there was an increase in crack propagation resistance, the G_{Ic} for the Nipol containing specimen was calculated. The G_{Ic} also showed an increase from 0.838 lb/in for MNS with 7.5% ATBN to 1.485 lb/in for the Nipol containing sample (Figure 4.35 and Table 4.3). This is a significant increase, but it comes at the expense of the modulus, which drops from a value of 509 ksi for the 7.5% ATBN control sample to a value of 378 ksi for the Nipol containing sample. Because of this substantial drop in the modulus, it is not clear whether the G_{Ic} increase represents actual toughening or is just an artifact of the decreased modulus.

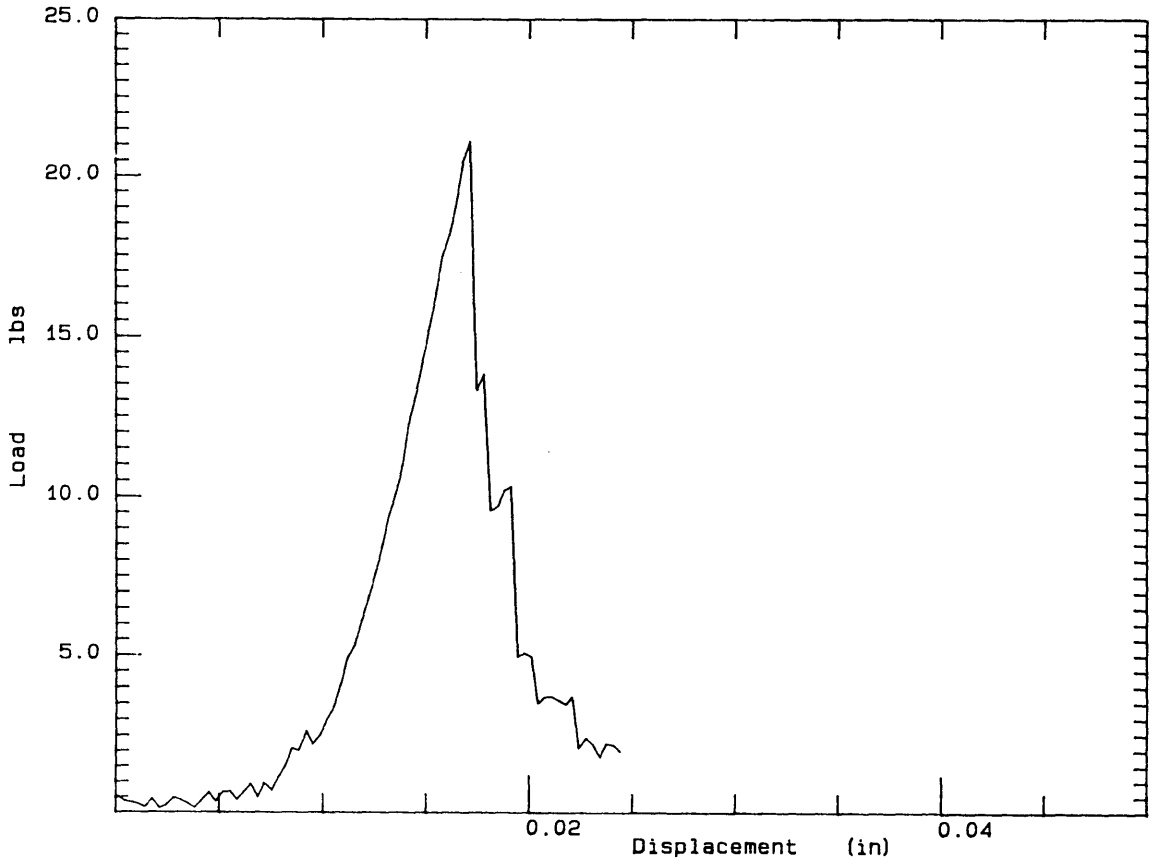

Figure 4.32- Load versus displacement curve for an MNS compact tension specimen containing 7.5% ATBN tested at a rate of 0.2 in/min.

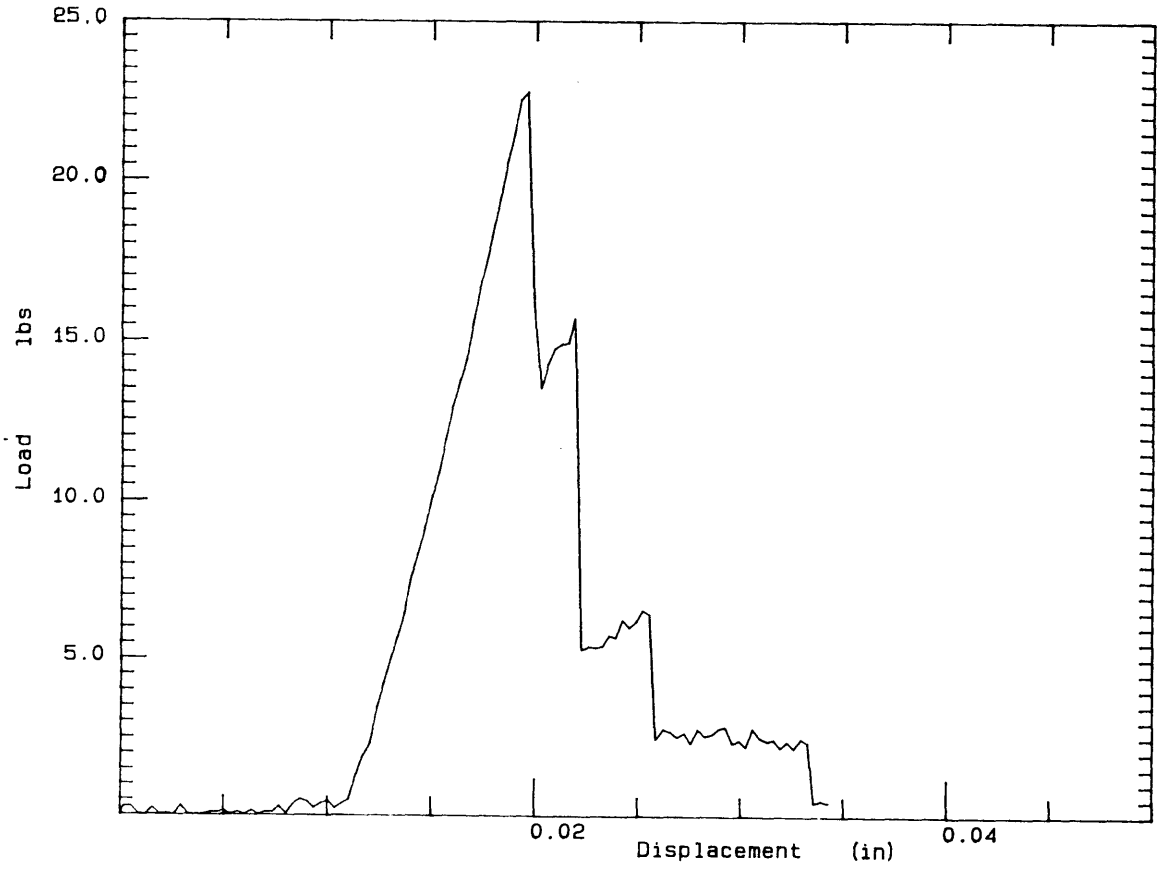

Figure 4.33- Load versus displacement curve for an MNS compact tension specimen containing 7.5% ATBN and 5% Nipol particles tested at a rate of 0.2 in/min.

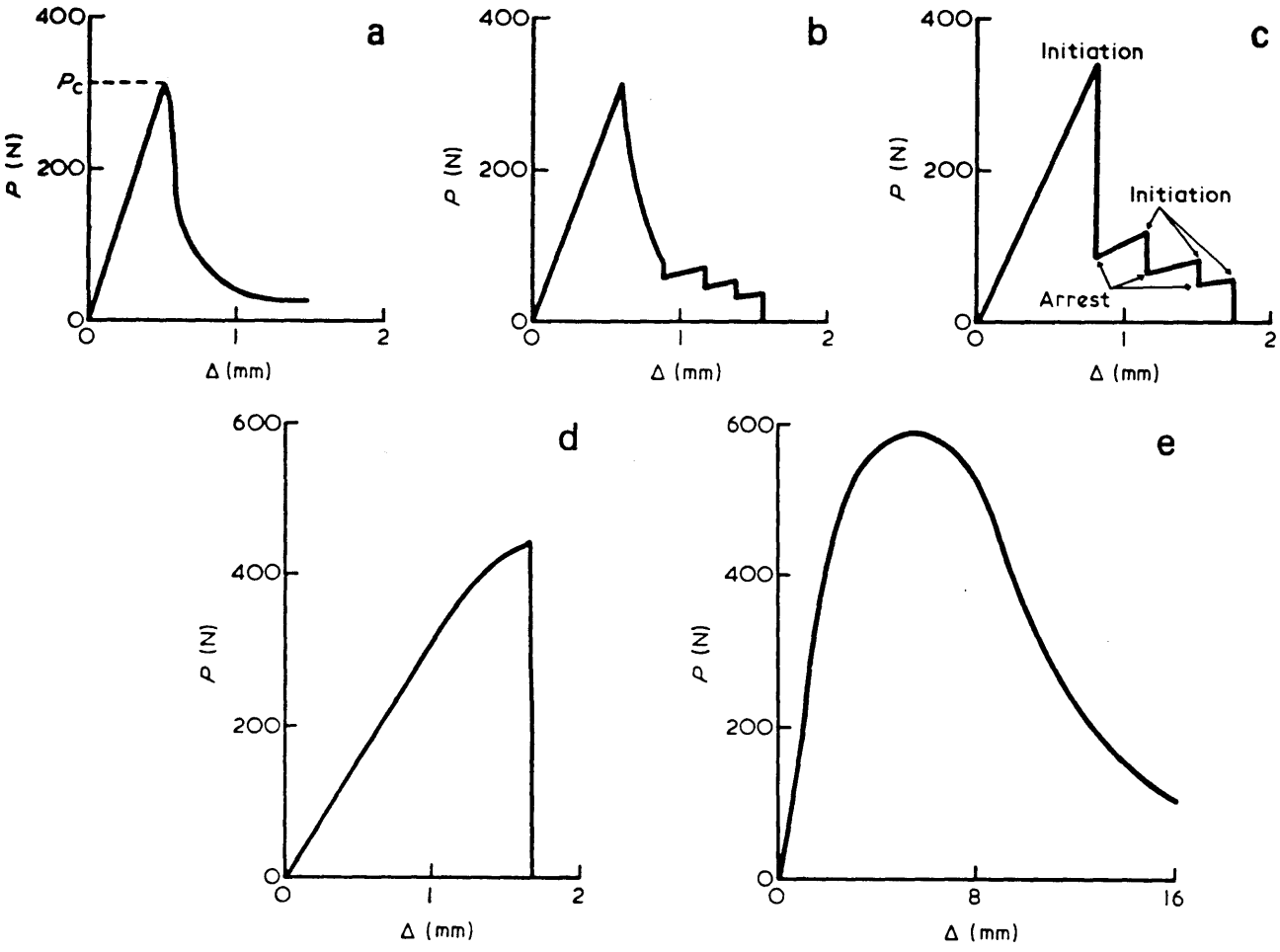

Figure 4.34- Schematic of load versus deflection curves for rubber-modified epoxy associated with different types of crack growth: a) brittle stable crack growth, b) transition between brittle stable and brittle unstable crack growth c) brittle unstable crack growth, d) transition between brittle unstable and ductile stable crack growth, and e) ductile stable crack growth.[61]

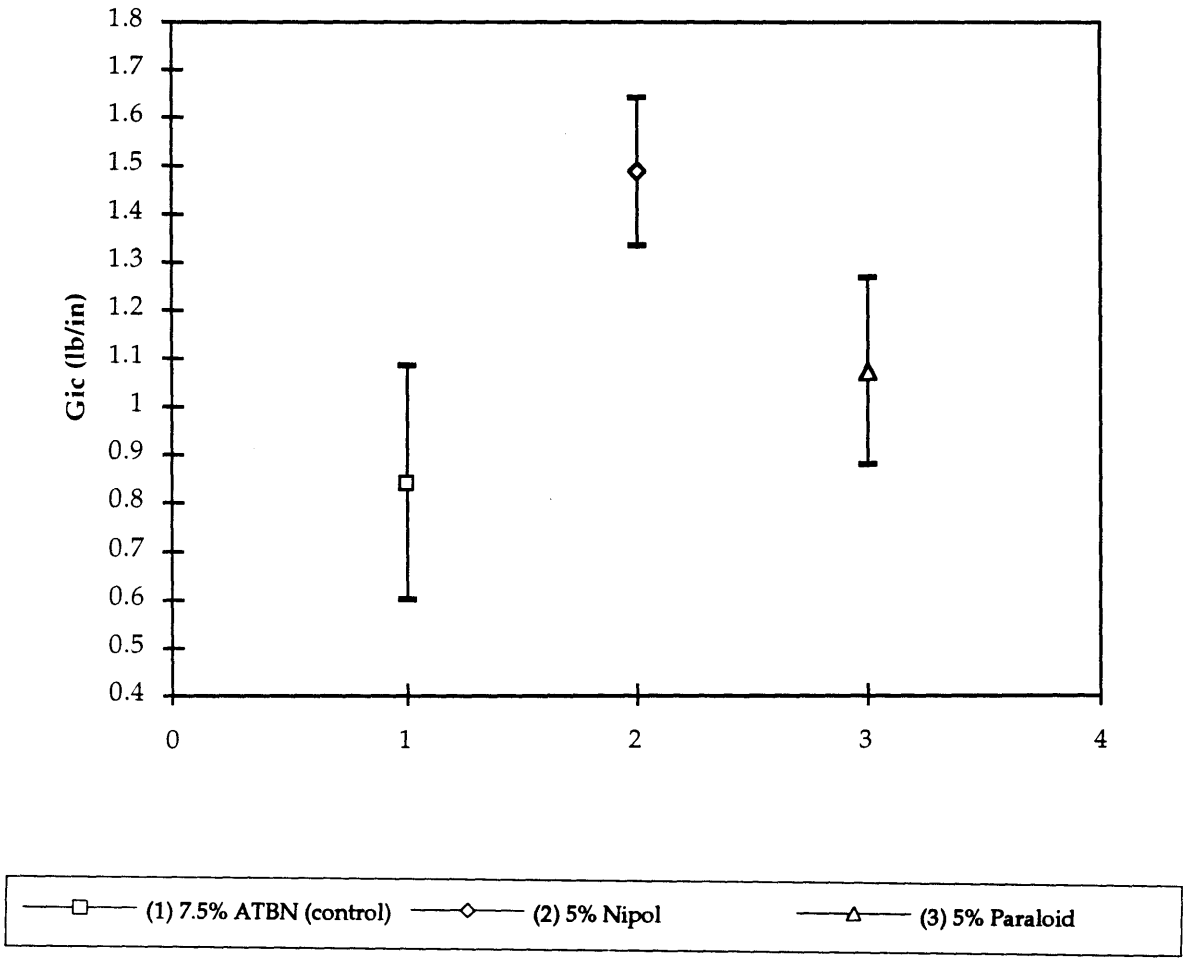

Figure 4.35- Gic values for MNS compact tension specimens containing 7.5% ATBN and samples containing 7.5% ATBN and either 5% Nipol or 5% Paraloid particles tested at a rate of 0.2 in/min.

The fracture toughness of the sample containing 5% Paraloid and that of the sample containing 2.5% fumed silica increased only slightly over the value for the control 7.5% ATBN sample. The Paraloid containing sample produced an average value of 0.6564 ksi*in$^{1/2}$. This low value of fracture toughness is especially surprising since the effective rubber content of this sample is also 12.5%. This puts the fracture toughness of this sample considerably below the value for the 12.5% ATBN sample. The load versus displacement curve for the Paraloid containing sample may help explain this unexpected result. The curve drops off very sharply, has a low area under the curve, and shows no evidence of crack arrest mechanisms (Figure 4.36). The G_{Ic} value for the 5% Paraloid sample increases to a value of around 1.10 lb/in., as compared to the value of 0.8380 lb/in. for the control 7.5% ATBN sample. However, this increase can again be attributed to the increased rubber content and simultaneous decrease in modulus to 406 ksi from 509 ksi for the 7.5% ATBN control specimen.

The average K_{Ic} value of the sample containing 7.5% ATBN and 2.5% fumed silica was around 0.6654 ksi*in$^{1/2}$. This value is also very close to that of the control 7.5% ATBN sample. The load versus displacement curve for this sample appears to be very similar to the control sample, both in area under the curve and crack arrest evidence (Figure 4.37). Thus, it appears that the addition of a small weight percent of fumed silica has no effect on the fracture properties of the MNS. Therefore, it seems that adding fumed silica to increase the viscosity of the uncured resin and keep the particle additives in solution will not have any adverse effects on the fracture properties.

4.2.1.2 Scanning Electron Microscopy

4.2.1.2.1 Nipol Particles

In order to determine the effect of the second phase particles on the morphology of the system, the fracture surfaces were examined using SEM. The polished surfaces of samples of the same composition were also examined using SEM so that the morphology of these samples could be observed unobscurred by the deformation process. In both cases, the samples

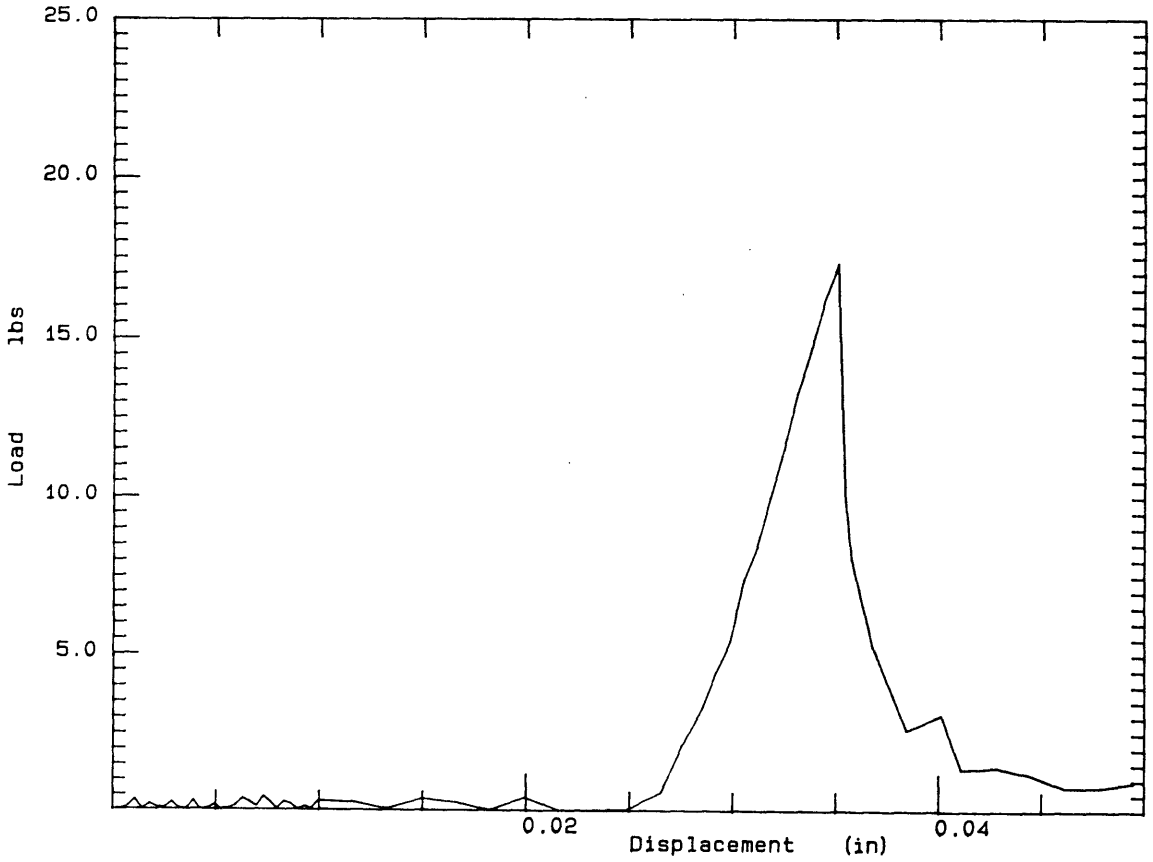

Figure 4.36- Load versus displacement curve for an MNS compact tension specimen containing 7.5% ATBN and 5% Paraloid particles tested at a rate of 0.2 in/min.

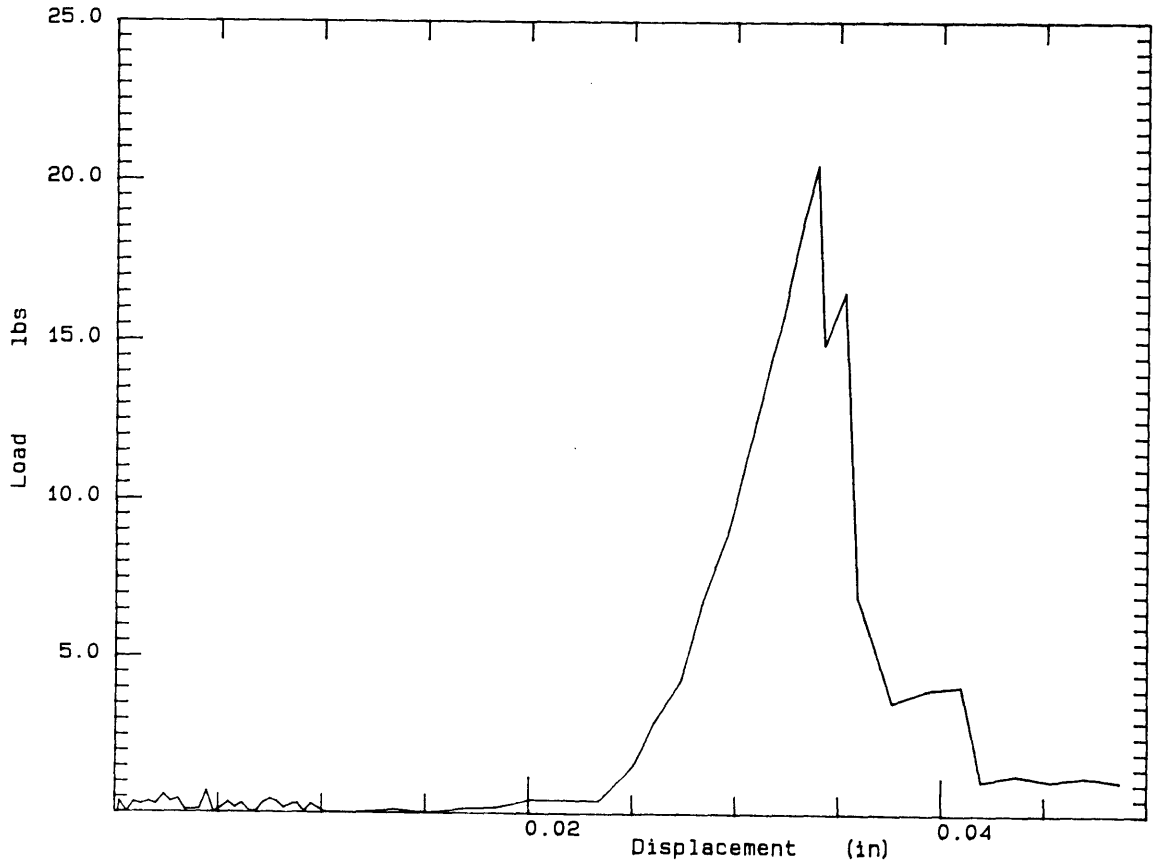

Figure 4.37- Load versus displacement curve for an MNS compact tension specimen containing 7.5% ATBN and 2.5% fumed silica particles tested at a rate of 0.2 in/min.

specimen containing 7.5% ATBN and 5% Nipol particles. The rubber domains on this surface appear as large blobs, and not the perfectly circular domains found for the control 7.5% ATBN specimen (Figure 4.5). As can be seen, the smaller, circular domains can still be found, and are often surrounded by or partially incorporated into the edges of the large Nipol domains. The diameter of the Nipol particles appear to be much larger than the 100 microns specified by the supplier.

Upon examining the unreacted Nipol particles under a light microscope at 40X, it appeared that the particles had clumped together to form larger blobs consisting of 5 or more small, spherical particles. When styrene monomer was added to these particles, they swelled dramatically until they burst their boundaries and coalesced together. Therefore, it is thought that the 100 micron Nipol particles were dissolved by the styrene monomer in the MNS system, then re-precipitated back out again to form large, amorphous rubber-rich domains. As there is a considerably lower volume fraction of circular ATBN-rich domains on the surface of this sample than seen for a typical 7.5% ATBN control sample, it is probable that the Nipol domains also contain a significant amount of ATBN.

When the polished surface of a sample from the same casting containing 7.5% ATBN and 5% Nipol particles was examined using backscattered electrons, it appears that the large, amorphous rubber-rich domains are composed of multiple phases (Figures 4.39 and 4.40). The darkest region in Figure 4.40 is a polyester-rich matrix occlusion. The darker of the rubber-rich portions appears to be ATBN-rich material, and the grainy rubber-rich portions are thought to contain the Nipol. Rubber domains with diameters between 0.5 and 1.5 microns can be identified in this grainy region. It would make sense that these domains are composed of Nipol, because the molecular weight of the butadiene in the Nipol particles is probably higher than that in the ATBN rubber. Thus, the Nipol rubber should form larger sized regions of pure rubber within the rubber-rich domains, which would stain more brightly than the smaller ATBN regions. The separation of the ATBN and the Nipol within the large domains is probably also due to the

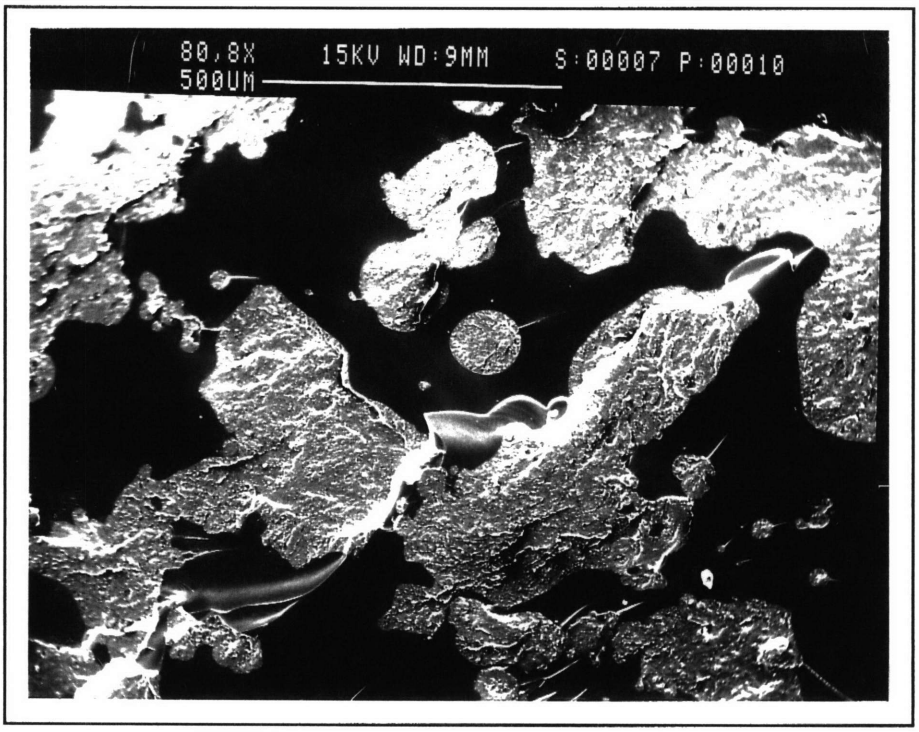

Figure 4.38- Fracture surface of an MNS compact tension specimen containing 7.5% ATBN and 5% Nipol particles.

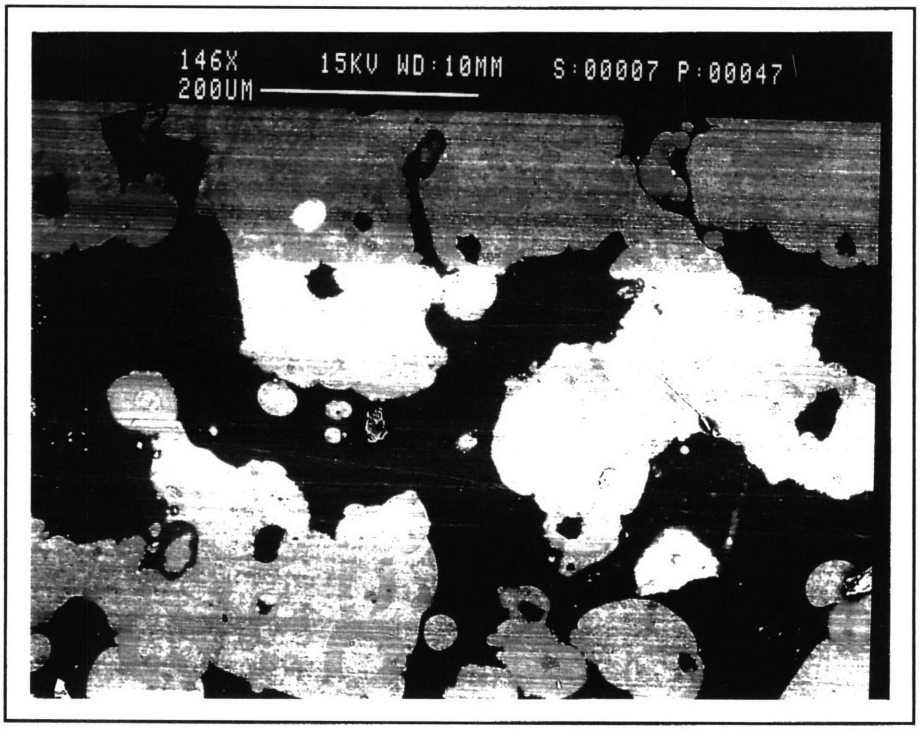

Figure 4.39- Backscattered image of the polished surface of an MNS specimen containing 7.5% ATBN and 5% Nipol particles.

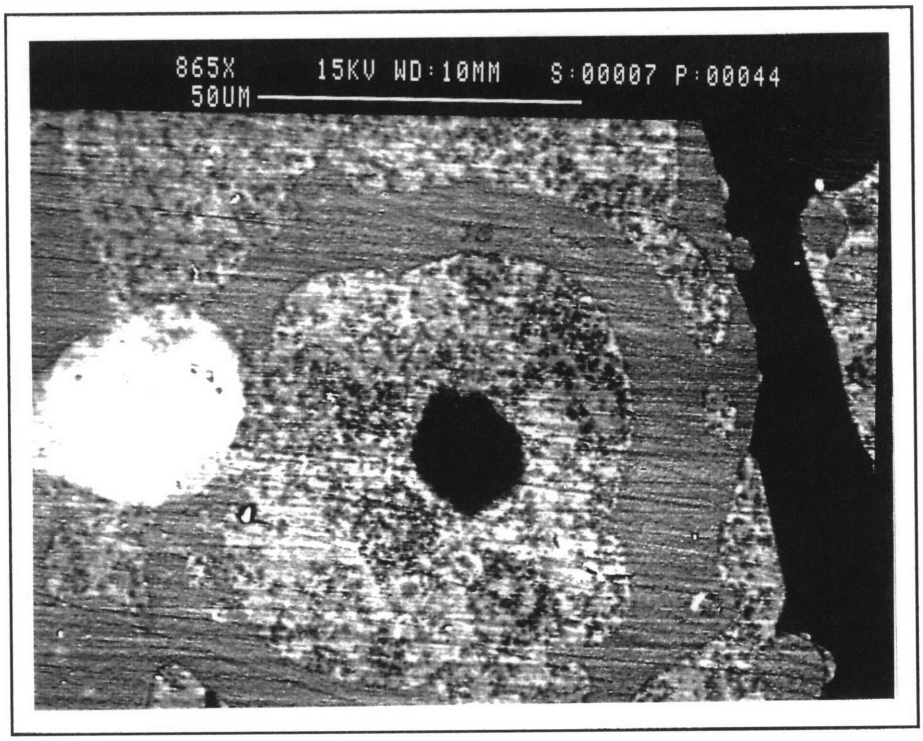

Figure 4.40- Backscattered image of the phase separation in a rubber-rich domain on the polished surface of an MNS specimen containing 7.5% ATBN and 5% Nipol particles.

differences in molecular weight of the two butadienes. The bright region in Figure 4.40 is probably a very rubber-rich domain of some sort. These domains were prevalent on the surface and may be a portion of the original Nipol particle that did not dissolve in the solution. The unusual miscibility between the two types of butadiene and the polyester-rich matrix is very interesting in this sample. The large rubber-rich domains almost make up a co-continuous network with the polyester-rich phase. This could explain why the samples containing the Nipol particles showed a small, but measurable, increase in fracture toughness over the 7.5% ATBN sample.

4.2.1.2.2 Paraloid Particles

Figure 4.41 contains a micrograph of the fracture surface of an MNS compact tension specimen containing 7.5% ATBN and 5% Paraloid particles. The morphology consists of a collection of Paraloid particles clumped into circular domains (Figure 4.42) that are surrounded by amorphous regions of ATBN-rich material. The polished surface of the sample containing Paraloid particles is shown in Figure 4.43. Neither the pMMA shell nor the butyl acrylate core of the Paraloid particles contains double bonds that can react with the osmium tetroxide. Therefore, the Paraloid-rich circular domains do not appear bright. These regions do, however, contain a few very bright ATBN occlusions. These occlusions do not appear to contain any Paraloid particles.

It also appears that the Paraloid particles attract the ATBN to their surfaces, as there is a significant amount of bright material present in the highly magnified view of the particle-rich domain (Figure 4.44). It is possible that the Paraloid particles rob the ATBN-rich domains of some of the ATBN. Notice that the brightest regions in Figure 4.43 are those immediately surrounding the particle-rich domains and the ATBN-rich occlusions within these regions. The migration of the ATBN to the surfaces of the particles, and out of the main portions of the domains, could explain why the fracture toughness of the specimens containing the Paraloid particles did not exhibit as large an improvement over the control specimens as was expected.

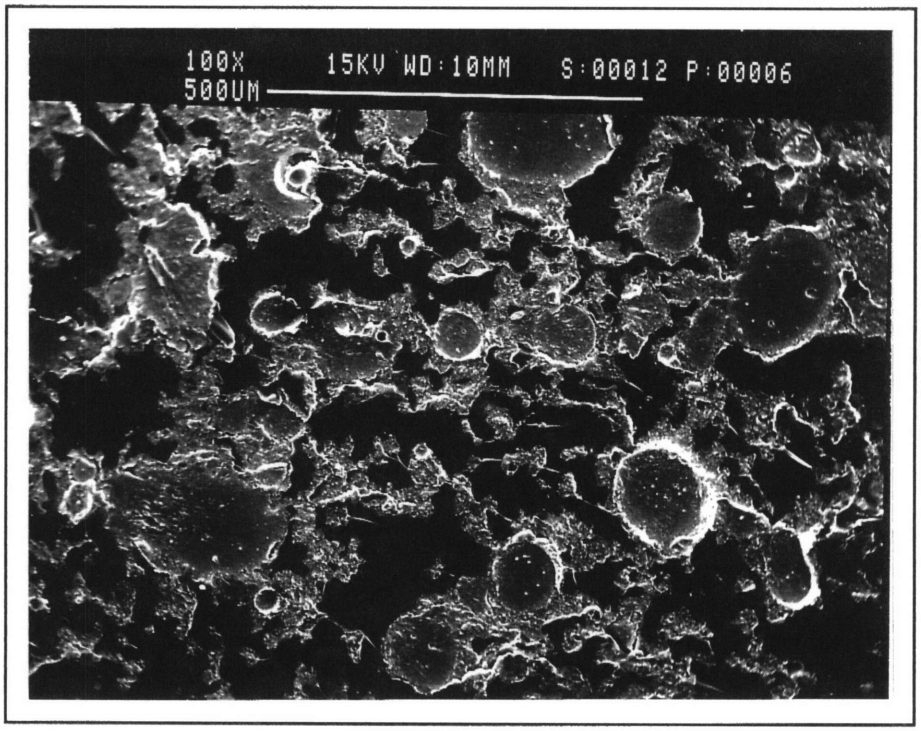

Figure 4.41- Fracture surface of an MNS compact tension specimen containing 7.5% ATBN and 5% Paraloid particles.

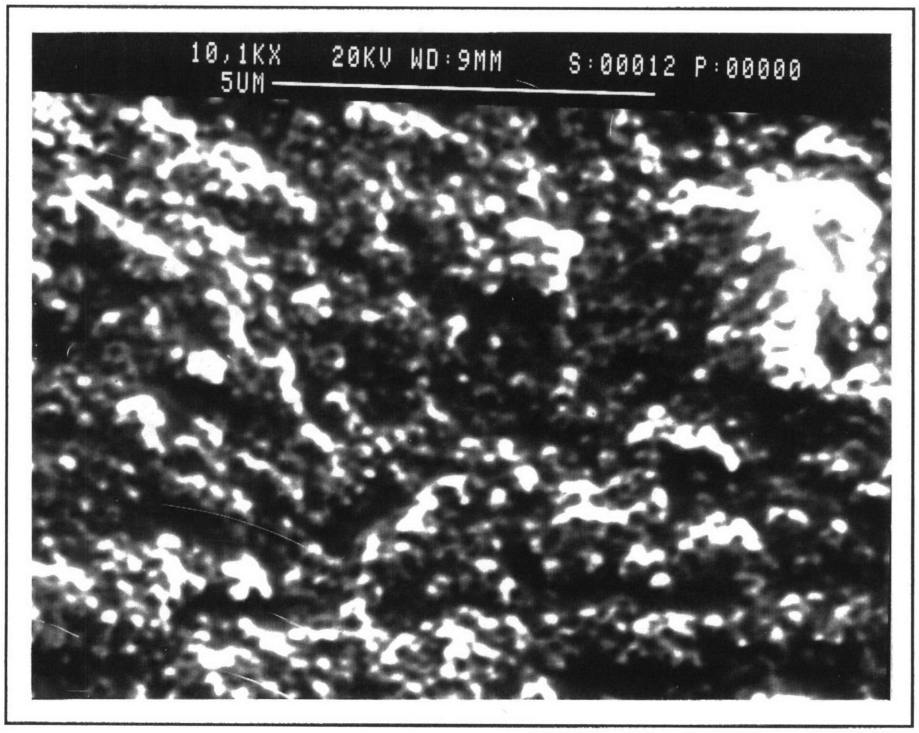

Figure 4.42- Paraloid particles within the circular domains on the fracture surface of an MNS compact tension specimen containing 7.5% ATBN and 5% Paraloid particles.

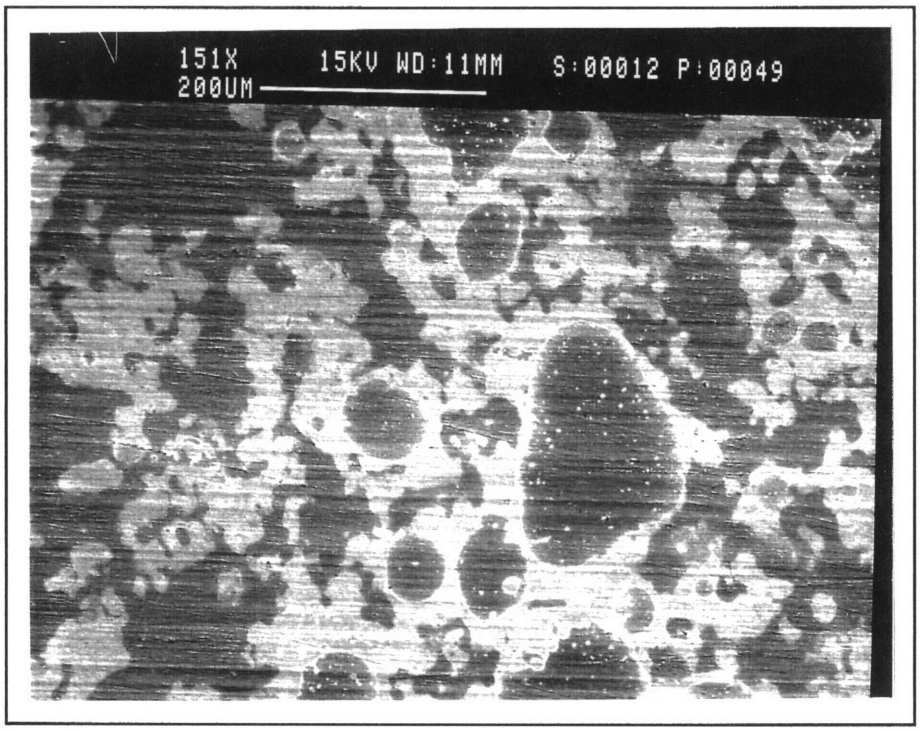

Figure 4.43- Backscattered image of the polished surface of an MNS specimen containing 7.5% ATBN and 5% Paraloid particles.

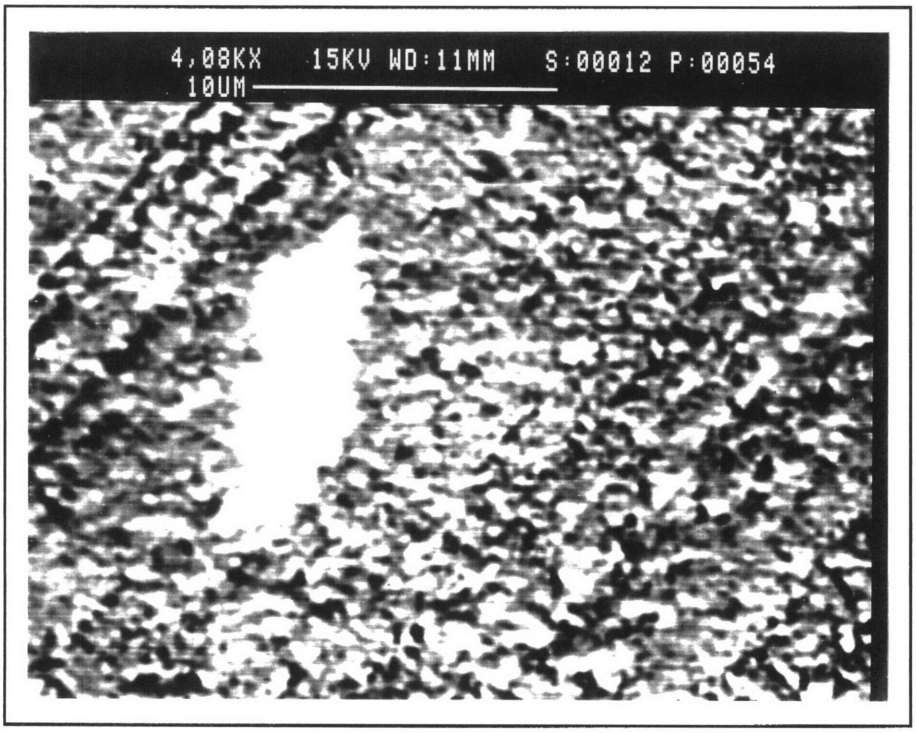

Figure 4.44- Backscattered image of a magnified rubber-rich domain containing Paraloid particles on the polished surface of an MNS sample containing 7.5% ATBN and 5% Paraloid particles.

4.2.1.2.3 Fumed Silica Particles

The fracture surface of the compact tension specimen containing 7.5% ATBN and 2.5% cabosil fumed silica particles is shown in Figure 4.45. The most evident difference between the morphology of this sample and that of the 7.5% ATBN control sample is that the ATBN domains are no longer perfectly spherical. Instead, the domains are basically circular with rough edges. This change in morphology is most likely the result of the large increase in resin viscosity caused by the addition of the fumed silica. The viscosity differences could affect the phase separation behavior. The polished surface of a sample of identical composition is shown in Figure 4.46. Evidence of fumed silica particles was found in both the brighter, well-defined domains as well as in the fuzzier domains (Figure 4.47). No evidence of particles was found in the matrix region. While the cabosil particles are found exactly where they were supposed to be for increased toughness, there was no accompanying increase in fracture toughness for these samples. This could be due to clumping of the particles. The indentations that provide the evidence for the existence of particles in the rubber-rich domains are much larger than would be expected to be formed by individual fumed silica particles. Thus, it is postulated that the fumed silica particles are clumped together within the ATBN-rich domains.

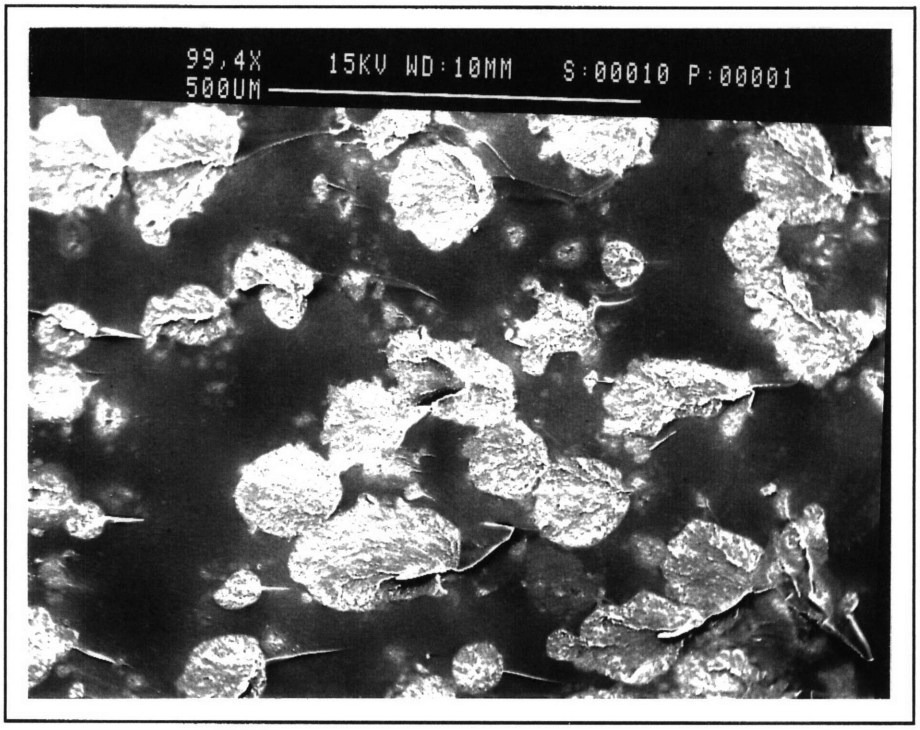

Figure 4.45- Fracture surface of an MNS compact tension specimen containing 7.5% ATBN and 2.5% fumed silica.

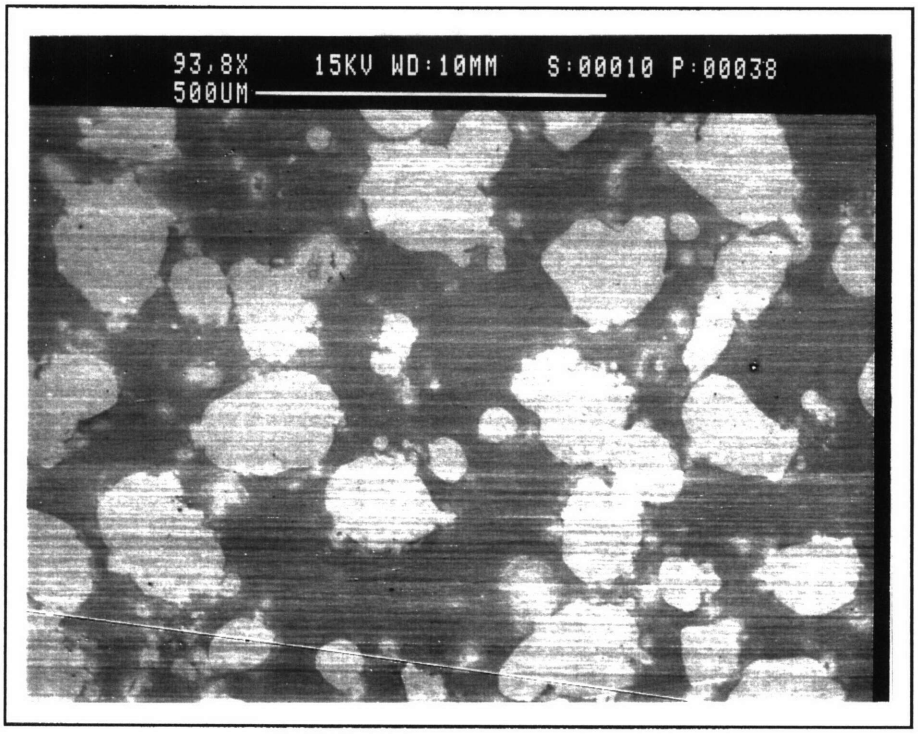

Figure 4.46- Backscattered image of the polished surface of an MNS sample containing 7.5% ATBN and 2.5% fumed silica.

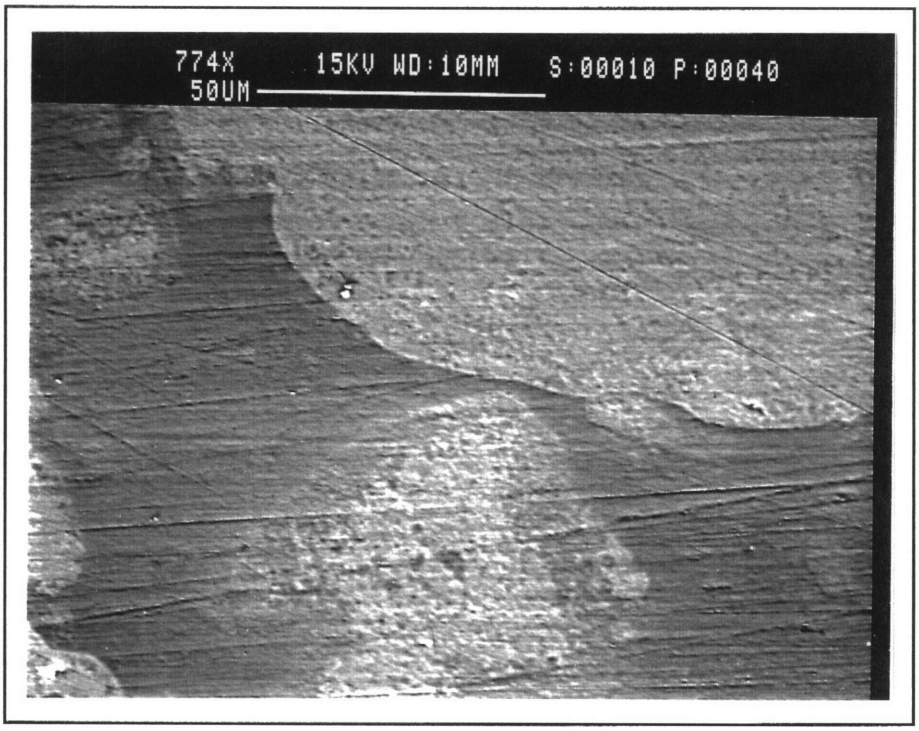

Figure 4.47- Backscattered image of fumed silica particles in ATBN-rich domains on the polished surface of an MNS specimen containing 7.5% ATBN and 2.5% fumed silica.

4.2.1.3 Dynamic Mechanical Analysis

Figure 4.48 contains the tanδ curves for samples containing 7.5% ATBN and either 5% Nipol particles, 5% Paraloid particles, or 2.5% Cabosil fumed silica particles, in addition to the control samples containing 0% ATBN and 7.5% ATBN. The values of the intensities and locations of the transitions are shown in Table 4.4. All three additives produce curves that have both a primary and secondary transition. All three additives also result in a broadening of the curves, which indicate an increased scale of heterogeneity.

The Nipol and Paraloid particles exhibit both primary and secondary transition peaks at almost identical temperatures of around 162°C and 111°C respectively. These primary transitions also occur at the same temperature as that for the 7.5% ATBN control samples. However, the values of the intensity of the primary transition for both the Nipol and Paraloid compositions, which are almost identical to each other at around 0.17, are much lower than that of around 0.19 for the 7.5% ATBN control specimens. This indicates a decrease in mobility of the polyester phase of the castings containing Nipol and Paraloid particles. The secondary transition in the sample containing Paraloid particles is more distinct than in that containing Nipol particles, and has a higher intensity of around 0.15 as opposed to an average of around 0.13 for the sample containing Nipol particles. This would indicate that the epoxy phase is less well mixed and posses more mobility in the specimen containing Paraloid particles than in that containing Nipol particles.

The primary transition for the samples containing Cabosil particles occurs at a slightly higher temperature than that of the 7.5% ATBN control specimens, while the secondary transition occurs at a slightly lower temperature than that of the 7.5% ATBN control specimen and is much less distinct. Both peaks also have lower intensities than the control. The lower intensities of the peaks indicate that the mobilities of both the polyester and epoxy have been reduced by the addition of cabosil. The fact that the secondary transition is very faint indicates that the epoxy is almost as well distributed as in the 7.5% ATBN control sample.

Table 4.4- Values of Tg and tan(d) for both primary and secondary transitions in MNS samples containing 7.5% ATBN and samples with 7.5% ATBN and either 5% Nipol, 5% Paraloid, or 2.5% Cabosil fumed silica particles as determined by DMA runs performed at a rate of 2°C per minute and a frequency of 5 Hz.

Sample	High Temperature Tg (°C)	Low Temperature Tg (°C)	High Temperature tan(d)	Low Temperature tan(d)
0% ATBN	147.6	112.3	0.2173	0.1709
7.5% ATBN	164.8	none	0.1930	none
9.5% ATBN	145.4	108.4	0.2323	0.1843
5% Nipol	163.0	111.4	0.1689	0.1346
5% Paraloid	160.9	111.2	0.1716	0.1513
2.5% Cabosil	169.6	104.3	0.1551	0.1073

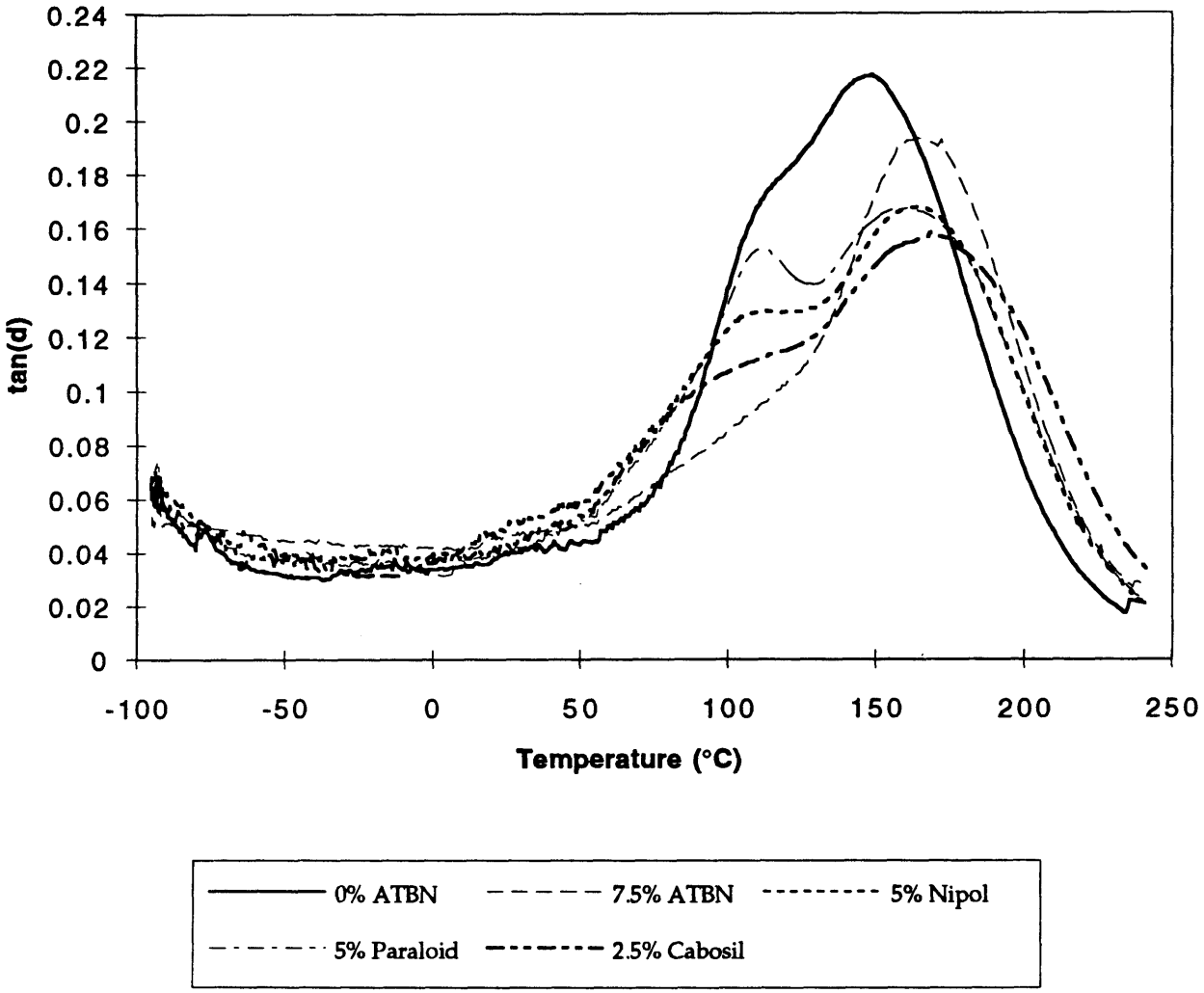

Figure 4.48- Tanδ curves as a function of temperature for MNS specimens containing 7.5% ATBN and samples with 7.5% ATBN and either 5% Nipol, 5% Paraloid or 2.5% Cabosil fumed silica particles determined by DMA performed in tensile mode at a heating rate of 2°C/min and a frequency of 5 Hz.

4.2.2 CTBN Liquid Rubber

Many studies have shown that carboxyl-terminated acrylonitrile butadiene (CTBN) liquid rubber forms in-situ rubber domains with diameters of 1-5 microns in epoxy resin.[20] In order to verify these findings, a casting was made containing solely epoxy resin and 10% CTBN liquid rubber. The fracture surface revealed CTBN domains in the 0.5-1.0 micron size range. Because the CTBN was found to form in-situ particles of the desired size in the epoxy resin system, an MNS casting was made containing 7.5% ATBN and 2.5% CTBN. The finished casting had phase separated into three distinct regions. The middle regions was by far the largest and had a grainy appearance. The top and bottom regions were much smaller in size and were completely transparent. However, the bottom region was slightly darker in color than the top region. A second casting of the same composition showed the same separation behavior. It is thought that the separation was due to the thermal gradient from the bottom to the top of the casting. Since the total rubber content in the ATBN and CTBN casting is 10%, which brings the level just to the phase inversion point in ATBN modified MNS, it is possible that these temperature differences became critical. If cross-linking was faster in the bottom of the casting, it could have pushed the rubber to the top of the casting.

4.2..2.1 Fracture Toughness

Figure 4.49 shows the fracture toughness values for samples taken from the top and middle portions of the 7.5% ATBN and 2.5% CTBN casting (The bottom region of the casting was too small to make compact tension specimens). Table 4.3 gives the values for the fracture toughness of samples taken from the top and middle regions. The average fracture toughness values for samples taken from the middle region of the CTBN containing casting is 0.6782 ksi*in$^{1/2}$. Considering that the total rubber content in this sample is 10%, the fracture toughness is not considerably higher than the value of 0.6465 ksi*in$^{1/2}$ for the 7.5% ATBN control sample. The load versus displacement curve for the sample taken from the 7.5% ATBN and 2.5% CTBN casting is slightly broader than for the 7.5% ATBN control sample, but does not show much evidence of crack arrest (Figure 4.50).

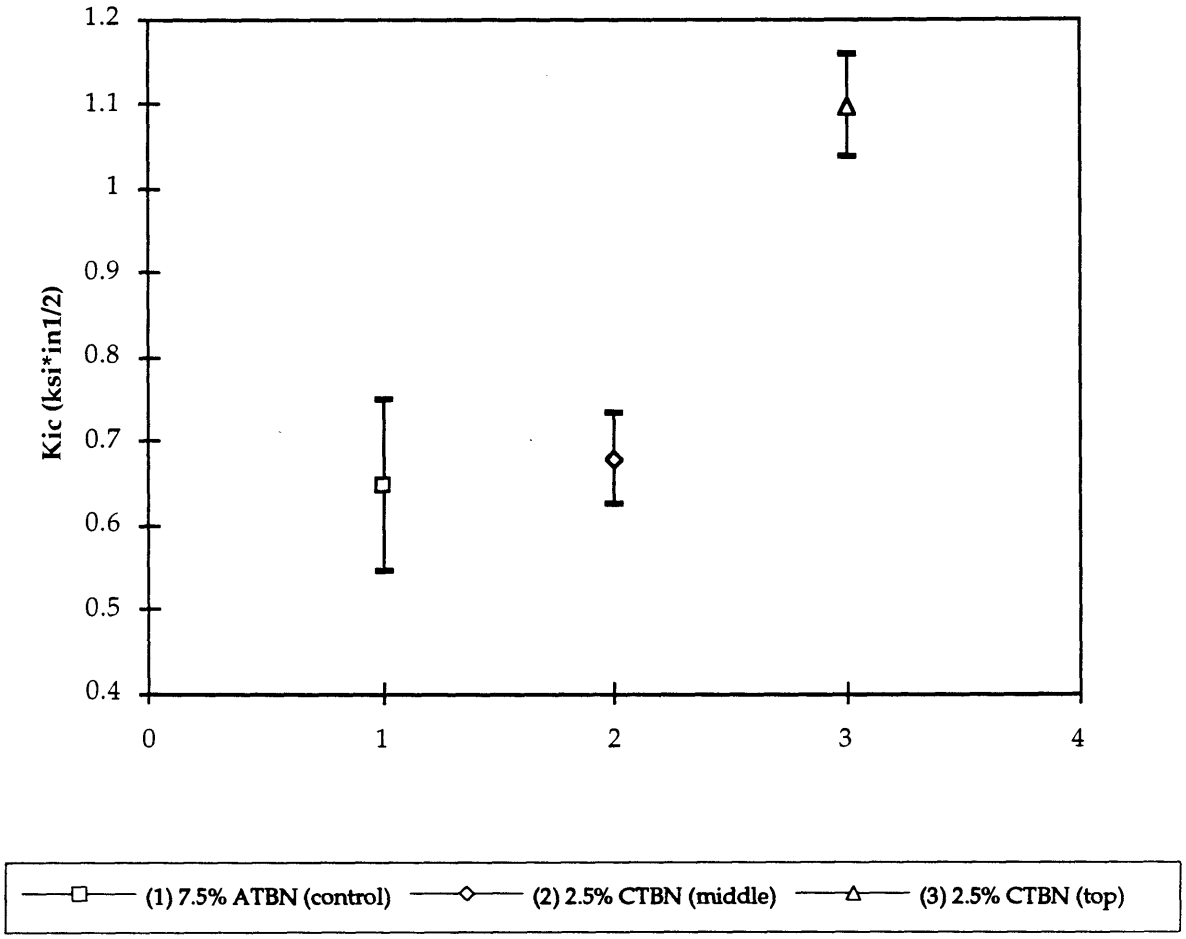

Figure 4.49- Fracture toughness values for MNS compact tension specimens taken from the top and middle of a casting containing 7.5% ATBN and 2.5% CTBN tested according to ASTM D 5045-93 at a rate of 0.2 in./min.

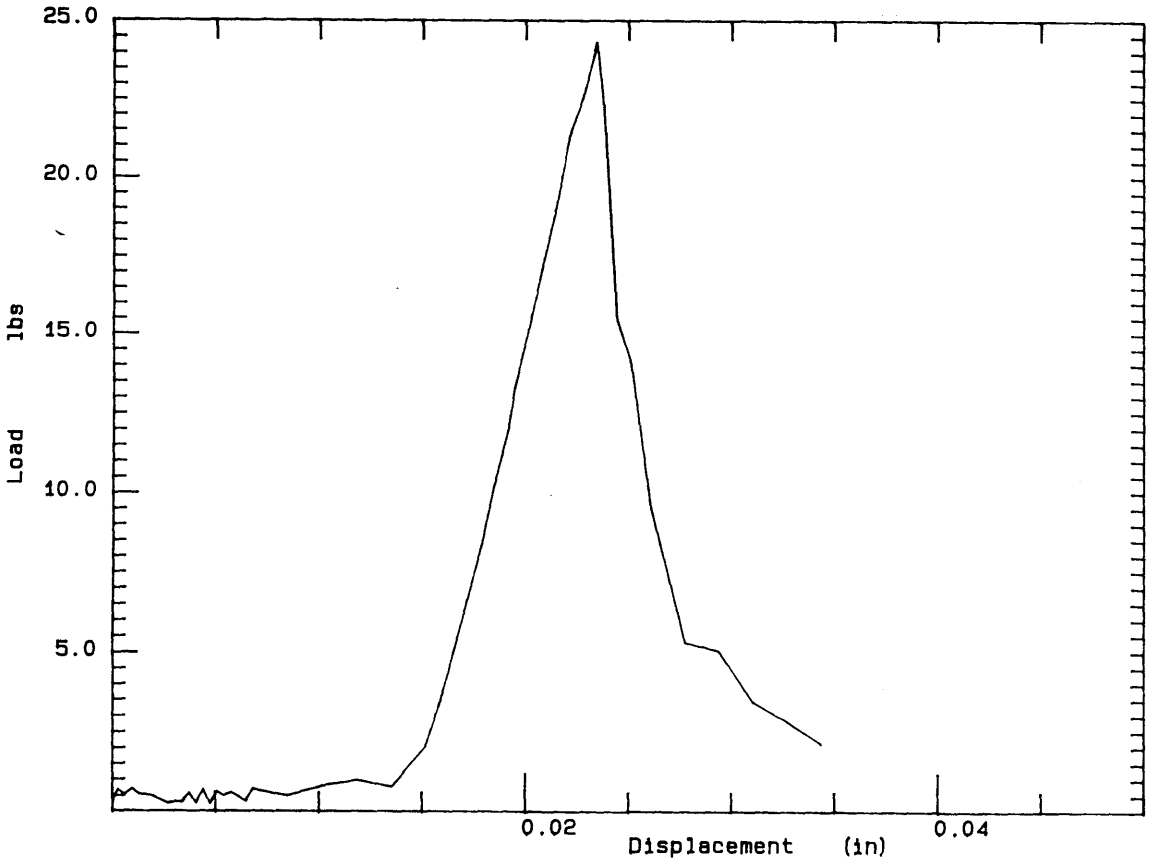

Figure 4.50- Load versus displacement curve for a compact tension specimen from the middle region of an MNS casting containing 7.5% ATBN and 2.5% CTBN tested at a rate of 0.2 in/min.

The GIC value for the sample taken from the middle region of the casting increases slightly over the value for the control 7.5% ATBN sample (Figure 4.51). However, the increase to 1.10 lb/in. can again probably be explained by the drop in modulus from 509 ksi for the 7.5% ATBN sample to 425 ksi for the sample with 2.5% CTBN. On the other hand, the fracture toughness of samples taken from the top portion of the casting containing 7.5% ATBN and 2.5% CTBN almost doubled to an average value of 1.0969 $ksi*in^{1/2}$. In addition, there is a huge area under the load versus displacement curve for this sample despite the lack of crack arrest evidence (Figure 4.52). This curve is not plotted on the same scale as the rest, due to the much higher stain level attained by this sample. This curve is very similar to that representing ductile stable crack growth shown in Figure 4.34.

4.2.2.2 Scanning Electron Microscopy

4.2..2.2.1 Middle Region

The fracture surface of a compact tension specimen taken from the middle region of the casting containing 7.5% ATBN and 2.5% CTBN is shown in Figure 4.53. Many of the rubber particles have undergone a great deal of deformation and cavitation. After the highly stretched rubber domains have failed, they no longer completely fill the hole they originally occupied. There are two types of cavitation behavior seen on the surface of this casting. The first type of cavitated domain is fairly flush with the matrix for most of the domain, but contains some void space where it doesn't completely refill the hole after the deformation process. This type of domain is represented by the domain located just to the right of center in Figure 4.54. The fracture surface of this domain is fairly brittle in appearance. This type of cavitation can also be observed on the polished surface of a sample of the same composition (Figure 4.55).

The second type of cavitation is represented by the domain located just to the left of center in Figure 4.54. The rubber has most likely pulled out of

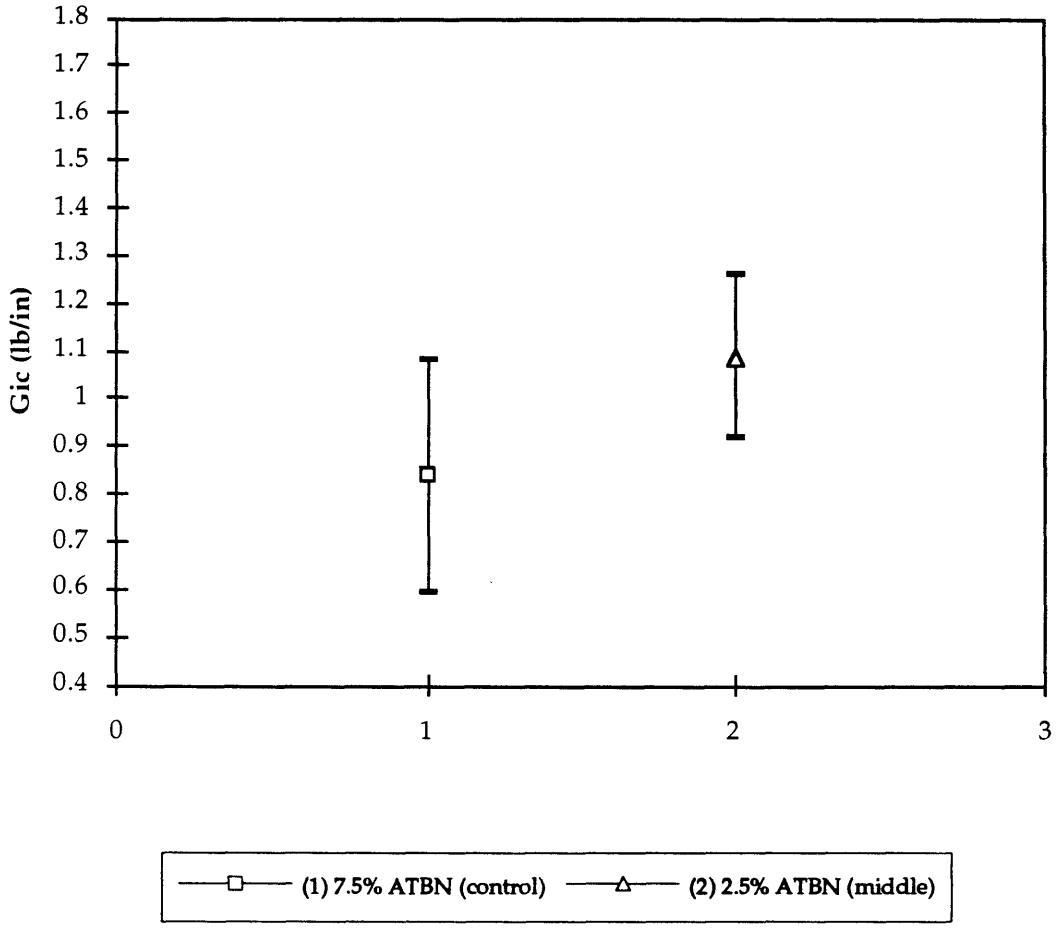

Figure 4.51- GIC values for MNS compact tension specimens containing 7.5% ATBN and samples from the top portion of a sample containing 7.5% ATBN and 2.5% CTBN tested at a rate of 0.2 in/min.

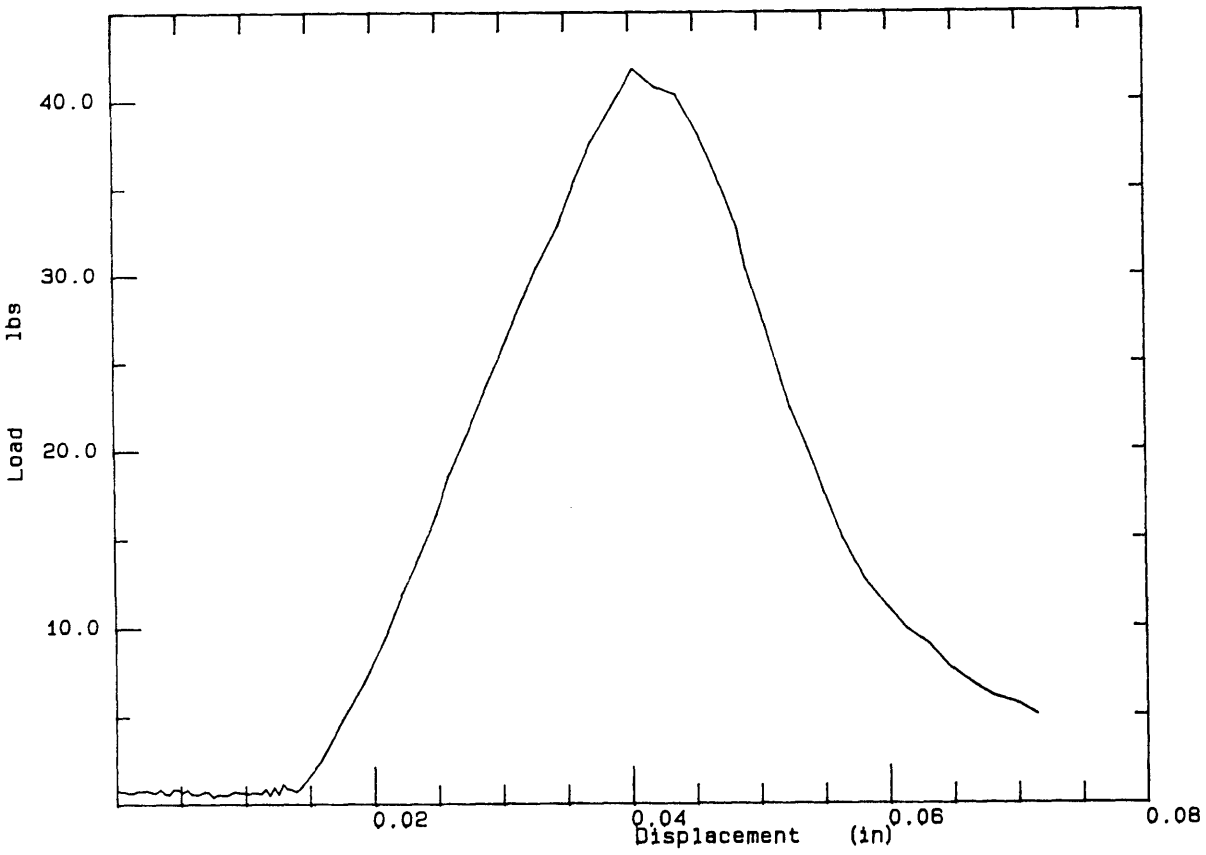

Figure 4.52- Load versus displacement curve for a compact tension specimen taken from the top region of an MNS casting containing 7.5% ATBN and 2.5% CTBN tested at a rate of 0.2 in/min.

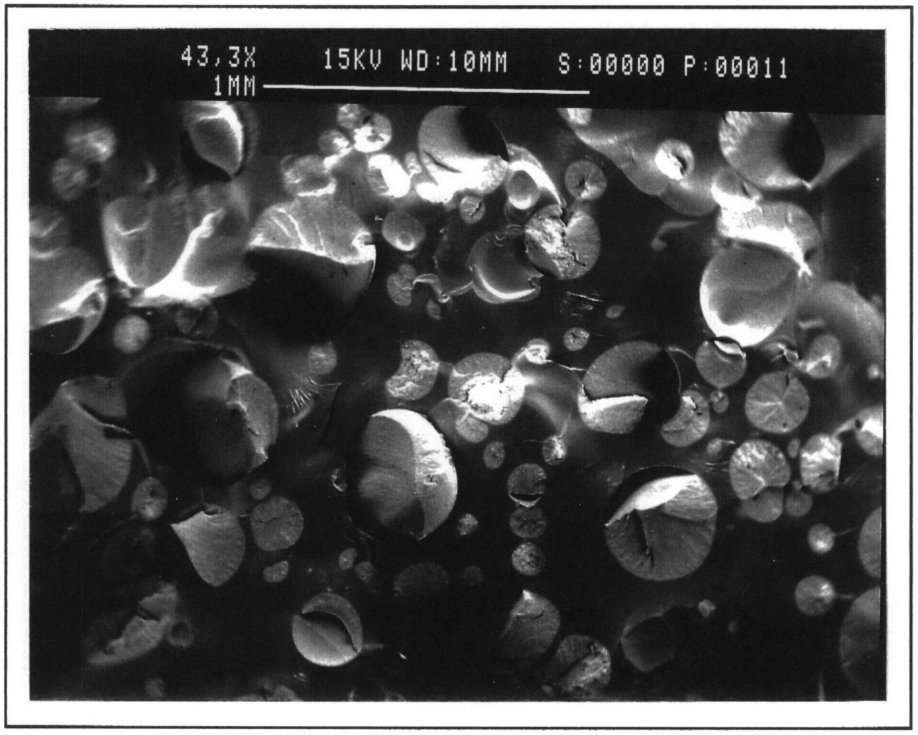

Figure 4.53- Fracture surface of a compact tension specimen taken from the middle region of an MNS casting containing 7.5% ATBN and 2.5% CTBN.

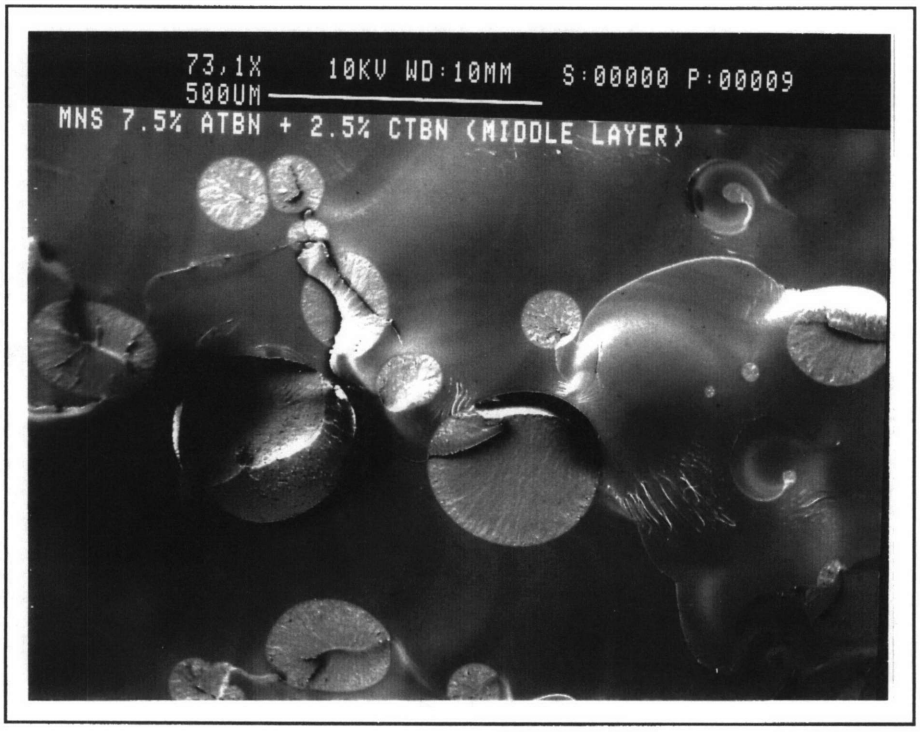

Figure 4.54- Two types of cavitation behavior on the fracture surface of a sample taken from the middle region of an MNS casting containing 7.5% ATBN and 2.5% CTBN.

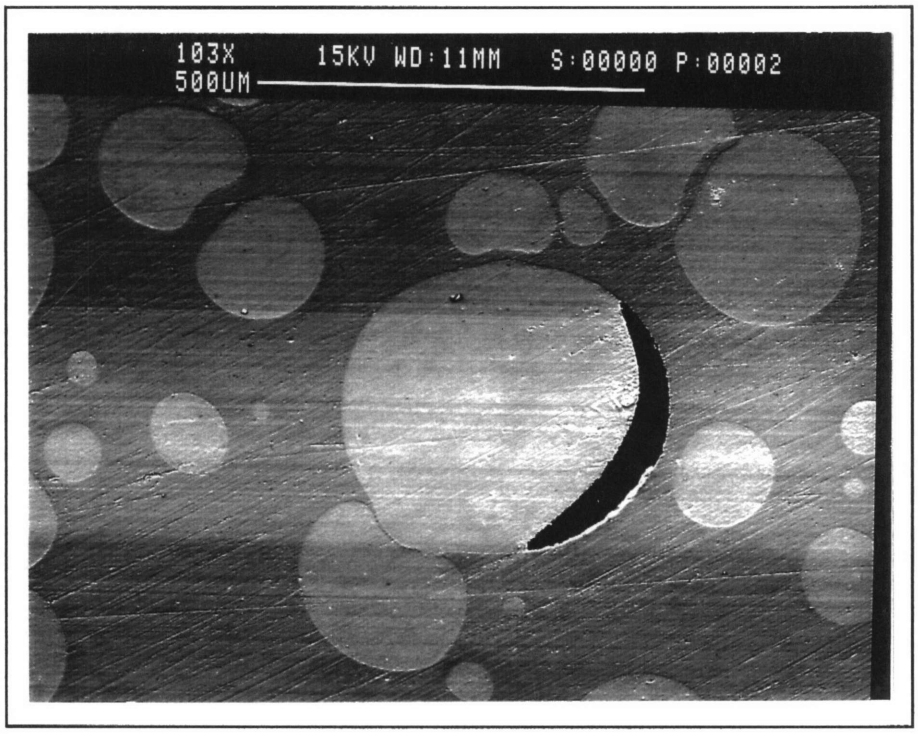

Figure 4.55- Backscattered image of a cavitated domain on the polished surface of a sample taken from the middle region of an MNS casting containing 7.5% ATBN and 2.5% CTBN.

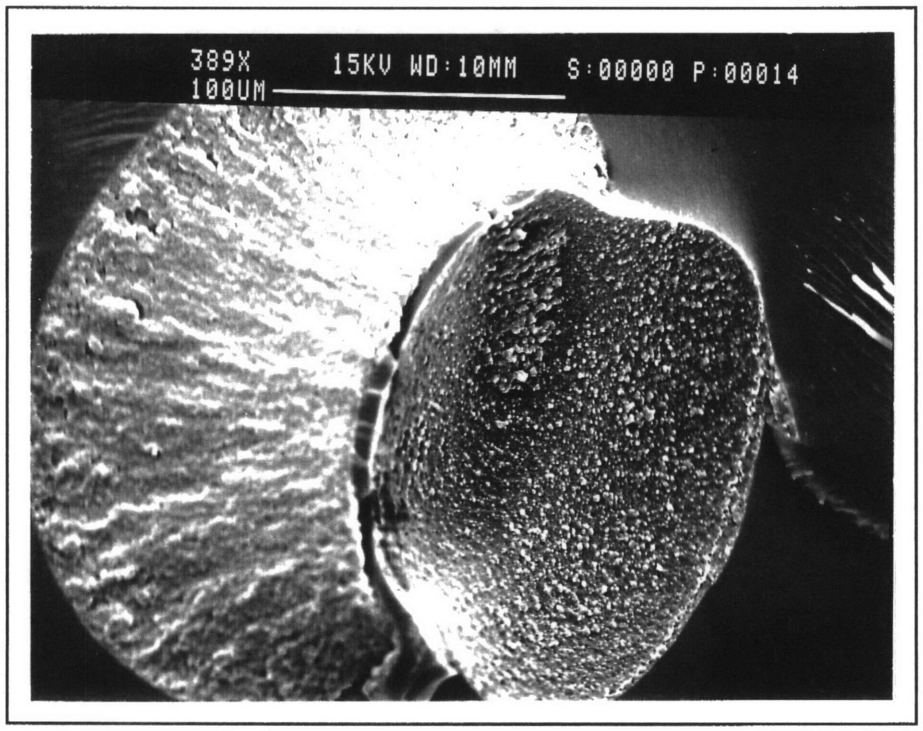

Figure 4.56- Crater left by a pulled-out rubber domain on the fracture surface of a sample taken from the middle region of an MNS casting containing 7.5% ATBN and 2.5% CTBN.

Figure 4.57- Three different types of rubber-rich domains on the fracture surface of a sample taken from the middle region of an MNS sample containing 7.5% ATBN and 2.5% CTBN.

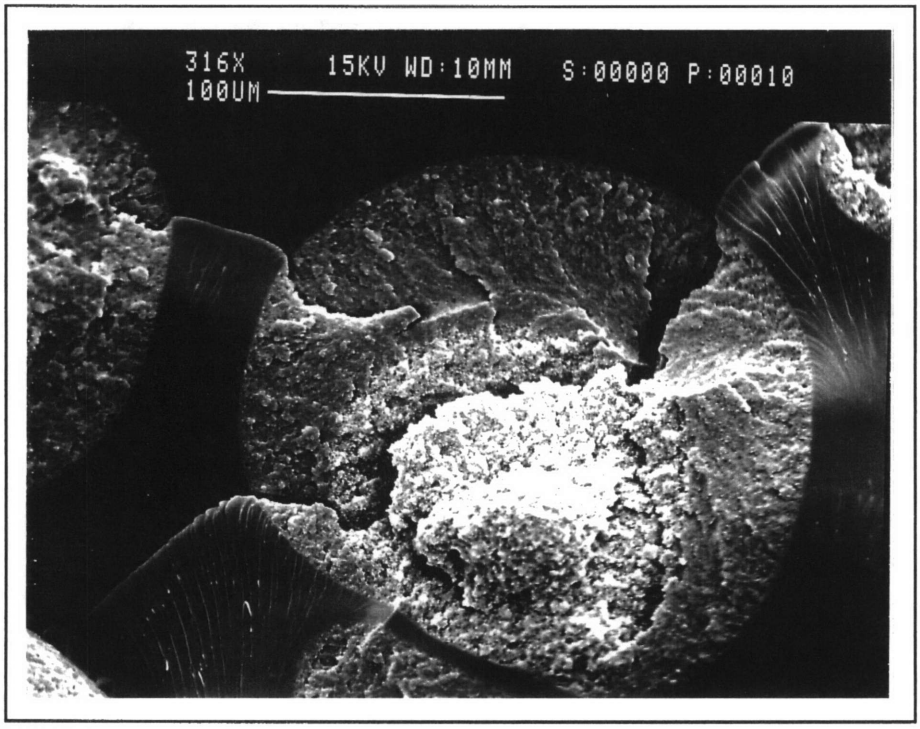

Figure 4.58- Two-phase rubber-rich domain on the fracture surface of a sample taken from the middle region of an MNS sample containing 7.5% ATBN and 2.5% CTBN.

the matrix on the other half of the specimen, thus leaving behind a crater on the fracture surface. These craters are prevalent on the fracture surface and can be seen in Figure 4.56. The surface of this domain shows a fair amount of deformation that might have occurred as the particle pulled out of the matrix. It seems that if the propagating crack hits close to the equator of a rubber domain, the domain will mostly shear in half. However, if the crack hits the domain much above or below the equator, the smaller portion of the domain will pull away from the matrix on the other side of the crack. Since both mechanisms appear to be energy absorbing mechanisms, it is surprising that the fracture toughness of this sample is not higher.

There are three remaining types of domains present on the fracture surface of the sample containing 2.5% CTBN. The first appears to contain predominately ATBN since its fracture surface appears to be fairly similar to the ATBN domains found in the 7.5% ATBN control specimen. This type of domain can be found on the right side of Figure 4.57. However, there is no crack into the matrix in the direction of crack growth for these domains in the 2.5% CTBN samples. Instead, there is deformation in the interior of the domain. Therefore, it is possible that either the domain contains some CTBN in addition to the ATBN, or that the addition of CTBN changed the method of crack propagation so as to cause a different deformation mode for the ATBN domains. There are also some domains that resemble ATBN in terms of their fracture surface and have cracks emanating from them into the matrix in the direction of crack growth. This type of domain can be found on the left side of Figure 4.54. These domains are much smaller than the domains with the internal deformation. The small domains have diameters in the range of less than 25 microns to 100 microns, while the larger domains have diameters of 200 microns and higher. It is possible that the different sizes of the domains result in different deformation mechanisms. The larger domains might tear, while the smaller ones might act as stress concentrators.

The final type of domain found on the surface of the 2.5% CTBN specimen appears to be part CTBN and part ATBN. The brittle region was assumed to be ATBN, while the more spongy region was thought to be composed of at least part CTBN. Some domains have CTBN cores and are surrounded by ATBN (Figure 4.58) while other domains have the opposite

morphology. Because, in both cases, there is a distinct boundary between the two materials, it appears that the CTBN and ATBN have phase separated to form the different layers. These domains were not common, however. For the most part, domains were either completely brittle or spongy in appearance. An example of the later type of domain appears in the center of Figure 4.57. It appears that this central region of the casting shows very complex phase separation characteristics.

4.2.2.2.2 Top Region

The fracture surface of a compact tension specimen taken from the top portion of the casting appeared to be homogeneous at all levels of magnification, and no second phase domains were visible. However, a large amount of plastic flow seems to have accompanied the fracture of this specimen, and the failure mechanism appears to be multi-planar (Figure 4.59). The extensive amount of plastic flow present on the surface of this sample, along with the extremely high values of fracture toughness obtained by these specimens, is consistent with a flexibilized rubber-rich matrix.

When the polished surface of a specimen taken from this region is examined using backscattered electrons, it is apparent that the continuous phase is rubber-rich and contains very small, discrete brittle domains (Figure 4.60). It is interesting that the ATBN and CTBN have reacted to form a continuous matrix with a uniform distribution of very small rubber domains rather than separating into separate phases. It is possible that the addition of 2.5% CTBN kicked the phase separation mechanism over to spinodal decomposition, and that the brittle domains are what is left over from the more typical nucleation and growth mechanism that forms the island morphology seen in the middle region of the casting.[57] This is possible since the phase inversion was found to occur at around 9% ATBN in the MNS formulation, and the total rubber content of the 2.5% CTBN system is 10%. It is also possible that more of the rubber migrated to the top portion of the casting, and that the top portion of the casting contains more than 10% rubber.

Figure 4.59- Plastic flow on the fracture surface of a sample taken from the top region of an MNS casting containing 7.5% ATBN and 2.5% CTBN.

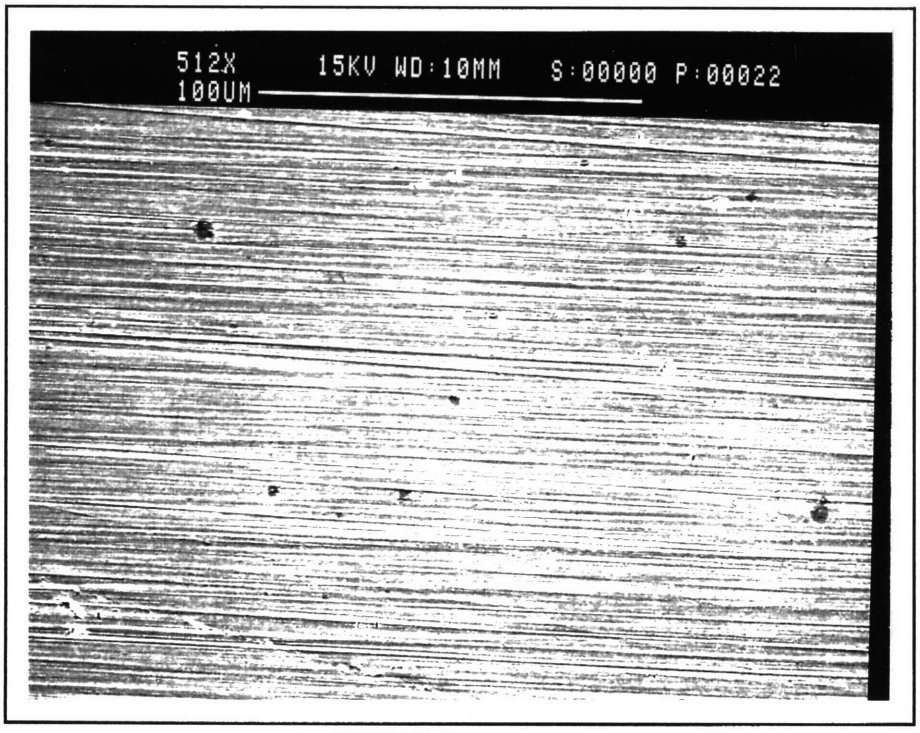

Figure 4.60- Backscattered image of discrete polyester-rich domains on the polished surface of a sample taken from the top region of an MNS casting containing 7.5% ATBN and 2.5% CTBN.

4.2.2.2.3 Transition Regions

In order to view the boundary between the top and middle regions of the casting, as well as that between the middle and bottom regions, strips of material that included each boundary were fractured using a razor blade and mallet. Figure 4.61 shows the boundary between the top region (on left) and the middle region (on right). The boundary is extremely sharp. The large domains to the right appear to be rubber domains (Figure 4.62). It is interesting to note that the domains are completely separated from each other. Even though the domains are deformed due to their close proximity to one another, there is a definite line of matrix material separating one domain from another. This transition zone with the large rubber-rich domains is very narrow, and soon the type of fracture surface typical of the central region of the casting is soon seen. In Figure 4.63, the left half of the micrograph continues to show the large rubber-rich domains, while the right half shows the domains typical of those found in the central region of the casting. As can be seen in this figure, all the cavitation, craters, and ATBN domains typically present in the central region of the casting are present in the region immediately adjacent to the boundary between the top and middle layers.

The boundary between the middle and bottom regions of the casting is shown in Figure 4.64. The left half of the micrograph shows the bottom region of the casting, which is completely featureless. Due to the lack of evidence of plastic flow on the fracture surface of the bottom region of this casting, and the fact that the specimen chipped very easily when fractured using a razor blade and mallet, it appears that the bottom portion of the casting does not contain much (if any) rubber. There are no second phase domains visible in the bottom region of the casting but, because of its brittle nature, it is probable that the material has not undergone a phase inversion. The right half of the micrograph in Figure 4.64 shows the presence of a few rubber domains which appear to be composed of ATBN, but these domains are located in the region of the transition zone closest to the middle region of the casting.

It appears that MNS castings of 7.5% ATBN with 2.5% CTBN are very complicated systems because of their proximity to the rubber content at which

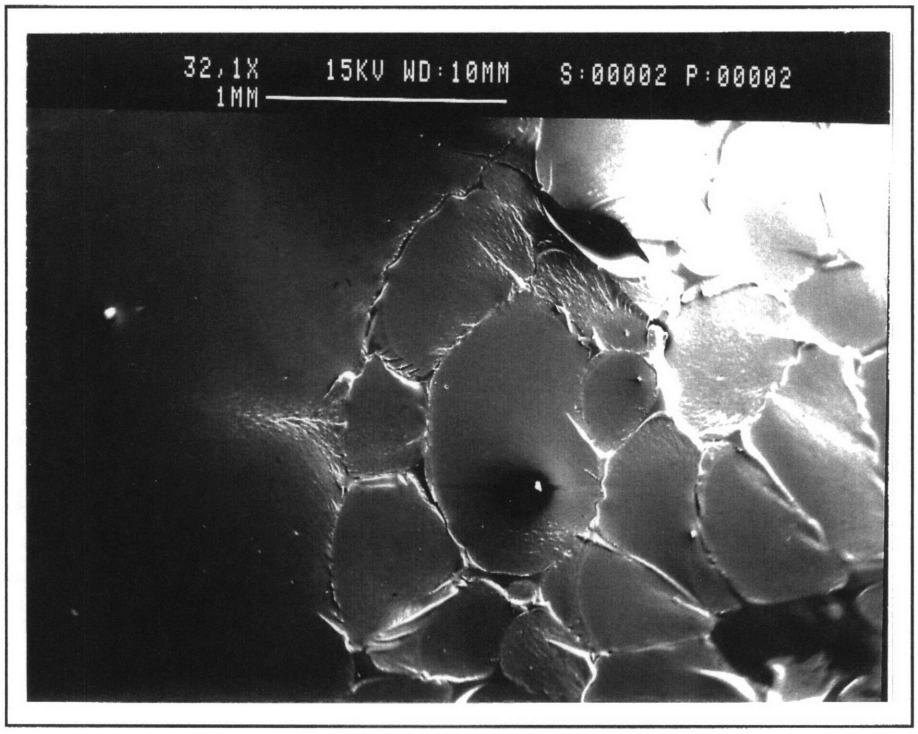

Figure 4.61- Transition zone between the top and middle regions of an MNS casting containing 7.5% ATBN and 2.5% CTBN.

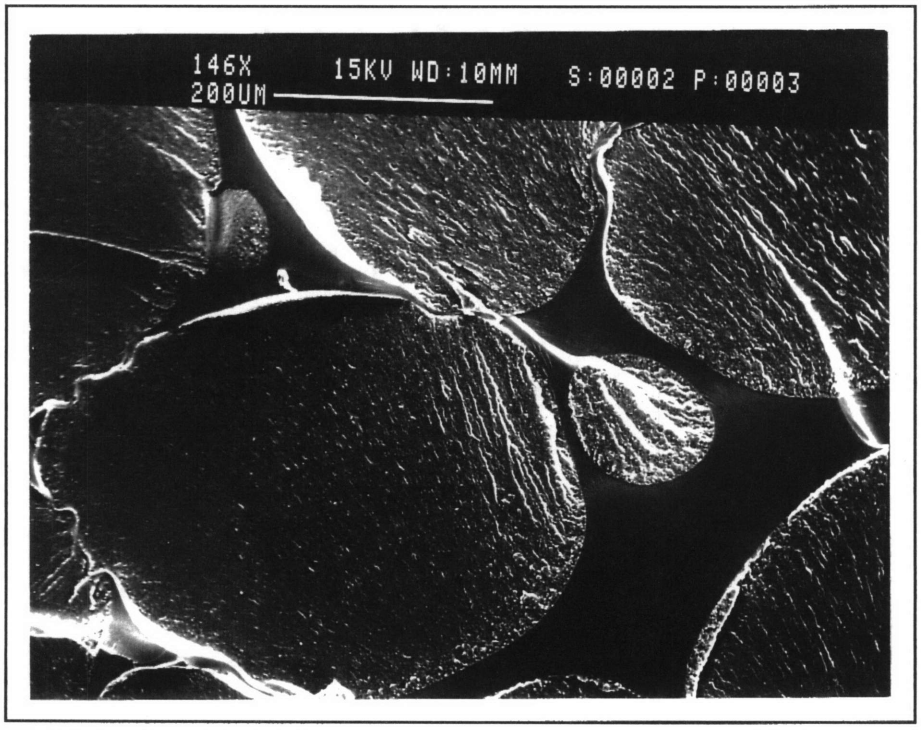

Figure 4.62- Rubber-rich domains near the transition zone between the top and middle regions of an MNS casting containing 7.5% ATBN and 2.5% CTBN.

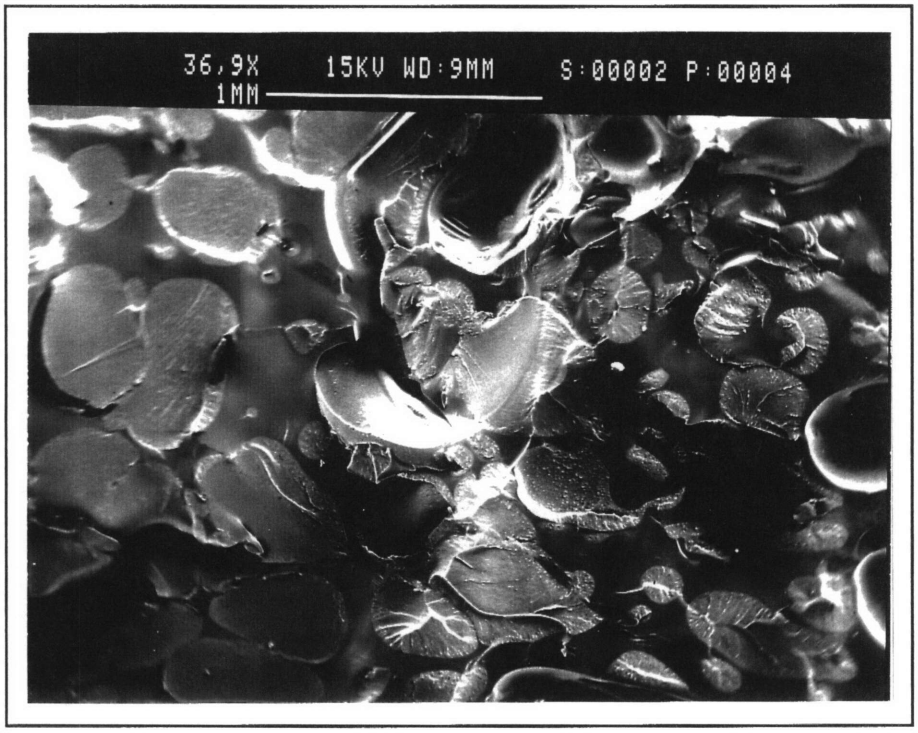

Figure 4.63- Morphology of the top portion of the middle region of a sample taken from an MNS casting containing 7.5% ATBN and 2.5% CTBN.

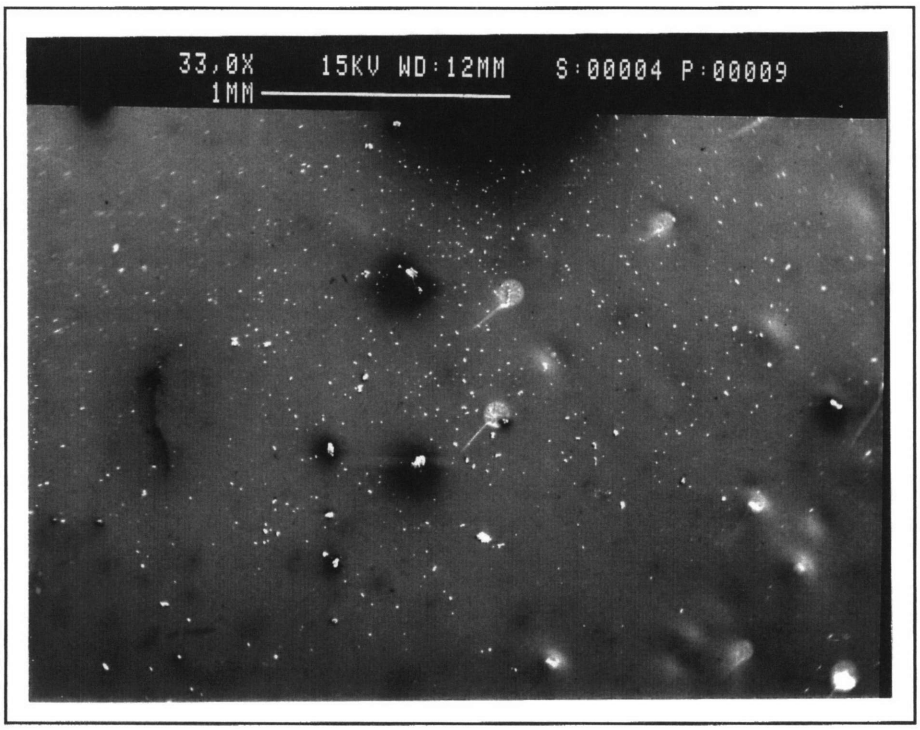

Figure 4.64- Transition zone between the middle and bottom regions of an MNS casting containing 7.5% ATBN and 2.5% CTBN.

phase inversion occurs. In all but the top region of the casting, the CTBN had prevented the phase inversion from occurring even though the combined rubber content exceeds the level for which the phase inversion was found to occur for MNS compositions containing only ATBN as the liquid rubber component. It appears that for compositions near the phase inversion point, any small difference in composition or heat treatment has a significant effect on the morphology of the casting. It appears that while the deformation in the domains within the middle region of the casting was extensive, this deformation was too isolated to provide a measurable increase in the fracture toughness of the sample. The large increase in the fracture toughness of the top region of the casting was the result of global deformation.

4.2.2.3 Dynamic Mechanical Analysis

Figure 4.65 contains the tanδ curves for samples machined from the middle and top portions of the casting containing 7.5% ATBN and 2.5% CTBN, as well as the 0% ATBN and 7.5% ATBN control samples. Table 4.5 contains average values for the temperatures and intensities of the transitions for these samples.

Table 4.5- Values of Tg and tan(d) for both primary and secondary transitions in for MNS samples containing 7.5% ATBN and samples taken from the top and middle regions of the casting containing 7.5% ATBN and 2.5% CTBN as determined by DMA runs performed at a rate of 2°C per minute and a frequency of 5 Hz.

Sample	High Temperature Transition (°C)	Low Temperature Transition (°C)	High Temperature tan(d)	Low Temperature tan(d)
0% ATBN	147.6	112.3	0.2173	0.1709
7.5% ATBN	164.8	none	0.1930	none
2.5% CTBN middle	176.0	77.9	0.1541	0.0708
2.5% CTBN top	095.7	none	0.3690	none

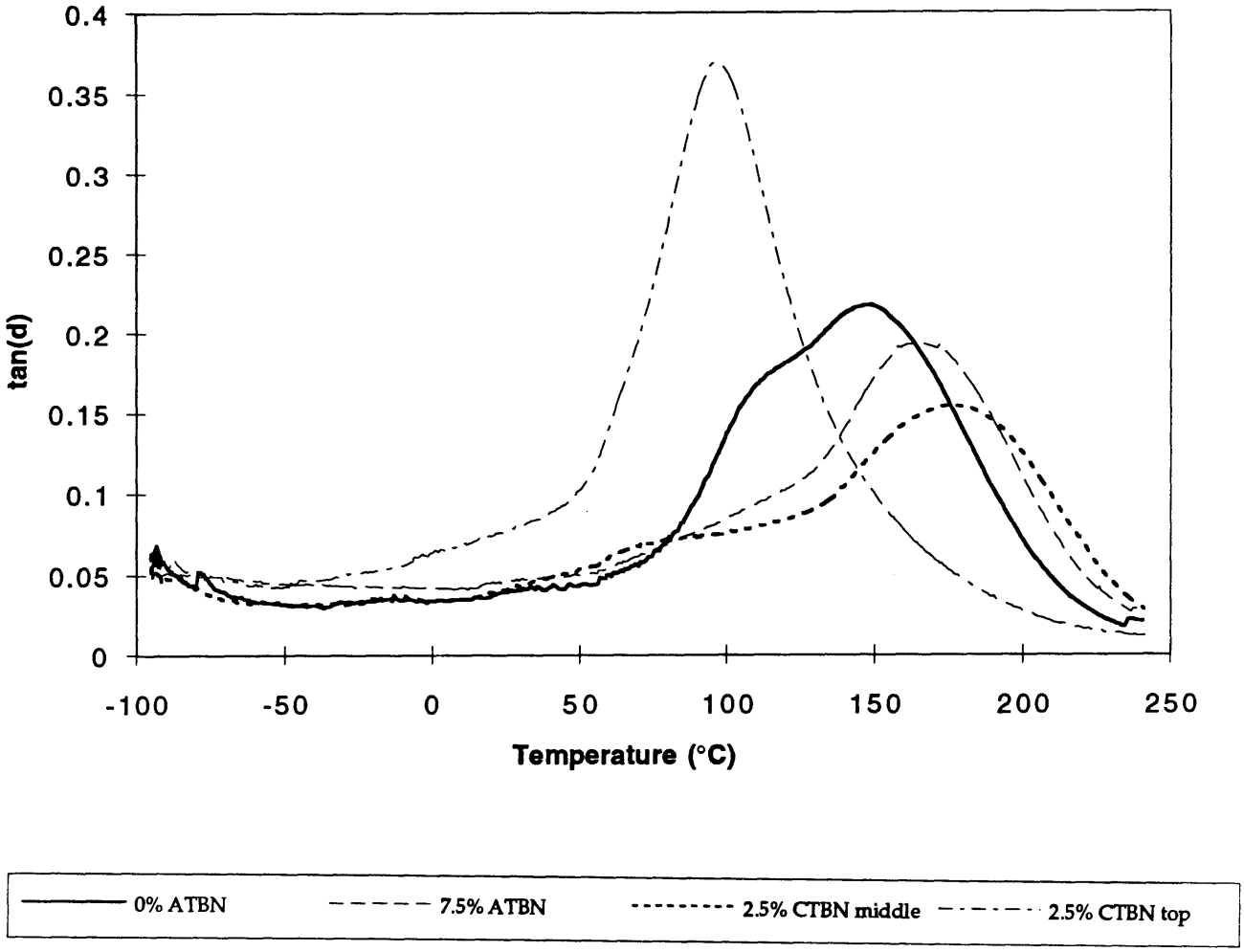

Figure 4.65- Tanδ curves as a function of temperature for samples taken from the top and middle portions of an MNS casting containing 7.5% ATBN and 2.5% CTBN as determined by DMA performed in tensile mode at a heating rate of 2°C/min and a frequency of 5 Hz.

The tanδ curve for the sample taken from the middle portion of the casting containing 7.5% ATBN and 2.5% CTBN possesses both a primary transition and a very faint secondary transition. The primary transition occurs at a much higher temperature than that of the 7.5% ATBN control specimen and has a much lower intensity. This indicates that the damping ability of the polyester is significantly reduced by the addition of the CTBN. The secondary transition for the samples taken from the middle region of the CTBN casting is very broad, and it is difficult to determine the exact transition temperature. There is a slight peak at around 73°C, but the center of the transition occurs at around 110°C. The intensity of this secondary transition is even lower than that of the 7.5% ATBN control sample. This indicates that either the epoxy does not form a very discrete element in this formulation, or it is immobilized by the addition of the CTBN. This could explain why the fracture toughness of this sample was not measurably higher than for the 7.5% ATBN control sample even though these was a fair amount of deformation evident on the fracture surface of the sample taken from the middle region of the 2.5% CTBN sample.

On the other hand, the tanδ curve for the sample taken from the top portion of the 2.5% CTBN casting has one very distinct, narrow peak at a temperature around that of the epoxy transition for the 7.5% ATBN control sample. This transition indicates that all of the epoxy has reacted with the rubber to form a continuous rubber-rich phase. As stated earlier, the fracture surface of a compact tension specimen taken from this region revealed a continuous rubber-rich matrix with only a few small, distinct polyester-rich domains. Therefore, it is not surprising that no peak occurs in the range of the polyester transition for this sample. The intensity of this peak is much higher than that for the 7.5% ATBN control sample, which indicates a high degree of mobility in this sample. This is consistent with the earlier hypothesis that the material in the top portion of the 2.5% CTBN casting had undergone a phase inversion to form a continuous flexibilized rubber-rich matrix. The tanδ and Tg values of this sample are around those for the samples containing 22.5% ATBN as tested by Subramaniam.[6] Therefore, either the majority of ATBN and CTBN in the system migrated to the top portion of the casting to increase the rubber content in this region, or the CTBN reacts with the ATBN to produce greater mobility at lower rubber

contents. The later theory is probably correct, since there seems to be a large amount of rubber present in the large central region of the casting. The large degree of mobility in the sample from the top region of the 2.5% CTBN sample could explain the extremely high fracture toughness values found for this sample.

4.2.3 Core-Shell Particles

There was some concern that the styrene monomer used as the carrier for the polyester resin disrupted the integrity of the second phase particles. For example, the Nipol particles seem to have been at least partially dissolved by the styrene monomer before re-precipitating back out to form large, amorous multi-phase domains that were not pure rubber. It was also thought that some of the styrene had penetrated the Paraloid particles and then polymerized to embrittle the particles. Therefore, several types of core shell particles with crosslinked pMMA shells and either crosslinked or partially crosslinked rubber cores were investigated with the expectation that they would keep their integrity in the presence of the styrene monomer. The three types of particles obtained from Rohm and Haas were EXL 5136, EXL 2691 and EXL 2330. The first particle contained a very heavily crosslinked butyl acrylate core and possessed an average particle dimension of slightly over 1 micron. The remaining two types possessed partially crosslinked butadiene cores with average particle sizes of 150 nm and 600 nm respectively. Both the casting containing 5% EXL 5136 particles and that containing 5% EXL 2330 particles displayed a very even distribution of particles and were opaque. On the other hand, the distribution of the particles in the casting containing 5% EXL 2691 particles was less good, and the casting was grainy in appearance.

4.2.3.1 Fracture Toughness

The fracture toughness values for samples containing 7.5% ATBN and 5% core-shell particles are plotted along with those of a control sample containing 7.5% ATBN in Figure 4.66. Table 4.3 contains the average toughness values for these samples. The fracture toughness values for the three different particle-containing compositions are almost identical. The

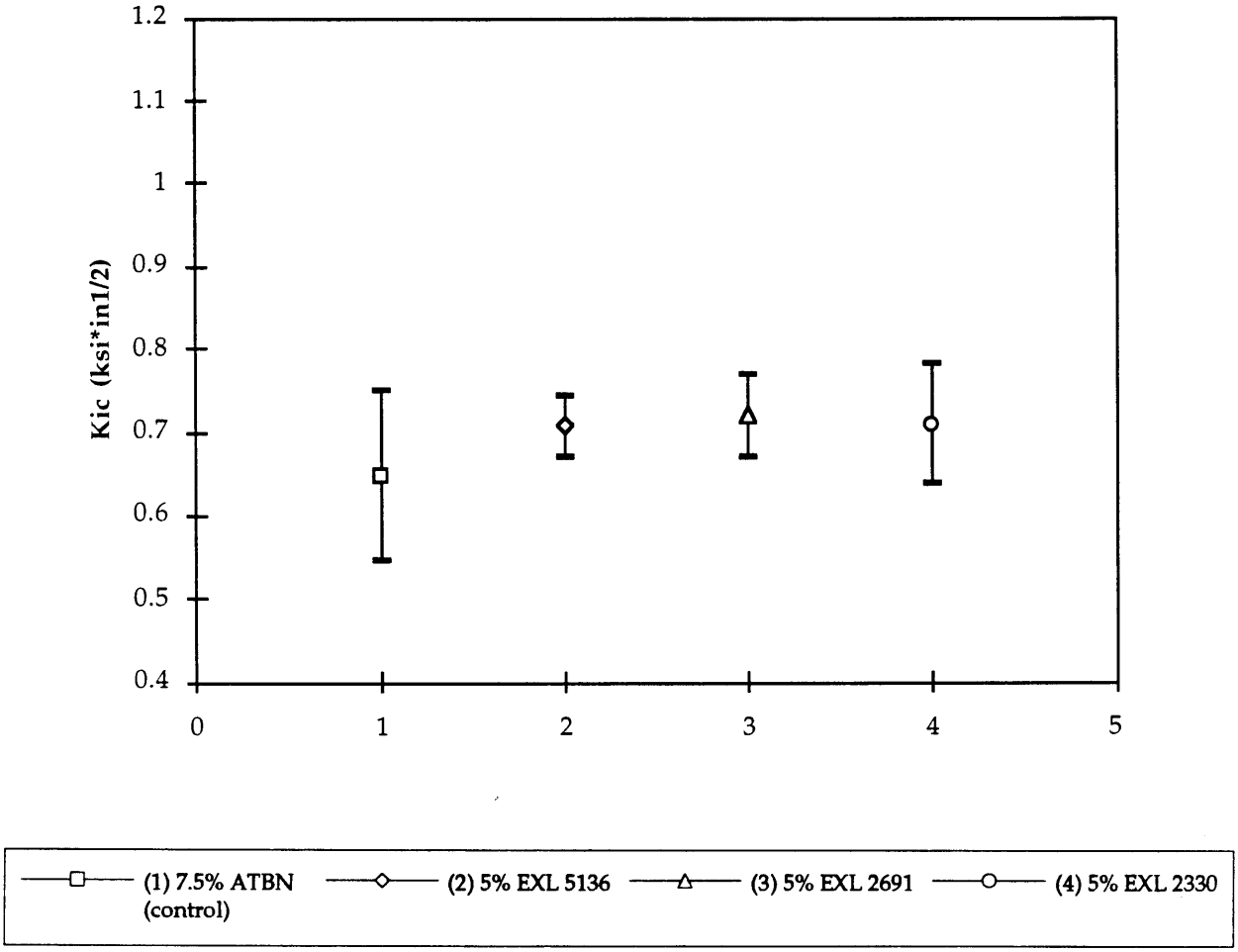

Figure 4.66- Fracture toughness values for MNS compact tension samples containing 7.5% ATBN and 5% core-shell particles tested according to ASTM D 5045-93 at a rate of 0.2 in./min.

samples containing 5% EXL 5136, 5% EXL 2691 and 5% EXL 2330 particles posses K_{Ic} values of 0.7072, 0.7197, and 0.7082 ksi*in$^{1/2}$ respectively. These values are only slightly higher than the value of 0.6465 ksi*in$^{1/2}$ obtained for the control MNS sample containing 7.5% ATBN. This is a surprising finding considering the additional rubber content in these systems.

The load versus displacement curves all samples containing core-shell particles appear to be very similar to each other, but exhibit slightly more evidence of crack arrest than the MNS control sample with 7.5% ATBN (Figures 4.67-4.69). While the particles do not appear to significantly increase the resistance to crack initiation, it is possible that they do improve the resistance to crack propagation. The G_{Ic} values do improve significantly for all three specimens, with values of 1.4567, 1.3756 and 1.3710 lb/in for the samples containing 5% EXL 5136, 5% EXL 2691 and 5% EXL 2330 particles respectively (Figure 4.70). This is a considerable improvement over the value of 0.8380 lb/in for the MNS control sample containing 7.5% ATBN. However, the increase in G_{Ic} is accompanied by a significant decrease in the modulus of the material; from 509 ksi for the control sample to values of 344, 378, and 369 ksi respectively for the compositions containing the core-shell particles. In addition, the effective rubber content for these samples is now 12.5%. For a 12% ATBN sample, the G_{Ic} value is 1.42 lb/ in with a modulus of 419 ksi. Therefore, the core-shell particles do not produce the desired toughening effect and don't prevent the decrease in modulus which accompanies the increased rubber content.

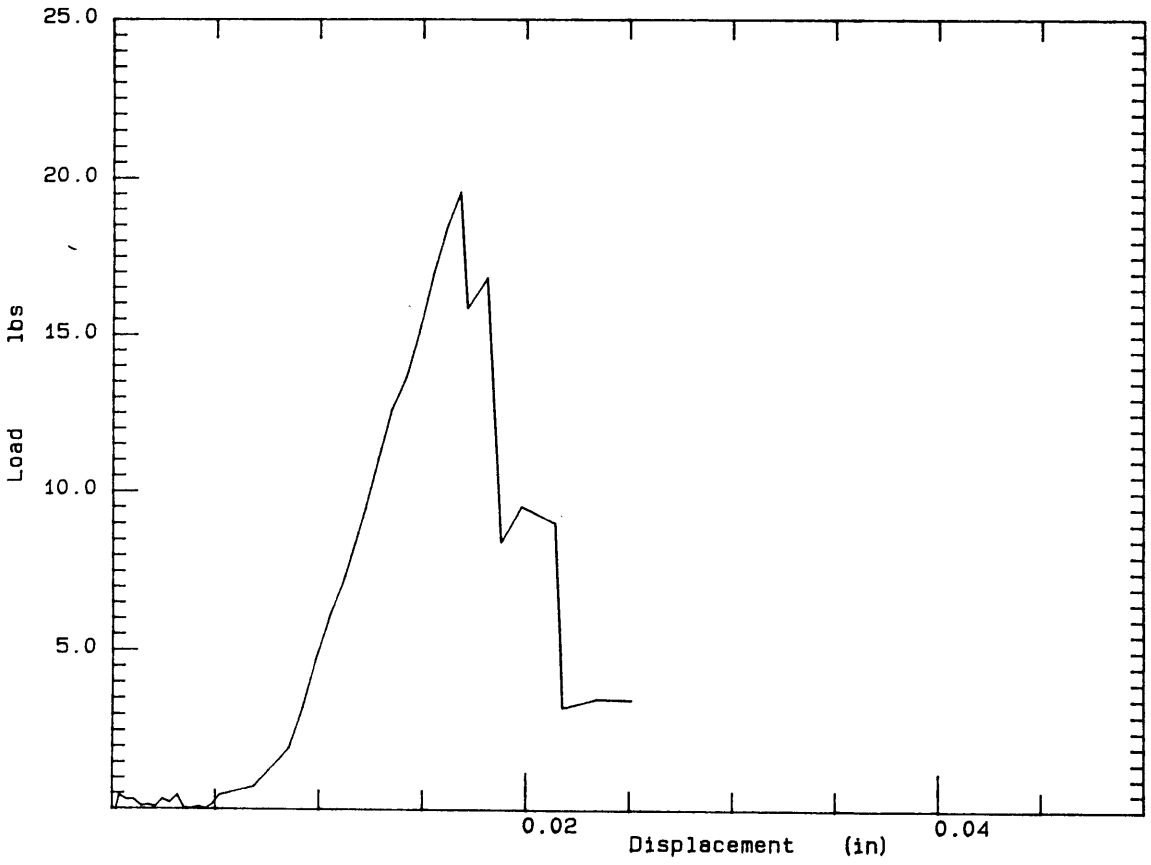

Figure 4.67- Load versus displacement curve for an MNS compact tension specimen containing 7.5% ATBN and 5% EXL 5136 particles tested at a rate of 0.2 in/min.

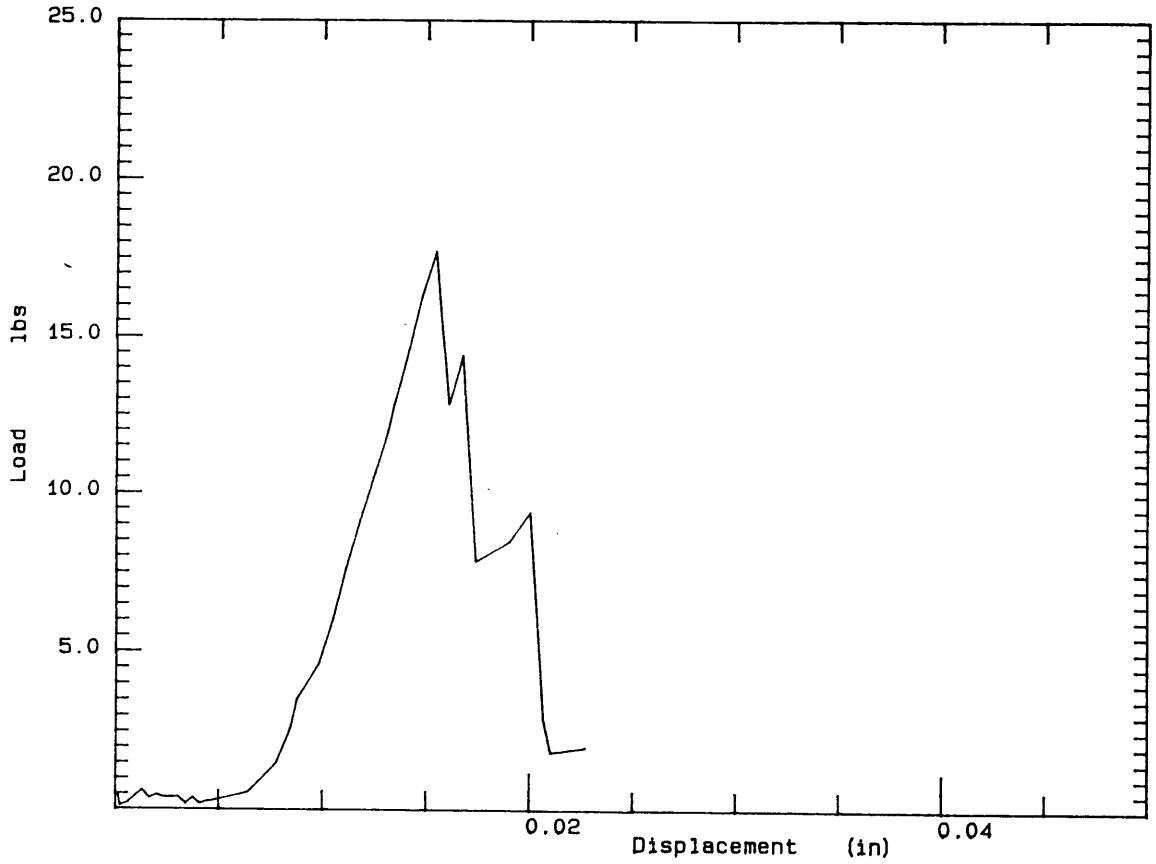

Figure 4.68- Load versus displacement curve for an MNS compact tension specimen containing 7.5% ATBN and 5% EXL 2691 particles tested at a rate of 0.2 in/min.

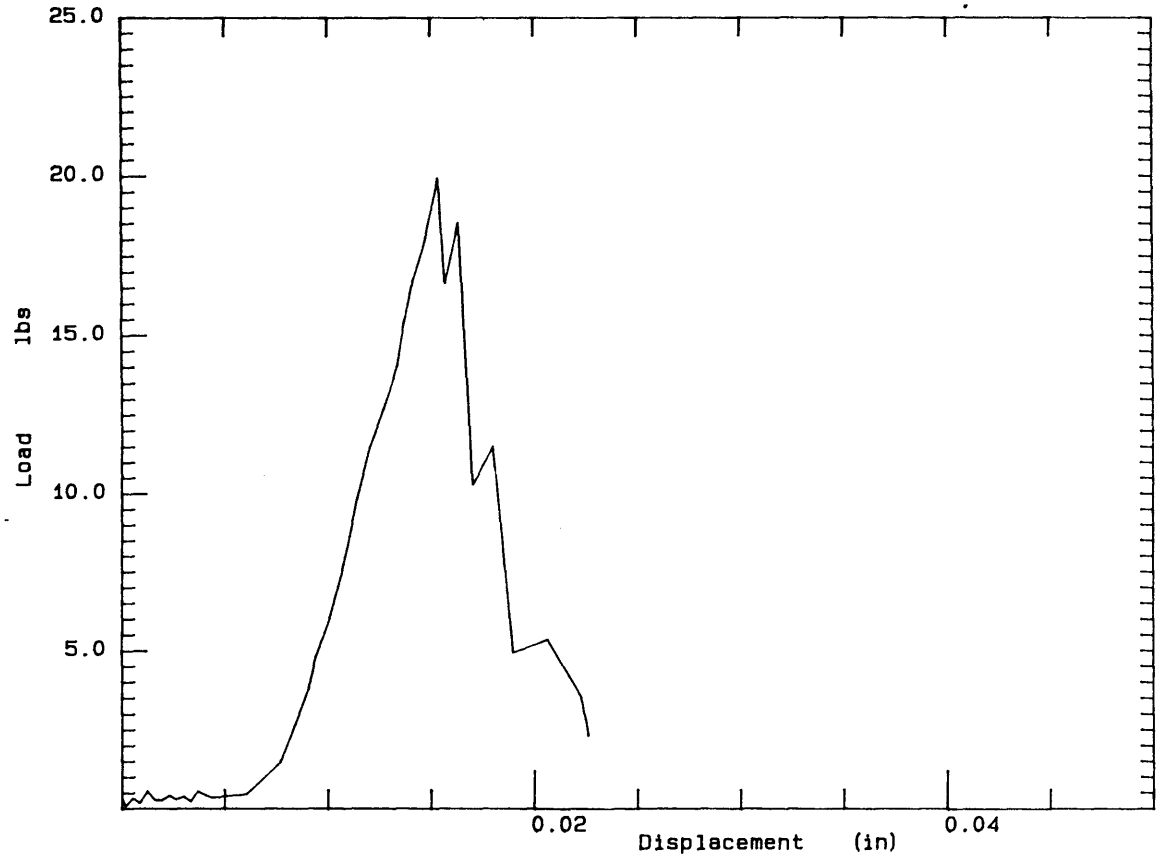

Figure 4.69- Load versus displacement curve for an MNS compact tension specimen containing 7.5% ATBN and 5% EXL 2330 particles tested at a rate of 0.2 in/min.

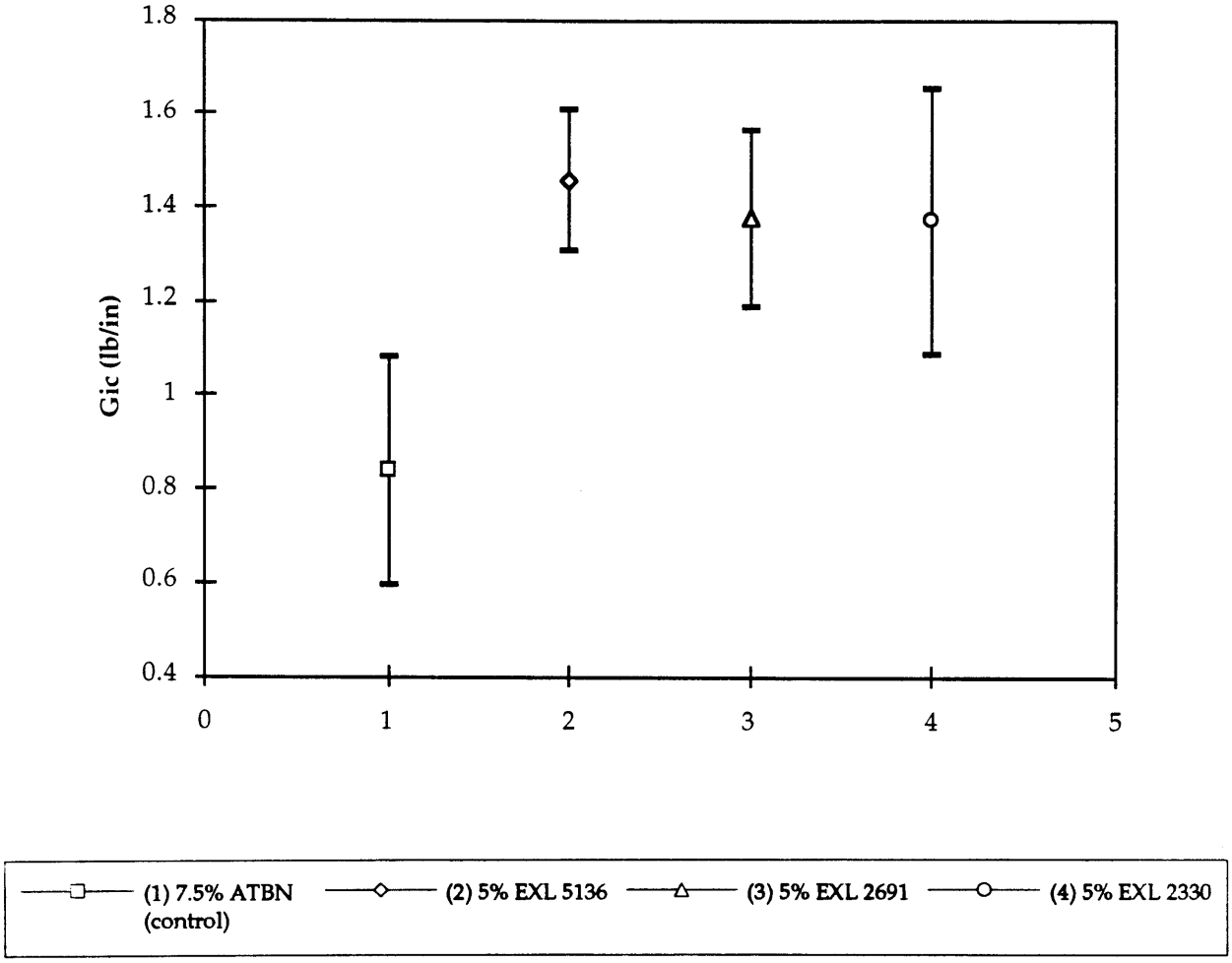

Figure 4.70- Gic values for MNS compact tension samples containing 7.5% ATBN and 5% core-shell particles tested according to ASTM D 5045-93 at a rate of 0.2 in./min.

4.2.3.2 Scanning Electron Microscopy

4.2.3.2.1 EXL 5136 Particles

The fracture surface of the sample containing 5% EXL 5136 particles is shown in Figure 4.71. The circular rubber-rich domains appear to deform more than is characteristic of the rubber-rich domains in the 7.5% ATBN control sample (figure 4.8). These domains also do not originate cracks into the matrix as do the rubber-rich domains in the 7.5% ATBN control sample. Since no core-shell particles appear to be located inside the rubber-rich domains, it does not appear that the additional deformation in these domains was the result of plastic flow induced by the core-shell particles acting as stress-concentrators within the rubber-rich domains. It is possible that the presence of the core-shell particles surrounding the domains serves to partially arrest the crack to slow its propagation and allow more time for the ATBN within the rubber-rich domains to deform.

All of the core-shell particles appear to be located in clusters around the ATBN domains (Figure 4.72). Within these clusters, the particles seem to have maintained their shape and do not appear to have dissolved in the styrene monomer during curing. There also appears to be fairly good adhesion between the matrix and the particles, as bits of matrix appear to be suck to the surfaces of exposed particles. The polished surface of a sample of the same composition is shown in Figure 4.73. The particles still appear to be located outside the main ATBN-rich domains. The particles appear dark, because neither the butyl acrylate core nor pMMA shell contain double bonds that can be stained by the osmium atoms. In the polished view, there still appears to be fairly good adhesion between the particles and the matrix (Figure 4.74). Even though the adhesion appears to be good for the EXL 5136 particles, the resulting fracture toughness of the sample did not increase significantly over the control value. This is probably due to the fact that the particles are located outside the main ATBN-rich domains. While it appears that the particles were able to trap some ATBN in the center of the clusters (Figure 4.75), they do not trap enough to form a complete domain and produce significant toughening.

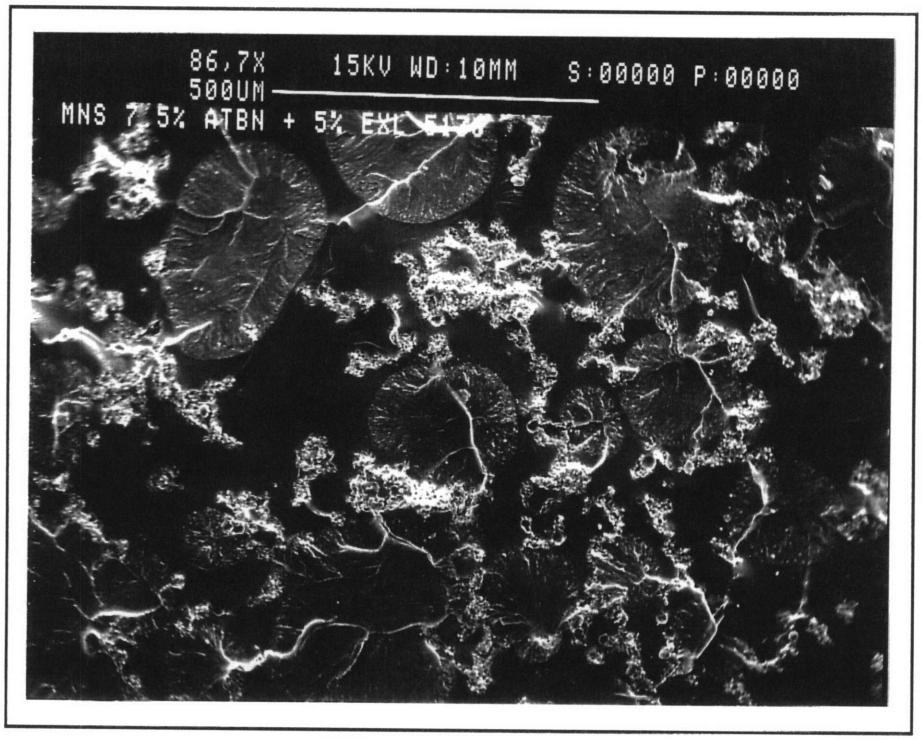

Figure 4.71- Fracture surface of an MNS compact tension specimen containing 7.5% ATBN and 5% EXL 5136 core-shell particles.

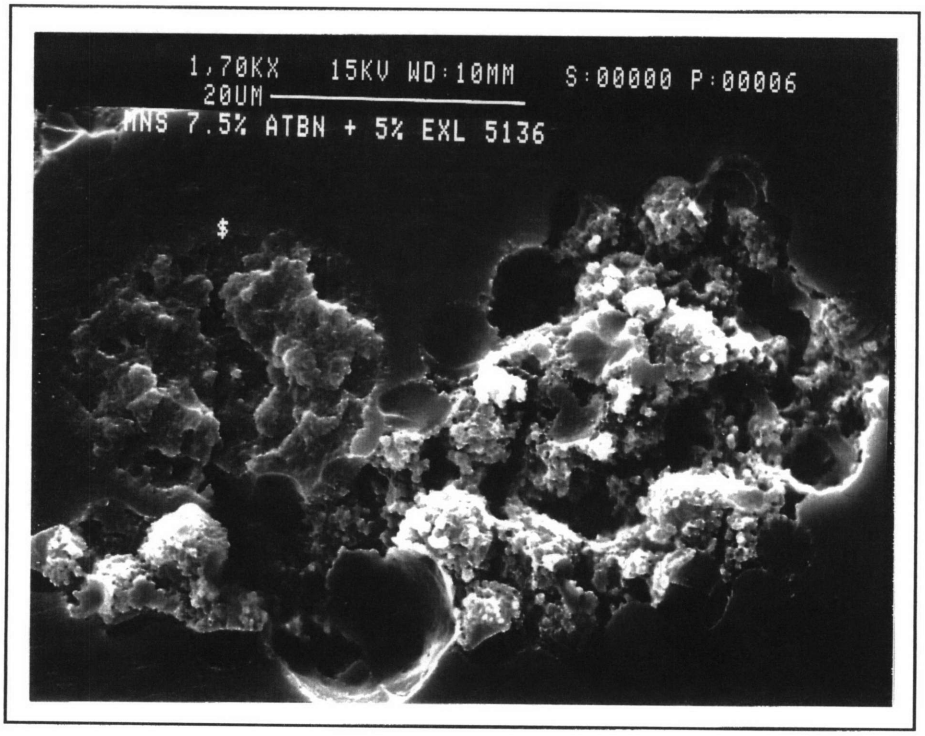

Figure 4.72- Clusters of EXL 5136 particles surrounding an ATBN-rich domain on the fracture surface of a compact tension specimen containing 7.5% ATBN and 5% EXL 5136 particles.

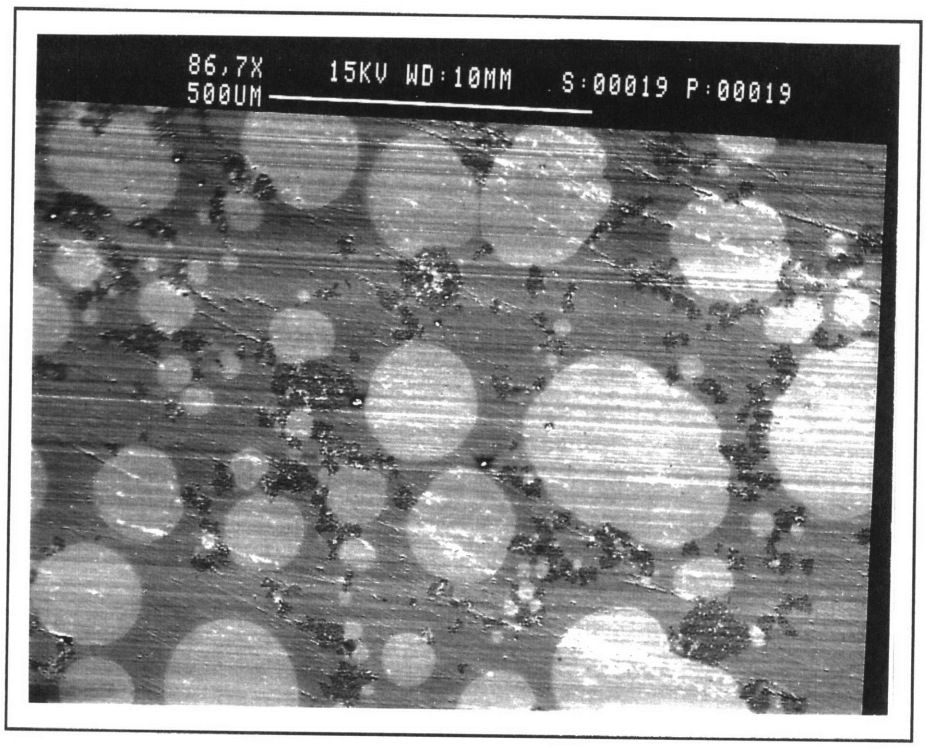

Figure 4.73- Backscattered image of the polished surface of an MNS specimen containing 7.5% ATBN and 5% EXL 5136 particles.

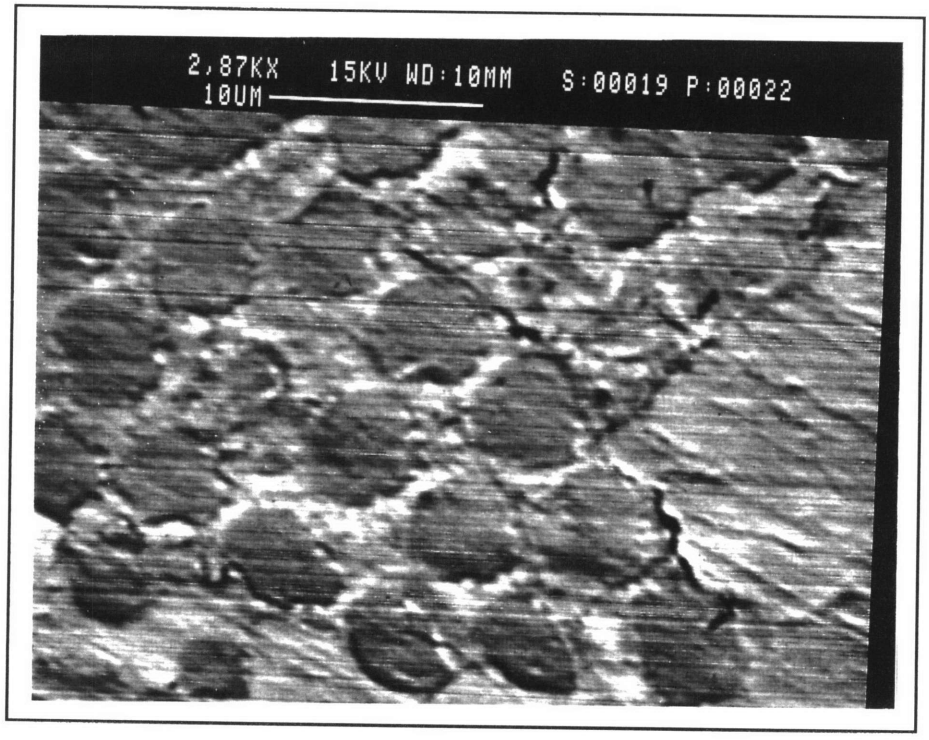

Figure 4.74- Backscattered image of well-adhered particles on the polished surface of an MNS specimen containing 7.5% ATBN and 5% EXL 5136 particles.

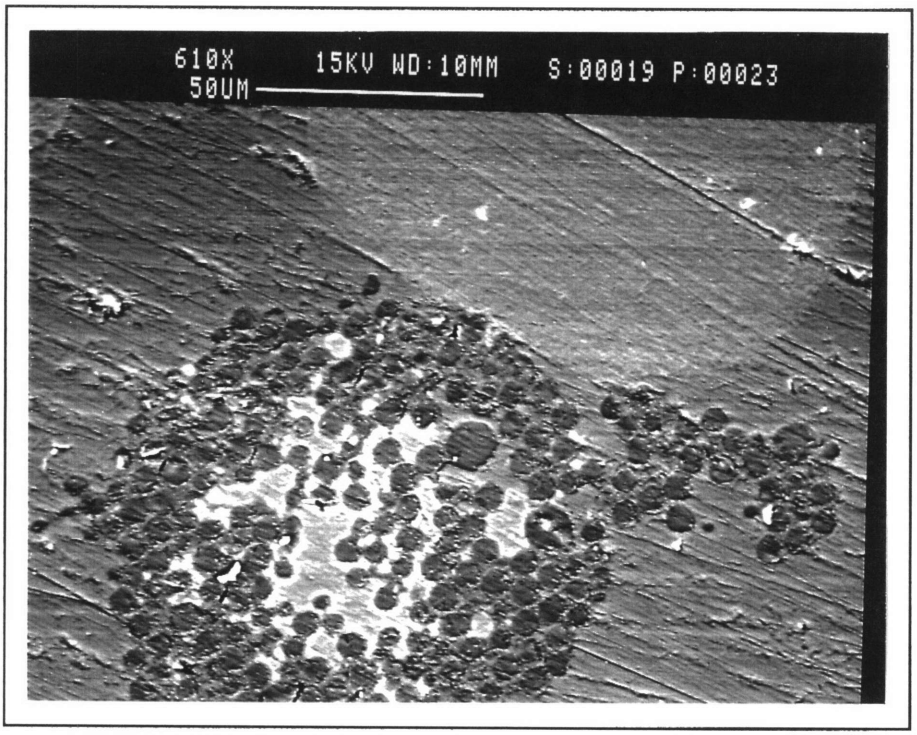

Figure 4.75- Backscattered image of trapped ATBN in a particle cluster on the polished surface of an MNS sample containing 7.5% ATBN and 5% EXL 5136 particles.

4.3.2.2 EXL 2691 Particles

Figure 4.76 shows the fracture surface of an MNS compact tension specimen containing 7.5% ATBN and 5% EXL 2691 particles. The surface is similar to that of the sample containing 5% Paraloid particles. It is covered with large, amorphous domains that appear to contain multiple small, brittle domains inside the larger, more deformed ones. The small, brittle domains appear to contain densely packed EXL 2691 particles with very little material in between them (Figure 4.77). Unlike the sample containing the Paraloid particles, the outer areas of the composite domains in the EXL 2691 sample also contain particles. There appears to be slightly more material between the particles in these regions, and there may be slightly better adhesion of particles (Figure 4.78). However, there is a large amount of pull-out visible in both regions of the particle-containing domains. The degree of particle adhesion and the amount of material between particles in the two types of regions is very hard to determine from these micrographs. Therefore, it is not understood why the degree of deformation is so much higher in some areas of the particle-containing domains than in others.

The polished surface of a sample containing 7.5% ATBN and 5% EXL 2691 core-shell particles is shown in Figure 4.79. The smoother, circular portions of the ATBN-rich domains apparent on the fracture surface appear to be more rubber-rich than the surrounding regions on the polished surface. This difference in rubber concentration is probably the result of the presence of the particles. However, particles were found in both types of ATBN-rich regions on the fracture surface. Magnified views of both types of ATBN-rich regions on the polished surface show evidence of the existence of particles, but no distinct particles. This is probably due to a combination of the fact that the particles are very small and the polishing was not fine enough, and that the butadiene cores of the EXL 2691 particles stain just as well as the surrounding ATBN. It is not possible, therefore, to determine why the ATBN tends to preferentially migrate to the circular regions.

The fracture surface of the sample containing 5% EXL 2691 particles also contains some domains that do not appear to be composite domains.

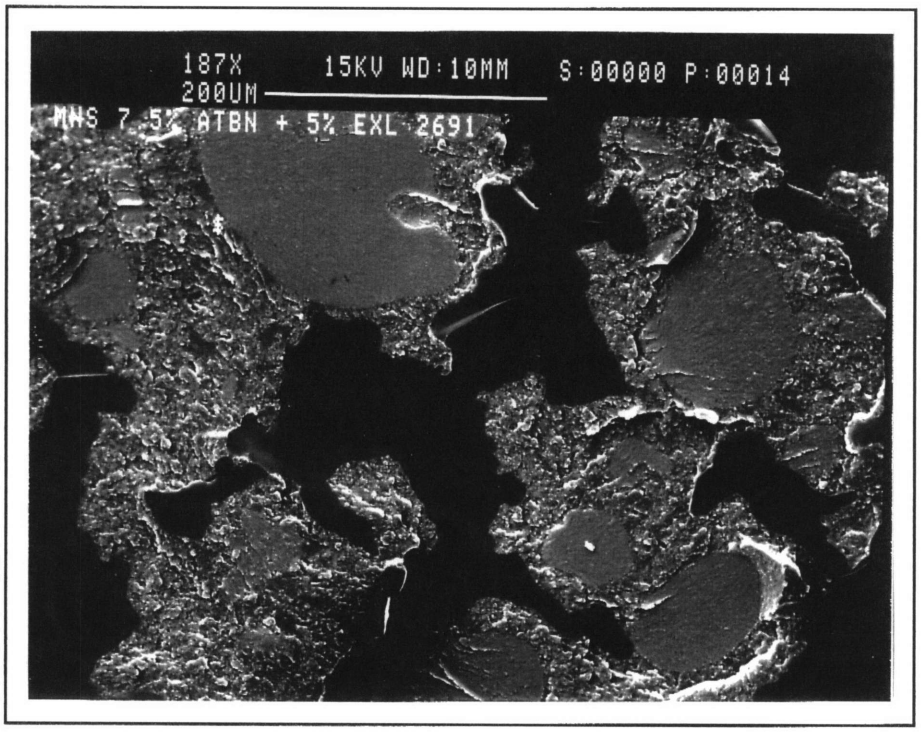

Figure 4.76- Fracture surface of an MNS compact tension specimen containing 7.5% ATBN and 5% EXL 2691 core-shell particles.

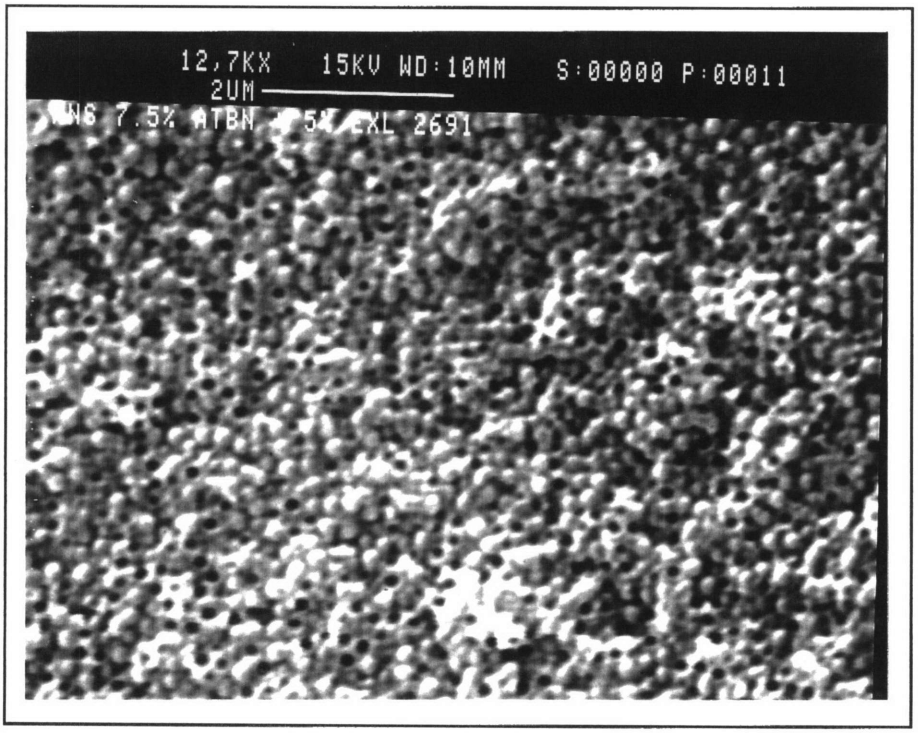

Figure 4.77- EXL 2691 particles within the smooth region of a rubber rich domain on the fracture surface of an MNS compact tension specimen containing 7.5% ATBN and 5% EXL 2691 particles.

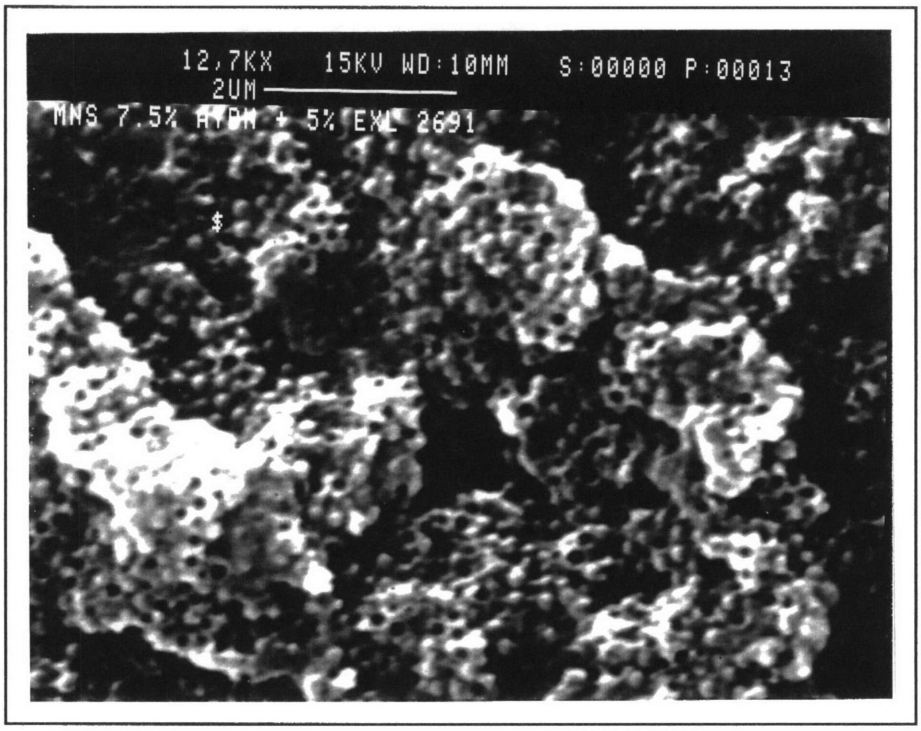

Figure 4.78- EXL 2691 particles in the rough region of a rubber-rich region of an MNS compact tension specimen containing 7.5% ATBN and 5% EXL 2691 particles.

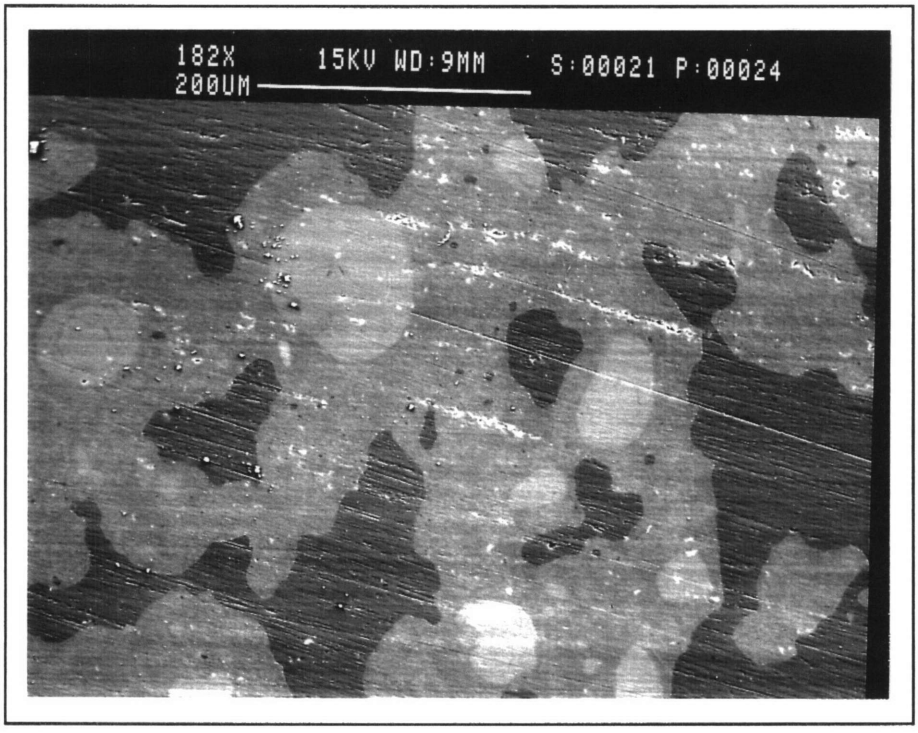

Figure 4.79- Backscattered image of the polished surface of an MNS specimen containing 7.5% ATBN and 5% EXL 2691 core-shell particles.

While some of these domains contain rubber particles in an arrangement similar to that of the rough regions of the composite particles, others show no signs of containing any particles. However, the majority of the domains found on the fracture surface did contain rubber particles. It is surprising, therefore, that the fracture toughness of this material wasn't higher. Small particles placed in domains containing small regions of ATBN should have produced a high degree of toughening. This is exactly the morphology that was desired for increased toughness. There are two possible explanations. First, the degree of adhesion between the particles and matrix may be poor. There did appear to be a significant amount of pull-out visible on the fracture surface. It was not possible to determine the degree of adhesion from the polished surface due to the similar staining capabilities of the ATBN and particles. The second explanation is that the particles were too small. The particles have diameters of around 150 nm, which is very close to the size estimated for the pure ATBN regions within the ATBN-rich domains. Thus, a bidistribution of particle sizes may not have been achieved.

4.2.3.2.3 EXL 2330 Particles

Figure 4.80 contains the fracture surface of a compact tension specimen from the casting containing 7.5% ATBN and 5% EXL 2330 particles. There were a few small, circular domains that did not appear to contain any particles. These domains were generally smaller than ATBN domains in the 7.5% ATBN control sample, but they did have cracks originating from them and propagating into the matrix. The majority of the domains were amorphous in shape and contained large amounts of EXL 2330 particles (Figure 4.81). These particles are not very distinct as individual spherical particles and showed no signs of pull-out of. Therefore, these particles were either well-adhered to the resin, or dissolved a bit and partially coalesced during curing, because they are

The polished surface of a sample from the same casting containing 7.5% ATBN and 5% EXL 2330 particles is shown in Figure 4.82. The ATBN-rich domains are not as continuous as they appear on the fracture surface, and are much smaller than for most of the samples containing 7.5% ATBN and secondary particles. The particles seem to be located mainly in the rough

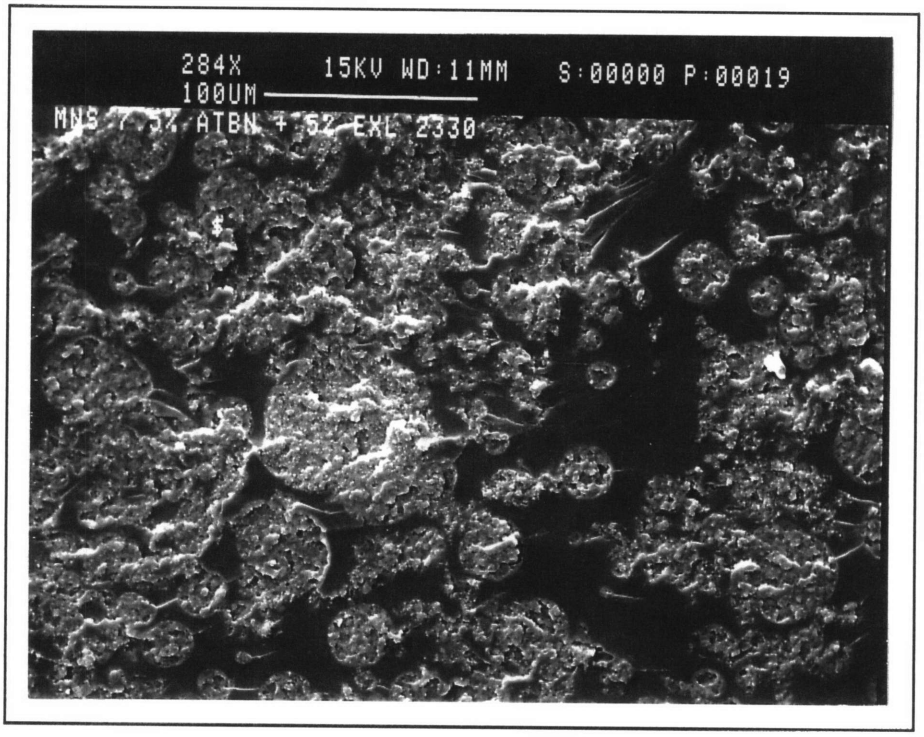

Figure 4.80- Fracture surface of an MNS compact tension specimen containing 7.5% ATBN and 5% EXL 2330 particles.

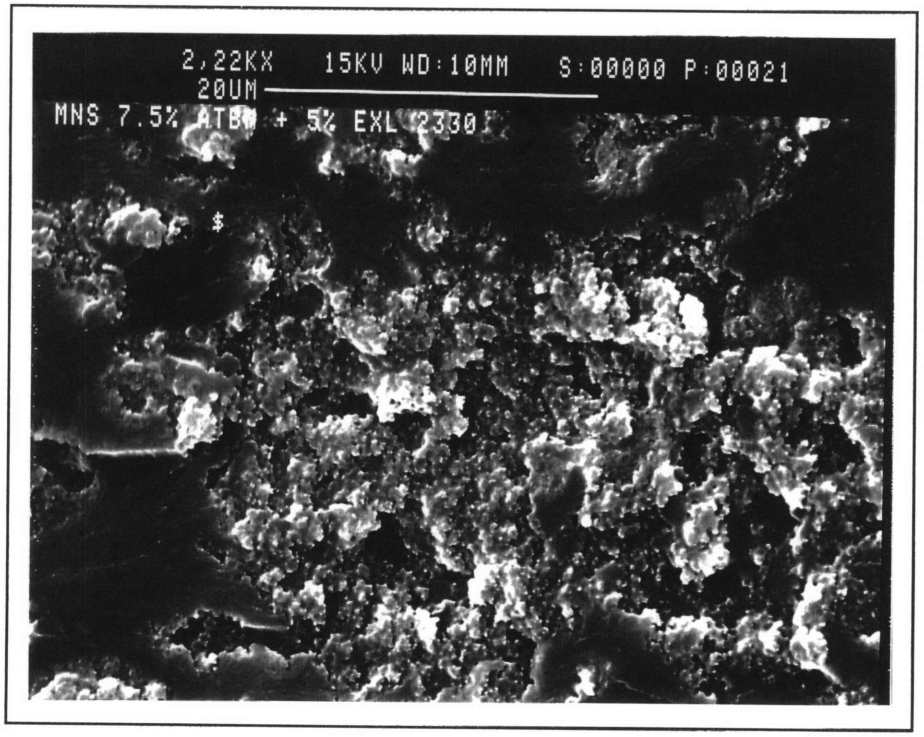

Figure 4.81- EXL 2330 particles within an amorphous rubber-rich domain on the fracture surface of an MNS compact tension specimen containing 7.5% ATBN and 5% EXL 2330 particles.

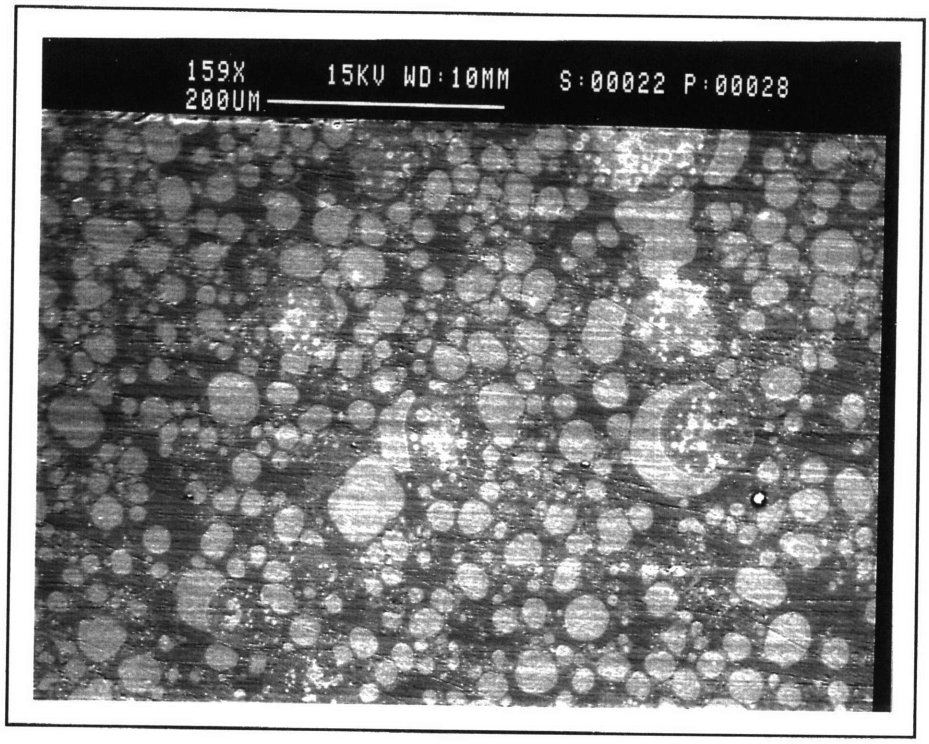

Figure 4.82- Backscattered image of the polished surface of an MNS specimen containing 7.5% ATBN and 5% EXL 2330 particles.

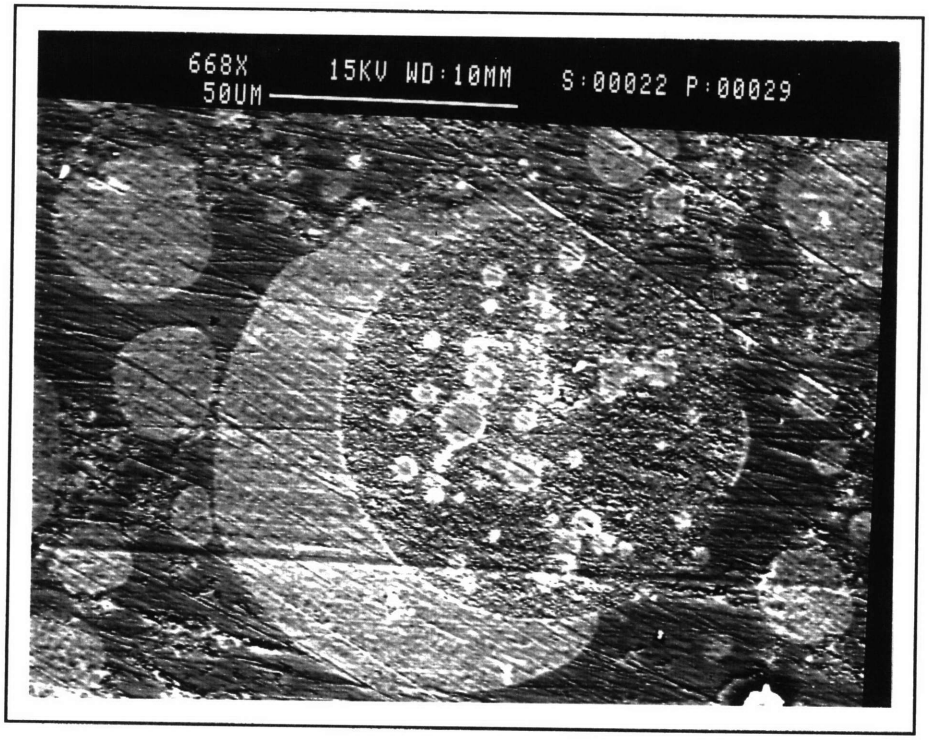

Figure 4.83- Backscattered image of particle containing domains on the polished surface of an MNS specimen containing 7.5% ATBN and 5% EXL 2330 particles.

regions of the large, two-phase domains shown in Figure 4.83. Again, neither the pMMA shell nor the butyl acrylate core of these particles can be stained by the osmium tetroxide, so the particles appear dark in these backscattered images. Neither the surrounding ATBN-rich portion of these domains nor the ATBN occlusions within the rough domains appear to contain any particles. Particles are found in the smaller, discrete rubber-rich domains shown in Figure 4.83 and in the relatively ATBN-free regions between the discrete ATBN-rich domains. The particles within the smaller ATBN-rich domains do not appear to be as densely packed as those in the relatively rubber-free regions.

The fracture surface of the casting containing 7.5% ATBN and 5% EXL 2330 particles showed very good adhesion between particles and matrix, and the polished surface showed that the particles were located within the ATBN-rich domains. However, the fracture toughness and G_{Ic} values still did not improve considerably over any of the other castings containing rubber particles. This is probably due to the fact that the majority of the particles were found in the domains that did not contain as much ATBN. It could also be due to the fact that the ATBN-rich domains which did contain particles were very small. Thus, the deformation may be too localized.

4.2.3.3 Dynamic Mechanical Analysis

Figure 4.84 contains the tanδ curves for samples containing 7.5% ATBN and either 5% EXL 5136, EXL 2691, or EXL 2330 core-shell particles, as well as the 0% ATBN and 7.5% ATBN control samples. Table 4.6 lists the temperatures and the intensities of the transitions. All three types of particles produced curves that exhibit both primary and secondary transitions. The primary transitions for all three types of particles occur at the same temperature as that for the 7.5% ATBN control specimen. However, the intensity of this transition occurs at a lower value of around 0.175 for each of the samples containing the EXL particles. The locations of the secondary transitions vary from around 102°C for the EXL 2691 particles to around 110°C for the EXL 5136 particles and the transitions are very distinct.

This distinct secondary transition indicates that the epoxy phase has formed larger microdomains with a higher degree of mobility than in the 7.5% ATBN control specimen. The mobility of the epoxy phase appears to correspond to the fracture toughness of the sample, as there is a measurable increase in toughness of the samples containing the EXL particles over the control 7.5% ATBN specimen. In addition, the sample with the EXL 2691 particles has the highest intensity secondary transition of the samples containing EXL particles and exhibits the highest fracture toughness of these samples. However, since the mobility of the polyester phase decreases with the addition of the EXL particles, the toughness of these samples is not quite as high as expected from the increased rubber content.

Table 4.6- Values of Tg and tan(d) for both primary and secondary transitions in for MNS samples containing 7.5% ATBN and 5% core-shell particles as determined by DMA runs performed at a rate of 2°C per minute and a frequency of 5 Hz.

Sample	High Temperature Transition (°C)	Low Temperature Transition (°C)	High Temperature tan(d)	Low Temperature tan(d)
0% ATBN	147.6	112.3	0.2173	0.1709
7.5% ATBN	164.8	none	0.1930	none
5% EXL5136	165.4	109.6	0.1755	0.1205
5% EXL2691	157.0	105.0	0.1767	0.1649
5% EXL2330	167.7	102.4	0.1747	0.1196

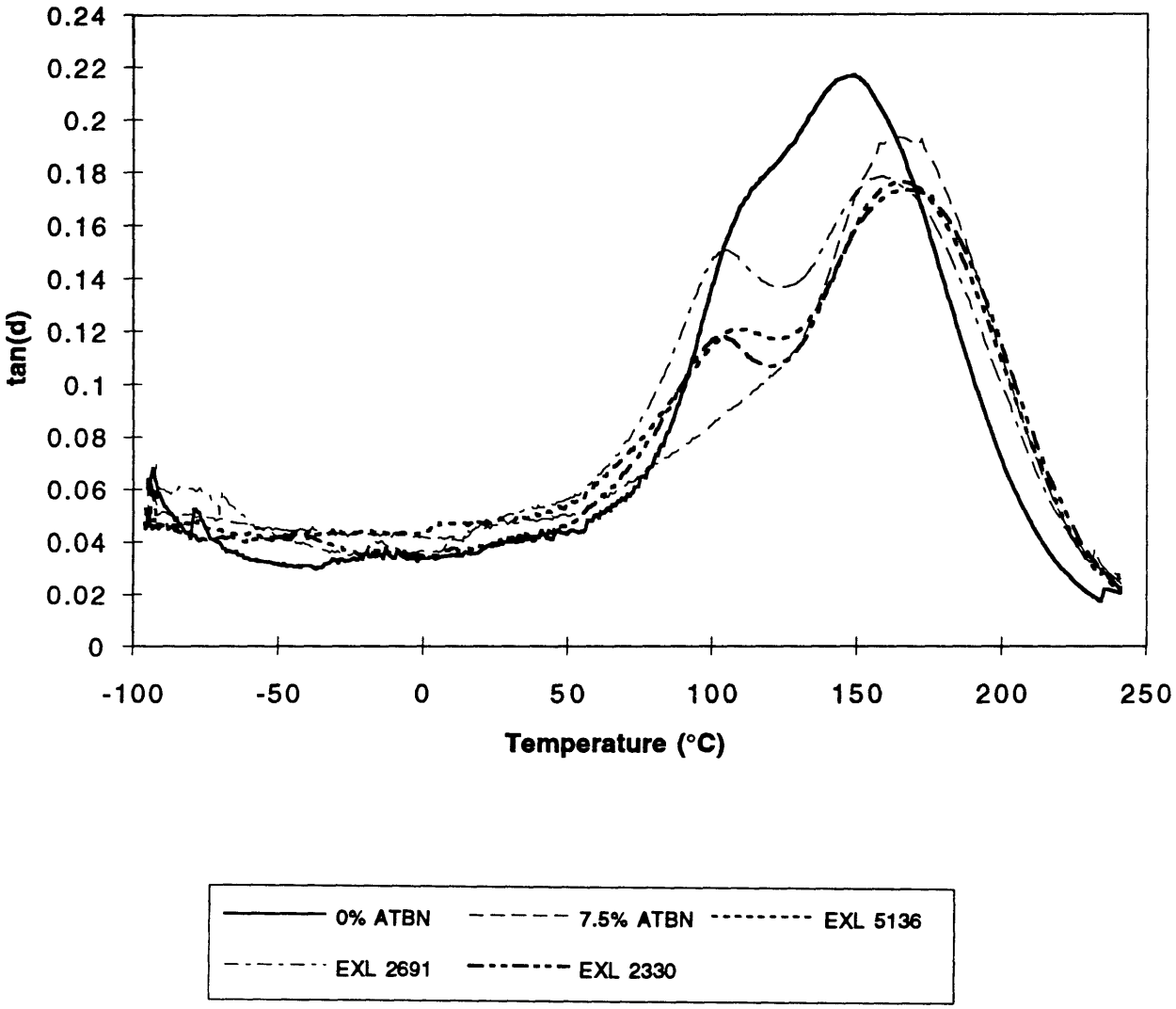

Figure 4.84- Tanδ curves as a function of temperature for MNS specimens containing 7.5% ATBN and 5% core-shell particles as determined by DMA performed in tensile mode at a heating rate of 2°C/min and a frequency of 5 Hz.

4.2.4 Glass Particles

In order to ensure that the styrene monomer did not dissolve or penetrate the second phase particles, glass spheres were investigated for use as second phase particles. As stated in the background section, voids were found to toughen as well as rubber particles in some cases. The crack bridging and subsequent rubber tearing mechanism was not found to be necessary for toughening as long as the second phase particles produced enough stress concentration to induce deformation in the surrounding matrix. Therefore, glass spheres should be capable of toughening matrices.

Two types of glass spheres were obtained from Potter's Industries. The first type was a solid sphere with a 2 micron diameter, and the second was a hollow sphere with a diameter of 8 microns. As discussed in the experimental section, the spheres were first reacted with a silanol based coupling agent to increase the degree of adhesion between the particles and MNS matrix. All castings containing 7.5% ATBN and 5% glass spheres also contained 0.5% fumed silica particles to increase the viscosity of the resin so as to prevent the dense glass particles from sinking to the bottom. The casting with the solid glass spheres showed a good distribution of particles and was transparent, while that with the hollow glass spheres was opaque. The opacity of the later casting was probably due to the different indices of refraction of the hollow glass spheres.

4.2.4.1 Fracture Toughness

The fracture toughness values for MNS samples containing 7.5% ATBN and either 5% solid glass spheres reacted with epoxy coupling agent, solid spheres reacted with amino coupling agent, or hollow glass spheres reacted with epoxy coupling agent are shown in Figure 4.85. The average K_{Ic} values for each specimen is shown in Table 4.3. The fracture toughness of the samples containing the solid glass spheres with either type of coupling agent actually decreases with respect to the control 7.5% ATBN specimen. The K_{Ic} value for the solid spheres reacted with the epoxy coupling agent falls only slightly to an average value of 0.6195 $ksi*in^{1/2}$, while that for the spheres

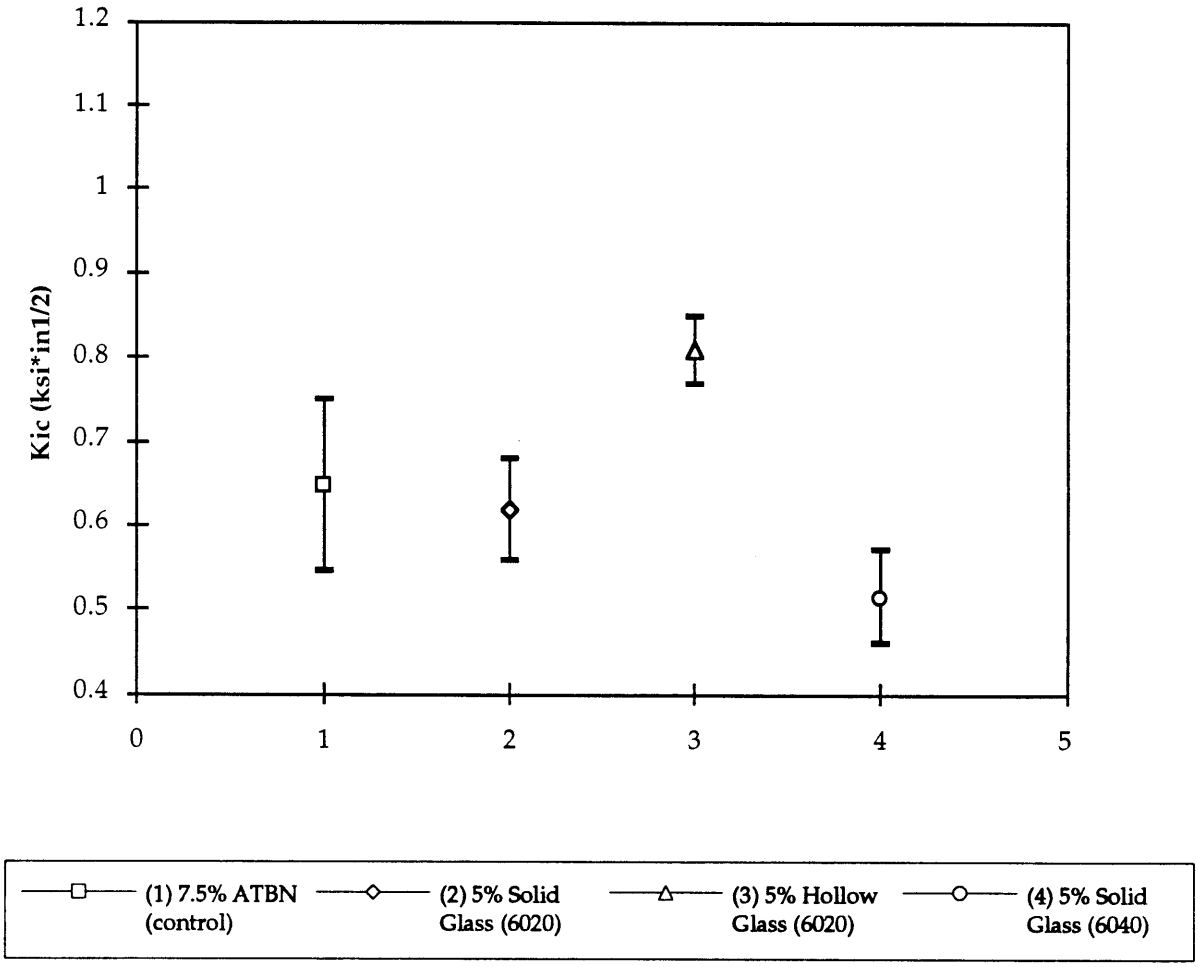

Figure 4.85- Fracture toughness values for MNS compact tension samples containing 7.5% ATBN and 5% solid glass spheres reacted with either epoxy or amino coupling agent or 5% hollow glass spheres reacted with epoxy coupling agent tested according to ASTM D 5045-93 at a rate of 0.2 in/min.

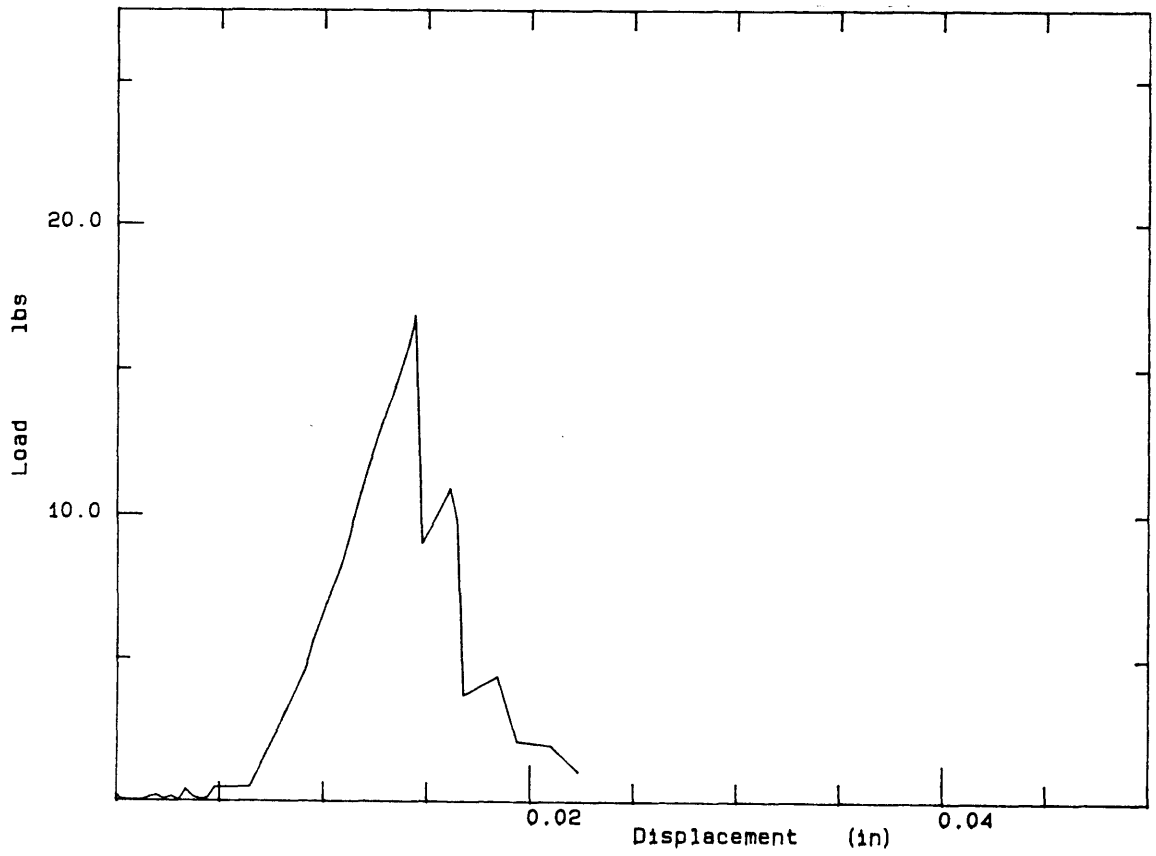

Figure 4.86- Load versus displacement curve for an MNS compact tension specimen containing 7.5% ATBN and 5% solid glass spheres reacted with epoxy coupling agent tested at a rate of 0.2 in/min.

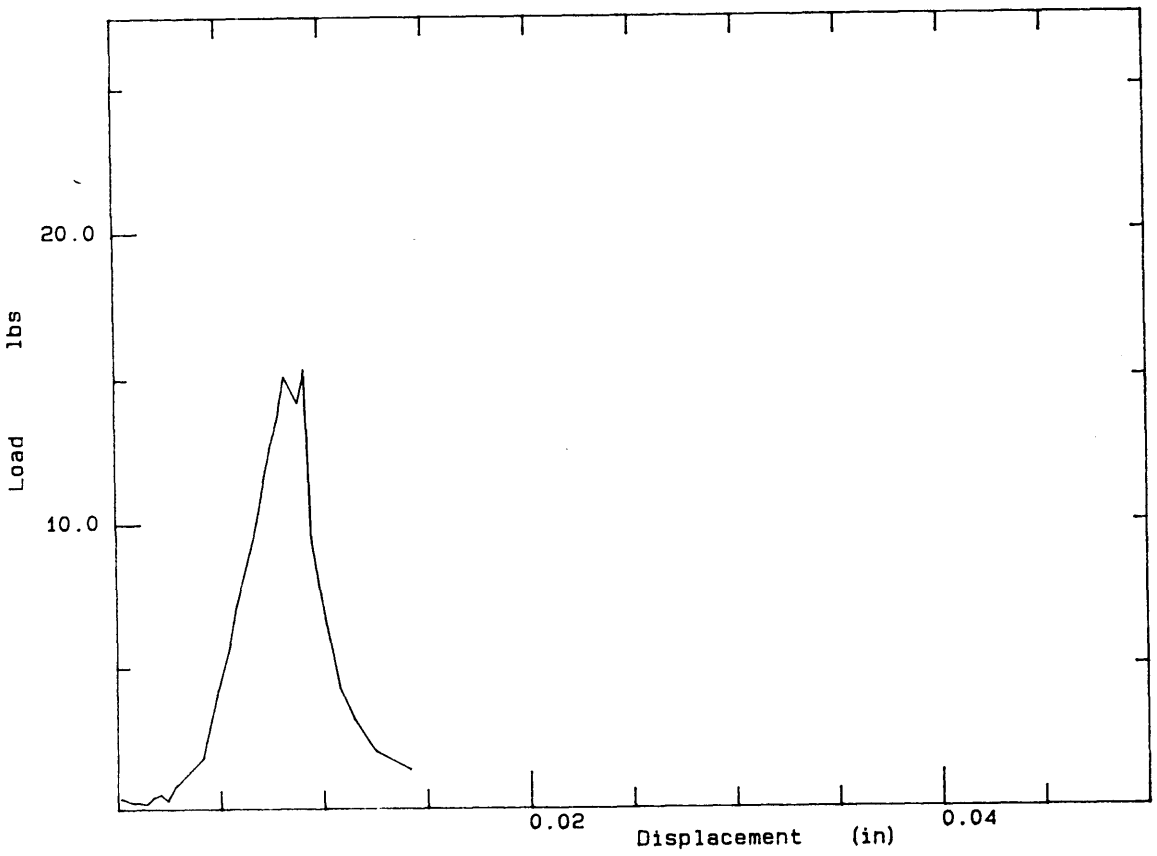

Figure 4.87- Load versus displacement curve for an MNS compact tension specimen containing 7.5% ATBN and 5% solid glass spheres reacted with amino coupling agent tested at a rate of 0.2 in/min.

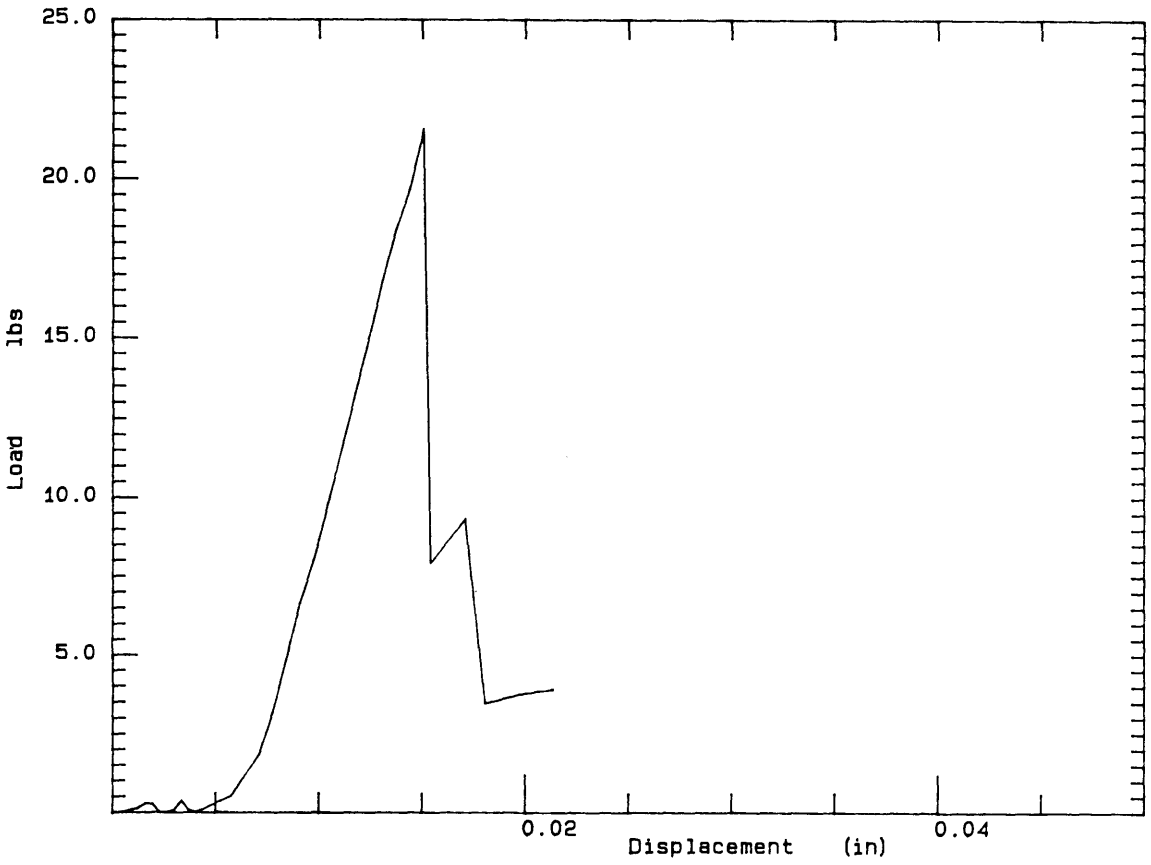

Figure 4.88- Load versus displacement curve for an MNS compact tension specimen containing 7.5% ATBN and 5% hollow glass spheres reacted with epoxy coupling agent tested at a rate of 0.2 in/min.

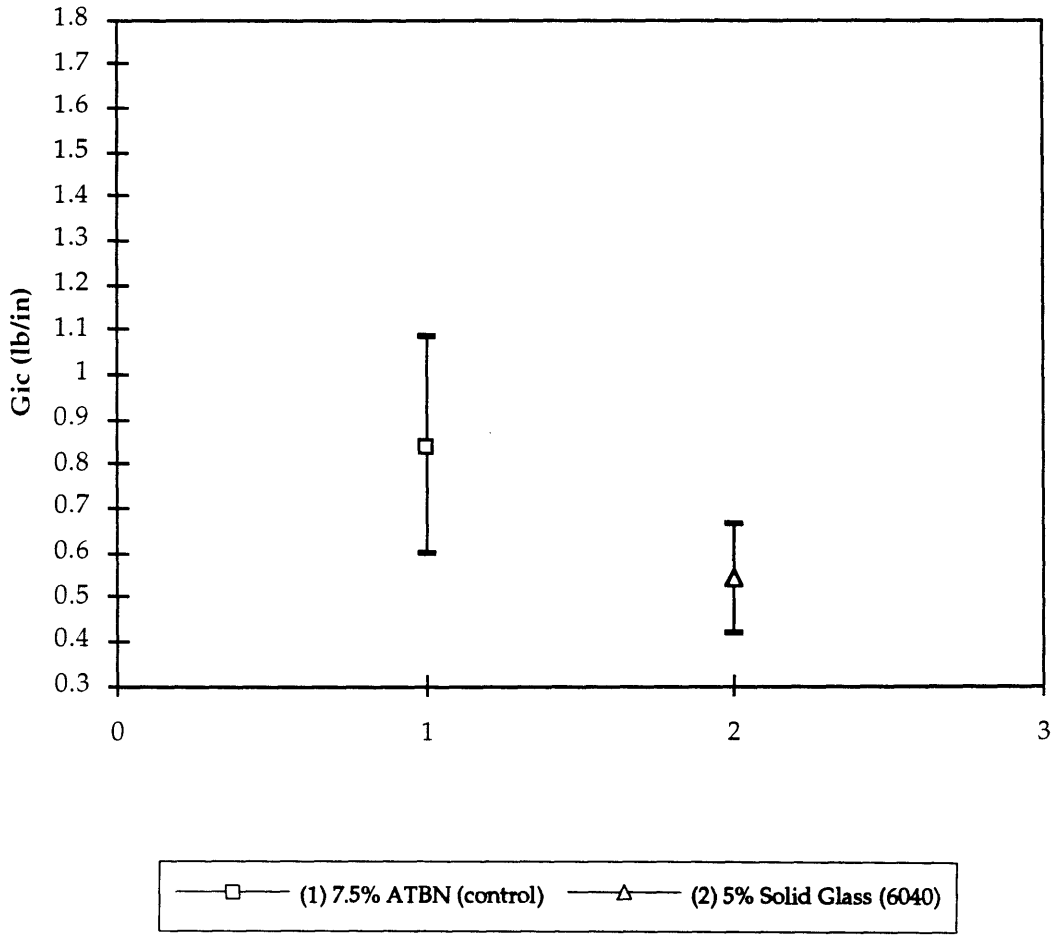

Figure 4.89- Average Gic values for MNS compact tension samples containing 7.5% ATBN and 5% solid glass spheres reacted with amino coupling agent tested according to ASTM D 5045-93 at a rate of 0.2 in/min.

reacted with the amino coupling agent drops considerably to a value of 0.5151 ksi*in$^{1/2}$. On the other hand, the sample containing 5% hollow glass spheres reacted with the epoxy coupling agent showed a considerable increase in fracture toughness to an average value of 0.8093 ksi*in$^{1/2}$. The load versus displacement curves for all three types of specimens are very similar and show a similar amount of crack arrest (Figures 4.86 - 4.88).

The average GIc value of the samples containing the solid glass spheres reacted with the amine compatible coupling agent is 0.54 lb/in, which is significantly lower than the value of 0.84 lb/in for the 7.5% ATBN control specimens (Figure 4.89). This is due to both the lower KIc values for these samples and the very high modulus values (of around 500 ksi) for the samples containing the solid glass spheres.

4.2.4.2 Scanning Electron Microscopy

4.2.4.2.1 Solid Glass Spheres (Z6020)

The fracture surface of the compact tension specimen containing 5% solid glass spheres reacted with the epoxy compatible coupling agent is shown in Figure 4.90. The surface shows the presence of ATBN domains that are about the same size as those found in the control 7.5% ATBN specimen. However, unlike the domains in the control specimen, the domains in the specimen containing 5% solid glass spheres are not completely circular. For the most part, the domains in the later specimen are composed of a particle-free ATBN center and a surrounding fringe of more deformed material containing the glass spheres. However, not all of the solid glass spheres in the casting were located at the edges of the ATBN domains. There were a number of smaller ATBN domains that contained solid glass spheres throughout (Figure 4.91). In either case, there was extremely poor adhesion between the spheres and the matrix even though the spheres were reacted with a coupling agent prior to being incorporated into the resin.

The polished surface of a specimen taken from the same casting is shown in Figure 4.92. It can be seen that the glass spheres attract ATBN to

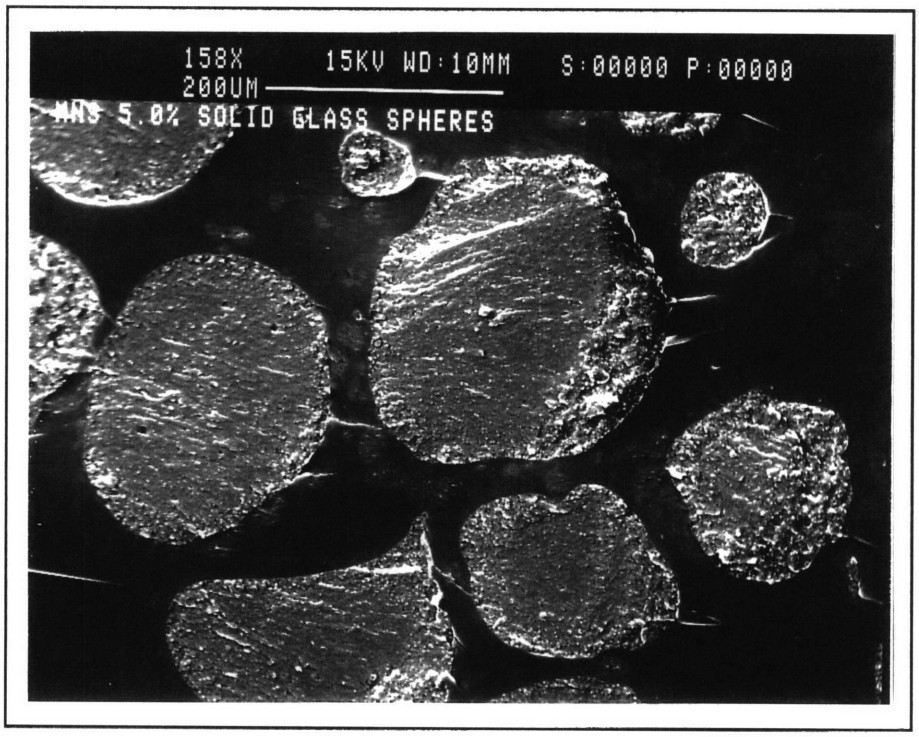

Figure 4.90- Fracture surface of an MNS compact tension specimen containing 7.5% ATBN and 5% solid glass spheres reacted with epoxy coupling agent.

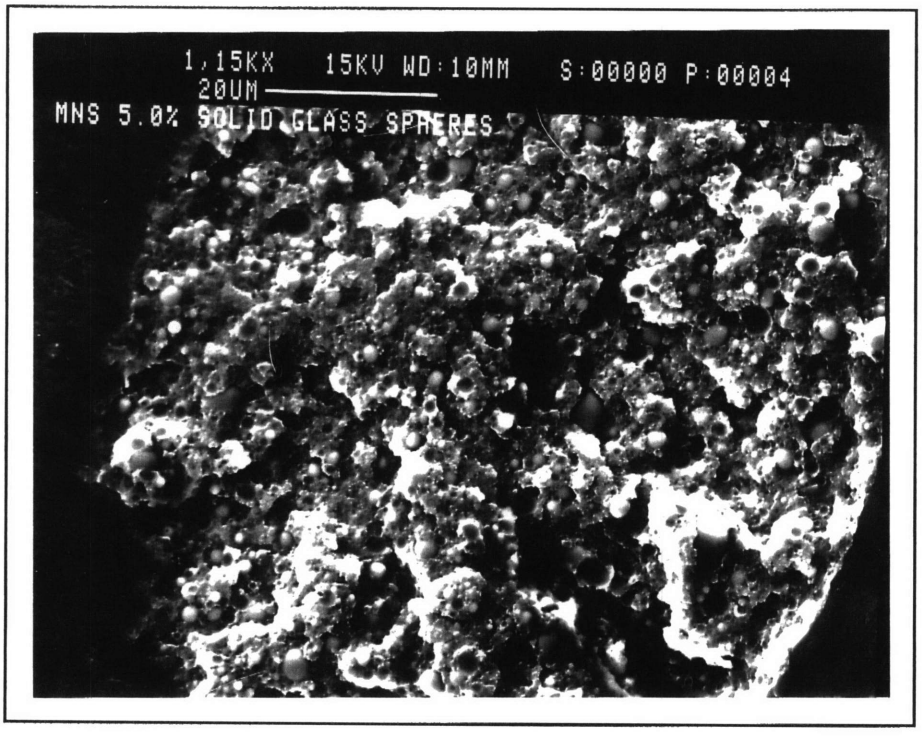

Figure 4.91- Glass spheres in an ATBN-rich domain on the fracture surface of an MNS sample containing 7.5% ATBN and 5% solid glass spheres reacted with epoxy coupling agent.

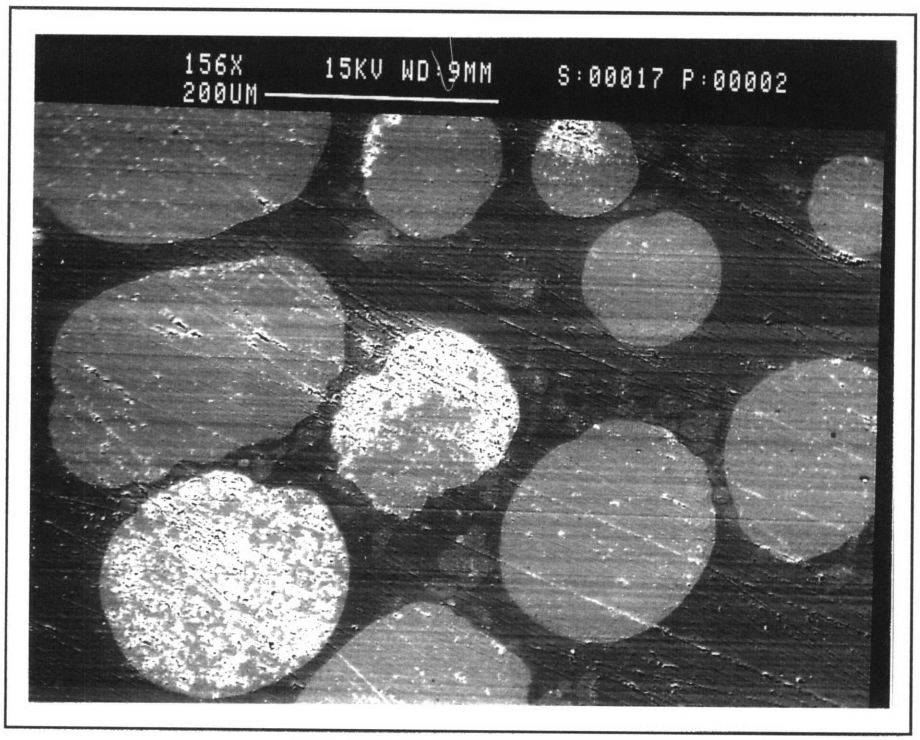

Figure 4.92- Backscattered image of the polished surface of an MNS specimen containing 7.5% ATBN and 5% solid glass spheres reacted with an epoxy coupling agent.

their surfaces. This could be the result of ATBN reacting with the epoxy functionality in the coupling agent. Thus, it appears that the drop in fracture toughness of these specimens with respect to the control 7.5% ATBN specimen is a result of the combination of very poor adhesion of the particles and the withdrawing of the ATBN from the main portions of the domains, thus, making the domains ATBN deficient.

4.2.4.2.2 Solid Glass Spheres (Z6040)

Figure 4.93 shows the fracture surface of a specimen containing 7.5% ATBN and 5% solid glass spheres reacted with the amino coupling agent. As expected, the glass spheres exhibit a much higher degree of adhesion than did the ones reacted with the epoxy compatible coupling agent (Figure 4.94). However, the amine compatible spheres are located outside of the ATBN domains rather than inside as found for the solid spheres reacted with the epoxy coupling agent. No glass spheres were found within the ATBN domains. While the spheres are not located inside the discrete ATBN domains, the polished surface of a sample of the same composition shows that the glass spheres attracted some of the ATBN to their surfaces and out of the discrete rubber-rich domains (Figure 4.95). The fact that the spheres attract the rubber is not surprising considering that the coupling agent used contains amino groups. However, the amount of rubber they attract is very small.

Thus, the extremely low fracture toughness of these samples is probably due to two factors. First, while the spheres themselves are well-adhered, they are located outside the ATBN-rich domains and the rubber they are able to attract to their surfaces is too small a quantity to produce effective toughening. Secondly, the removal of the ATBN from the main domains diminishes the effectiveness of these domains.

4.2.4.2.3 Hollow Glass Spheres (Z6020)

Figure 4.96 shows the fracture surface of the specimen containing 5% hollow glass spheres reacted with the epoxy compatible coupling agent. Unlike the specimen with the solid glass spheres reacted with the epoxy coupling agent, the ATBN domains in this sample tended to coalesce in

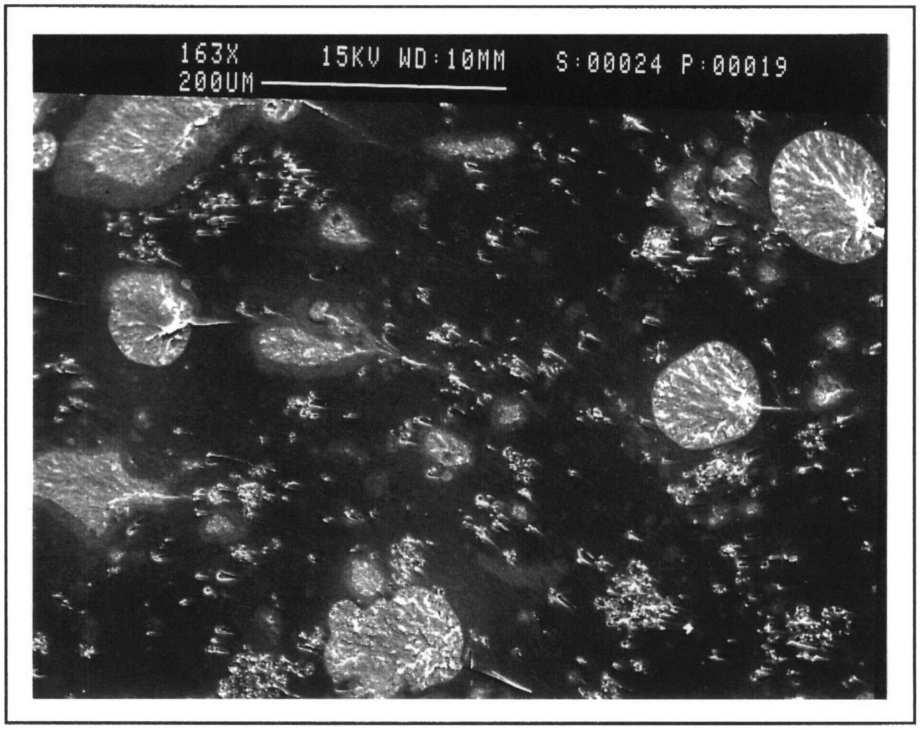

Figure 4.93- Fracture surface of an MNS compact tension specimen containing 7.5% ATBN and 5% solid glass spheres reacted with an Z6040 coupling agent.

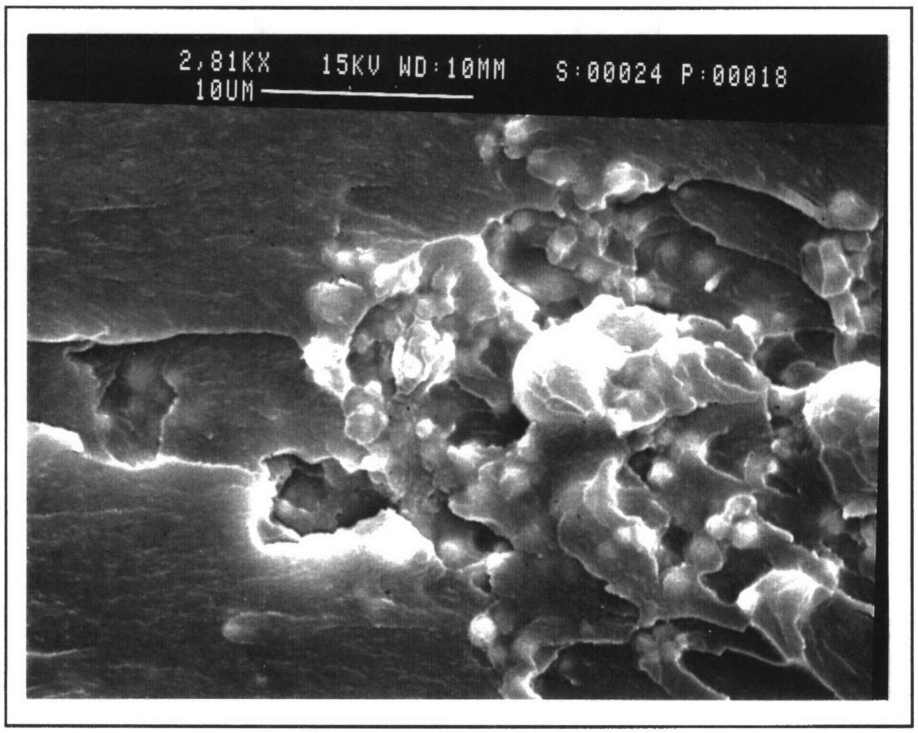

Figure 4.94- Well-adhered glass spheres on the fracture surface of an MNS compact tension specimen containing 7.5% ATBN and 5% solid glass spheres reacted with an Z6040 coupling agent.

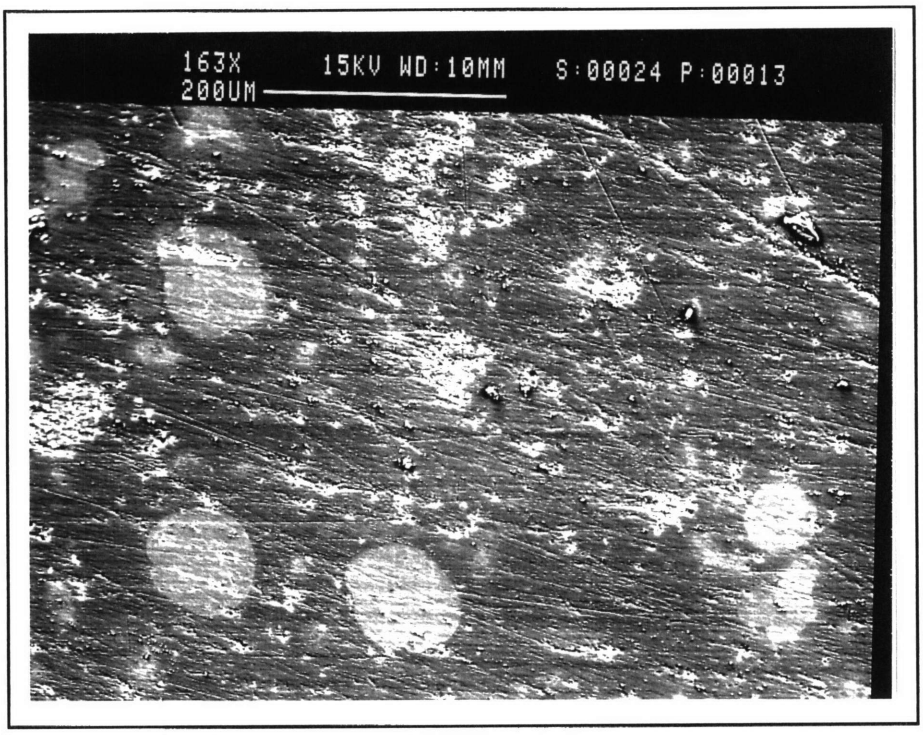

Figure 4.95- Backscattered image of the polished surface of an MNS specimen containing 7.5% ATBN and 5% solid glass spheres reacted with an Z6040 coupling agent.

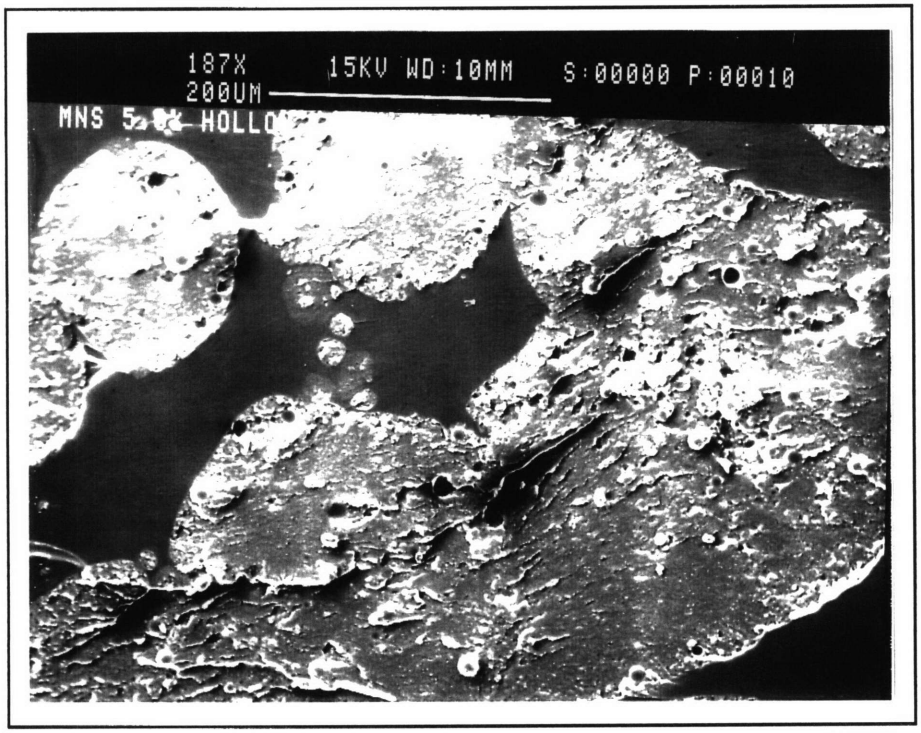

Figure 4.96- Fracture surface of an MNS compact tension specimen containing 7.5% ATBN and 5% hollow glass spheres reacted with the Z6040 coupling agent.

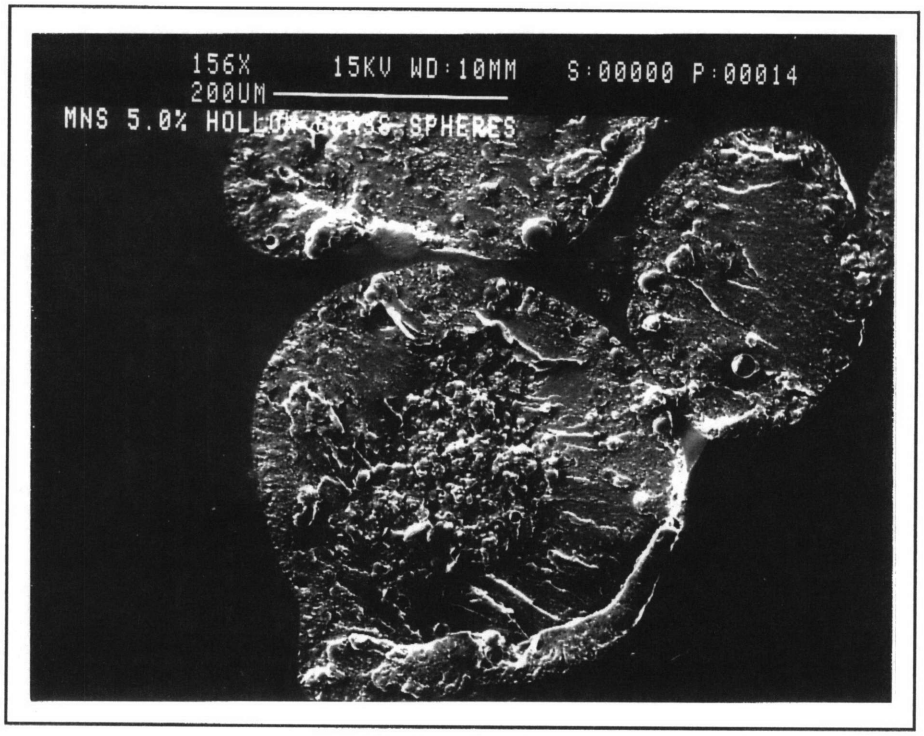

Figure 4.97- Glass spheres in rubber-rich domains on the fracture surface of an MNS compact tension specimen containing 7.5% ATBN and 5% hollow glass sphere reacted with the Z6020 coupling agent.

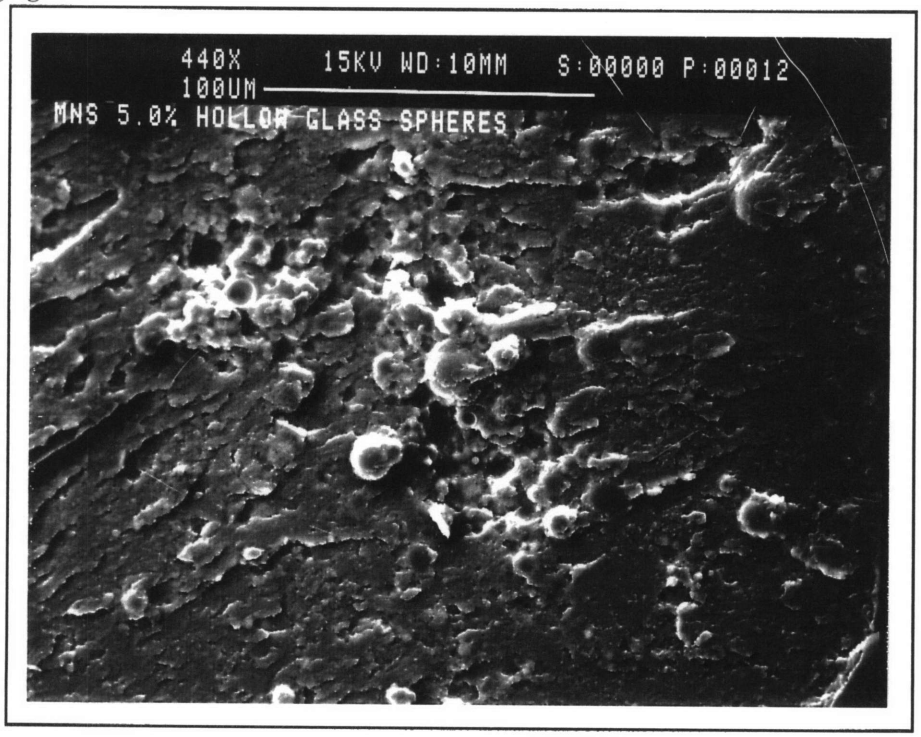

Figure 4.98- Well-adhered glass spheres on the fracture surface of an MNS compact tension specimen containing 7.5% ATBN and 5% hollow glass spheres reacted with the Z6020 coupling agent.

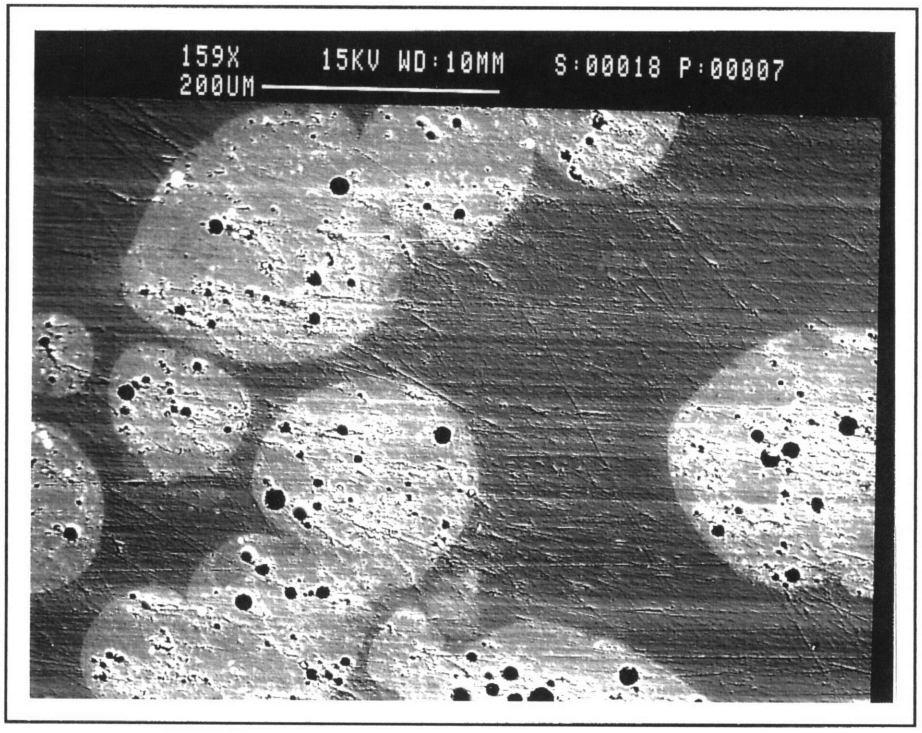

Figure 4.99- Backscattered image of the polished surface of an MNS specimen containing 7.5% ATBN and 5% hollow glass spheres reacted with Z6020 coupling agent.

places. This would explain the opacity of this sample. While some of the hollow spheres were found in the fringes of the ATBN domains, the majority of the spheres were found in the centers of the domains (Figure 4.97). The hollow spheres found on the fringes of the domains lacked good adhesion, but many of the spheres found in the center of the domains showed pieces of resin still adhered to their surfaces (Figure 4.98). The polished surface of a specimen taken from the same casting is shown in Figure 4.99. Although the particles still seem to attract the ATBN to their surfaces, they do not seem to have as severe of a withdrawing effect as the solid spheres reacted with the epoxy coupling agent. This could be due to the fact that the hollow spheres are much more uniformly distributed in the ATBN domains. The extremely well-adhered and well-distributed particles located within the ATBN-rich domains is exactly the desired morphology for a toughened system. This explains the significant increase in the fracture toughness for these specimens over the control 7.5% ATBN specimens.

4.2.4.3 Dynamic Mechanical Analysis

Figure 4.100 contains the tanδ curves for samples containing 7.5% ATBN and either 5% solid glass spheres reacted with Z6020 coupling agent, solid glass spheres reacted with Z6040 coupling agent, or hollow glass spheres reacted with Z6020 coupling agent as well as the 0% ATBN and 7.5% ATBN control samples. Table 4.7 contains the values of the temperatures and intensities of the transitions for these samples. The curve for the solid glass spheres reacted with the amine coupling agent (Z6040) contains one single peak at a temperature of 166°C and is almost identical to that of the 7.5% ATBN control sample. It is possible that the amine functionalities in the coupling agent serve to further increase the crosslinking of the epoxy. Thus, the mobility of the epoxy would be suppressed, and no secondary transition would occur. In addition, the mobility of the polyester phase is also decreased by the addition of the solid glass spheres with amino (Z6040) coupling agent. Thus, it is not surprising that this sample has an extremely low fracture toughness.

On the other hand, the tanδ curves for both the solid and hollow glass spheres reacted with the epoxy compatible coupling agent (Z6020) possessed

both primary and secondary peaks and are almost identical to each other. The primary peaks occur at the same temperature as that for the 7.5% ATBN specimen, but with a slightly lower intensity of around 0.175. The secondary peaks both occur at around 110°C. The intensity of the secondary transitions is similar to those of the casting containing the Nipol particles. It is curious that the tanδ curves of these two specimens are so similar when the sample with the hollow glass spheres exhibits substantially higher toughness properties than that with the solid glass spheres. It appears that increasing the mobility of the epoxy phase is not a sufficient condition for increasing the fracture toughness of the sample. It was found from the SEM micrographs of these two samples that the degree of adhesion of the solid glass spheres was very poor, while that of the hollow spheres was exceptionally good. The combination of the good adhesion of particles and the increased mobility of the epoxy phase in the sample containing the hollow spheres resulted in good energy absorption mechanisms for this sample.

Table 4.7- Values of Tg and tan(d) for both primary and secondary transitions in for MNS samples containing 7.5% ATBN and either 5% solid glass spheres reacted Z6020 coupling agent, solid glass spheres reacted with Z6040 coupling agent, or hollow glass spheres reacted with Z6020 coupling agent as determined by DMA performed in tensile mode at a heating rate of 2°C/min and a frequency of 5 Hz.

Sample	High Temperature Transition (°C)	Low Temperature Transition (°C)	High Temperature tan(d)	Low Temperature tan(d)
0% ATBN	147.6	112.3	0.2173	0.1709
7.5% ATBN	164.8	none	0.1930	none
5% Solid 6020	162.8	112.0	0.1777	0.1242
5% Hollow 6020	159.8	106.6	0.1681	0.1271
5% Solid 6040	166.8	none	0.1882	none

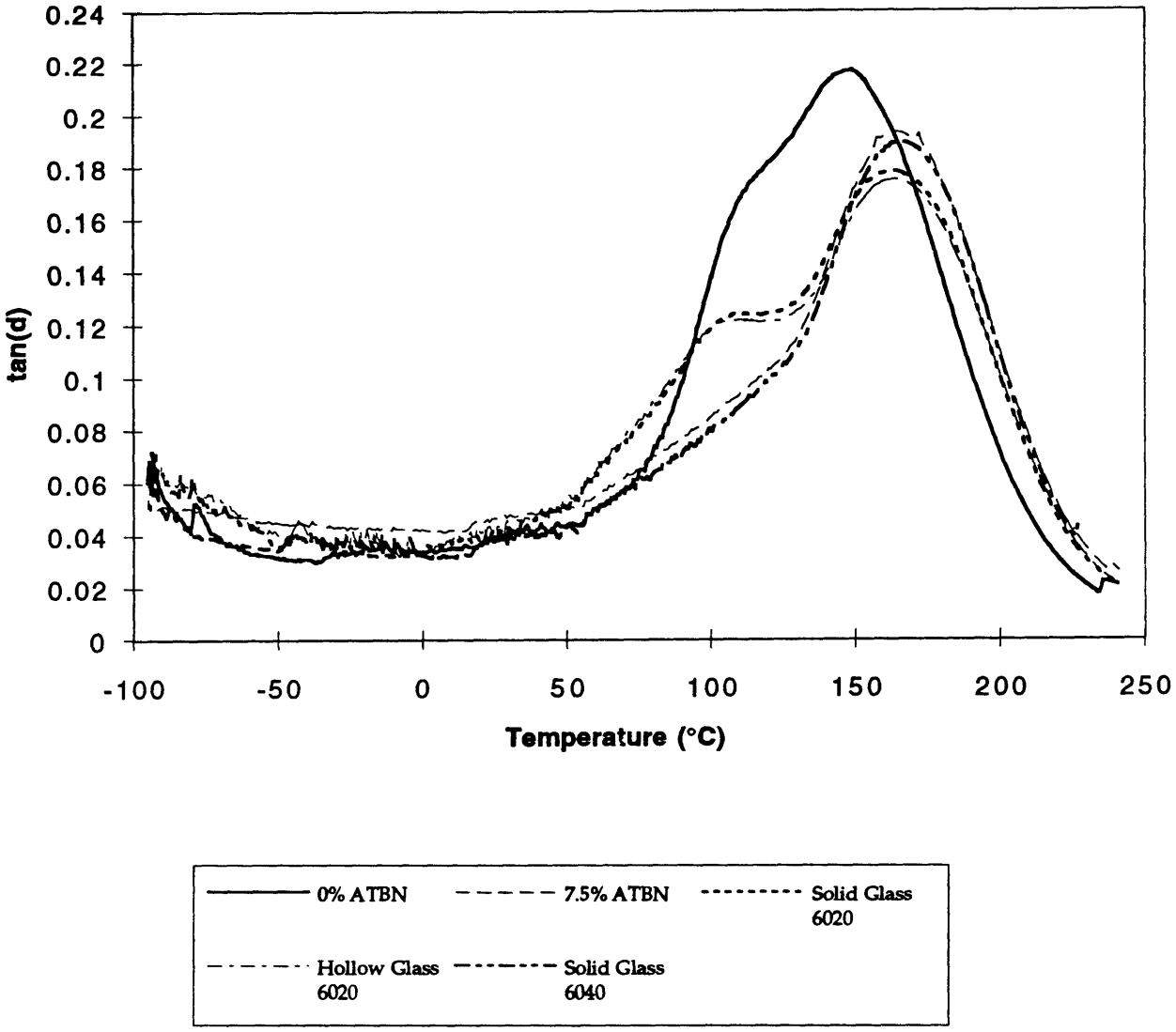

Figure 4.100- Tanδ curves as a function of temperature for MNS specimens containing 7.5% ATBN and either 5% solid glass beads reacted Z6020 coupling agent, solid glass beads reacted with Z6040 coupling agent, or hollow glass beads reacted with Z6020 coupling agent as determined by DMA performed in tensile mode at a heating rate of 2°C/min and a frequency of 5 Hz.

4.2.5 PDMS Particles

From the above results, it appears that while well-adhered second phase particles with diameters close to 1 micron located inside the ATBN-rich domains can produce a measurable increase in toughness properties, the real toughness increases were achieved only when the continuous phase became rubber-rich. This was the case for the top portion of the casting containing 2.5% CTBN. Also, it was still possible that some of the styrene monomer had penetrated the pre-formed rubber particles to reduce their deformabiliy (this was evidenced by the lack of a low temperature rubber transition in the DMA curves of any of the samples containing pre-formed rubber particles). Therefore, castings containing 9.5% ATBN and 5% PDMS particles were produced. A rubber content of 9.5% ATBN is just high enough to ensure a continuous rubber-rich phase in MNS. The PDMS particles were chosen because they were believed to be more resistant to penetration by the styrene monomer. Three types of PDMS particles were investigated. All had a particle size of around 5 microns. The differences came in the form of the coatings, which contained either amino, epoxy or silanol groups.

4. 2.5.1 Fracture Toughness

The fracture toughness values for the sample containing 7.5% ATBN and 5% PDMS particles are shown in Figure 4.101, and the average values are given in Table 4.3. The average fracture toughness values for the samples containing the amino and epoxy groups are 0.6873 and 0.7169 ksi*in$^{1/2}$ respectively, which is slightly higher than for the control 7.5% ATBN casting. The low value of 0.6446 ksi*in$^{1/2}$ for the fracture toughness of the sample containing the PDMS particles with silanol groups is probably the result of the poor distribution of particles observed in this sample. The silanol PDMS particles congregated into clumps with diameters of a few millimeters that were visible to the naked eye. However, all of the samples containing PDMS particles had lower fracture toughness values than MNS castings containing 9.5% ATBN. This indicates that the additional rubber content, both in the form of ATBN and the PDMS particles, was the cause of the slight increase in fracture toughness over the 7.5% ATBN control sample.

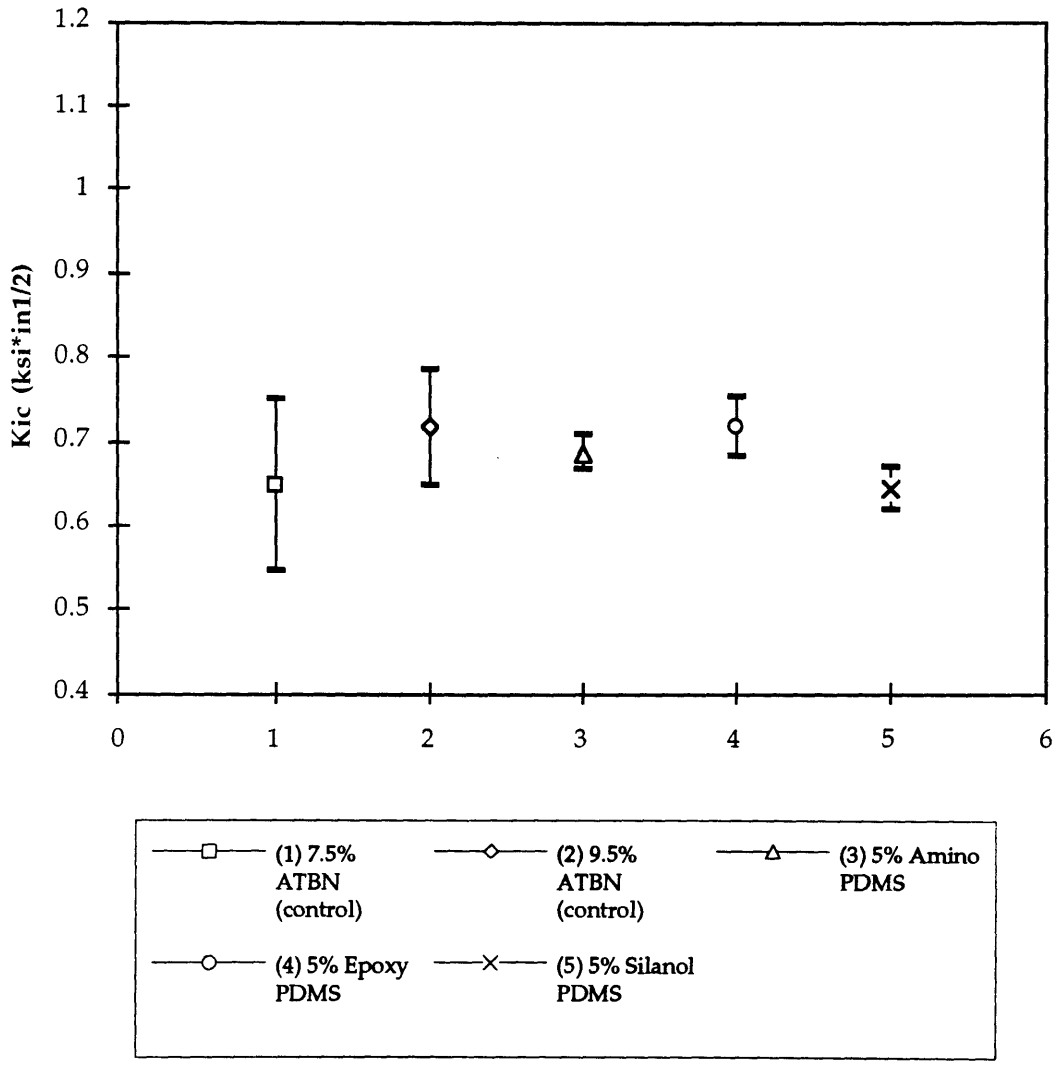

Figure 4.101- Fracture toughness values for MNS compact tension samples containing 9.5% ATBN and 5% PDMS particles tested according to ASTM D 5045-93 at a rate of 0.2 in/min.

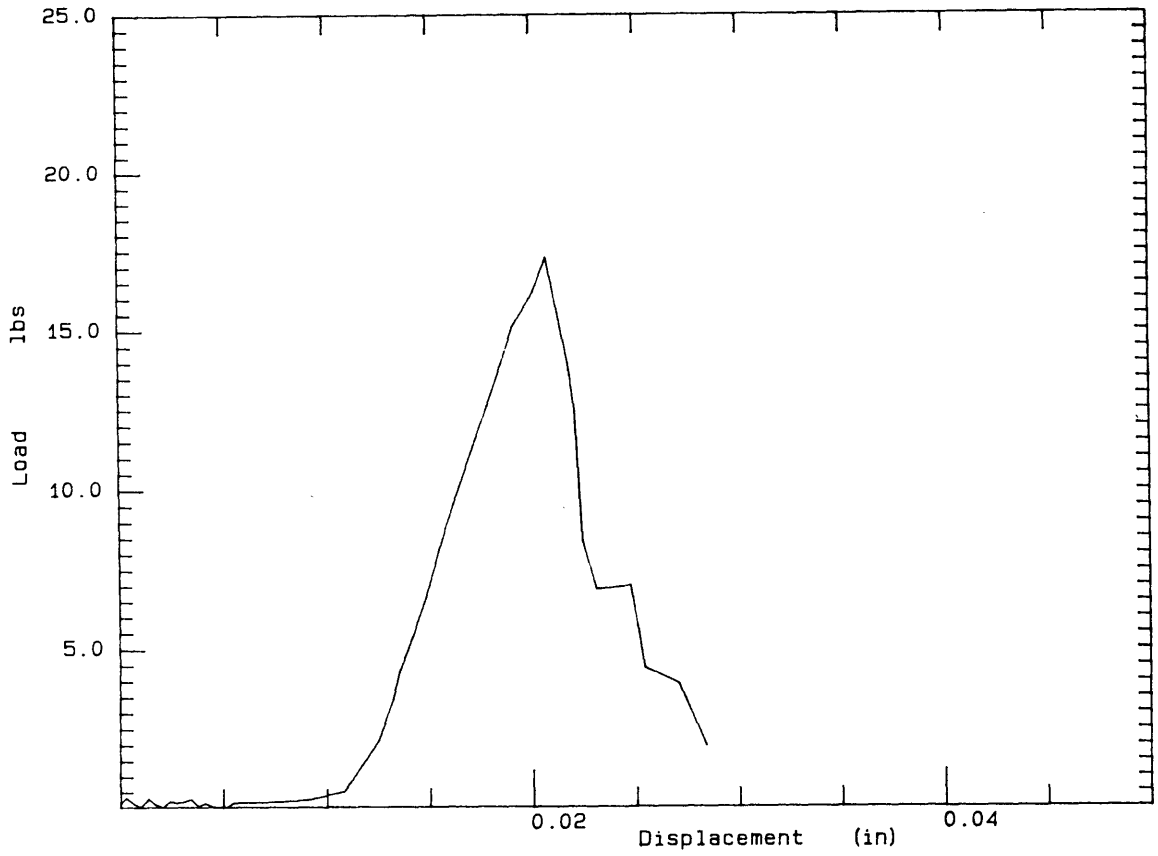

Figure 4.102- Load versus displacement curve for an MNS compact tension specimen containing 9.5% ATBN and 5% amino PDMS particles tested at a rate of 0.2 in/min.

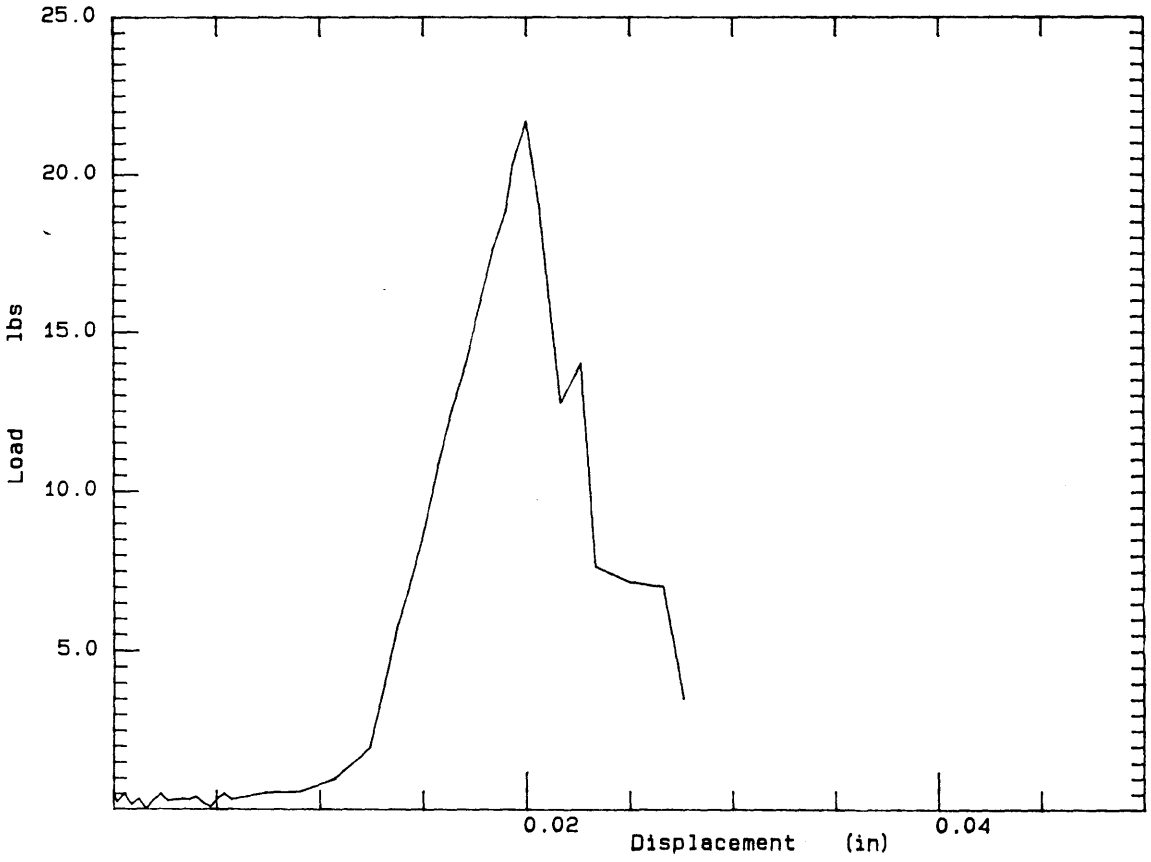

Figure 4.103- Load versus displacement curve for an MNS compact tension specimen containing 9.5% ATBN and 5% epoxy PDMS particles tested at a rate of 0.2 in/min.

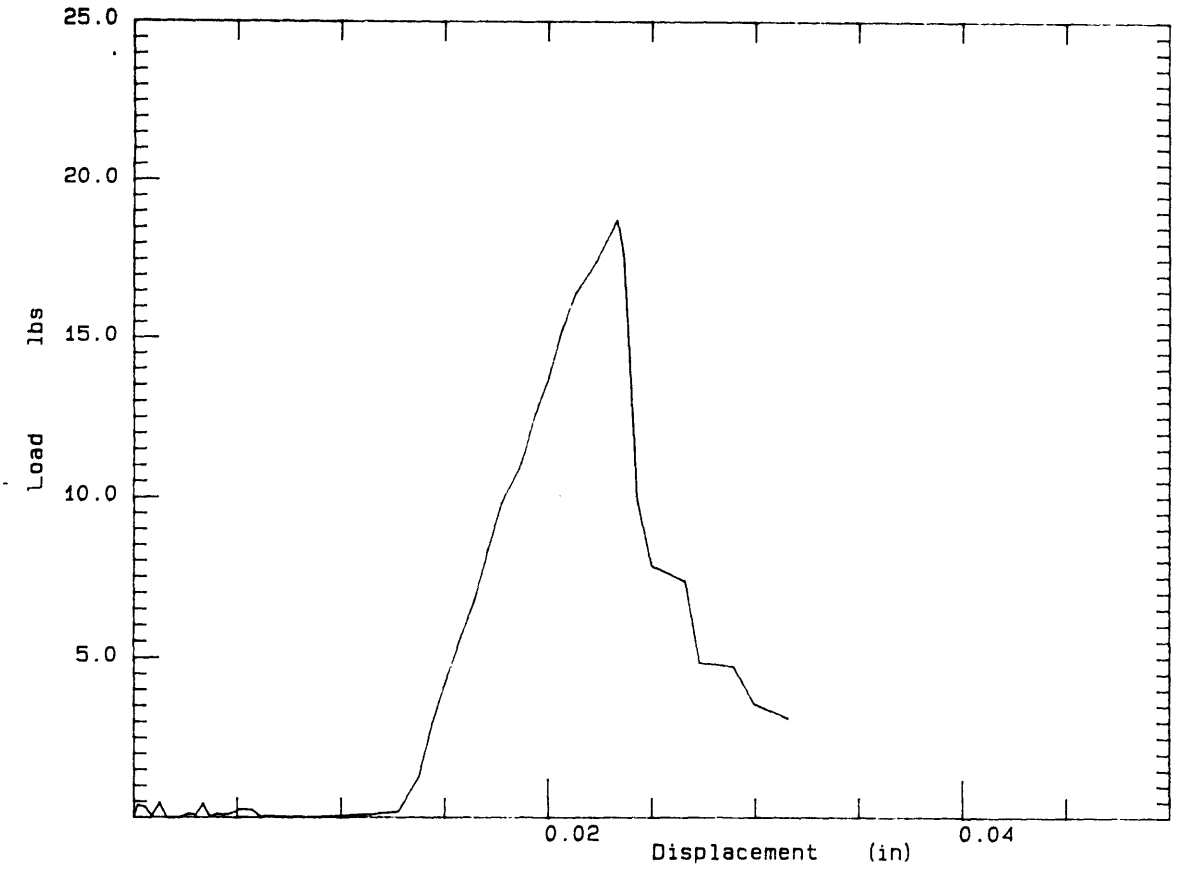

Figure 4.104- Load versus displacement curve for an MNS compact tension specimen containing 9.5% ATBN and 5% silanol PDMS particles tested at a rate of 0.2 in/min.

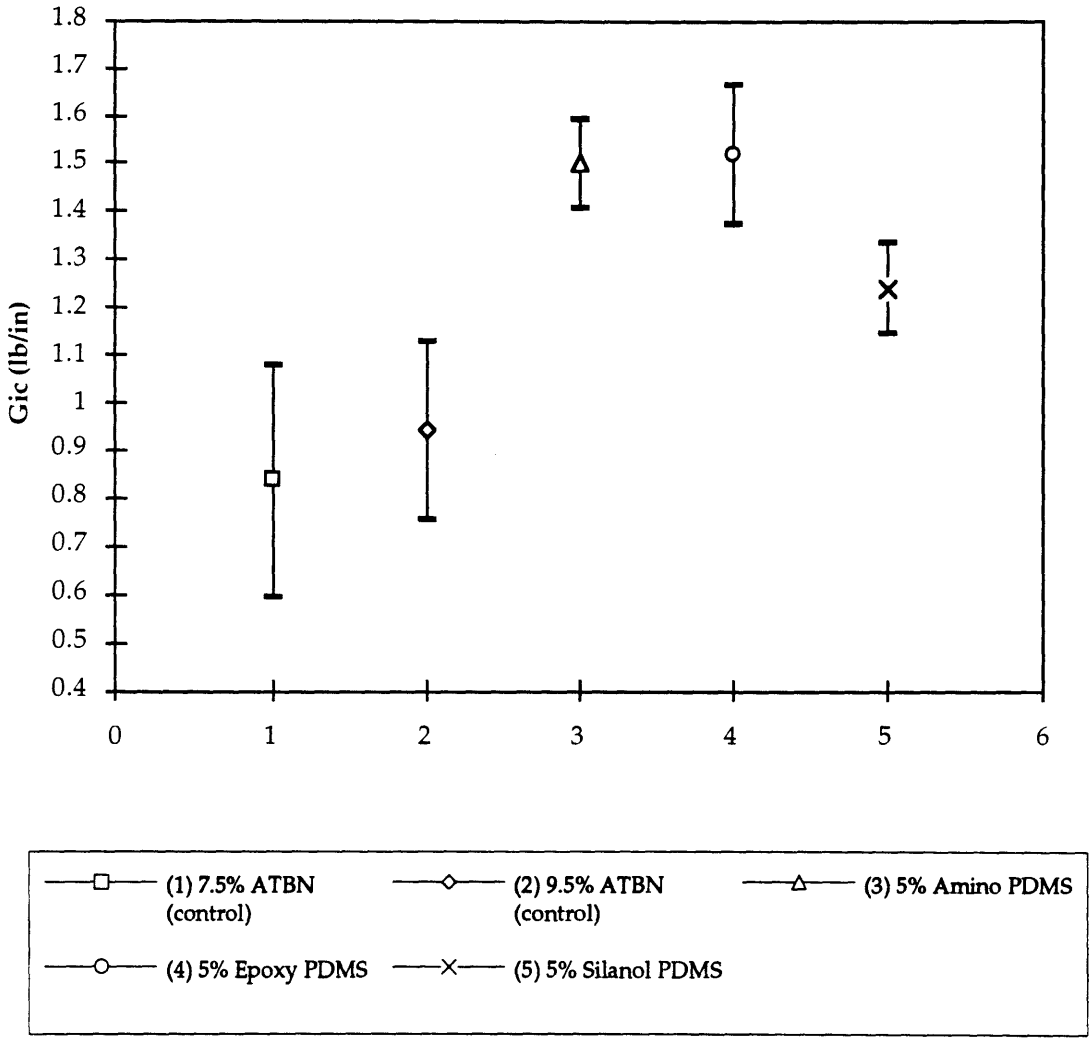

Figure 4.105- Average GIC values for MNS compact tension samples containing 9.5% ATBN and 5% PDMS particles tested according to ASTM D 5045-93 at a rate of 0.2 in/min.

The load versus displacement curves for the samples containing the PDMS particles show only minimal evidence of crack arrest (Figures 4.102-4.104). However, the samples containing 9.5% ATBN and the amino or epoxy compatible PDMS particles show a very significant increase in G_{Ic} to 1.5 lb/in. This is a considerable increase over both the 7.5% ATBN and 9.5% ATBN control specimens (Figure 4.105). The increase over the 9.5% ATBN control value could be attributed to the much lower modulus values of around 330 ksi for these samples and the greater total rubber content. The sample containing the Silanol PDMS has a slightly higher G_{Ic} value than the 9.5% ATBN control specimen, but a much lower modulus.

4.2.5.2 Scanning Electron Microscopy

4.2.5.2.1 Amino PDMS Particles

The fracture surface of a sample containing 9.5% ATBN and 5% Amino PDMS particles is shown in Figure 4.106. Note that even though the casting contains 9.5% ATBN, the continuous phase is still polyester-rich. Without the additional rubber particles, MNS samples with ATBN contents as low as 9% have been found to exhibit a continuous rubber-rich phase. Instead, the ATBN domains still constitute the discontinuous phase. The PDMS particles have somehow managed to suppress the phase inversion. The amino PDMS particles appear to be very poorly adhered, as there is extensive evidence of particle pull-out (Figure 4.107). The particles are also found to be located only in the middle of the large, amorphous ATBN-rich domains and not in the smaller, circular domains.

The polished surface of a sample taken from the same casting appears in Figure 4.108. All the PDMS particles appear to be inside the amorphous domains and not inside the smaller, circular ATBN-rich domains. The PDMS particles appear dark in these backscattered images because they do not contain any unsaturation for the osmium atoms to react with. The PDMS particles appear to attract ATBN to their surfaces as all of the particles are surrounded by bright material (Figure 4.109). The ATBN probably reacts with the amino groups on the surfaces of the PDMS particles. It is probable that when the ATBN is attracted to the surfaces of the PDMS particles, the ATBN

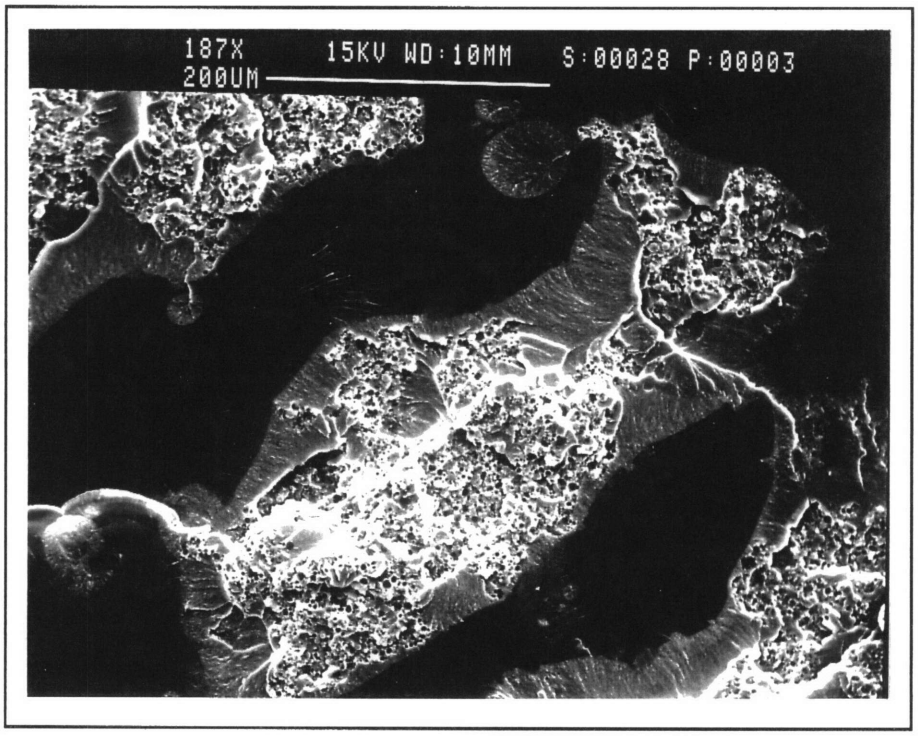

Figure 4.106- Fracture surface of an MNS compact tension specimen containing 9.5% ATBN and 5% amino PDMS particles.

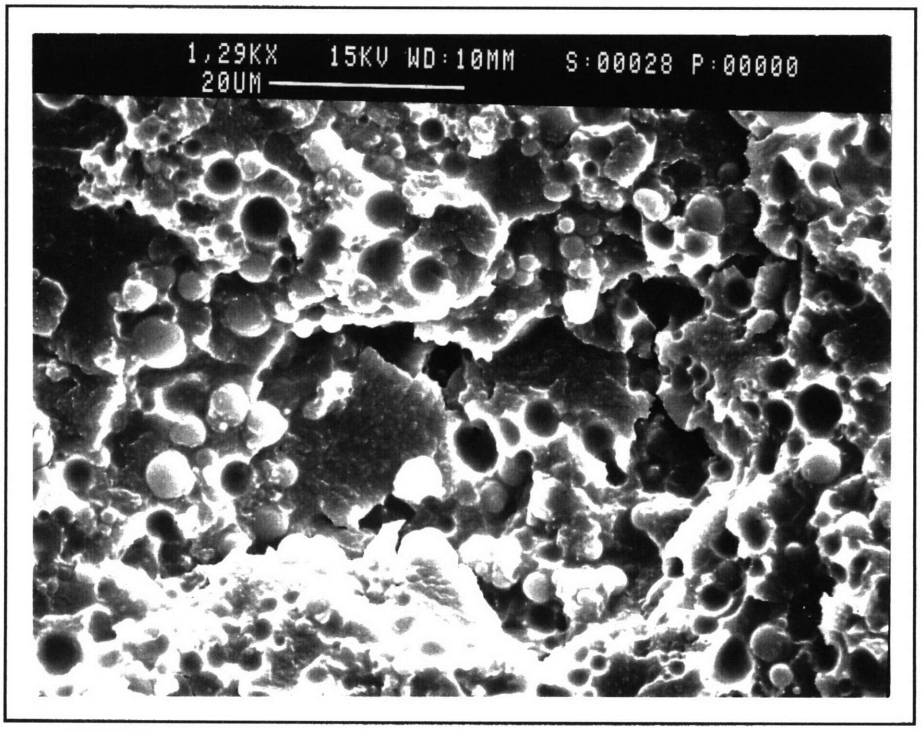

Figure 4.107- Evidence of pulled out particles in a rubber-rich domain on the fracture surface of an MNS compact tension specimen containing 9.5% ATBN and 5% amino PDMS particles.

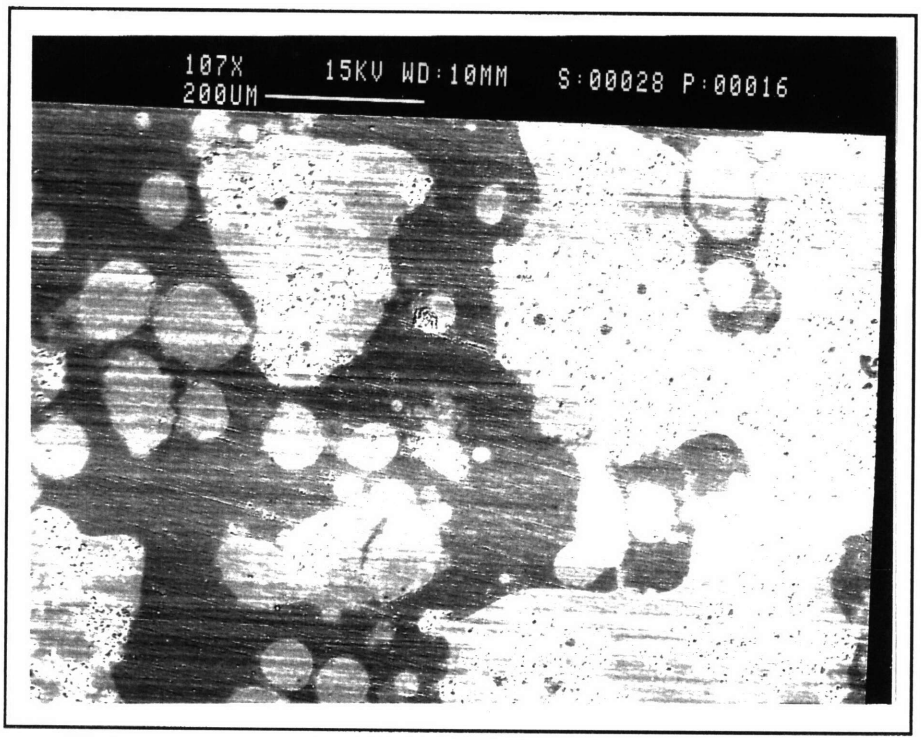

Figure 4.108- Backscattered image of the polished surface of an MNS sample containing 9.5% ATBN and 5% amino PDMS particles.

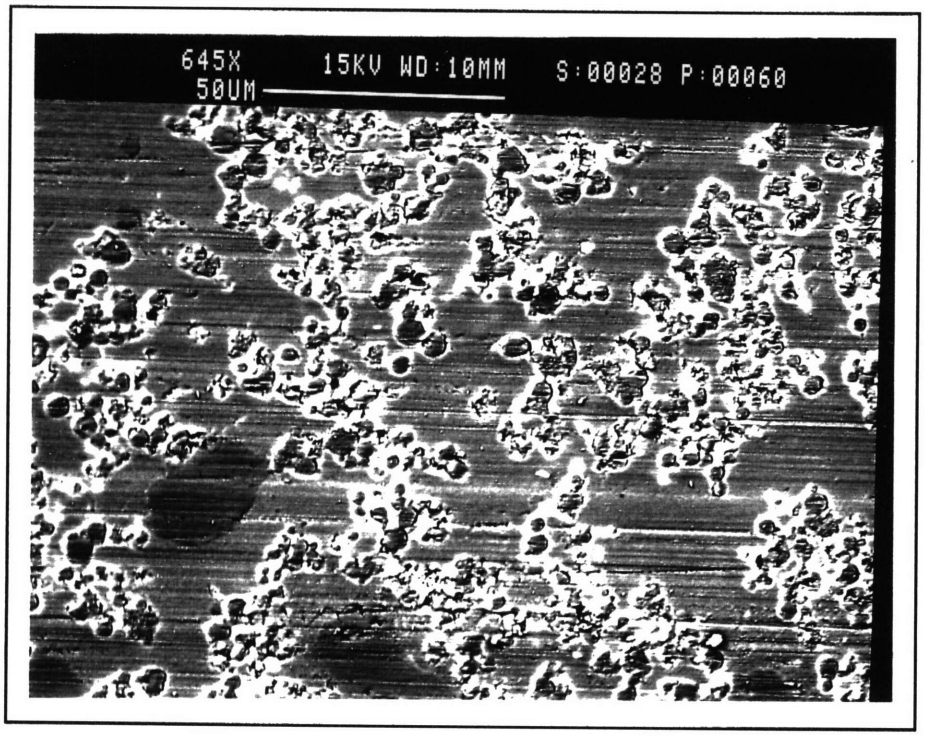

Figure 4.109- Backscattered image of PDMS particles in a rubber-rich domain on the polished surface of an MNS sample containing 9.5% ATBN and 5% amino PDMS particles.

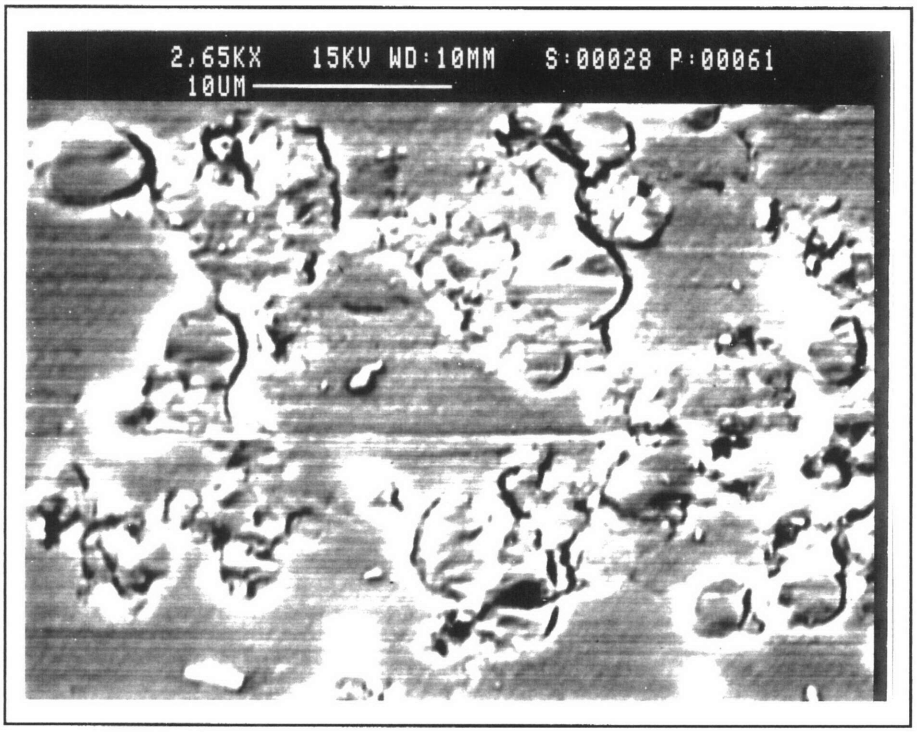

Figure 4.110 - Backscattered image of poorly-adhered PDMS particles on the polished surface of an MNS sample containing 9.5% ATBN and 5% amino PDMS particles.

cannot evenly distribute itself throughout the system, and the phase inversion is suppressed. Even though there is a large rubber content in this sample, the fracture toughness does not show an improvement over any of the samples containing 7.5% ATBN and secondary particles. In fact, the fracture toughness and modulus are actually lower than for a sample containing 9.5% ATBN without additional rubber particles. This could be due to the fact that the phase inversion did not occur as expected for this system. It could also be due to the extremely poor adhesion between the particles and matrix (Figure 4.110). Because of the poor adhesion, the PDMS particles are not capable of contributing much of a toughening effect. The GIc does show some improvement, but it is accompanied by such a large drop in modulus that it is hard to attribute the GIc increase to an increase in toughness.

4.2.5.2.2 Epoxy PDMS Particles

Figure 4.111 shows the fracture surface of a specimen containing 9.5% ATBN and 5% Epoxy PDMS particles. Again, the casting did not undergo the expected phase inversion. It appears that the volume fraction of ATBN domains is fairly equal to that of the brittle domains and that both domains are semi-continuous. This suggests that the phase separation mechanism occurred by spinodal decomposition rather than by nucleation and growth. The epoxy PDMS particles are located within the amorphous ATBN domains and are well distributed. The epoxy PDMS particles also appear to have very poor adhesion and a broad distribution of particle sizes (Figure 4.112).

Figure 4.113 shows the well-distributed Epoxy PDMS particles on the polished surface of a sample with the same composition. It appears that the phase inversion was prevented due to ATBN accumulation at the surfaces of the PDMS particles rather than an even distribution throughout the ATBN-rich domains. Even though the rubber-rich domains are large and co-continuous, the fracture toughness is not as high as expected due to the suppression of the phase inversion and the poor adhesion of the PDMS particles.

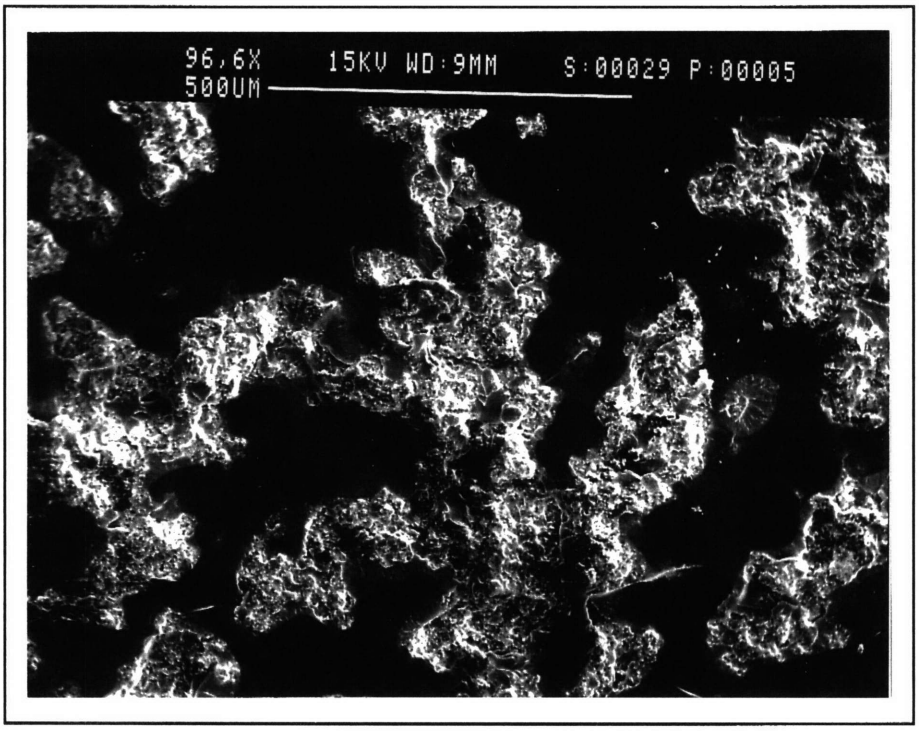

Figure 4.111- Fracture surface of an MNS compact tension specimen containing 9.5% ATBN and 5% Epoxy PDMS particles.

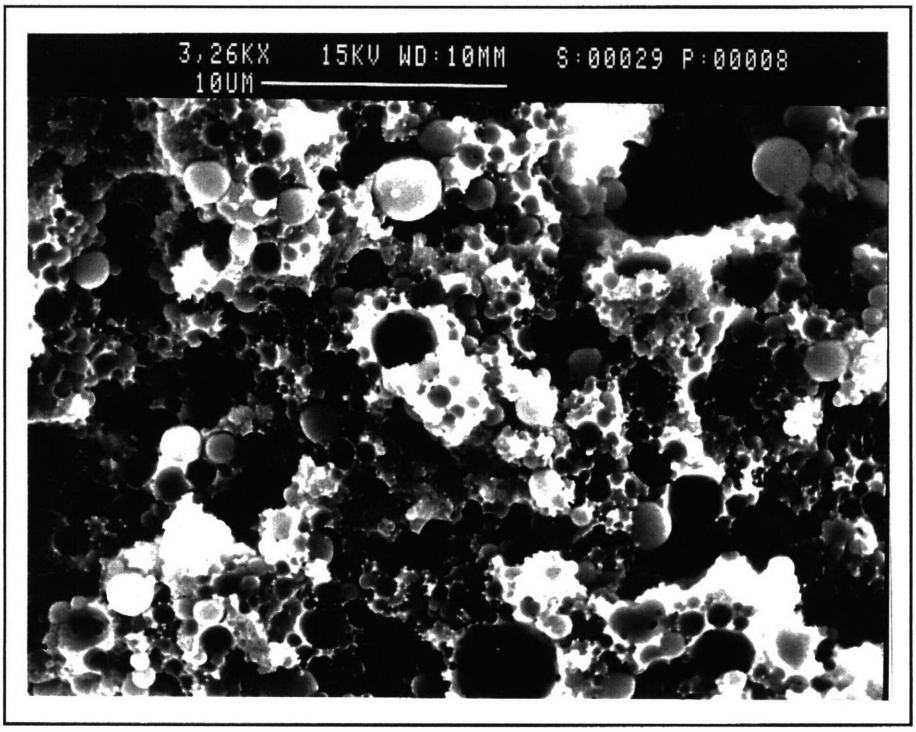

Figure 4.112- Poorly-adhered PDMS particles in a rubber-rich domain on the fracture surface of an MNS sample containing 9.5% ATBN and 5% Epoxy PDMS particles.

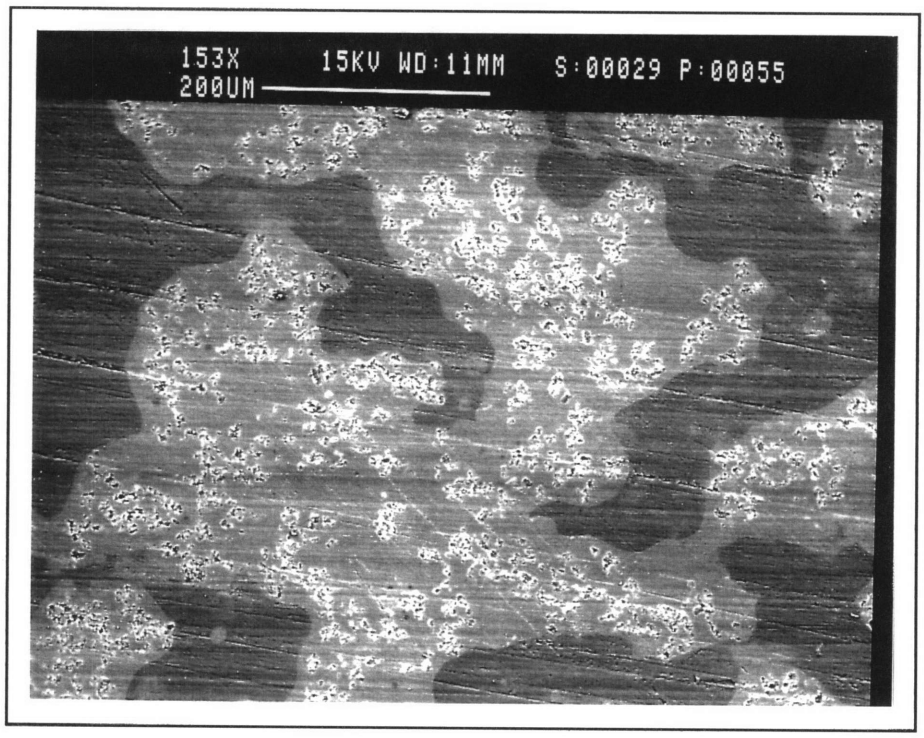

Figure 4.113- Backscattered image of the polished surface of an MNS specimen containing 9.5% ATBN and 5% Epoxy PDMS particles.

4.2.5.2.3 Silanol PDMS Particles

The fracture surface of a specimen containing 9.55 ATBN and 5% silanol PDMS particles is shown in Figure 4.114. There appears to be a slightly higher volume fraction of ATBN domains than brittle material. However, this sample continues to contain the ATBN-rich domains as a discontinuous phase. As was seen in the sample containing the amino PDMS particles, the silanol PDMS particles appear to be clumped into the center of large, amorphous ATBN-rich domains. The smaller, circular ATBN domains do not appear to contain particles. The large domains also appear to have an outer rim of particle-free ATBN. However, the PDMS-containing domains are a good deal larger than those in the sample with amino PDMS particles. This is probably due to the problems encountered in dispersing the silanol PDMS particles during the mixing process. The degree of adhesion of the silanol PDMS particles is very poor and there is a broad distribution of particle sizes (Figure 4.115).

The polished surface of a specimen taken from the same casting is shown in Figure 4.116. This time, instead of the ATBN-rich domains forming a co-continuous phase with the polyester-rich phase, the surface consists of large, amorphous ATBN-rich domains containing PDMS particles and many polyester-rich occlusions. The very dark regions in the ATBN-rich domains are the cross sections of the silanol PDMS particles which do not contain any unsaturation for the osmium to stain. The lighter gray regions of these domains are the polyester-rich occlusions (Figure 4.117). These large domains are surrounded by many smaller ATBN-rich domains that do not appear to contain any particles. This large and small domain structure is probably formed because the silanol PDMS particles tended to clump together. It appears that the phase inversion was suppressed by the PDMS particles drawing the ATBN to their surfaces and out of the domains. The lack of a significant increase in toughness properties can be attributed to the lack of a phase inversion and poor adhesion of the PDMS particles.

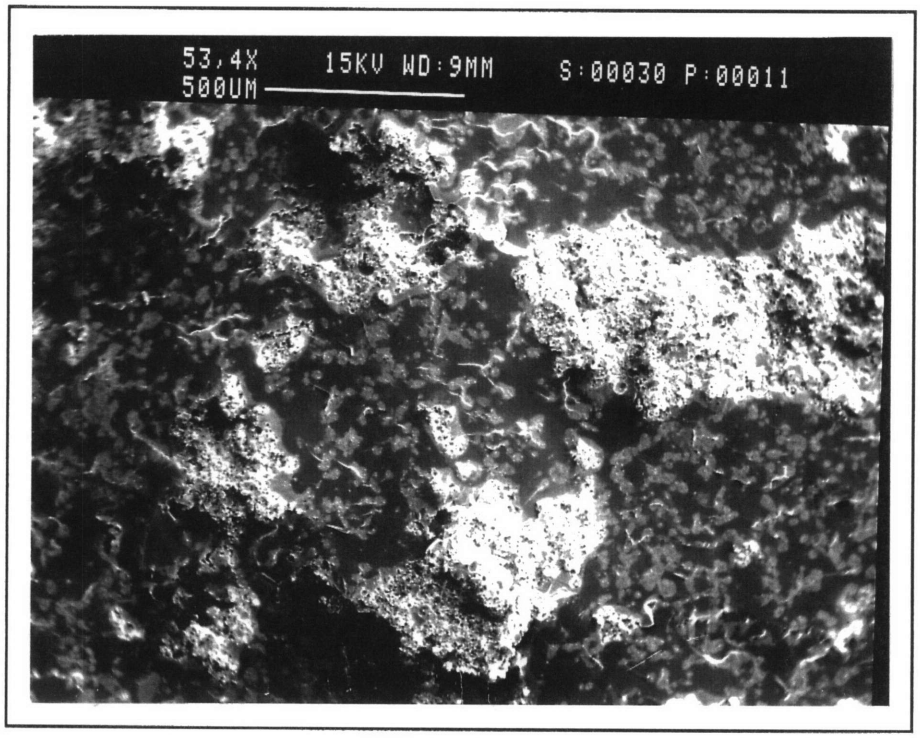

Figure 4.114- Fracture surface of an MNS compact tension specimen containing 9.5% ATBN and 5% Silanol PDMS particles.

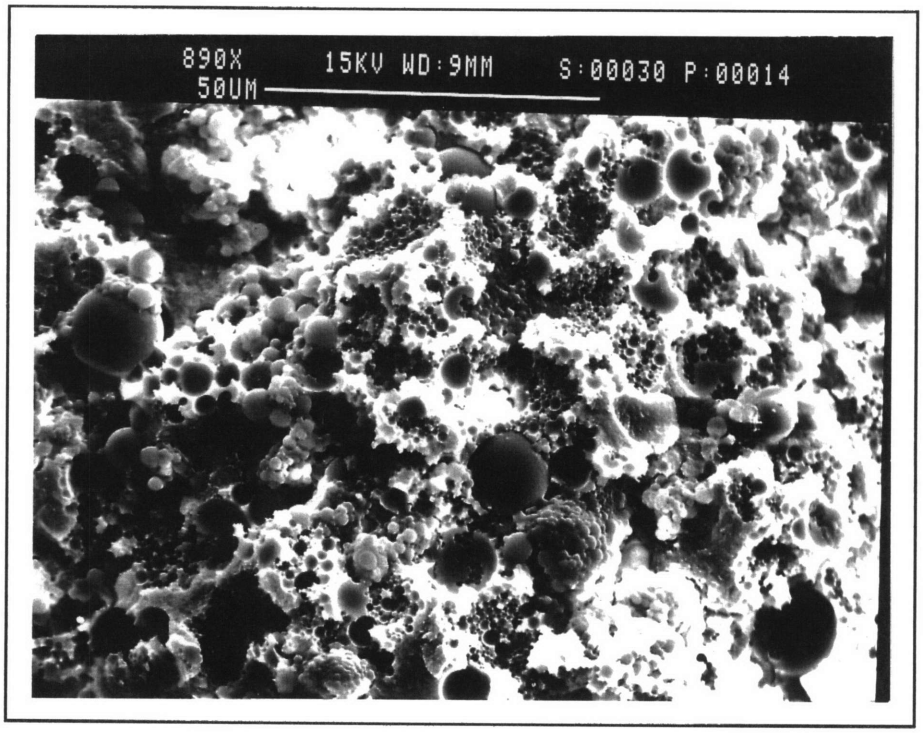

Figure 4.115- Poorly-adhered PDMS particles in a rubber-rich domain on the fracture surface of an MNS sample containing 9.5% ATBN and 5% Silanol PDMS particles.

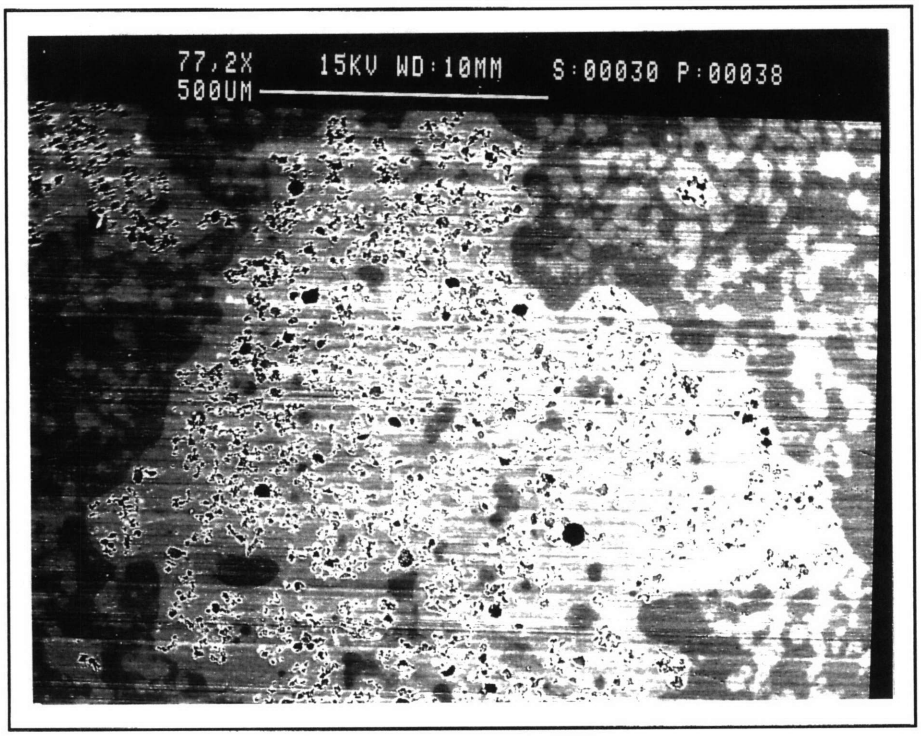

Figure 4.116- Backscattered image of the polished surface of an MNS sample containing 9.5% ATBN and 5% Silanol PDMS particles.

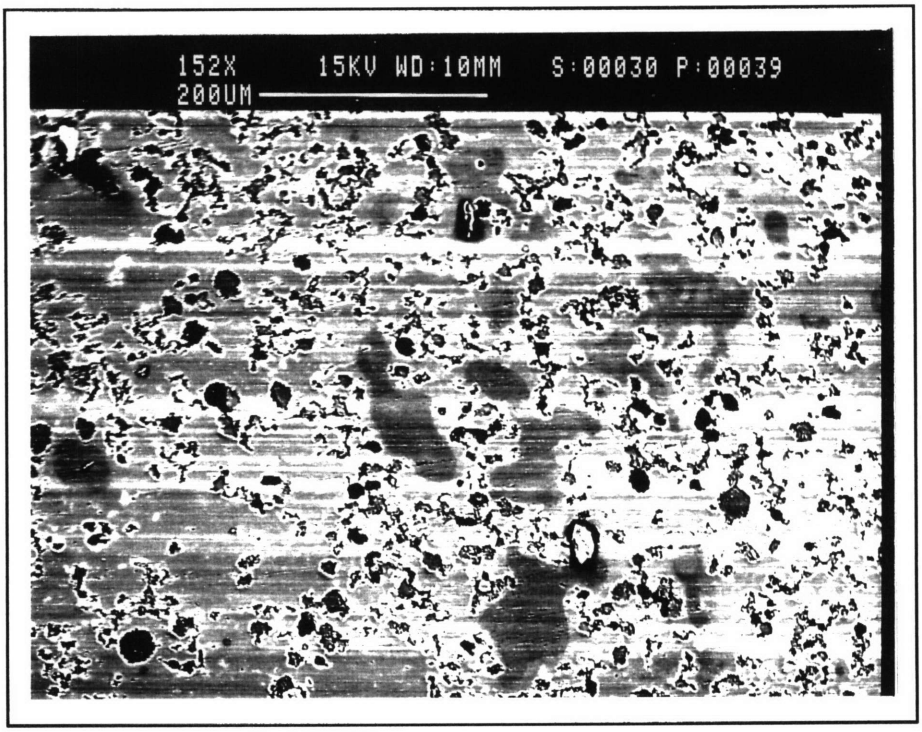

Figure 4.117- Backscattered image of an ATBN-rich domain on the polished surface of an MNS sample containing 9.5% ATBN and 5% Silanol PDMS particles.

4.2.5.3 Dynamic Mechanical Analysis

Figure 4.118 contains the tanδ curves for samples containing 9.5% ATBN and 5% amino, epoxy or silanol compatible PDMS particles, as well as the 0% ATBN and 9.5% ATBN control samples. Table 4.8 contains the values of the intensities and locations of the transitions. All three types of particles resulted in tanδ curves with both primary and secondary peaks. However, while the 9.5% ATBN control sample had a primary peak at around 110°C and a secondary peak at around 146°C, the locations of the primary and secondary peaks for the samples containing the PDMS particles occurred at similar locations to those of the 7.5% ATBN control samples. The peaks of the primary and secondary transitions for the samples containing the PDMS particles occurred at temperatures of around 160°C and 105°C respectively. This is probably due to the fact that the PDMS particles suppress the phase inversion.

Table 4.8- Values of Tg and tan(d) for both primary and secondary transitions in for MNS samples containing 9.5% ATBN and 5% PDMS particles as determined by DMA performed in tensile mode at a heating rate of 2°C/min and a frequency of 5 Hz.

Sample	High Temperature Transition (°C)	Low Temperature Transition (°C)	High Temperature tan(d)	Low Temperature tan(d)
0% ATBN	147.6	112.3	0.2173	0.1709
7.5% ATBN	164.8	none	0.1930	none
9.5% ATBN	145.4	108.4	0.2323	0.1843
5% Amino PDMS	157.5	104.2	0.1632	0.1233
5% Epoxy PDMS	157.6	105.3	0.1757	0.1379
5% Silanol PDMS	163.0	106.2	0.1660	0.1170

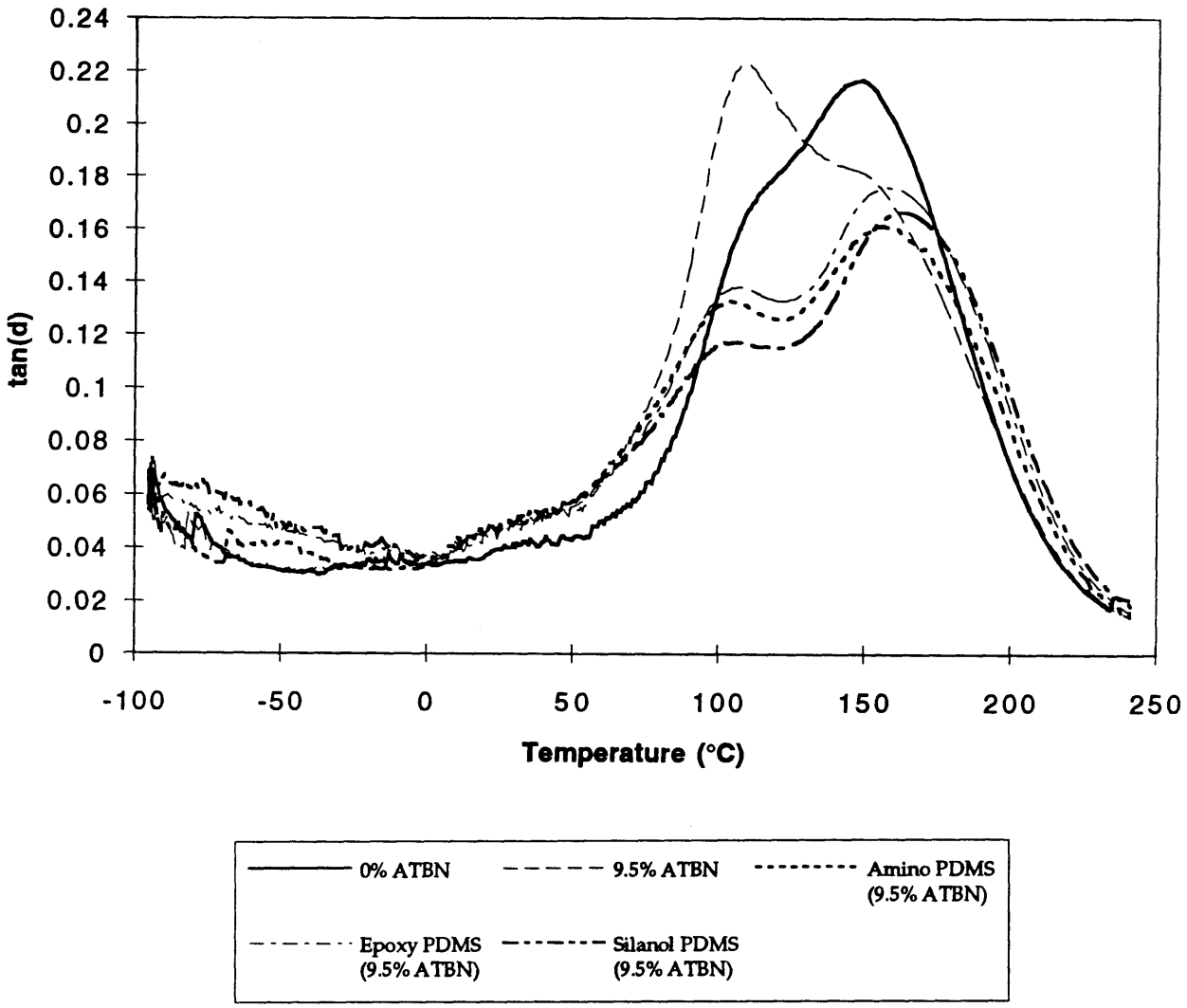

Figure 4.118- Tanδ curves as a function of temperature for MNS specimens containing 9.5% ATBN and 5% PDMS particles as determined by DMA performed in tensile mode at a heating rate of 2°C/min and a frequency of 5 Hz.

The curves of all three types of samples containing PDMS particles are very similar to each other and posses transitions at almost identical temperatures. The intensities of the transitions are also very similar to each other. However, the mobility of the epoxy phase, as indicated by the intensity of the low temperature shoulder, appears to relate to the fracture toughness. The sample with the epoxy PDMS particles exhibited the highest intensity shoulder of the samples containing PDMS particles and also the highest fracture toughness of these specimens. The sample containing the silanol PDMS particles exhibited the lowest intensity secondary transition and also the lowest fracture toughness. In addition, both the primary and secondary transitions occurred at higher temperatures for the sample containing the silanol PDMS particles than for the other samples containing PDMS particles. It is not surprising that the fracture toughness of the sample with the silanol PDMS particles is considerably lower than the other two samples containing PDMS particles.

It appears that the main reason that fracture toughness of the samples containing 9.5% ATBN and 5% PDMS particles is so low despite the high ATBN content is that the mobility of the epoxy phase is not any higher than in any of the specimens containing 7.5% ATBN and secondary particles observed in this study. This is probably due to the fact that the PDMS particles seem to attract the ATBN to their surfaces rather than allowing it to react with the epoxy to flexibilize it. In addition, the poor adhesion of the PDMS particles makes them ineffective in inducing any further deformation mechanisms that could lead to increased toughness.

4.2.6 12% ATBN and Glass Spheres

As discussed above, the fracture toughness of the compositions containing 9.5% ATBN and 5% PDMS samples were disappointingly low for two reasons. First, the presence of the PDMS particles seemed to suppress the phase inversion that should have occurred at 9.5% ATBN. It is believed that the ATBN was attracted to the surfaces of the PDMS particles rather than being free to evenly distribute itself throughout the resin to form a continuous rubber-rich phase. The second reason that the desired toughness was not achieved with the samples containing PDMS particles was that the

degree of adhesion between the PDMS particles and the matrix was extremely poor. Thus, this study produced a final composition, which contained 12% ATBN and 5% hollow glass spheres reacted with the epoxy compatible coupling agent (Z6020). The high ATBN content was chosen because it is sufficiently above the content that produces a phase inversion in pure MNS samples. The hollow glass spheres reacted with Z6020 coupling agent were chosen because they were found to posses the highest degree of adhesion and produce the highest fracture toughness values of any of the particles investigated in this study.

4.2.6.1 Plane Strain Fracture Toughness

Figure 4.119 shows the fracture toughness values of the sample containing 12% ATBN and 5% hollow glass spheres reacted with the epoxy compatible coupling agent. Table 4.9 contains the average fracture toughness values for all samples containing glass spheres, as well as for the 7.5% ATBN and 12% ATBN control specimens.

Table 4.9- Mechanical properties of MNS compact tension specimens containing various glass spheres.

Sample	K_{Ic} ksi*in1/ 2	Modulus ksi	G_{Ic} lb/ in
0% ATBN	0.45	590	0.34
7.5% ATBN Control	0.6465 (0.1017)	508.7	0.8380 (0.2427)
12% ATBN Control	0.7716 (0.0535)	419.7	1.4187 (0.1963)
5% Solid Glass 6020	0.6195 (0.0609)		
5% Hollow Glass 6020	0.8093 (0.0402)		
5% Solid Glass 6040	0.5151 (0.0562)	495.5	0.5409 (0.1210)
5% Hollow Glass 6020*	0.8184 (0.0609)	461.1	1.4585 (0.2133)

* Samples contain 12% ATBN.
All other samples contain 7.5% ATBN.

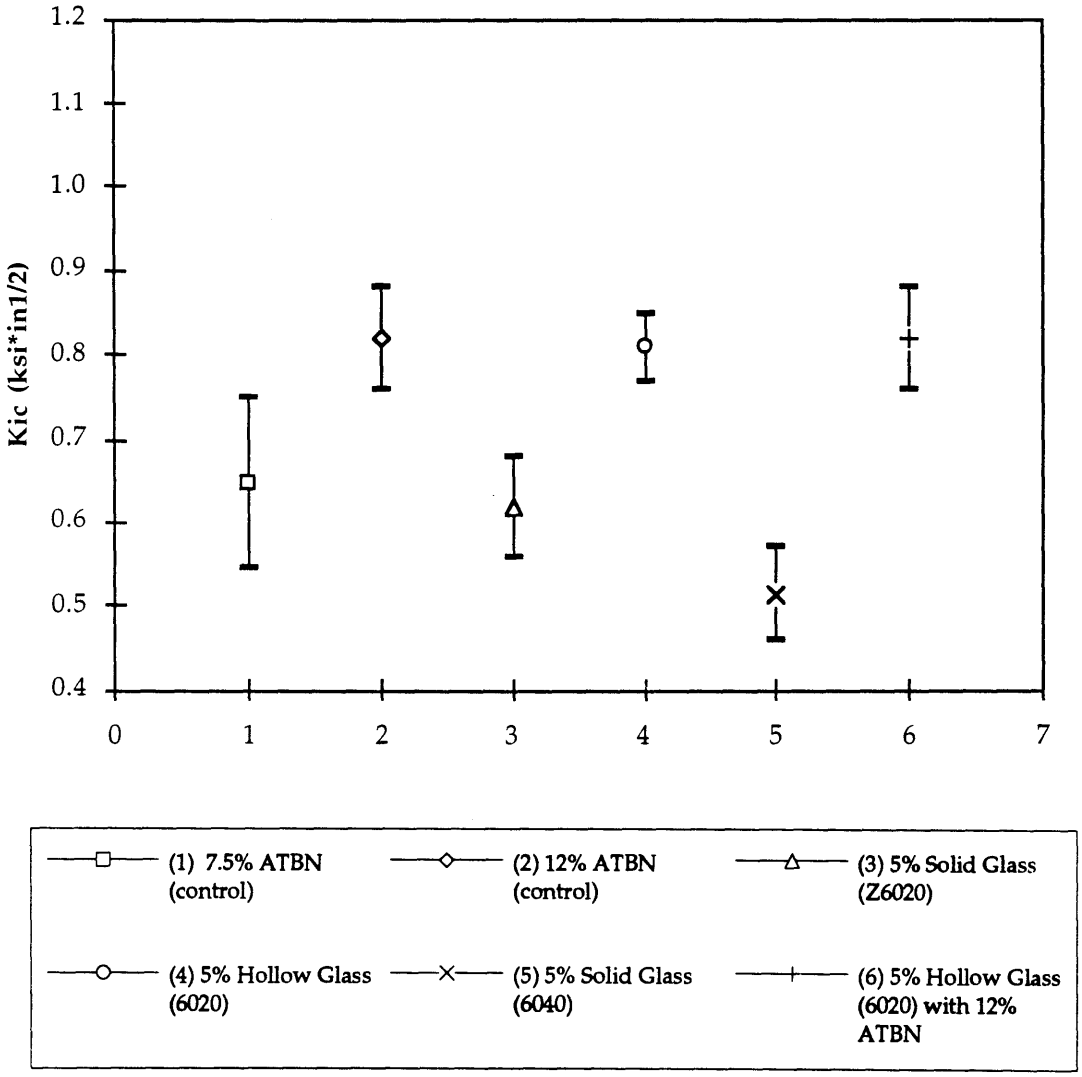

Figure 4.119- Fracture toughness values for MNS compact tension samples containing 7.5% ATBN and 5% solid glass spheres reacted with either epoxy or amino coupling agent or 5% hollow glass spheres reacted with epoxy coupling, or 12% ATBN with 5% hollow glass spheres reacted with epoxy coupling agent tested according to ASTM D 5045-93 at a rate of 0.2 in/min.

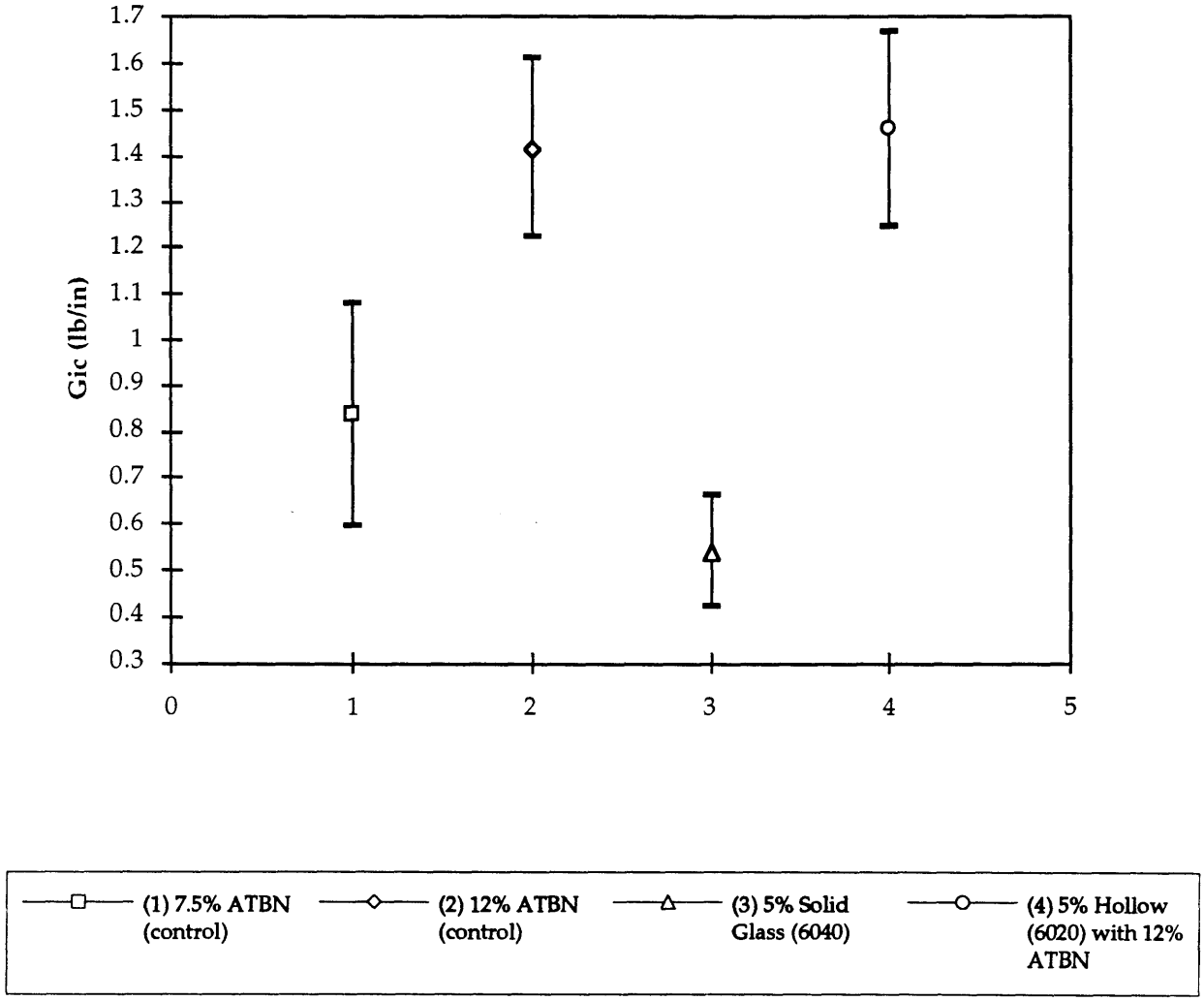

Figure 4.120- Average Gic values for MNS compact tension samples containing 7.5% ATBN and 5% solid glass spheres reacted with either epoxy or amino coupling agent or 5% hollow glass spheres reacted with epoxy coupling, or 12% ATBN with 5% hollow glass spheres reacted with epoxy coupling agent tested according to ASTM D 5045-93 at a rate of 0.2 in/min.

The fracture toughness of the sample containing 12% ATBN and 5% hollow glass spheres is only slightly higher than that for the sample with 7.5% ATBN and glass spheres. This is surprising considering the higher rubber content in the sample containing 12% ATBN. However, the sample containing 12% ATBN and glass spheres showed a measurably higher fracture toughness than the 12% ATBN control sample, with a value of 0.8184 $ksi*in^{1/2}$ rather than 0.7716 $ksi*in^{1/2}$. In addition, the modulus of the sample containing the glass spheres is measurably higher than that of the 12% ATBN control sample with a value of 461 ksi as opposed to the severe drop to 419 ksi for the 12% ATBN control sample. As a matter of fact, the modulus of the sample containing 12% ATBN and 5% glass spheres is considerably higher than that of any of the other particle-containing compositions discussed in this study (except for the sample with the solid glass spheres that showed an extremely low fracture toughness) (Table 4.3). It is also interesting that despite the high modulus, the sample with the 12% ATBN and glass spheres has a higher G_{Ic} value (with a value of 1.4585 lb/in) than the control 12% ATBN sample and comparable G_{Ic} values to the rest of the samples examined in this study (Figure 4.120).

4.2.5.2 Scanning Electron Microscopy

Figure 4.121 shows the fracture toughness of a sample containing 12% ATBN and 5% hollow glass spheres reacted with the epoxy compatible coupling agent (Z6020). Despite the very high rubber content in this sample, the rubber still forms discrete domains. The volume fraction of these domains is extremely high. There are several different types of ATBN-rich domains present on the surface of this sample. The first type is very large, amorphous and shows little evidence of deformation. These domains tend to contain clumps of glass spheres. One such domain is exhibited in the top center of Figure 4.121.

The second type of domain exhibited on the fracture surface of the 12% ATBN and hollow glass sphere sample is shown in Figure 4.122. These domains exhibit a high degree of plastic flow and may or may not contain clumps of glass particles (Figure 4.123). However, looking closely at the domain in Figure 4.123, the plastic flow of the surface of this domain does

appear to radiate out from a few well-adhered glass spheres and from the clump of well-adhered spheres in the upper right corner of the micrograph.

The final type of ATBN-rich domain is similar to the small, circular domains with cracks emanating from them as was characteristic of the fracture surfaces of pure MNS samples with rubber contents less than 9% ATBN (Figure 4.124). These small, ATBN-rich domains seem to be interspersed with single, well-adhered glass spheres (Figure 4.125). In general, the glass spheres are found to be located in clumps within the relatively undeformed domains, either in clumps or well-dispersed in the domains exhibiting large amounts of flow, or singly in the matrix phase. In all cases, the degree of adhesion of these particles appears to be extremely good with almost no evidence of particle pull-out (Figure 4.126). In fact, the degree of adhesion of these particles appears to be so good that the hollow spheres fracture rather than debonding from the matrix (Figure 4.127). Therefore, the cavities seen on the surface of this sample are generally fractured hollow spheres rather than craters left by debonded particles.

Thus, while the addition of the hollow glass spheres appears to suppress the phase inversion in the 12% ATBN sample, the well-adhered spheres appear to initiate enough energy absorbing mechanisms to increase the fracture toughness measurably, with minimal drop in the modulus. Despite the high modulus, this composition is also able to support a high resistance to crack propagation. Thus, the use of glass spheres to further increase the toughness of a rubber modified system without serious detriment to the mechanical properties looks promising.

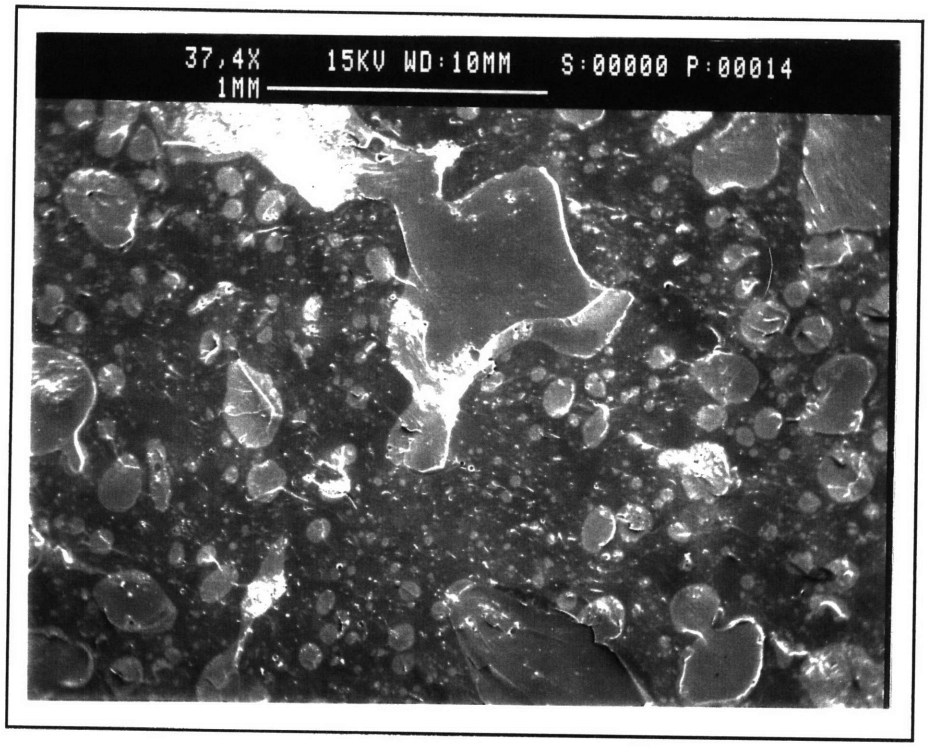

Figure 4.121- Fracture surface of an MNS compact tension specimen containing 12% ATBN and 5% hollow glass spheres reacted with epoxy coupling agent.

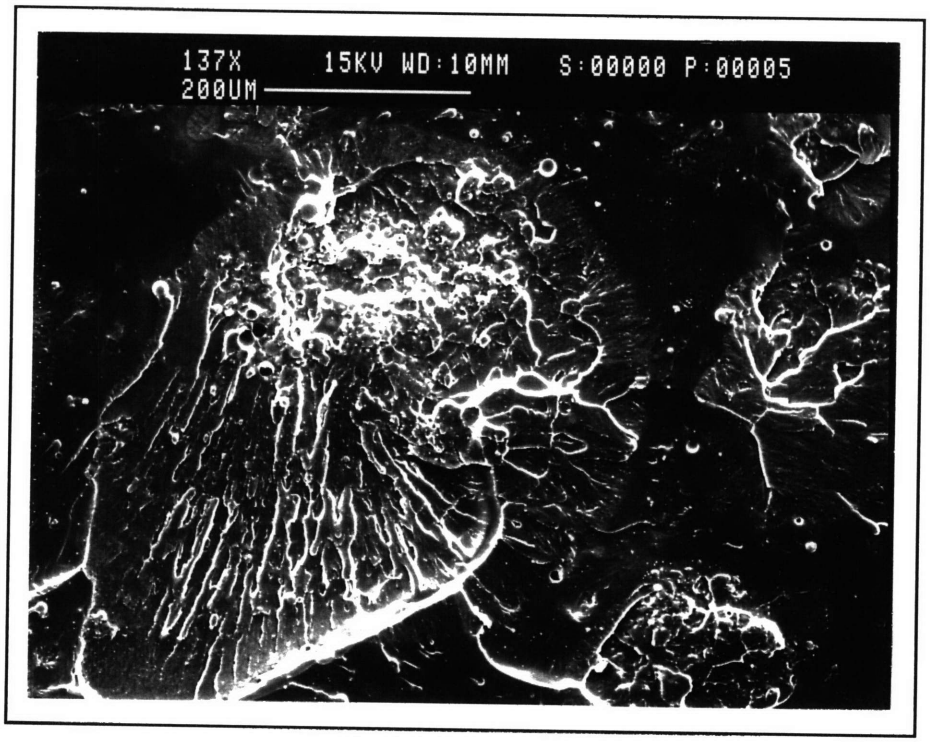

Figure 4.122- Glass spheres within a highly deformed rubber-rich domain on the fracture surface of an MNS specimen containing 12% ATBN and 5% hollow glass spheres reacted with epoxy coupling agent.

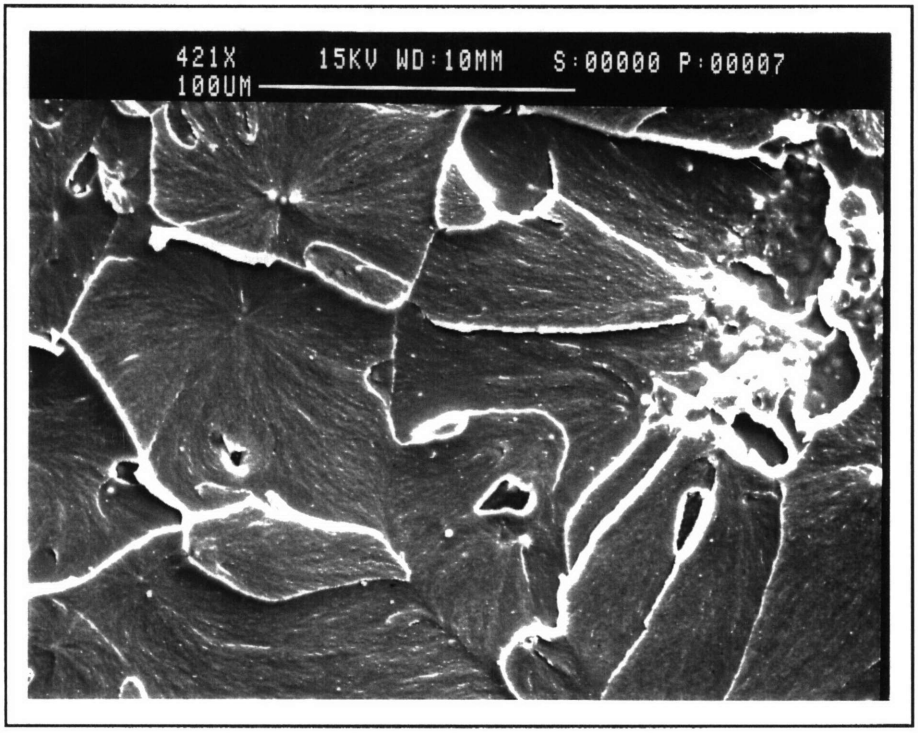

Figure 4.123- Extensive plastic flow emanating from glass spheres in a rubber-rich domain on the fracture surface of an MNS sample containing 12% ATBN and 5% hollow glass spheres reacted with an epoxy coupling agent.

Figure 4.124- Small rubber-rich domains and well-adhered glass spheres on the fracture surface of an MNS compact tension specimen containing 12% ATBN and 5% hollow glass spheres reacted with an epoxy coupling agent.

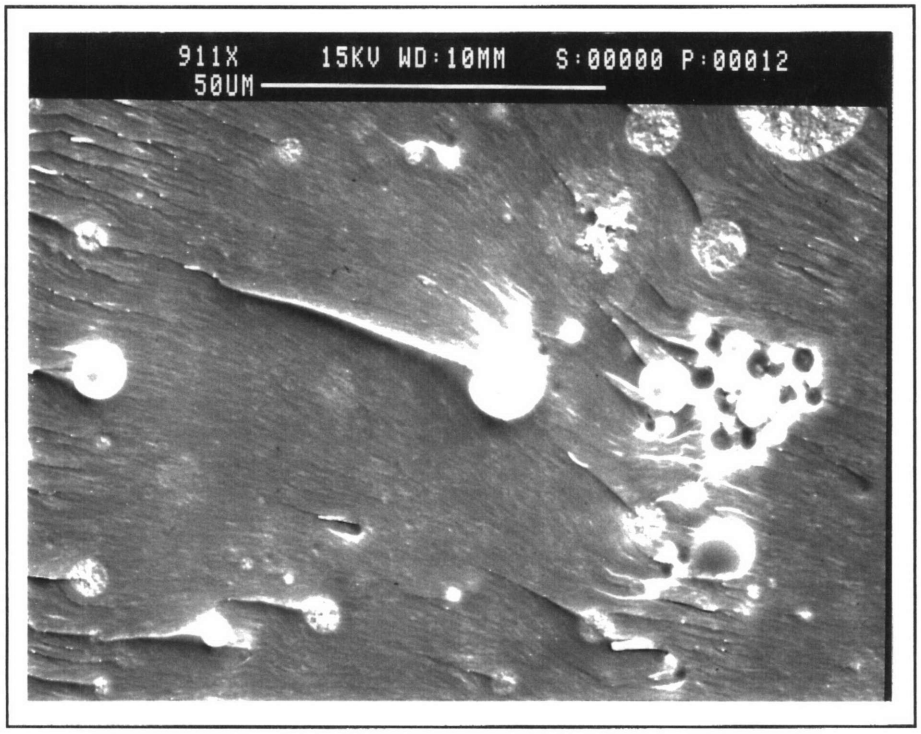

Figure 4.125- Well-adhered glass spheres on the fracture surface of an MNS compact tension specimen containing 12% ATBN and 5% hollow glass spheres reacted with an epoxy coupling agent.

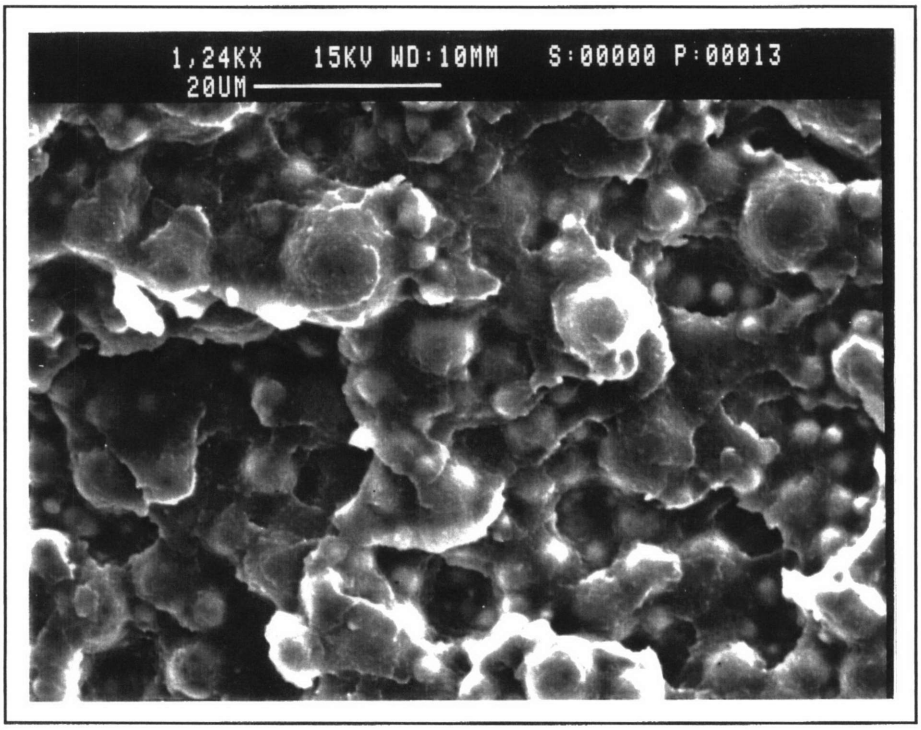

Figure 4.126- Well-adhered glass spheres on the fracture surface of an MNS compact tension specimen containing 12% ATBN and 5% hollow glass spheres reacted with an epoxy coupling agent.

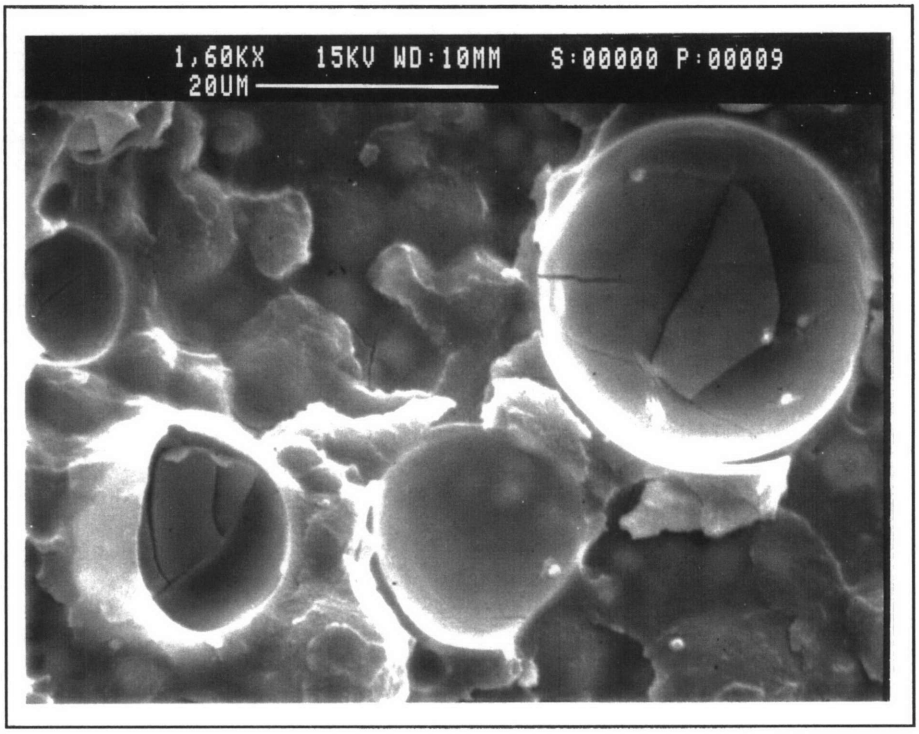

Figure 4.127- Cleaved glass spheres on the fracture surface of an MNS compact tension specimen containing 12% ATBN and 5% hollow glass spheres reacted with epoxy coupling agent.

5.0 Conclusions

This study shows that the addition of rubber modified epoxy to an otherwise brittle unsaturated polyester network can produce measurable improvements in toughness properties. While the addition of epoxy alone appears to produce a more mobile system, addition of the liquid rubber is necessary to produce the desired increase in toughness properties. However, these toughening effects are only substantial at rubber contents higher than about 8.5%. The addition of 8% ATBN results in slightly more than a 1.1 fold increase in plane strain fracture toughness (K_{Ic}), and a 1.5 fold increase in the strain energy release rate (G_{Ic}) over a pure polyester and epoxy system. This is accompanied by a small drop in modulus. When the ATBN content is increased to 9%, the K_{Ic} increases by a factor of 1.7 and the G_{Ic} by a factor of 3.2 over the pure polyester and epoxy system. With increasing rubber content, both the K_{Ic} and G_{Ic} continue to rise, but the modulus has dropped by a factor of 1.5 by the time the rubber content reaches 10%.

It was determined that the dramatic change in properties at rubber contents of around 9% was caused by a drastic change in the morphology of the system that occurs at these rubber contents. With the addition of around 9% ATBN, the morphology changes from a brittle polyester-rich matrix containing discrete rubbery domains to a continuous flexibilized matrix with brittle inclusions. At rubber contents below about 9%, it is believed that most of the ATBN reacts with the epoxy, as this reaction is favored. While the ATBN may flexibilize the epoxy to some extent, it does not affect the continuous polyester-rich phase. In addition, it is possible that due to the amine end groups on the liquid rubber used in this study, the ATBN may serve to further crosslink the epoxy. At low rubber contents, these ATBN crosslinks are probably very short and cannot absorb large amounts of energy through the typical uncoiling mechanisms.

At high rubber contents, there is probably sufficient ATBN to react with both the epoxy and a significant portion of the polyester to flexibilize both. It also appears to phase separate to produce a more uniform distribution of components. At these high rubber contents, the ATBN segments are probably much longer, and an epoxy rubber blend may form. This creation of an

overall flexibilized matrix phase is thought to be responsible for the measurable increase in toughness properties at high rubber contents. However, it is accompanied by a significant decrease in mechanical and thermal properties.

In general, the addition of small, second phase particles to MNS containing low rubber contents did not produce as large of an increase in toughness properties as expected. While the presence of the majority of these particles seemed to increase the mobility of the epoxy phase (as evidenced by the creation of a distinct, low temperature transition in the DMA curves), they did not appear to induce the deformation necessary to provide a substantial increase in toughness properties. Early in the study, it was observed that large scale deformation mechanisms were crucial to producing higher degrees of toughening. For example, the large, amorphous domains formed by ATBN and re-precipitated Nipol particles provided large regions of flexibilized material. This composition produced one of the higher increases in toughness properties. However, by far the largest increase in fracture toughness was observed in samples taken from the top region of the casting containing 2.5% CTBN. These samples had a continuous rubber-rich matrix, which showed extensive evidence of global deformation upon fracture. From DMA analysis, it was apparent that the system was extremely homogeneous and had a very high degree of mobility. However, the thermal properties of the material were sacrificed, as the transition appeared at a much lower temperature.

This failure of most of the second phase additives to initiate large scale energy-absorbing mechanisms appears to be either the result of the location of the particles or the poor degree of adhesion between the particles and matrix. When the particles are located outside the ATBN-rich domains, they cannot induce adequate deformation mechanisms, as it is much harder to induce flow in the polyester-rich matrix than in the ATBN-containing domains. In addition, when the particles are not well adhered, they are even less effective in inducing deformation in the matrix. Instead, their contribution comes through debonding. However, when adhesion is poor, not much energy is absorbed by debonding and the effect on toughness is minimal. A final problem caused by the addition of the second phase particles was that many of

these particles attracted ATBN to their surfaces. This resulted either in a depletion of distributed rubber within the ATBN-rich domains (in the case of samples with low ATBN contents), or a suppressed phase inversion (in samples with rubber contents greater than 9%). In either case, the volume of flexibilized material capable of undergoing substantial energy absorbing deformation was reduced by the addition of many types of particles.

On the other hand, a significant degree of toughening was produced by the addition of the hollow glass spheres reacted with Z6020 coupling agent. These particles were extremely well adhered and were located within the ATBN-rich domains. When the rubber content of the samples was low (7.5% ATBN), the toughening effect of these particles seemed to come mostly from debonding and fracturing of the well-bonded particles. There was not much evidence of large scale energy absorbing mechanisms. When the ATBN content was raised to 12%, large scale deformation was seen. The glass spheres did manage to suppress the phase inversion, so the ATBN-rich phase continued to form discrete domains even at this high rubber content. These large domains, which contained the well-adhered spheres, exhibited a good deal of plastic deformation. This deformation appeared to be initiated by the glass spheres as it tended to expand radially from individual particles. Plastic flow was also evident in some of the domains with clumps of particles. It is possible that even though the phase inversion was suppressed by the glass spheres, the existing large domains contain a higher rubber concentration and, therefore, posses more deformation potential. The presence of the glass spheres provided the stress concentration necessary to initiate the process. As a result, the K_{IC} increased by a factor of 1.8 and the G_{IC} by a factor of 4.2 over the pure polyester and epoxy system. In addition, the modulus of this sample only decreased by a factor of 1.3 despite the high rubber content.

Thus, it appears that this combination of the well-adhered glass microspheres within discrete rubber-rich domains has the potential to produce considerable increases in the toughness properties of an otherwise brittle polyester and epoxy system without significant deterioration of the mechanical and thermal properties. As the isolated particles seemed to produce considerable amounts of plastic flow, it is possible that even more significant increases in toughness could be achieved if the distribution of the

glass spheres were improved. In addition, it would be worthwhile to investigate the addition of the hollow microspheres to a system with an even higher ATBN content (or one containing both ATBN and CTBN) in an attempt to produce a continuous rubber-rich phase. It is possible that the presence of these well-adhered glass spheres could initiate a substantial amount of deformation in a continuous flexibilized matrix, while at the same time limiting adverse effects on the mechanical and thermal properties.

APPENDIX

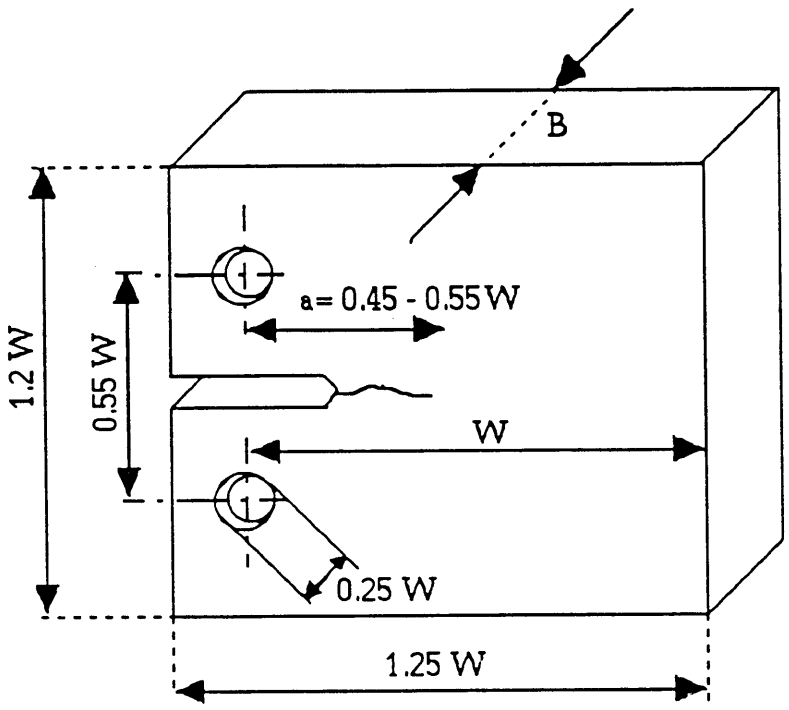

Figure A3.1- Schematic of compact tension specimen used for measuring the plane strain fracture toughness (ASTM D 5045-93).

REFERENCES

1) Ashby, M.F., D.P.H. Jones, *Engineering Materials 2: An introduction to Microstructures, Processing and Design* (Oxford: Pergamon Press, 1986), pp.169-174.

2) McCrum, N.G., C.P Buckley and C.B. Bucknal, *Principles of Polymer Engineering* , (Oxford: Oxford University Press, 1988), pp.209-252.

3) Supplemental Information for Program Competition 94-02. May, 1994.

4) *Composite Materials Technology: Processes and Properties*, Mallick, P.K. and S. Newman eds. (Hanser Publishers: New York, 1990).

5) Hsieh, K.H., J.S. Tsai, K.W. Chang, *Journal of Materials Science*, **26**, 5877, (1991).

6) Subramaniam, R., *Synthesis and Modification of Unsaturated Polyester Resins*, MIT Sc.D. Thesis, 1993.

7) Suspene, L. J. Gerard, J. Pascault, *Polymer Engineering and Science*, **30**, 1585, (Dec. 1990).

8) Suspene, L., D. Sage, J.P. Pascault, *Journal of Applied Polymer Science*, **41**, 2677, (1990).

9) Kausch, H., *Polymer Fracture* , (Springer-Verlag: Berlin,1987), pp.332-362.

10) Yamamoto T., H. Furukawa, *Polymer*, **36**, 2389, (1995).

11) Clegg, D.W., A.A. Collyer, *The Structure and Properties of Polymeric Materials*, (The Institute of Materials: London, 1993), pp.116-119.

12) Riew, C.K., E.H. Rowe, A.R. Siebert, in "Toughness and Brittleness of Plastics"; Deanin, R.D.; Crugnola, A.M., Eds.; ACS ADVANCES IN CHEMISTRY SERIES No. 154; American Chemical Society: Washington, D.C., 1976: 326-43.

13) Kambour, R.P. "A Review of Crazing and Fracture in Thermoplastics," Report No. 72CRD285, in General Electric Company Technical Information Series, (Oct. 1972).

14) Donald, A.M., E.J. Kramer, *Polymer*, **23**, 483, (July 1982).

15) Yamamoto T., H. Furukawa, *Polymer*, **36**, 2393, (1995).

16) Sultan, J.N., F.J. McGarry, *Polymer Engineering and Science*, **13**, 29, (Jan. 1973).

17) Manzione, L.T., J.K. Gillham, C.A. McPherson,*Journal of Applied Polymer Science*, **26**, 889 (1981).

18) Maazouz, A., H. Sautereau, J.F. Gerard, *Polymer Bulletin*, **33**, 67, (1994).

19) Hedrick, J.L., I. Yilgor, M. Jurek, *Polymer*, **32**, 2020, (1991).

20) Sankaran, S., M. Chandra, *Journal of Applied Polymer Science*, **39**, 1635, (1990).

21) Iijima, T., M. Tomoi, J. Yamasaki, H. Kakiuchi, *European Polymer Journal*, **26**, 145, (1990).

22) Iijima, T, M. Tomoi, T. Tochimoto, H. Kakiuchi, *Journal of Applied Polymer Science*, **43**, 463, (1991).

23) Wang, H.B., S.J. Li, J.Y. Ye, *Journal of Applied Polymer Science*, **44**, 789 (1992).

24) Manzione, L.T., J.K. Gillham, McPherson, *Journal of Applied Polymer Science*, **26**, 907, (1981).

25) Kunz, S.C., J.A. Sayre, R.A. Assink, *Polymer*, **23**, 1897, (1982).

26) Kinloch, A.J., S.J. Shaw, D.A. Tod, *Polymer*, **24**, 1141 (1983).

27) Kunz-Douglas, S., P.W.R. Beaumont, M.F. Ashby, *Journal of Materials Science*, **15**, 1109, (1980).

28) Kim, D.S., K. Cho, J.H. An, C.E. Park, *Journal of Materials Science*, **29**, 1854, (1994).

29) Hsieh, K.H., J.L. Han, *Journal of Polymer Science: Part B: Polymer Physics*, **28**, 783, (1990).

30) Parker, D.S., H-J. Sue, J. Huang, A.F. Yee, *Polymer*, **31**, 2267, (Dec. 1990).

31) Martsucelli, E., P. Musto, G. Ragosta, G. Scarinzi, E. Bertotti, *Journal of Polymer Science: Part B: Polymer Physics*, **31**, 619 (1993).

32) Okamoto, M., Y. Shinoda, *Polymer*, **34**, 4868, (1993).

33) Yee, A.F., D. Li, X. Li, *Journal of Materials Science*, **28**, 6392, (1993).

34) Penczek, P., "IPNs, Semi-IPNs and Related Systems Based on Unsaturated Polyester Resins," in *Advances in Interpenetrating Polymer Networks*, eds. D. Klempner and K.C. Frisch (Technomic Publishing: Lancaster, PA, 1989), pp.239-259.

35) Dompas, D., G. Groeninckx, *Polymer*, **35**, 4760, (1994).

36) Kim, H., H. Keskkula, D.R. Paul, *Polymer*, **32**, 2372, (1991).

37) Min, B.G., Z.H. Stachurski, J.H. Hodgkin, *Journal of Applied Polymer Science*, **50**, 1511, (1993).

38) Dompas, D., G. Groeninckx, *Polymer*, **35**, 4743, 1994.

39) Wrotecki, C., P. Heim, P. Gaillard, *Polymer Engineering ans Science*, **31**, 213, (February 1991).

40) Dompas, D., G. Groeninckx, *Polymer*, **35**, 4750, (1994).

41) Wrotecki, C., P. Heim, P. Gaillard, *Polymer Engineering and Science*, **31**, 218, (Feb. 1991).

42) Kinloch, A.J., D.G. Gilbert, S.J. Shaw, *Journal of Materials Science*, **21**, 1051, (1986).

43) Bagheri, R., R. Pearson, *Polymer*, **36**, 4883, (1995).

44) Sankaran, S., M. Chanda, *Journal of Applied Polymer Science*, **39**, 1635, (1990).

45) Di Liello, V., E. Martuscelli, P. Musto, G. Ragosta, G. Scarinzi, *Journal of Polymer Science: Part B: Polymer Physics*, **32**, 409, (1994).

46) Hsieh, K.H., J.L. Han, *Journal of Polymer Science: Part B: Polymer Physics*, **28**, 783, (1990).

47) Sankaran, S., *Journal of Applied Polymer Science*, **39**, 1459, (1990).

48) Abbate, M., E. Martuscelli, P. Musto, G. Ragosta, G. Scarinzi, *Journal of Polymer Science: Part B: Polymer Physics*, **32**, 395, (1994).

49) Tong, S.N., P.T. Wu, *Journal of Reinforced Plastics and Composites*, **9**, 299, (May 1990).

50) Ullett, J., R. Chartoff, *Polymer Engineering and Science*, **35**, 1086, (July 1995).

51) Kim, D.S., K. Cho, J.H. An, C.E. Park, *Journal of Materials Science Letters*, **11**, 1197, (1992).

52) Sperling, L.H. "IPNs Around the Word," in *Advances in Interpenetrating Polymer Networks*, eds. D. Klempner and K.C. Frisch (Technomic Publishing: Lancaster, PA, 1989), pp.1-7.

53) Frisch, H.L., K.C. Frisch, D. Klempner, *Polymer Engineering and Science*, **14**, 646, (Sept. 1974).

54) Meyer, G.C., P.Y. Mehrenberger, *European Polymer Journal*, 13, 383, (1977).

55) Fox, R.B., J.J. Fay, U. Sorathia and L.H. Sperling in *Sound and Vibration Damping with Polymers*, eds. R.D. Corsaro and L.H. Sperling, ACS Symp. Series No. 424, Amer. Chem. Soc., Washington, DC, (1990).

56) Iijima, T., M. Tomoi, A. Suzuki, H. Kakiuchi, *European Polymer Journal*, **27**, 851, (1991).

57) J.W. Park and S.C. Kim,*Phase Separation and Morphology Development during Curing of Toughened Thermosets.*, Department of Chemical Engineering, Korea Advanced Institute of Science and Technology, unpublished.

58) Figure 1 in Dompas, D., G. Groeninckx, *Polymer*, **35**, 4743, 1994.

59) Figure 7 in Kunz-Douglas, S., P.W.R. Beaumont, M.F. Ashby, *Journal of Materials Science*, **15**, 1109, (1980).

60) Figure 3.40 in Subramaniam, R., *Synthesis and Modification of Unsaturated Polyester Resins*, MIT Sc.D. Thesis, 1993.

61) Figure A 2.1 in Subramaniam, R., *Synthesis and Modification of Unsaturated Polyester Resins*, MIT Sc.D. Thesis, 1993.

62) Figure 4 in Kinloch, A.J., S.J. Shaw, D.A. Tod, *Polymer*, **24**, 1141 (1983).